

DISS. ETH NO. 27897

Synthesis, Characterization and Competitive Adsorption of Comb Copolymer Dispersants

A thesis submitted to attain the degree of
DOCTOR OF SCIENCES
(Dr. sc. ETH Zurich)

presented by

STEFANIE ANNE WECKWERTH

M.Sc. Polymer Science, *Universität Bayreuth*

born on 14.09.1991

accepted on the recommendation of

Prof. Dr. Robert J. Flatt
Dr. Hela Bessaies-Bey
Prof. Dr. Torben Gädt
Dr. Wolfgang Radke

2022

*"I have approximate answers and possible beliefs and
different degrees of certainty about different things,
but I'm not absolutely sure of anything"*

— RICHARD P. FEYNMAN

Acknowledgement

The research work of this thesis was realized in the group of Physical Chemistry of Building at Materials at ETH Zürich. Funding for my work was partly provided by the Swiss National Fund (project no. 172481) titled “Molecular control of cement hydration through tailored chemical admixtures”. I want to thank the SNF for their financial support.

First, I want to acknowledge the members of my defense jury who revised this manuscript, namely, my supervisor Prof. Dr. Robert J. Flatt, Prof. Dr. Torben Gädt, Dr. Hela Bessaies Bey and Dr. Wolfgang Radke. I also want to thank Prof. Dr. Ioannis Anastasopoulos, who was the chairman of the doctoral examination. Moreover, I want to express my gratitude to Dr. André Striegel for reading my manuscript and joining the defense. I want to thank all of them for their interest in my work and making this doctoral examination a pleasant experience. Unfortunately, and due to the current circumstances, we could not meet in person but, anyway, it was a very enjoyable event for me.

Besides, I want to acknowledge all people who contributed to the success of this work by helping me with experiments and their expertise: Robert Temme for his work on the competitive adsorption part, Weiqing Xu, Arnesh Das and Luca Michel for BET and XRD measurements. Moreover, Dr. Francesca Breviglieri for her help with cloud point determinations. I also want to acknowledge Dr. Giulia Gelardi for getting me started with chromatography.

Many of my experiments would not have been possible without the support by Sika AG, Switzerland, who supplied me with many polymers. Special thanks go to Dr. Lukas Frunz and Jürg Weidmann who were very supportive over the years and helped me out multiple times, when I called the “PCE Hotline” and asked for more material.

But of course, some people deserve my **special gratitude**.

I want to start with my supervisor, Prof. Robert Flatt. Thanks, **Robert**, for giving me the chance to pursue a PhD at PCBM. I came to ETH as a polymer chemist, with no clue about cement or concrete. This did not stop you from believing in my work and giving me a lot of freedom in shaping the scientific aspects of my thesis. I appreciated your input, in particular when we were writing publications. You took the time to critically discuss and argue with me. And in the end, I had the feeling that we were both happy and satisfied with the results.

Next, I want to express my deepest gratitude to Wolfgang Radke. Thanks, **Wolfgang**, for spontaneously “joining” my PhD. In 2018, I was kind of stuck with my work on PCE chromatography. You motivated me to pursue dual detection, and I am very proud that we even published this part of my thesis together. I appreciated every email exchange, scientific advice, but also your sense of humor a lot. It was an honor to also have you on my thesis committee.

At this point, I do not only want to mention Wolfgang, but all PSS team members that I was in contact with over the years, among them, Dr. Martina Adler. **Martina**, your paper was the basis for my PhD. Thanks, for meeting and supporting me with scientific advice, and thanks for helping me multiple times *via* Team Viewer, when I was struggling with WinGPC or any other technical issue, you saved me more than once! Another PSS member, I want to address, is Dr. Daniela Held. Thanks, **Daniela**, for recommending me to talk with Wolfgang and Martina.

I consider myself very lucky that I got support from another expert for polymers and chromatography, Dr. André Striegel. Thanks, **André**, for meeting me in Frankfurt in 2018. Your advice on my work but also your advice before my defense helped me to develop a lot of confidence in my work.

Moreover, I want to mention Robert Temme. It was my luck to find you as a student assistant. You carried out so many experiments and helped me a lot to improve the competitive adsorption procedure. You significantly contributed to the success of this work with your workforce, patience and ambition. Thanks for coming to Zürich, **Robert!**

Of course, I am thankful to all PCBM and corrosion group members who supported me within the last 5 years in one way or the other. Here, I want to mention my (former) office mates of E16, **Weiying**, **Ana** and **Federica**. It was fun to work along with you in our “multinational” office. In particular, I am grateful to Federica. We started our PhD journey almost at the same time, and I am very

happy that after all this time, we are still in contact as friends. I love to follow your adventure in the US and am already curious what happens next.

I want to continue with **Andrea, Andi, Martin, Heinz, Lukas** and **Lex**. Thanks for giving me the chance to talk German from time to time. A particular "thank you" goes to Heinz. I loved discussing with you, listening to your stories and jokes, and I really think we should revive the "Flachwitz-Freitag".

At this point, I cannot miss to mention Patrick. Thanks, **Patrick**, for showing me that my ability to understand Swiss German must improve when I want to survive in Switzerland. You know that I understood only 30% of what you told me when we had lunch for the first time. Since then, I can confidentially say that I understand now about 75% (even when you talk with Steffi). Thanks for having become a good friend along the way.

Sometimes, I almost forget that there was a time before Zürich. My studies started in Bayreuth, and I am very thankful to all people who made my studies a memorable experience. During my bachelor studies, Dr. Munish Chanana hired me as a student assistant. Thanks, **Munish** for giving me the chance to get started with research. It was a very pleasant coincidence that we met again some years afterwards at ETH.

Everyone who pursues a PhD knows about the ups and downs. And here I must thank one person in particular. Thanks, **Federico**! In the most desperate moment of my PhD, you did not even try to give advice using words, but you came back from Italy with a lopy-eared bunny and wanted me to choose a second one. Ever since, **Banjo** and **Fanta** have become the most lovable and memorable part of my time in Zürich. I am more than grateful to have you three in my life.

My PhD shows the end to more than a decade of studies and figuring out whom I want to become. I must admit, it was a hell of a journey that I will never forget. I learned so many things, not only science and research, but this period also shaped my personality. All this had not been possible without my parents.

Thanks **Mum** and **Paps** for giving me the freedom, strength, and confidence to pursue my goals. No matter, if I changed my mind from becoming a local journalist, to teacher, to chemist, to polymer chemist, to "something with concrete". You always had my back and ensured me that what I was doing was exactly the right thing to do. I owe you for that!

But not only my parents, also **Lena, Jan** and **Martina** went with me through all these phases. Since I moved to Switzerland (and already before), your numbers are the most dialed on my phone. Thanks for being a part of my life since forever!

Mission PhD is accomplished. I am looking forward to new adventures and making new memories.

Abstract

Poly(carboxylate ether) (PCE) superplasticizers have become an indispensable part in modern concrete formulations. On the market, a broad variety of chemically different PCEs is available. However, the performance of a PCE does not exclusively depend on the chemical nature of the monomers. Indeed, their molecular structure and dispersity have a significant impact on performance and plasticizing abilities. To this date, a lot of research empirically describes the impact of average molecular parameters on the performance of PCEs, but falls short of predictive models considering parameter distributions. At the same time, there is a lack of analytical protocols that enable a comprehensive analysis of molecular dispersity.

Indeed, the notion "*dispersity*" is often applied to acknowledge solely the width of the molar mass distribution (MMD). However, PCEs are characterized by a high degree of molecular heterogeneity. This means that dispersity is not restricted to variations in molar mass, but also applies to distributions of the molecular parameters, such as backbone length, grafting ratio and potentially side chain length.

A better understanding of dispersity is crucial for the prediction of structure-performance relations of PCEs. This thesis draws attention to their complex dispersity and reveals how molecular parameters affect the competitiveness of PCEs for adsorption at the cement surface. More specifically, the thesis contributes to the field of PCE research in four main aspects:

First of all, versatile protocols for the synthesis of PCE model structures with low dispersity and systemic variations of the molecular parameters are presented. Well-defined model structures are crucial for identifying structure-performance relations, but also to develop analytical methods that allow to characterize molecular heterogeneity.

Subsequently, this thesis opts for a better use of liquid chromatography (LC) for PCE analytics. LC-based protocols are developed that enable to investigate molecular heterogeneity within PCEs. Such versatile and refined analytical tools are essential to get an insight into the polymeric fractions of PCEs that ultimately determine their qualities as superplasticizers.

For instance, size exclusion chromatography (SEC) with dual concentration detection is suggested to quantify the comonomer composition of PCEs. While common SEC analysis solely targets the MMD, the dual concentration method gives information on the PCE composition in dependence on their molecular size. Moreover, it is revealed how and to what extent the synthesis pathway affects the chemical dispersity of PCEs.

Furthermore, reverse-phase high performance liquid chromatography (RP-HPLC) with solvent gradients is presented as a suitable tool to separate PCEs according to the grafting ratio. Thus, this method gives an insight into the chemical composition distribution (CCD). Limitations of RP-HPLC are discussed, and complementary SEC experiments allow a profound 2D-analysis of PCEs targeting the CCD in the first and MMD in the second chromatography dimension.

Besides providing analytical tools to study dispersity, the effect of molecular parameters on PCE adsorption and competition is studied. For this purpose, a novel experimental approach is presented that enables to quantify the competitive adsorption between PCE molecules of different molecular parameters, *i.e.* different charge density, backbone length and side chain length. The presented results confirm the existence of competitive adsorption phenomena among PCE molecules as a consequence of their molecular characteristics. In this context, the impact of molecular heterogeneity of PCEs is discussed. A thermodynamic framework is established to interpret the results. It offers the first theoretical model capable to discriminate the adsorption competitiveness of a PCE in relation to its molecular structure.

All in all, this thesis presents a comprehensive approach to synthesize and analyze PCEs before investigating their adsorption behavior. Herein, the thesis opts for a better use of polymer analytics and polymer physics in combination with basic thermodynamics and fundamental cement chemistry to provide a better understanding of competitive adsorption phenomena. Most importantly, it is emphasized that reliable structure-performance relations can only be established when the applied PCEs are well-characterized regarding their molecular parameters.

Zusammenfassung

Poly(carboxylate ether) (PCE) basierte Verflüssiger sind ein essenzieller Bestandteil moderner Beton-Formulierungen. Tatsächlich ist heute eine grosse Auswahl an PCEs erhältlich, welche sich in ihrer chemischen Zusammensetzung unterscheiden. Die Leistung und Effektivität eines PCEs hängt dabei nicht ausschliesslich von dessen chemischer Natur ab. Darüber hinaus haben die molekulare Struktur und die Dispersität einen erheblichen Einfluss auf die Leistung und Verflüssigungseigenschaften. In der Literatur findet man zahlreiche Arbeiten, welche den Einfluss von gemittelten molekularen Parametern auf die Verflüssigungseigenschaften beschreiben. Hierbei ist auffällig, dass Parameter Verteilungen häufig nicht genügend Beachtung geschenkt wird. Des Weiteren fehlt es an analytischen Protokollen, welche eine umfassende Analyse der molekularen Dispersität ermöglichen.

In der Tat wird der Begriff "*Dispersität*" häufig lediglich mit der Breite der Molekulargewichtsverteilung (MMD, molar mass distribution) in Zusammenhang gebracht. Allerdings zeichnen sich PCEs durch ein hohes Mass an Dispersität aus. Dies bedeutet, dass Dispersität nicht auf Variationen der molaren Masse beschränkt sind, sondern auch auf molekulare Parameter, wie beispielsweise Länge der Hauptkette (engl. backbone), deren Pfropfdichte und möglicherweise auch Seitenkettenlänge zutreffen.

Ein umfassender Einblick in die Dispersität ist essenziell, um Parameter-Wirkungs Vorhersagen zu treffen. In der vorliegenden Dissertation wird der Fokus auf die komplexe Dispersität von PCEs gelegt und dabei untersucht, wie sich molekulare Parameter auf deren Kompetitivität bezüglich der Adsorption an der Zementoberfläche auswirken. In folgenden vier Punkten leistet diese Arbeit einen Beitrag zur PCE-Forschung:

Zunächst werden Protokolle zur Synthese von PCEs vorgestellt, welche die Herstellung von Modellstrukturen mit geringer Dispersität unter systematischer Variation der molekularen Parameter ermöglichen. Modellstrukturen sind essenziell,

um Parameter-Wirkungs-Vorhersagen (oder Struktur-Wirkungs-Vorhersagen) zu treffen. Darüber hinaus spielen Modell-PCEs eine wichtige Rolle bei der Entwicklung analytischer Methoden zur Charakterisierung molekularer Heterogenität.

Des Weiteren hat es sich diese Arbeit zum Ziel gesetzt, aufzuzeigen, wie Flüssigchromatographie (LC, liquid chromatography) optimal in der PCE-Analytik eingesetzt werden kann. Deshalb werden im Zuge dieser Arbeit LC-basierte Protokolle entwickelt, welche die Untersuchung molekularer Heterogenität unter PCE-Molekülen ermöglichen. Flexible und präzise Analysemethoden sind essenziell, um einen Einblick in die PCE-Fractionen zu erhalten, welche letztendlich deren Eigenschaften als Verflüssiger bestimmen.

Zunächst wird Grössenausschluss-Chromatographie (SEC, size exclusion chromatography) mit dualer Konzentrationsdetektion vorgeschlagen, um die Comonomer-Zusammensetzung von PCEs zu quantifizieren. Während in gewöhnlichen SEC Experimenten lediglich die Molekulargewichtsverteilung bestimmt wird, ermöglicht es die duale Konzentrationsdetektion, Informationen bezüglich der PCE-Zusammensetzung in Abhängigkeit von der Molekülgrösse zu erhalten. Des Weiteren wird aufgezeigt, inwiefern und in welchem Ausmass sich der Syntheseweg auf die chemische Dispersität auswirkt.

Darüber hinaus wird Umkehrphasen-Flüssigkeitschromatographie (RP-HPLC, reverse-phase high performance liquid chromatography) unter der Nutzung von Lösungsmittelgradienten als Methode vorgestellt, welche es zulässt, PCEs nach deren Pflöpfungsdichte aufzutrennen. Folglich, ermöglicht diese Methode einen Einblick in die chemische Zusammensetzungsverteilung (CCD, chemical composition distribution). Limitierungen der RP-HPLC Methode werden diskutiert und ergänzende SEC Experimente werden durchgeführt, um eine umfassende 2D-Analyse von PCEs zu erhalten, welche einen Einblick in CCD und MMD gewährleistet.

Nachdem verschiedene analytische Methoden vorgestellt wurden, welche dem Zweck der Charakterisierung von Dispersität dienen, wird die Auswirkung der molekularen Parameter auf kompetitive Adsorption an der Zementoberfläche untersucht. Hierzu wird ein neuartiger experimenteller Ansatz präsentiert, welcher es zulässt, kompetitive Adsorption zwischen PCEs unterschiedlicher molekularer Parameter (z.B. Pflöpfungsdichte/Ladungsdichte, Hauptkettenlänge und Seitenkettenlänge) zu quantifizieren. Die Resultate bestätigen die Existenz von kompetitiver Adsorption zwischen PCE-Molekülen als Folge deren molekularer Eigenschaften. Im Zuge dessen wird

auch die Rolle von Dispersität diskutiert. Des Weiteren wird ein thermodynamisches Rahmenkonzept etabliert, welches die Interpretation der experimentellen Resultate ermöglicht. Es ist das erste thermodynamische Modell, welches es ermöglicht, die Affinität und Kompetitivität von PCEs im Hinblick auf deren molekulare Struktur zu unterscheiden.

Die vorliegende Dissertation beinhaltet einen umfassenden Ansatz zur Synthese und Analyse von PCEs, sowie eine Untersuchung deren Adsorptionsverhaltens. Demnach hat es sich diese Arbeit zum Ziel gesetzt, Polymeranalytik und Polymerphysik in Kombination mit grundlegender Thermodynamik und Zementchemie gezielt einzusetzen, um ein besseres Verständnis bezüglich kompetitiver Adsorption zu erhalten. Hierbei muss betont werden, dass zuverlässige Aussagen bezüglich Struktur-Wirkungs-Mechanismen nur getroffen werden können, wenn PCEs bezüglich ihrer molekularen Parameter hinlänglich untersucht werden.

Contents

Acknowledgements	i
Abstract	v
Zusammenfassung	vii
List of Figures	xvii
List of Tables	xxi
Acronyms & Abbreviations	xxiii
0. Introduction	1
0.1. Background Section	1
0.2. Objective of the Thesis	3
0.3. Structure of the Manuscript	5
0.4. List of Publications	7
1. State of Art	9
1.1. Poly(carboxylate ethers)	9
1.1.1. Molecular Characteristics	9
1.1.2. Model of Gay and Raphael	10
1.1.3. Dispersity of PCEs	12
1.1.4. Working Mechanism - DLVO Theory	14
1.1.5. Solubility of PCEs	16
1.2. PCE Adsorption	17
1.2.1. Adsorption Basics	17
1.2.2. Adsorption Isotherms	18
1.2.3. The Impact of Dispersity	19
1.2.4. Impact of Molecular Parameters	19

1.3. Competitive Adsorption	20
1.3.1. Competition with Admixtures	21
1.3.2. Competition among PCEs	21
1.3.3. Adsorption Equilibrium	22
1.4. Chemical Variety in PCEs	22
1.4.1. Backbone Chemistry	22
1.4.2. Sidechain Chemistry	24
1.5. PCE Synthesis	25
1.5.1. Grafting of Precursor Backbones	26
1.5.2. Free Radical Copolymerization	27
1.5.3. RAFT-Polymerization	28
1.6. Characterization of Average Parameters	30
1.6.1. PCE Composition	30
1.6.2. Conformation in Solution	31
1.6.3. Molar Mass Averages	32
1.7. Characterization of Parameter Distributions	33
1.7.1. The Importance of Liquid Chromatography	33
1.7.2. Basics about Liquid Chromatography Modes	34
1.8. Size Exclusion Chromatography	36
1.8.1. Basics about SEC	36
1.8.2. Dual Concentration Detection	39
1.9. Liquid Chromatography at Critical Conditions	41
1.9.1. Basics about LCCC	41
1.9.2. LCCC of PCEs	42
1.10. Liquid Adsorption Chromatography	43
1.10.1. Basics about LAC	43
1.11. Gradient Polymer Elution Chromatography	44
1.11.1. Solvent Gradient Interaction Chromatography	44
1.11.2. Temperature Gradient Interaction Chromatography	46
1.12. 2D-Chromatography	46
1.13. Implications of the State of the Art	49
2. Synthesis of Poly(carboxylate ethers)	51
2.1. Context	51
2.2. Nomenclature of PCEs	52
2.3. RAFT Polymerization	53
2.3.1. Chemicals	53

2.3.2.	Synthesis Protocol	53
2.3.3.	Calculation of Molecular Parameters	55
2.3.4.	Molar Mass Distribution	56
2.3.5.	Monitoring the Reaction Progress	57
2.3.6.	Different Side Chain Lengths	58
2.3.7.	Living Character of RAFT	60
2.3.8.	Concentration Detection via UV-Vis Spectroscopy	61
2.3.9.	Hydrolytic Stability of the RAFT group	63
2.4.	Free Radical Copolymerization	65
2.4.1.	Chemicals and Synthesis Protocol	65
2.4.2.	Molar Mass and Grafting Density	66
2.5.	Grafting <i>via</i> Polymer-analogous Esterification	67
2.5.1.	Standard Grafting Protocol	68
2.5.2.	Size Exclusion Chromatography	69
2.5.3.	Methacrylic G-PCEs	69
2.6.	Materials and Characterization Protocols	70
2.6.1.	Purification and Storage	70
2.6.2.	Size Exclusion Chromatography	70
2.6.3.	¹ H-NMR	72
2.6.4.	Titration	73
2.6.5.	UV-Vis-Spectroscopy	76
3.	Liquid Chromatography - Part I	77
	SEC with Dual Concentration Detection	77
3.1.	Context	77
3.2.	Strategy	78
3.3.	Materials and Methods	79
3.3.1.	Applied Polymers for Dual Detection	79
3.3.2.	Size Exclusion Chromatography	80
3.3.3.	Mobile Phase and Detection Wavelength	81
3.3.4.	Response Factor Determination	81
3.4.	Results and Discussion	83
3.4.1.	Evaluation of Dual Concentration Results	83
3.4.2.	Mixtures of PMAA and PPEGMA Homopolymers	84
3.5.	Dual Detection SEC of PCEs	86
3.5.1.	Comparison with ¹ H-NMR	86

3.5.2. Homogeneity of PCEs produced by Esterification	87
3.5.3. Impact of Backbone Length	88
3.5.4. PCEs from Free Radical Copolymerization	90
3.6. Conclusion	92
3.7. Appendix <i>Chapter 3</i>	94
4. Liquid Chromatography - Part II	99
RP-HPLC with Solvent Gradients	99
4.1. Context	99
4.2. Strategy	100
4.3. Applied Polymers	100
4.3.1. Nomenclature	102
4.3.2. RAFT-Polymers	102
4.3.3. Grafting of Precursor Backbones	102
4.3.4. Free Radical Copolymerization	103
4.4. Instrumentation	103
4.4.1. Size Exclusion Chromatography	103
4.4.2. RP-HPLC	103
4.4.3. Development of the Solvent Gradient	104
4.5. Results and Discussion	106
4.5.1. Gradient RP-HPLC of Polymers with Low Dispersity	106
4.5.2. Variations of Side Chain Length	108
4.5.3. Variations of Backbone Length	110
4.5.4. Gradient Experiments of PCEs from Free Radical Copolymer- ization	111
4.5.5. Fractionation and 2D-Chromatography	113
4.6. Comprehensive LC Analysis of PCEs	117
4.7. Conclusion	119
4.8. Implications for Admixture Research	120
4.8.1. Mapping Dispersity	120
4.8.2. Identification of PCE Species	121
4.8.3. Structure-Performance-Relations: An Example	122
5. Competitive Adsorption Part I	125
Impact of Charge Density and Backbone Length	125
5.1. Context	125

5.2. Strategy	127
5.2.1. Basic Concept and Methodology	127
5.2.2. Assessing Molecular Level Effects	127
5.3. Materials	129
5.3.1. Cement	129
5.3.2. PCEs	129
5.4. Experimental Methods	131
5.4.1. Standard Mixing Protocol	131
5.4.2. Competitive Adsorption Protocol	132
5.4.3. Adsorption Isotherms	133
5.5. Results	136
5.5.1. Calculations and Data Treatment	136
5.5.2. Experimental Outcome	138
5.6. Discussion	139
5.6.1. Rationalizing Affinity and Dispersity	139
5.6.2. Basic Thermodynamics of the Exchange	142
5.6.3. Exchange on a Unit Surface	144
5.6.4. Rationalizing Free Energy and Partition	149
5.6.5. Connecting Theory with Results	154
5.7. Conclusion	163
5.8. Appendix <i>Chapter 5</i>	165
5.8.1. Influence of W/C	165
5.8.2. Removal of Excess PCE	166
5.8.3. Desorption with Sulfates	167
5.8.4. Alternative Adsorbed Conformation	167
6. Competitive Adsorption Part II	171
On the Role of Side Chains	171
6.1. Context	171
6.2. Materials and Methods	172
6.2.1. Cement	172
6.2.2. PCEs with different Side Chain Length	173
6.2.3. Adsorption Isotherms from TOC	173
6.2.4. Mixing Protocol and Data Treatment	175
6.3. Results and Discussion	175
6.3.1. Experimental Outcome	175

6.3.2. Thermodynamics of the Adsorption Process	176
6.3.3. Master Curve	179
6.4. Conclusion	180
7. Conclusion and Outlook	183
7.1. Accomplished Results	183
7.1.1. PCE Analysis	183
7.1.2. Adsorption Studies and Structure Performance Relations . .	184
7.2. Implications for Admixture Research	185
7.3. Future Opportunities	187
A. Lower Critical Solution Temperature	189
A.1. Context	189
A.2. Materials and Methods	189
A.2.1. Applied PCEs	189
A.2.2. Turbidity measurements	190
A.3. Solubility Behavior of PCEs	191
A.3.1. Impact of C/E and pH	191
A.3.2. Impact of Side Chain Length	192
A.3.3. Impact of Salt and Ionic Strength	193
A.4. Implications for Chromatography	193
Bibliography	197
Curriculum Vitae	216

List of Figures

Figure 1.1.	Molecular structure of a comb-shaped PCE featuring a PMAA backbone and PEG side chains.	10
Figure 1.2.	PCE representation and phase diagram according to Gay and Raphaël	11
Figure 1.3.	Schematic representation of PCE dispersity.	13
Figure 1.4.	Schematic representation of the adsorption of PCE molecules onto the surface of cement grains.	15
Figure 1.5.	Schematic describing force-distance curves between cement particles (substrate and cantilever tip).	16
Figure 1.6.	Representative adsorption isotherms of polymer samples with high and low dispersity.	18
Figure 1.7.	Chemical structures of several PCE types.	23
Figure 1.8.	Monomers for the synthesis of Organo- silane modified PCEs.	25
Figure 1.9.	Grafting process (polymer-analogous esterification) for the synthesis of MPEG-type PCEs.	26
Figure 1.10.	Free radical copolymerization route for the synthesis of MPEG-type PCEs.	27
Figure 1.11.	Representative molecular structure of a trithiocarbonate RAFT agent and a RAFT-PCE.	29
Figure 1.12.	RAFT equilibrium between active and dormant species of two growing chains.	29
Figure 1.13.	Schematic of a liquid chromatography setup.	34
Figure 1.14.	Dependence of the molar mass (M) on the retention volume for different LC modes.	36
Figure 1.15.	Schematic representation of a Zimm plot.	38
Figure 1.16.	Hypothetic 2D-analysis of PEGMA.	48
Figure 2.1.	Chromatograms of R-PCEs-C/E-19 synthesized by RAFT copolymerization of PEGMA-19 and MAA.	57

Figure 2.2.	Conversion of comonomers (PEGMA-19 and MAA) in dependence of time.	58
Figure 2.3.	Synthesis of R-PCEs with short side chains.	59
Figure 2.4.	Synthesis of R-PCEs with long side chains.	60
Figure 2.5.	Living Character of the RAFT synthesis.	61
Figure 2.6.	UV-Vis absorption spectra of R-PCE-1.9-19 recorded between 260 and 800 nm.	62
Figure 2.7.	UV-Vis absorption spectra of R-PCE-1.9-19 solutions.	63
Figure 2.8.	Hydrolytic Stability of R-PCEs in aqueous media	64
Figure 2.9.	SEC Analysis of FRC-PCEs synthesized by free radical copolymerization in aqueous media.	67
Figure 2.10.	SEC Analysis of a PCE prepared by polymer analogous esterification.	69
Figure 2.11.	¹ H-NMR spectrum of a PCE with PMAA backbone and MPEG side chains including peak assignments.	72
Figure 2.12.	Monitoring the reaction progress of a RAFT polymerization.	73
Figure 2.13.	Titration of PCEs	74
Figure 3.1.	Molecular structure of a comb shaped PCE featuring a PMAA backbone and PEG side chains with <i>P</i> repeating units.	79
Figure 3.2.	UV-Vis absorption spectra of various polymers and solvents.	82
Figure 3.3.	Chromatogram of PMAA and PPEGMA and response factor calibration for dual detection analysis.	83
Figure 3.4.	Analysis of homopolymer mixtures using dual detection.	85
Figure 3.5.	Comparison of copolymer composition in G-PCEs (○) and FRC-PCEs (●) calculated from ¹ H-NMR data and dual concentration detection SEC.	87
Figure 3.6.	Chromatograms of various G-PCE samples with different C/E ratio.	89
Figure 3.7.	Influence of backbone length on PCE composition.	90
Figure 3.8.	Dual detection SEC analysis of FRC-PCEs with different C/E ratio.	91
Figure 3.9.	Dual detection SEC analysis of an alternative G-PCE with high C/E ratio.	94
Figure 3.10.	Degradation mechanisms of carboxylic acid groups within the PCE backbone	95
Figure 3.11.	Chromatogram of G-PCE-3.0 before and after freeze-drying.	96
Figure 4.1.	Chromatography at Critical Conditions of MPEG and solvent gradient development for RP-HPLC.	105

Figure 4.2.	RP-HPLC experiments using solvent gradients of water and ACN for several R-Polymers.	107
Figure 4.3.	Impact of side chain length on retention of PCEs in a RP-HPLC experiment with solvent gradients.	109
Figure 4.4.	Impact of backbone length on retention of G-PCEs in a RP-HPLC experiment with solvent gradients of ACN/Water.	110
Figure 4.5.	RP-HPLC experiments using solvent gradients of water and ACN for several PCEs.	112
Figure 4.6.	Schematic 2D-analysis (RP-HPLC×SEC) of a linear, monofunctional MPEG homopolymer and a bifunctional PEG.	114
Figure 4.7.	2D-Chromatography of FRC-PCEs using RP-HPLC in the first dimension and SEC in the second dimension (RP-HPLC–SEC).	115
Figure 4.8.	Calculated contour plot of a PCE containing two species.	121
Figure 5.1.	Schematic describing the concept of the competitive adsorption study.	128
Figure 5.2.	Molecular structure of a PCE with PMAA backbone and PEG side chains using the notation according to Gay, Raphaël and Flatt.	130
Figure 5.3.	Adsorption isotherms of all applied PCEs determined by TOC and depletion calculation.	134
Figure 5.4.	UV-Vis absorption spectra of different pore solutions.	135
Figure 5.5.	Adsorption isotherms from UV-Vis and comparison with TOC.	135
Figure 5.6.	Total amount and weight fraction of adsorbed PCEs during competitive adsorption experiments.	139
Figure 5.7.	Molar mass distribution of all applied PCEs: R-PCE-2.9 (a) and G-PCEs (b).	140
Figure 5.8.	Molar mass distribution of the PCE backbones.	141
Figure 5.9.	Schematic describing how a change in the molecular parameter x_A results in dynamic processes to re-establish equilibrium conditions.	151
Figure 5.10.	Verification of Equation 5.32. The data of the simultaneous experiment was fitted by linear regression.	155
Figure 5.11.	Comparison between experimental data of the <i>simultaneous</i> series and calculated values according to the dispersity model.	158
Figure 5.12.	Distribution of partition, $Y_{G,i}$ and adsorbed mass, $m_{G,i,ad}$ of the sub-fractions within the G-PCE calculated with K^*	159
Figure 5.13.	Replot of $\Delta G_{Ex}^{o,Area}$ vs. $ \Delta N_i^{-0.3} (N_i - 1) $	161

Figure 5.14. Adsorption data illustrating the challenge posed by low W/C pastes and the solution to this issue proposed in the current paper.	165
Figure 5.15. Verification of an alternative adsorption models (Stretched-out backbone).	168
Figure 5.16. Verification of the "Mushroom Slice" model.	169
Figure 6.1. Adsorption isotherms of all applied PCEs determined by TOC and depletion calculation.	174
Figure 6.2. (a) Amount of adsorbed PCEs during competitive adsorption experiments. (b) Corresponding number of adsorbed PCE molecules.	176
Figure 6.3. Verification of Equation 6.3. The data of the competitive experiments was fitted by linear regression.	179
Figure 6.4. Master curve obtained by combining data from competitive adsorption experiments with focus on P and N .	180
Figure A.1. Plot of transmission vs. temperature as obtained from turbidity measurement of a PCE solution.	191
Figure A.2. Cloud points of PCE copolymers as a function of C/E at different pH values.	192
Figure A.3. Impact of side chain length, pH and presence of different salts on the solubility behavior of PCEs.	193

List of Tables

Table 1.1. Dimensionless shape factor for various geometries and molecular architectures as reported by Burchard <i>et. al.</i>	32
Table 2.1. Applied PEGMA Monomers.	53
Table 2.2. Experimental conditions and conversions of several RAFT copolymerizations.	54
Table 2.3. Information on number-average molar mass and C/E ratio of several R-PCEs.	56
Table 2.4. Applied Chemicals for free radical copolymerization of PCEs with different grafting degree.	65
Table 2.6. Information on SEC and 1H-NMR characterization of the FRC-PCEs.	66
Table 2.7. Information on precursor backbone and side chains used for polymer analogous esterification.	70
Table 3.1. Average Molecular characteristics of applied PCEs.	80
Table 3.2. Response factors for PMAA and PPEGMA.	84
Table 3.3. Ratio RI/UV signal of G-PCE-3.0 before and after freeze-drying the sample.	96
Table 4.3. Characteristics of PCEs located in different sectors of a contour plot obtained by RP-HPLCxSEC as shown in Figure 4.8.	122
Table 4.4. Delay in hydration of various PCE samples.	124
Table 5.1. XRD analysis of the applied cement powder (%).	129
Table 5.2. Molecular characteristics of applied PCEs applied in <i>Chapter 5</i>	131
Table 5.3. Sub-fractions of the PCE backbones.	142
Table 5.4. Number of molecules (X_i) and charges (Z_i) per 100 nm ²	146
Table 5.5. Equilibrium constants: K was determined according to Equation 5.15.	159
Table 6.1. XRD analysis of the applied cement powder (%).	173
Table 6.2. Molecular characteristics of applied PCEs.	174

List of Tables

Table 6.3. Number of molecules (X_i) and charges (Z_i) per 100 nm². 178

Acronyms & Abbreviations

AFM Atomic Force Microscopy.

C-S-H Calcium Silicate Hydrate.

CP Cloud Point.

CTA Chain Transfer Agent.

DC Decorated Chain.

DLS Dynamic Light Scattering.

DLVO Derjaguin Landau Verwey Overbeek.

ELSD Evaporative Light Scattering Detectors.

EO Ethylene Oxide.

EXAFS Extended X-Ray Absorption Fine Structure.

FBW Flexible Backbone Worm.

FRC Free Radical Copolymerization.

GPEC Gradient Polymer Elution Chromatography.

IC Interaction Chromatography.

IR Infrared.

LAC Liquid Adsorption Chromatography.

LC Liquid Chromatography.

LCCC Liquid Chromatography at Critical Conditions.

LCST Lower Critical Solution Temperature.

MALLS Multi Angle Laser Light Scattering.

MAPS N-maleic- γ -aminopropyl triethoxysilane.

MAPTMS 3-(trimethoxysilyl) propyl methacrylate.

MMD Molar Mass Distribution.

MPEG Methoxy poly(ethylene glycol).

PC Portland Cement.

PDADMAC Poly(diallyl dimethyl ammonium) chloride.

PEGMA Poly(ethylene glycol) methacrylate.

PMAA Poly(methacrylic acid).

PMS Poly(melamine sulfonates).

PNS Poly(naphthalene sulfonates).

RAFT Reversible Addition-Fragmentation Chain Transfer.

RI Refractive Index.

SANS Small Angle Neutron Scattering.

SBS Stretched Backbone Star.

SBW Stretched Backbone Worm.

SCM Supplementary Cementitious Materials.

SEC Size Exclusion Chromatography.

SGIC Solvent Gradient Interaction Chromatography.

SP Superplasticizer.

SSA Specific Surface Area.

TGIC Temperature Gradient Interaction Chromatography.

TOC Total Organic Carbon.

0.1. Background Section

Water-soluble polymers are widely applied as dispersing agents for aqueous particle dispersions, including gypsum [1], limestone [2], silica [3] and concrete [4]. Indeed, in concentrated particle suspensions, the use of dispersants is essential to improve the (colloidal) stability, but also to adjust the rheological behavior. A common type of dispersants are comb copolymers based on poly(carboxylate ether) (PCE) chemistry. The backbone of PCE combs is given by a poly(carboxylic acid) onto which poly(alkylene glycol) side chains are grafted [5–7].

In the construction sector, PCEs belong to the broader family of chemical admixtures referred to as superplasticizers (SPs) [4, 6]. Their usage has reached an estimated volume of more than 3 million tons per year (based on 30 % liquid concentration) [6, 8]. A particular benefit of using PCEs is that they facilitate producing concrete with decreased environmental impact and improved rheology without compromising the final performance and strength of the building material [9].

Due to the charged carboxylic acid groups along the backbone, the PCE molecules tend to adsorb to the surface of mineral phases in cement [6, 10]. Upon adsorption, interparticle attractions are reduced due to steric hindrance between the non-adsorbing side chains, resulting in a decreased yield stress and improved fluidity [10–12].

The relevance of PCEs as dispersants can only be understood by referring to the extraordinary role of concrete as a building material. Each year, more than 10 km³ of concrete are used on construction sites all over the world [9]. According to the low costs of its ingredients, its broad availability, and its convenient handling, it has not

been possible to replace concrete by any other building material so far. The most common binder used in concrete production is Portland Cement (PC). During the production of PC, an essential step involves limestone decarbonation, resulting in the release of CO₂ [9, 13].

Considering the amounts of cement produced, this explains why PC manufacturing is responsible for about five percent of the man-made global CO₂ emission per year. A major way of mitigating this is to replace part of the “ordinary cement” by “supplementary cementitious materials” (SCMs). The resulting materials are referred to as blended cements and are essential to decrease the environmental impact of concrete use. However, the extent of replacement is limited by several factors, in particular the reduced early strength of blended cements. One way of compensating for this is to reduce the amount of water, which has a negative impact on rheology, but can be largely compensated by adding admixtures such as PCEs. Apart from this, early hydration of blended cements can be boosted by adding activators and/or accelerators [14–19].

Consequently, the formulation of modern cement with increased performance and low environmental impact increasingly requires the use of admixture combinations. This increases the risk of incompatibilities that might impair the performance of the individual admixtures [20–26].

To reliably predict the performance of admixtures and their combinations, it is therefore essential to precisely understand how they work on cement. In this regard, while there has been extensive research focused on the working mechanisms of various admixtures [11, 27], there is still a lack of reliable and scientifically based models that enable to predict the performance of admixtures and their combinations. Indeed, the choice and formulation of admixtures and their dosages often relies on empirical data as well as simple trial and error [28].

PCEs have been subject to research for more than four decades. While the main working mechanisms are understood, it is still challenging to correlate the molecular structure of the comb copolymer with the macroscopic properties of cement. In other words, it is difficult to draw conclusions on structure-function or structure-performance relations.

One topic that has major consequences on rheological properties of concrete, but also hydration kinetics, is competitive adsorption [23, 29–32]. This topic has “haunted” the research community for the past decades. While a lot of progress

has been made, there is still a lack of detailed quantitative studies, in particular, in relation to competitive adsorption among PCE molecules with different molecular structures. Indeed, this issue is highly relevant for the formulation of efficient commercial products, a topic of which the sensitivity increases for blended cements.

In common studies, PCEs are compared by their "performance", meaning that their ability to modify the rheological behavior of cementitious pastes is characterized referring to their dosage in the paste [33–35]. In this course, the complex nature of PCEs is often insufficiently characterized. Indeed, PCE characterization is often restricted to determination of average values of molar mass and grafting density. While being very useful, the molecular heterogeneity within a PCE, (*i.e.* variations in grafting density, molar mass, and architecture) remains neglected.

This negligence is mainly due to a lack of versatile tools and characterization methods that allow to elucidate information on parameter distributions. Size exclusion chromatography (SEC) serves as method to approach the molar mass distribution (MMD) of PCEs [36]. Here, the width of the MMD can be acknowledged by referring to the dispersity index. Notably, the dispersity in molar mass can be affected by variations in backbone length, grafting density or architecture. Hence, it is not enough to refer to variations in molar mass. Indeed, two PCEs with identical comonomers and identical average properties regarding grafting ratio and molar mass can be composed by molecules with completely different composition. Thus, additional methods are needed to precisely map the molecular heterogeneity.

0.2. Objective of the Thesis

This thesis embraces the idea that PCE performance may be predicted and optimized through a more detailed understanding of its chemical structure - function relations. More specifically, it tackles two poorly treated subjects: First the characterization of molecular heterogeneity and second, the role of molecular structure and dispersity on adsorption.

Despite the availability of many types of PCEs on the market, we have selected to use MPEG-type PCEs that consist of a poly(methacrylic acid) (PMAA) backbone and methoxy poly(ethylene glycol) (MPEG) side chains. The reasons for choosing this PCE type are manifold. For instance, such polymers can be synthesized with systemic variations in molecular parameters pursuing various synthesis strategies.

Moreover, they have a good stability against hydrolysis at high pH. And most importantly, over the last decades, their solution properties, *i.e.* the coil dimensions in solution, have been thoroughly investigated.

The starting point of this thesis is focused on the development of versatile synthesis protocols that allow the realization of PCE structures with defined characteristics using various synthesis techniques, among them RAFT copolymerization. The synthesis of model PCEs with well-characterized parameter averages is fundamental for further method development and adsorption studies.

Subsequently, this thesis gives a deep insight into the molecular heterogeneity of PCEs obtained from different synthesis pathways. For this purpose, different liquid chromatography methods are applied. For instance, size exclusion chromatography with dual concentration detection is used to elucidate information on the grafting ratio in dependence on molecular size of PCEs.

The presented dual detection approach allows for the first time, to reveal and quantify, how different synthesis routes can lead, for a same average composition, to different distributions of molecular structures. This result is important for both, academia and industry. While in the first case it will raise important questions in terms of interpreting structure-function relations, in the second it will open new means to optimize products by modifying structural dispersity.

Besides, the potential of reverse-phase liquid chromatography (RP-HPLC) using solvent gradients to characterize PCEs regarding their grafting ratio is presented. Hence, the chemical composition distribution of PCEs is targeted. Complementing SEC experiments reveal the advantages of 2D-chromatography for a profound analysis of MMD and CCD.

While the first part of this thesis is dedicated to the synthesis of PCEs and to the analysis of molecular heterogeneity using LC-based methods, the second part of this thesis is focused on adsorption of PCEs at the cement surface.

More specifically, this thesis aims to present a new experimental method that reveals competitive adsorption between PCE molecules with different molecular characteristics. Experimental results are interpreted by deriving a thermodynamic model that allows to describe and predict the competitive adsorption behavior between PCE molecules in dependence on molecular parameters. A combination of basic thermodynamics and polymer physics is applied to show how and to what extent

backbone length, grafting ratio and side chain length impact the competitiveness of PCE molecules for adsorption at the cement surface. These results underline the role of molar mass dispersity on adsorption, and point to the fact that chemical structure dispersity may be equivalently important to consider.

All in all, this thesis aims to combine a thorough characterization of PCEs and their molecular structure with applications in cement paste to study their adsorption behavior. Thus, this work provides the means to study competition between PCEs on a molecular level. This marks a milestone for admixture research on its way towards reliable structure-performance predictions.

Hence, the main goal of this thesis is to combine fundamental polymer science and thermodynamics with applied cement research, opting for a better use of analytical methods in admixture research.

0.3. Structure of the Manuscript

Chapter 0 gives a general introduction to this thesis as well as objective and structure of the manuscript.

Chapter 1 contains a comprehensive state-of-the-art laying the groundwork for the research of this thesis. In the first part of the chapter (*Section 1.1-1.6*), the research field of PCEs is introduced. After presenting general information on PCEs, the topic of adsorption onto the cement surface and competitive phenomena are presented. Moreover, the issue of dispersity and molecular heterogeneity are highlighted. Information on the chemical variety of PCEs used in cement and concrete technology is summarized, and different synthesis routes for the preparation of these structures are presented. Subsequently, the second part of the chapter (*Section 1.7-1.10*) elaborates on the characterization of molecular parameters and parameter distributions by polymer chromatography. Besides size exclusion chromatography, also the concepts of liquid chromatography at critical conditions and liquid adsorption chromatography are described. All chromatographic techniques are introduced regarding their relevance for PCE characterization. Finally, in *Section 1.13*, the concept behind this work and its main goal is put in context with previous research.

Chapter 2 is focused on materials and methods regarding PCE synthesis and characterization of average molecular parameters. Protocols for the polymerization

of PCEs with different molecular design are described. More specifically, various synthesis routes including RAFT (short for reversible-addition-fragmentation chain-transfer polymerization) copolymerization, polymer-analogous esterification and free radical copolymerization are pursued. The molecular parameters of PCEs were investigated by various techniques, among them size exclusion chromatography (SEC) and $^1\text{H-NMR}$. All characterization protocols are described in detail. However, *Chapter 2* is not purely descriptive as the outcome of various synthesis and characterization experiments is discussed. The synthesis of PCEs with systemic variations in molecular parameters provides the basis for further research.

Subsequently, the main outcome of this PhD thesis is presented in *Chapter 2-Chapter 6*. Parts of these chapters were published in peer-reviewed research articles with *Stefanie Anne Weckwerth* as a first author. Information on the publications is given in *Section 0.4*.

Chapter 3 presents a method to investigate the PCE composition (*i.e.* grafting ratio) of PCEs in dependence on their molecular size. More precisely, the addition of a UV detector to a standard SEC device with refractive index detector allows to monitor the grafting ratio along the elution axis in a SEC chromatogram. This enables to compare the molecular heterogeneity of PCEs obtained from different synthesis techniques. It is shown that the synthesis pathway has a significant impact on the chemical heterogeneity within a PCE.

In *Chapter 4*, liquid adsorption chromatography using solvent gradients is elaborated as a potential tool to reveal chemical heterogeneity in PCEs. Experiments are carried out in reverse-phase mode. Thereby, the method is shown to separate PCEs according to their grafting ratio. Limitations of the method and coelution phenomena are addressed. Finally, the relevance of 2D-chromatography for precisely mapping molecular heterogeneity and identifying different PCE species is pointed out. *Chapter 4* is concluded by giving an example how the molecular dispersity in PCEs is likely to affect macroscopic properties (*e.g.* cement hydration retardation).

Chapter 5 presents a new experimental approach to measure competitive adsorption between PCE molecules of different molecular structure, *i.e.* different charge density. The chapter includes a detailed materials and methods section. Subsequently, a thermodynamic framework is established to interpret the results. It offers the first theoretical model capable to discriminating *a priori* the adsorption competitiveness of a PCE in relation to its molecular structure.

In *Chapter 6*, the role of side chain length on competition between PCE molecules for adsorption onto cement is revealed. The results are discussed referring to the previously established thermodynamic model. Thus, *Chapter 6* presents complementary information to the previous chapter.

In *Chapter 7*, the results achieved in this thesis are summarized and the thesis is concluded by presenting an outlook regarding future developments in PCE characterization and the relevance of scientifically based models to predict PCE performance based on their physico-chemical parameters.

In *Appendix A*, the solubility behavior of PCEs in dependence on molecular parameters is investigated using turbidity measurements. The grafting ratio is shown to have a significant impact on the lower critical solution temperature (LCST). Finally, a concept is presented that suggests temperature gradients to separate PCEs within a chromatographic analysis by taking advantage of the LCST behavior.

0.4. List of Publications

Parts of the work presented in this monograph were published as research articles in scientific journals or conference volumes, with *Stefanie Anne Weckwerth* as first author. Connections between research papers and the underlying manuscript are indicated at the beginning of each chapter.

“A Method for Characterizing the Chemical Heterogeneity of Comb-Copolymers and its Dependence on Synthesis Routes”, *Polymers* **2021**, 13(12):1921, [doi:10.3390/polym13121921](https://doi.org/10.3390/polym13121921)

“Experimental Method and Thermodynamic Model for Competitive Adsorption between Polycarboxylate Comb-Copolymers”, *Cement and Concrete Research*, **2022**, Volume 151, 106523, [doi:10.1016/j.cemconres.2021.106523](https://doi.org/10.1016/j.cemconres.2021.106523)

“Side Chains and the Competitive Adsorption between Poly(carboxylate ethers)”, *ACI Conference Paper, Supplementary Volume, SP-167*, Milano, **2022**, 13th International Conference on Superplasticizers and Other Chemical Admixtures in Concrete

Chapter **1**

State of Art

Parts of the present chapter were published in the *Introduction* and *Background* of the research articles listed below. All elements that were taken from these publications were entirely written by *Ms. Weckwerth* and revised by *Prof. Flatt*.

Weckwerth *et al.*, *Cement and Concrete Research*, **2022**, Volume 151, 106523,
[doi:10.1016/j.cemconres.2021.106523](https://doi.org/10.1016/j.cemconres.2021.106523)

Weckwerth *et al.*, *Polymers*, **2021**, 13(12):1921,
[doi:10.3390/polym13121921](https://doi.org/10.3390/polym13121921)

1.1. Poly(carboxylate ethers)

1.1.1. Molecular Characteristics

The market of poly(carboxylate ether) superplasticizers (PCEs) has grown substantially since their invention in the middle 1980s. Today, a variety of PCEs is commercially available. In fact, the term PCE does not refer to one single type of polymer, but a family of comb-shaped copolymers with a range of different chemistries [4, 6]. The backbone of the combs is usually comprised by a poly(carboxylate), whereas the side chains of the PCEs are commonly given by a derivate of poly(alkylene glycol). The archetype of PCE is given by a poly(methacrylic acid) (PMAA) backbone onto which methoxy poly(ethylene glycol) (MPEG) side chains are grafted [10]. An example for the molecular structure of a corresponding PCE is shown in Figure 1.1. Due to the high pH in concrete (pH 13), the carboxylate groups of the backbone are deprotonated and serve as anchor groups to adsorb onto positively charged cement

grains, whereas the side chains are non-adsorbing and reach into solution inducing steric hindrance [4, 10, 11].

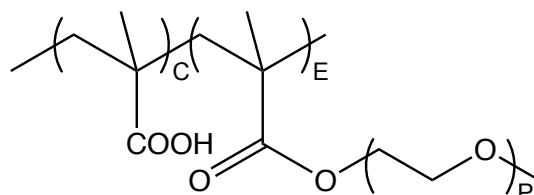


Figure 1.1. Molecular structure of a comb-shaped PCE featuring a PMAA backbone and PEG side chains with P repeating units. C notes the number of MAA units in the backbone, and E refers to the number of side chain bearing backbone units. Hence, the degree of polymerization of a PCE is given by $C+E$. The repartition of C and E along the backbone depends on the synthesis procedure and can be random-, gradient- or block-like.

1.1.2. Model of Gay and Raphael

From a molecular structure point of view, common PCEs comprise a poly(carboxylate) backbone onto which side chains are grafted [4, 6]. Gay and Raphaël [37] suggested a model to describe the solution conformation and thermodynamics of homopolymer combs. This was also found to be applicable to comb copolymers such as PCEs [10, 36, 38]. Herein, the polymer backbone is defined as an assemblage of n structural repeating units, each containing N monomers and one side chain of P monomers (Figure 1.2a) Hence, the structural unit N can be taken as a measure for the grafting ratio of the backbone. More precisely, N is equal to the average side-chain to side-chain distance along the backbone. The number of groups between two side chains is $N-1$, which in literature is also often termed C/E ratio, referring to the molar ratio between carboxylic acid (C) units and esterified (E) units bearing side chains. The molecular structure of the PCE presented in Figure 1.1 can be noted according to Gay and Raphaël [37] as shown Figure 1.2b. However, the notation is only valid for homogeneously grafted PCEs as gradients and irregularities of the grafting density are not sufficiently considered [38, 39].

Considering a comb-like homopolymer in a good solvent, Gay and Raphaël [37] derived various possible chain conformations, which are depicted in the phase diagram shown in Figure 1.2c. Depending on the relative ratio between the molecular

^aThe phase diagram presented in Figure 1.2c was reprinted from [10]

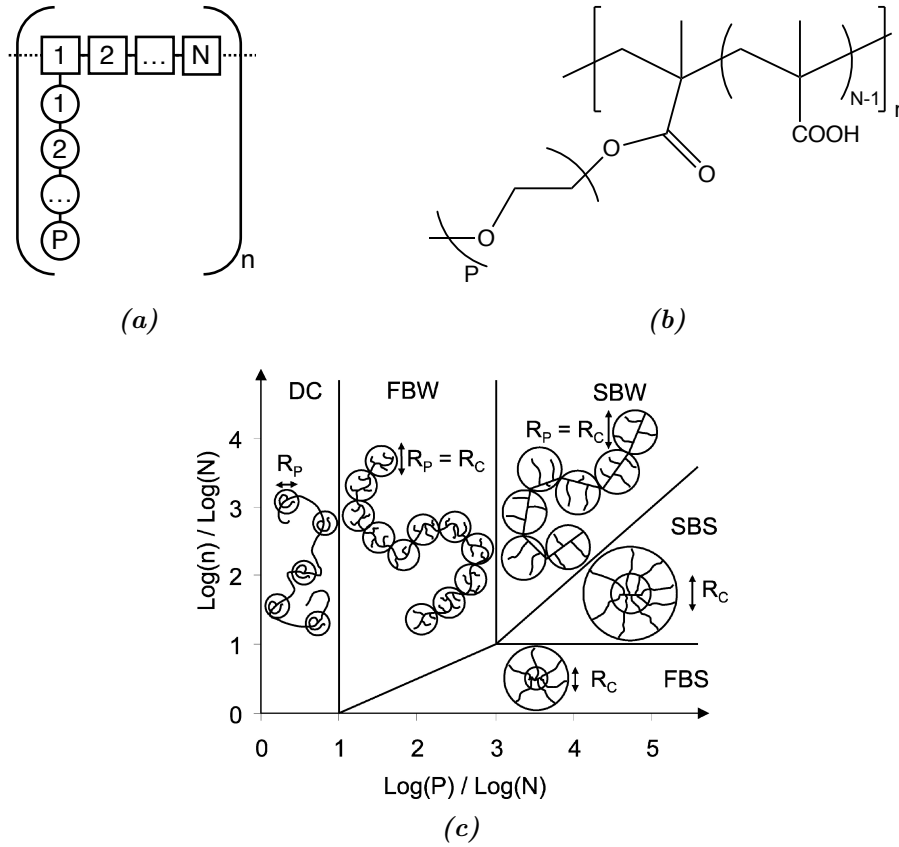


Figure 1.2. PCE representation according to Gay and Raphaël [37]: (a) Schematic comb copolymer (b) Molecular structure representation. (c) Phase diagram for comb polymers in a good solvent according to Gay and Raphaël. The different domains are the following: decorated chain (DC), flexible backbone worm (FBW), stretched backbone worm (SBW), stretched backbone star (SBS), flexible backbone star (FBS).^a

parameters N , P and n , different conformation regimes are distinguished, namely decorated chain (DC), flexible backbone worm (FBW), stretched backbone worm (SBW) and stretched backbone star (SBS).

Following thermodynamics, the core radius R_C can be calculated by minimizing the *Flory free energy*. Flatt *et al.* [10] extended the model to comb copolymers making it applicable to PCEs. A corresponding expression for R_C and the radius of gyration R_G is given in Equation 1.1-1.2. The expression was derived for flexible backbone worms, which can be considered the most relevant conformation among SPs. In this regime, the polymer chain behaves as an ideal chain of cores with radius R_C [10].

$$R_C = \left(\left(\frac{a_N}{a_P} \right) \frac{(1 - 2\chi)}{2} \right)^{1/5} a_P \cdot P^{7/10} N^{-1/10} \quad (1.1)$$

$$R_G = \left(\left(\frac{a_N}{a_P} \right)^2 \frac{(1 - 2\chi)}{2} \right)^{1/5} a_P \cdot P^{2/5} N^{1/5} n^{3/5} \quad (1.2)$$

where a_N represents the backbone monomer size (0.25 nm for methacrylates), and a_P the side chain monomer size (0.36 nm for ethylene oxide, EO). χ is the *Flory- Huggins- Parameter* accounting for the solubility of the PCE (0.37 for PEO at 25 °C) [10].

Gelardi [36] and Emaldi [38] recently validated the scaling laws by comparing the predictions given by Equation 1.2 with measurements of the radius of gyration obtained from SANS (short for small angle neutron scattering) and light scattering experiments.

1.1.3. Dispersity of PCEs

PCEs are synthetic polymers. Unlike several biopolymers (*e.g.* proteins), synthetic polymers are multicomponent materials. On the molecular level, they reveal an assembly of macromolecules with different chain lengths. Consequently, the molar mass of a PCE is not given by a distinct value but can be described by a distribution [39–42].

The shape and width of the molar mass distribution (MMD) depend on the type of reactants, polymerization mechanism, kinetics, and reaction conditions. PCE synthesis commonly involves at least one step of free radical polymerization [4, 6] and this type of polymerization is known to yield disperse polymers. For homogeneously grafted PCEs, the dispersity of molar mass is mainly reflected in a distribution of the backbone length. Many studies aiming to investigate the impact of molecular structure and architecture of a PCE onto its performance reduce the dispersity to the dimension of molar mass [4, 28, 38, 43–46].

However, PCEs are synthetic copolymers consisting of two comonomers. Hence, the molecular complexity is extended by variations of the chemical composition. More precisely, the number of charges and side chains per backbone varies within

a certain range. Thus, also the C/E ratio is disperse. In addition to numerical variations of C/E, also the repartition of charges and side chains along the backbone varies. Besides a statistical distribution, gradient and block conformations exist (Figure 1.3) [39, 47]. Moreover, it is worth noting that variations in the molecular parameters and architecture do not solely affect molar mass, but also the dimensions of the PCE coils in solution (*i.e.* radius of gyration R_G and hydrodynamic radius R_H) [36, 38].

Looking at Figure 1.3, the multidimensional dispersity becomes clear. Indeed, the most relevant parameters impacting the total dispersity of a PCE are the number and repartition of charges and the backbone length. On the contrary, the impact of variations in side chain length on dispersity can be considered of minor importance for PCEs composed by only one type of side chain.

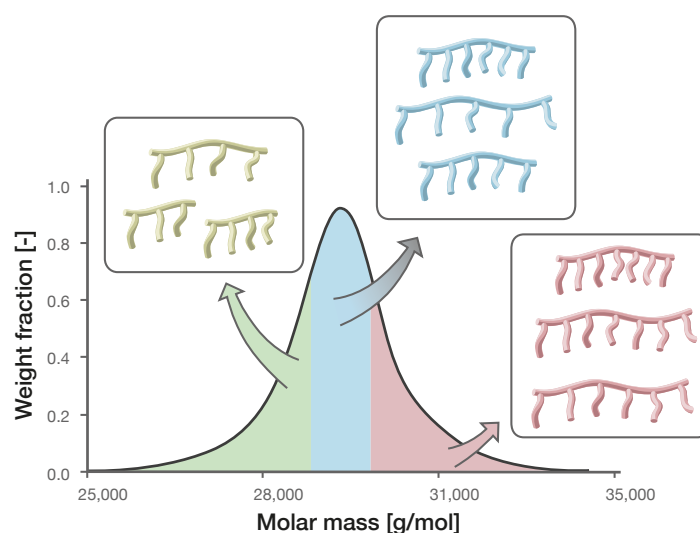


Figure 1.3. Schematic representation of dispersity of PCE molecules. Each chromatographic fraction may consist of molecules having a distribution of structural parameters.^b

Indeed, the length of the side chains is the molecular parameter that can be controlled most accurately in PCE synthesis. Side chains are usually given by derivatives of PEG, which are synthesized by anionic polymerization that allows to obtain polymers of very narrow dispersity. The most common side chain length in commercially relevant PCEs lies approximately between $P=10$ and 150 [6, 42].

^bIllustration by Fabian Rudy, www.andraia.ch

In PCE physics, the side chain length is mainly connected with the induction of steric hindrance between the surface of two cement particles [10, 11, 48]. Referring to the model presented in [10], the radius R of an adsorbed PCE hemisphere is proportional to $P^{7/10}$ indicating that side chains are reaching into solution. However, the side chains are not stretched out completely, but adapt a coiled conformation.

1.1.4. Working Mechanism - DLVO Theory

The importance of PCEs as dispersants for cementitious materials becomes clear when dealing with the stability of the cement paste. A suspension of cement particles suffers a poor colloidal stability, resulting in particle agglomeration. This negatively impacts its workability and rheological behavior.

Particle stability, aggregation and coagulation can be described with the DLVO-theory. In the 1940s *Derjaguin, Landau, Verwey* and *Overbeek* (DLVO) published a theory that allows to explain and predict the coagulation of an aqueous particle dispersion in correlation with the ionic strength of the aqueous phase [11, 49].

DLVO states that stability and coagulation is the result of an interplay between attractive (*i.e.* *Van der Waals* forces) and repulsive forces (*i.e.* electrostatic double layer repulsion). *Van der Waals* forces can be considered as short-distance forces that promote aggregation, whereas electrostatics stabilize the particle dispersion. The interaction range of the electrostatic double layer highly depends on the ionic strength of the aqueous phase. An increased ionic strength leads to a decreased *Debye* length meaning that the electrostatic interaction radius is shielded [11, 49].

In cement suspensions, the main source of stabilization is given by electrostatic repulsion between the positively charged surfaces. However, due to the high ionic strength of the pore solution in cement (100-200 mM) [46, 50, 51], the surface potential is widely screened by counter ions leading to a dramatic reduction of the *Debye* length. Consequently, electrostatic repulsion is only effective at very short distance from the cement surface. In this range *Van der Waals* attraction dominates and induces particle agglomeration [11, 49].

Without an additional stabilizing force, cement particle aggregation cannot be avoided. This causes an increased yield stress and poor fluidity of concrete. Here PCEs come into play. Whereas the chemistry and conformation of PCEs

varies, the underlying working mechanism as dispersing agent is the same. The carboxylate groups of the backbone adsorb to the cement surface. Upon adsorption, electrostatic bonds between the carboxylic groups along their backbone and Ca^{2+} ions on the cement surface are formed. Subsequently, the side chains introduce steric hindrance between cement particles and enhance the stability of the cement dispersion. Figure 1.4 shows a schematic representation of the working mechanism.

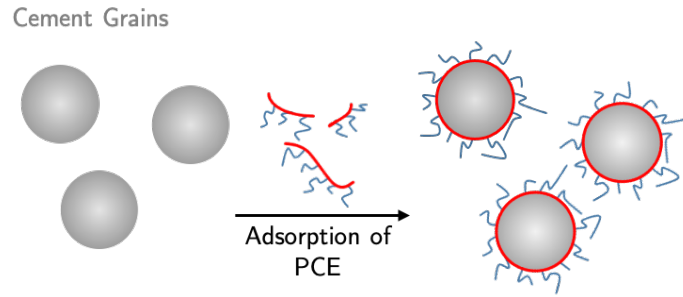


Figure 1.4. Schematic representation of the adsorption of PCE molecules onto the surface of cement grains to induce steric hindrance between the particles.

With regard to the DLVO theory, the interparticle potential (E_{total}) between cement grains can be regarded as the sum of *Van der Waals* attraction (E_{VdW}), electrostatic repulsion (E_{el}) and a steric hindrance component (E_{steric}) as described in Equation 1.3:

$$E_{total} = E_{VdW} + E_{el} + E_{steric} \quad (1.3)$$

Assessing steric hindrance forces between particles is delicate. A common tool to study inter-particle forces is colloidal probe atomic force microscopy (AFM). Flatt *et al.* [10] used this technique to measure forces between a flat calcium silicate hydrate (C-S-H) substrate and a C-S-H-modified cantilever tip. Figure 1.5 shows a schematic describing their findings. Upon approaching the tip to the substrate, an attractive (negative) force occurred at short distances. This force can be assigned to *van der Waals* interaction that cause particle aggregation. Modification of the C-S-H surfaces with PCE revealed the existence of a repulsive force. The repulsive force was shown to scale with the side chain length, confirming that the choice of side chains length has a significant impact on steric stabilization of cement particles.

Using an expression of the *Flory free energy* for adsorbed PCEs and applying the *Derjaguin* approximation allowed to calculate the interaction force between two

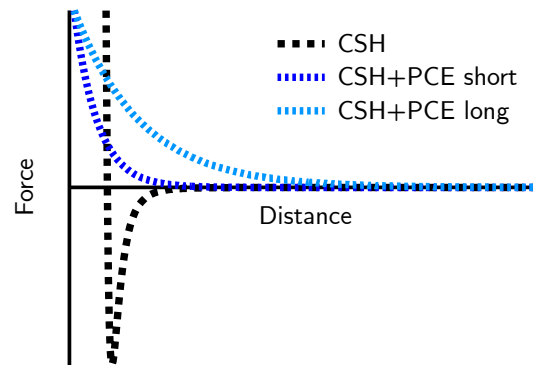


Figure 1.5. Schematic describing forces-distance curves between cement particles (substrate and cantilever tip). Negative forces are attractive and positive forces are repulsive. With increasing side chain length, the onset of repulsion shifts towards longer distances, indicating that the side chain length has a significant impact on steric stabilization. PCE-short refers to a PCE with short side chains compared to PCE-long.

cement particles in dependence of molecular parameters of a PCE. Notably, the magnitude of the steric force does not solely depend on the molecular parameters of the PCE but also on the surface coverage [52].

1.1.5. Solubility of PCEs

PCEs are predominantly used in cement and concrete technology. Thus, many studies focus on their characteristics and behavior at alkaline pH levels (and high ionic strength) intending to imitate the pore solution. For acidic pH levels, PCEs reveal a particular thermo-responsive behavior that can be characterized by the so-called lower critical solution temperature (LCST). LCST polymers exhibit a phase transition from soluble to insoluble upon heating the solution [53]. The LCST of a PCE depends on its molecular parameters. In particular, the length of the side chains P and the grafting ratio N have a significant impact on the LCST [54, 55].

Becer *et al.* [54] found that for $P= 10-20$ and of $C/E= 0-8$, the LCST of methacrylic MPEG-PCEs can be adjusted between 15 °C and 95 °C. They describe the LCST as the consequence of intramolecular interactions (*i.e.* hydrogen bonding) between the protonated carboxylic acid group of the backbone (*i.e.* MAA) and the PEG side chains. Thus, the LCST decreases for increasing C/E . For pH values significantly higher than the pK_a of PMAA (4.65-5.35 as reported in [56]), the PCE is entirely soluble in water up to the boiling point. On the contrary, at pH 2 or

lower, a highly charged PCE might precipitate below room temperature. While the characteristic of a LCST might not be relevant to understand the behavior of PCEs in cement pore solution, it is highly relevant to improve synthesis and characterization techniques.

In polymer physics, the LCST is defined as the critical temperature below which the components of a polymer solution are miscible for all compositions meaning that increasing the temperature above that point results in phase separation [53]. In polymer analytics, the LCST of polymer solutions can be determined by monitoring the increase of the hydrodynamic radius in temperature-dependent dynamic light scattering experiments [57]. Instead of accessing the LCST, it is also common to refer to the cloud point (CP) to characterize the solubility behavior. It can be determined from turbidity observations [55] or measurements [54].

1.2. PCE Adsorption

1.2.1. Adsorption Basics

In terms of adsorption onto cement particles, the behavior of PCE molecules can be rationalized as physisorption of an anionic polyelectrolyte onto an oppositely charged substrate [48]. Whether adsorption takes place or not depends on the net adsorption energy experienced by the polymer segments, as well as entropic factors regarding the surface, the polymer, and the solution. For this, contributions regarding free energy between polymer – surface, polymer – solvent and surface – solvent must be considered [5, 57–60].

From a thermodynamic point of view, the adsorption of PCEs onto surfaces is driven by enthalpy and entropy. Enthalpy favors the adsorption as the formation of electrostatic bonds between carboxylate and Ca^{2+} is exothermic [58–60]. Moreover, the adsorption of a PCE is connected with a net increase of the entropy due to the release of numerous ions and water molecules from the surface [12, 61].

1.2.2. Adsorption Isotherms

A key parameter in adsorption is the adsorbed amount per unit area of surface in dependence of the amount of polymer left in solution. Therefore, adsorption isotherms are a common tool to study this process. Adsorbed amounts are best plotted against solution concentration to see if the process involves an equilibrium between surface and solution.

Figure 1.6 (dashed line) shows a representative adsorption isotherm of a polymer with low dispersity and high affinity for the surface. For low solution concentrations, a very high adsorption can be observed. For higher concentrations, the isotherm ends in a plateau, indicating surface saturation. Typical plateau values are in the order of few mg per m². Adsorption of organic compounds is typically determined by measuring depletion from solution using total organic carbon (TOC) measurements [30, 62, 63].

It is worth noting that plotting adsorption versus dosage can be useful to identify situations where the process may rather involve precipitation, which would then be seen as a linear relation extending over a very large range of dosage. Similar behaviors can manifest themselves in cases where a fraction of the polymer has a very strong affinity and another not [64].

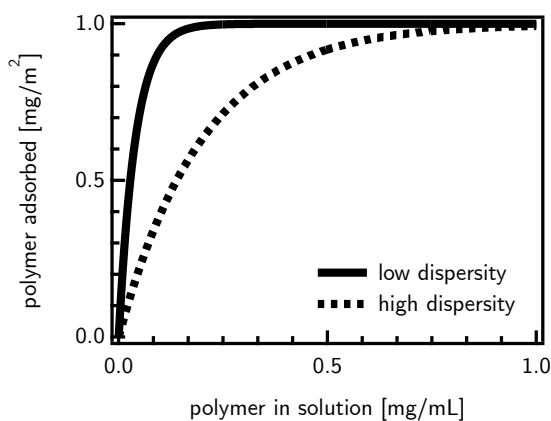


Figure 1.6. Representative adsorption isotherms of polymer samples with high and low dispersity. The isotherms are based theoretical considerations regarding polymer adsorption as described in [62].

1.2.3. The Impact of Dispersity

Isotherms of polymers with higher dispersity (*e.g.* PCEs) do not feature a well-defined plateau, but rather more rounded adsorption isotherms. (Figure 1.6, dashed line) Such cases are also found for low molar mass molecules, since they have a low affinity for the surface. Indeed, an important feature of polymer adsorption is that increasing molar masses generally increases the affinity for surfaces. In first order, this is because large polymers displace more solvent molecules from the surface when they adsorb and therefore have a larger positive adsorption entropy. Consequently, polymers with a broad molar mass distribution also show a distribution regarding affinity for adsorption. Coming back to PCEs, the distribution of affinity depends on the molar mass distribution but also on the distribution of C/E ($=N+1$) and the molar mass of the side chains (proportional to P) [12, 52, 62, 63].

1.2.4. Impact of Molecular Parameters

The adsorption plateau for a PCE can be experimentally determined from adsorption isotherms. In the past there have been multiple attempts to correlate the area that one molecule occupies on the surface with its average molecular parameters of N , P , and n (see Figure 1.2a). The different approaches are based on different conformations of the adsorbed molecules.

The simplest attempt to describe the conformation of adsorbed PCEs is assuming that the surface occupancy is indirectly proportional to the backbone length Equation 1.4. In this case, the backbone is stretched out on the surface while the uncoiled side chains extend into solution. Hence, the adsorbed area per molecule S_i is not affected by the length of the side chains P , but only by the length of the backbone.

$$S_i \propto N_i \cdot n_i \quad (1.4)$$

Besides neglecting the role of P onto adsorption, also the impact of charge density is not sufficiently represented in Equation 1.4. A more elaborated model was suggested by Flatt *et al.* [10] by assuming that the surface conformation of an adsorbed PCE molecule can be described by a chain of hemispheres ("Hemisphere Model"). They found the radius of one hemisphere after minimization of the *Flory*

free energy. This gives access to calculate the area S_i occupied by each PCE molecule on the cement surface as follows:

$$S_i = \frac{\pi}{\sqrt{2}} a_N \cdot a_P \left(2\sqrt{2} (1 - 2\chi) \frac{a_N}{a_P} \right)^{0.4} P_i^{0.9} N_i^{0.3} n_i \quad (1.5)$$

According to Equation 1.5, PCE molecules of high charge density and long backbones occupy more space on the surface. Importantly, it must be noted that P also impacts the space per molecule. Although being considered as non-adsorbent, the coiled side chains indirectly require space on the surface by hindering adsorption of potential neighbor molecules. The "Hemisphere Model" was found to feature a suitable correlation between surface area and molecular parameters.

Similar scaling relations to the "Hemisphere Model" can be found by referring to the so-called "Mushroom Slice Model". In this case, the PCE segments are considered to adsorb not as a hemisphere but a mushroom slice [10]:

$$S_i = \left(\frac{3}{8} \right)^{0.25} \left(\frac{a_N}{a_P} \right)^{0.25} (1 - 2\lambda)^{0.25} a_N \cdot a_P P_i^{0.75} \cdot N_i^{9/16} \cdot n_i \quad (1.6)$$

The exact scaling relations between molecular parameters and required surface area have not been confirmed so far. However, AFM colloidal probe experiments showed that Equation 1.5 and 1.6 capture main trends [10].

1.3. Competitive Adsorption

The working mechanism of several admixtures such as superplasticizers (SPs), viscosity modifiers or retarders is based on the adsorption of molecules on the surface of cement particles [12]. Thus, there may be a competition between different admixture molecules for adsorption sites at the liquid-solid interface. Moreover, some activators or accelerators are calcium salts, of which the counter ions, while of second order importance for hydration, may impact the adsorption of some organic compounds. Thus, understanding competitive adsorption between different species including organic admixtures as well as inorganic ions (*e.g.* sulfate ions) is crucial for robust concrete mix design [10, 12, 22].

1.3.1. Competition with Admixtures

Competitive adsorption phenomena in cement have been subject of research in the last decades, with probably the first concerns about the issue expressed with respect to hydroxyl ions [65]. Most importantly however was the concern over the competition between sulfate ions and PCEs. In the milestone work by Yamada *et al.* [65], it was shown that sulfate ions limit the amount of available adsorption sites for PCE molecules. Hence, it is now accepted that the dispersion efficiency of PCEs is impaired by competition with sulfate ions [32, 64, 66–68], even if the extent to which this occurs depends on the molecular structure of the PCE among other factors [69]. Moreover, competitive adsorption between PCE molecules and other organic admixtures, *i.e.* viscosity modifiers [23, 70] or retarders [23, 29, 31, 71] was also demonstrated.

1.3.2. Competition among PCEs

Notably, competition for the cement surface is not restricted to competition between different types or species of admixtures. Formulated SPs might contain blends of different PCEs that compete for the surface. For instance, PCEs with different water-reduction and slump-keeping properties can be blended to meet the user's demands [21, 72]. However, it has to be noted that PCEs are synthetic polymers that are disperse regarding their molar mass and molecular structure. In terms of adsorption behavior, broadly distributed polymers may be considered as multicomponent mixtures from which all individual components are competing for adsorption on the surface. Therefore, also competition within a PCE has to be considered [73]. It can be expected that this plays a role and changes the distribution of the adsorbed fraction with respect to the original composition since several studies have shown that in equilibrium conditions compounds with high affinity for the surface adsorb preferentially over low-affine compounds [12, 62].

For concentrations well below surface saturation, all molecules find an available adsorption site on the surface. Upon the onset of saturation, fractions with high affinity get adsorbed more extensively, possibly even entirely, whereas low affine molecules adsorb less effectively and are displaced towards the liquid phase. As a result, there is an increase of the low-affinity compounds in solution [62, 74]. In this regime, also excluded volume interactions of the adsorbed molecules start having a

significant impact on the free energy of the system [10, 63]. When the surface is fully saturated, the concentration of the high-affine components in solution increases more substantially (or begins to be present if up to then it was fully adsorbed). Finally, a dynamic equilibrium between adsorbed and dissolved species is established. One molecule can desorb to give access to the surface to another molecule of identical nature while maintaining a state of minimum free energy [62, 74].

1.3.3. Adsorption Equilibrium

The existence of a dynamic equilibrium was proven by Pefferkorn *et al.* [75] and was later discussed by de Gennes [63]. The work of de Gennes marks a milestone in polymer physics at interfaces. With respect to PCEs, transferring his theories means that there must be a dynamic equilibrium between PCEs at cement surfaces and in solution. Considering the multidimensional dispersity of PCEs, the nature of this equilibrium is expected to be influenced by structural parameters of the PCE molecules.

1.4. Chemical Variety in PCEs

Since their invention in the 1980s, PCEs have undergone a significant development. In 2014, the global volume of produced PCE dispersions (approximate solid content of 60%) surpassed 3 million tons [8, 46]. Today, a great variety of chemically different PCEs is available including MPEG, APEG, VPEG, HPEG, and IPEG among many others [4, 6]. These dispersants differ not only in chemical components, but also in their performance as cement plasticizers. Chemical structures of several above-mentioned PCE types are shown in Figure 1.7.

1.4.1. Backbone Chemistry

The backbones of the PCEs commonly contain units of methacrylic acid, acrylic acid or maleic acid. Their carboxylate groups can serve as anchors to attach side chains *via* ester or amide bonds (MPEG-type). However, these moieties are prone to hydrolysis in alkaline conditions. Losing side chains relates to a change in adsorption

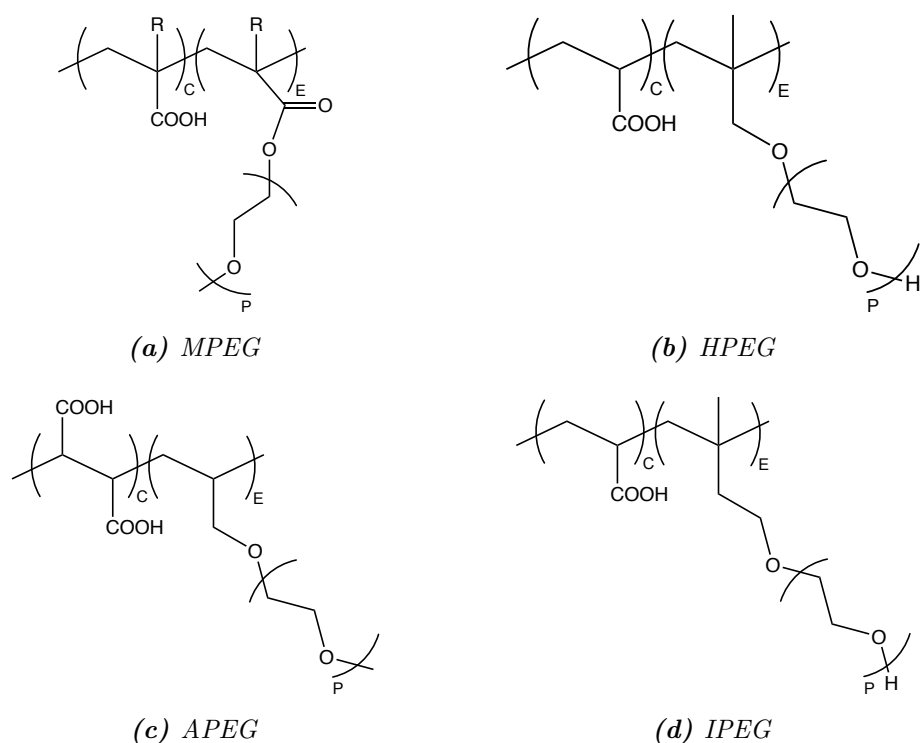


Figure 1.7. Chemical structures of several PCE types. *C* and *E* notes the number of repeating units of comonomers in the backbone. *P* gives the number of EO units in the side chain. (a) Molecular structure of a MPEG-PCE. The rest *R* indicates the possibility of acrylic ($R=H$) and methacrylic ($R=Methyl$) chemistry. (b)–(d) typical copolymers of HPEG, APEG and IPEG with acrylic or maleic acid.

and performance characteristics. Therefore, amide and ester functionalities can be substituted by more stable bonds such as ether or imide bonds [6, 76, 77].

PCEs including α -methallyl poly(ethylene glycol) (HPEG) are a prominent example of a PCE where side chains are connected *via* an ether bond. HPEG-PCEs are superior to MPEG-PCEs regarding hydrolytic stability. But also, their performance as SPs was demonstrated to be different from the MPEG-type. Recent results by Plank *et al.* [33, 78] show that HPEG-PCEs show a remarkable fluidification of cements blended with calcined clays (up to 50 % replacement). Other macromonomers featuring an ether bond are based on vinyl ether (VPEG), isoprenol ether (IPEG) and allylether (APEG) chemistry [4, 79].

The backbone chemistry of a PCE has a significant impact on the adsorption behavior. For example, when comparing (meth)acrylic PCEs with maleic acid PCEs (Figure 1.7a and 1.7c), the higher charge density in the maleic backbone has an impact

on the adsorption behavior due to the vicinity of adjacent carboxylic groups [80]. With adsorption being driven by the formation of exothermic bonds, an increased number of anchor groups correlates with more possible contact points with the surface. However, a high number of adjacent charges might also compromise the flexibility of the backbone and can induce mutual repulsion upon adsorption [62]. Therefore, it is important to tailor the charge density along the backbone. This can either be done by regulating the ratio of carboxylic units to side chains (*i.e.* decrease of C/E) or by inserting a third monomer as spacer molecule. In this case, the PCE can be characterized as a terpolymer [79, 81, 82].

To this day, PCEs with carboxylate groups show the benchmark in SP technology. Besides carboxylate groups, other ionic groups and functionalities can be incorporated into PCEs. Commonly, only a part of the carboxylic units gets replaced. For this purpose, sulfonate, phosphonate or quaternary ammonium can be used [6]. In a recent study, Stecher *et al.* [76] suggested phosphate containing PCEs as viable alternative to traditional methacrylic MPEG-PCEs. The investigated PCE terpolymers showed a better dispersing ability as well as higher sulfate and clay tolerance compared to their copolymer counterparts [76, 83].

Moreover, introducing silyl functionalities into a methacrylic backbone can be beneficial to increase adsorption at high grafting ratios [84]. The main difference between ionic anchor groups and organo-silyl groups is the fact that the silyl functionalities can form covalent bonds with the C-S-H surface. The presence of such bonds was confirmed by ^{29}Si -NMR [85–87] and EXAFS (short for extended X-ray absorption fine structure) [86]. The occurrence of covalent bonds prevents desorption of PCEs which has a significant impact on the adsorption process as it can be regarded as irreversible and non-dynamic. Organo-silane modified PCEs show less sensitivity for sulfate competition [85, 87] what can be seen as a consequence of irreversibly anchoring on the cement surface. Figure 1.8 shows the molecular structure of two silylated comonomers used for PCE synthesis [76, 83].

1.4.2. Sidechain Chemistry

Modern PCE technology almost exclusively uses derivatives of poly(alkylene glycols) as side chains. Among them, PEG is dominating the market with few exceptions where poly(propylene oxide) (PPO) is incorporated alongside with PEG. Here, the number of PEG side chains (EO units) is usually higher than the one PPO (PO units).

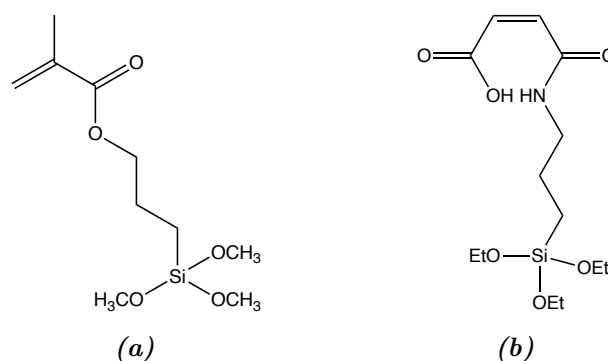


Figure 1.8. Monomers for the synthesis of Organo- silane modified PCEs. (a) 3-(trimethoxysilyl) propyl methacrylate (MAPTMS), (b) N-maleic- γ - aminopropyl triethoxy silane (MAPS).

With PPO being more hydrophobic than the PEG counterparts, they compromise the water solubility of PCEs [6, 8].

Typical PEG side chains feature a molar mass between 500 and 5000 ($P \approx 10$ -115). Thus, for most PCEs the backbones are longer compared to the side chains meaning that they can be ascribed to the FBW regime according to Gay and Raphaël [10, 37].

Few PCEs make use of other side chain chemistries than PEG/PEO. One of them are PAAM-type PCEs which contain PEG side chains together with poly(amido amine). This type of PCEs can be applied in concretes with extremely low water content ($w/c < 0.2$) suggesting that N-bearing side chains might be advantageous compared to PEG/PPO at low w/c . The exact working mechanism of such PCEs is still under investigation. However, N-bearing polymers are barely available at a comparable price to PEG/PPO [8].

1.5. PCE Synthesis

The different comonomers demand different synthesis strategies and conditions. From a synthesis point of view, the biggest advantage of PCEs compared to older generations of SPs (*i.e.* poly(naphthalene sulfonates) (PNS) and poly(melamine sulfonates) (PMS)) is the fact that they can be produced by radical polymerization techniques instead of polycondensation reactions [6]. Regarding synthesis route for PCEs, reaction conditions and choice of monomers, PCE synthesis offers high flexibility. Thus, the microstructure of the combs can be influenced by changing

molecular parameters like grafting degree, side chain length or backbone length. Another parameter that must be controlled is the distribution of side chains along the backbone. In the following, three techniques are presented that can be applied for the synthesis of a PCE with PMAA backbone and MPEG side chains (MPEG-type) as shown in Figure 1.1.

1.5.1. Grafting of Precursor Backbones

The first route implies grafting of mono-hydroxylated PEG onto PMAA in a polymer-analogous esterification process. The PMAA precursor backbone is formed prior to grafting by free radical polymerization of MAA. The two-step synthesis procedure is shown in Figure 1.9

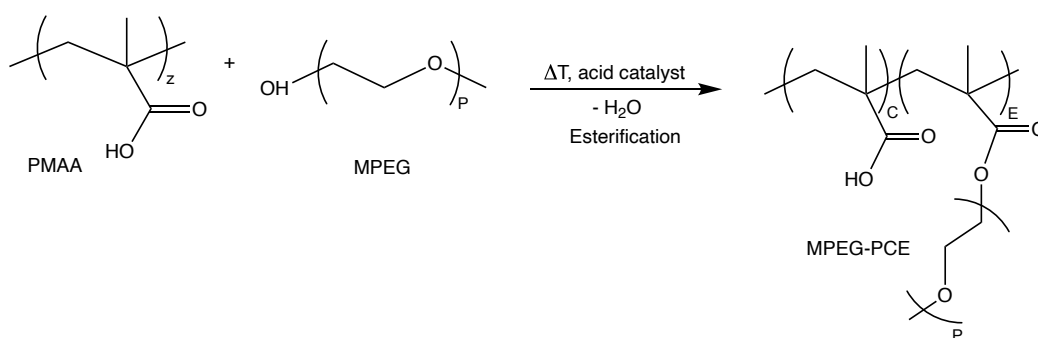


Figure 1.9. Grafting process (polymer-analogous esterification) for the synthesis of MPEG-type PCEs. The product can be considered as a homogenous graft with statistical distributed side chains along the backbone.

As a result of rather low conversion rates, the product contains residual MPEG which can cause excessive air entrainment when applied in concrete [88]. To obtain high conversions during the esterification, the grafting step is usually carried out in melt and under vacuum. While this technique is often used on the lab scale for research purposes, it is less relevant on industrial scale. However, grafting offers the advantage that the repartition of charges and side chains along the backbone is rather homogeneous [4, 6, 43]. This makes grafting suitable for the preparation of model PCEs for scientific studies as they can be described by the model and scaling relations found by Gay and Raphaël [37] and Flatt [10].

1.5.2. Free Radical Copolymerization

Alternatively, MAA can be copolymerized with a poly(ethylene glycol) methacrylate (PEGMA) macromonomer. The copolymerization is commonly carried out under free radical conditions (FRC) in aqueous media (Figure 1.10) [47]. Whereas grafting is known to yield homogeneously grafted PCEs, FRC yields more heterogeneous microstructures [43]. The backbone length can partially be controlled using chain transfer agents (CTAs) such as mercaptans or hypophosphite [4]. However, the sequence of monomers along the backbone depends on copolymerization parameters of the individual monomers. Besides statistical copolymers, also alternating, gradients or even block conformations can be obtained [38, 43].

Klier *et al.* [89] determined the copolymerization parameter of PEGMA ($M = 500\text{--}1000\text{ g/mol}$) and MAA in aqueous solution (D_2O) at low pH. It was shown that both comonomers show similar reactivity, enabling the synthesis of PCEs with statistical (random) distribution of monomers. However, acidic conditions cannot be applied to very short side chains.

For increased pH values, MAA was found to be less reactive than the PEGMA macromonomers. The difference in the copolymerization parameters alters the statistical incorporation of comonomers into the growing chains, and the PCE composition is not proportional to the feed. Depending on the exact copolymerization parameters, alternating, strictly alternating, gradient and more “blocky” structures are obtained [43, 47]. Moreover, Smolne *et al.* [90] reported on a change of the reactivity parameters with concentration. All in all, the exact reactivity ratio between PEGMA and MAA depends on a series of factors. To precisely control the monomer repartition of the backbone, all these impacts have to be considered.

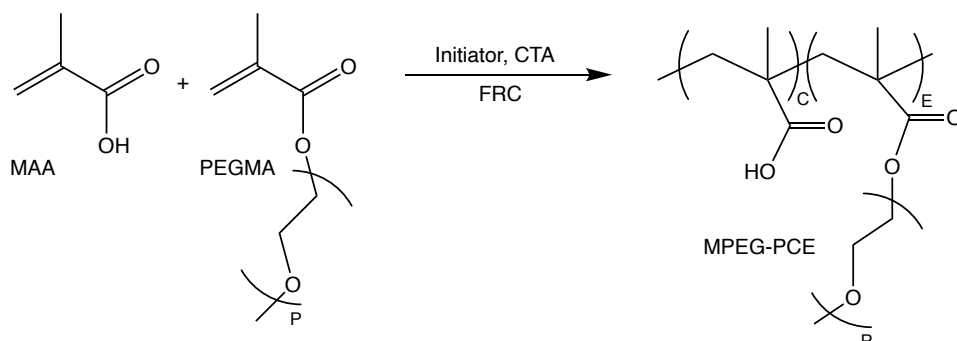


Figure 1.10. Free radical copolymerization route for the synthesis of MPEG-type PCEs. The repartition of monomers depends on the exact reaction conditions.

As an example, for a PCE with alternating monomers, the copolymerization of APEG macromonomers with maleic acid anhydride can be mentioned. Neither of the comonomers undergoes homopolymerization resulting in a strictly alternating sequence of monomers along the backbone as described in literature [4, 91].

FRC is the most important technique for the PCE synthesis on industrial scale, as it is applicable to a variety of relevant comonomers and can be carried out in aqueous media. The polymerization process can be divided into three main stages: initiation, chain growth (propagation) and termination. During propagation, transfer processes can cause the termination of the growing chain [92]. For instance, this happens when a hydrogen atom (*e.g.* from the solvent) is transferred to the polymer radical. While the chain growth is terminated, the remaining solvent radical might initiate the growth of a new polymer chain. Chain transfer occurs randomly and leads to a decrease of the degree of polymerization and an increase of dispersity. As mentioned above, the use of CTAs allows to decrease the occurrence of random transfer and initiation reactions. Notably, conventional CTAs only limit random transfer up to a certain extent [92].

1.5.3. RAFT-Polymerization

Both strategies, grafting and FRC imply at least one step of free radical polymerization. Consequently, the PCE product exhibits a broad heterogeneity in terms of molar mass and chemical composition. Better control over a polymerization can be obtained using “living polymerization techniques”. Indeed, several papers suggesting RAFT (short for reversible addition- fragmentation chain transfer) for the synthesis of PCEs by controlled techniques have been published in the last decade. Due to their “living” character, these procedures are suitable to decrease the dispersity PCE to $M_w/M_n < 1.1$. The low dispersity of the MMD indicates higher uniformity among the PCE molecules. But it must be noted that RAFT does not necessarily yield a homogeneously grafted product. Analogue to FRC, the reactivity ratio of the comonomers is the criterion for statistical, alternating, gradient or block monomer distributions [93–95].

The RAFT process is very similar to conventional free radical copolymerization. However, it involves the use of a particular chain transfer agent (often called RAFT agent) that mediates the polymerization *via* reversible chain-transfer processes.

Typical RAFT agents are thiocarbonylthio compounds such as dithioesters or trithiocarbonates (Figure 1.11a) [96, 97].

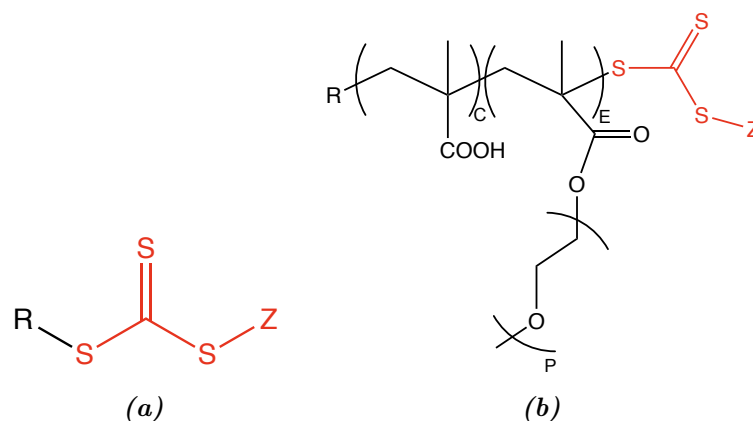


Figure 1.11. (a) Chemical structure of a typical trithiocarbonate RAFT agent. (b) α - ω -modified RAFT-PCE. The attached functional group strongly absorbs UV light [98, 99].

In contrast to FRC, where the CTA limits random chain transfer, RAFT agents allow to attain full control over the growing chain end. Thus, the RAFT process is characterized by “living” kinetics. In a typical RAFT synthesis, the polymerization is initiated by a radical initiator that reacts with a monomer. Subsequently, the monomer radical connects with the RAFT agent. As soon as all RAFT agents are activated, an equilibrium between active chains and dormant species is established. Ideally, transfer only happens within the RAFT equilibrium (Figure 1.12). This allows to precisely adjust the degree of polymerization (DP_n) from the ratio of monomer to CTA [96, 100, 101].

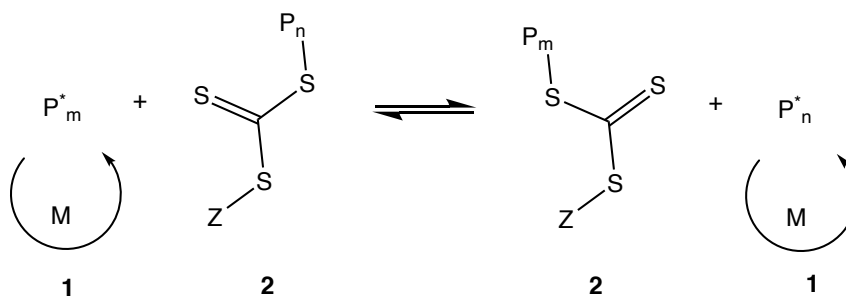


Figure 1.12. RAFT equilibrium between active and dormant species of two growing chains. (1) propagating radical P_i^* (active) that adds monomer M to the chain end (2) polymer-RAFT-adduct (dormant species).

Because of the polymerization mechanism, each PCE backbone is modified at both ends ($\alpha - \omega$ modification). One end carries the so-called Z-group, which is attached *via* a thiocarbonylthio moiety (Figure 1.11b)

This functionality strongly absorbs light in the UV-Vis range. This characteristic can be used for concentration detection or end group analysis of the synthesized PCE by UV-Vis spectroscopy. It must be considered that the Z-group is prone to hydrolysis, in particular at high pH as found in cement pore solution [97, 98].

When first applied to PCEs, RAFT synthesis was carried out in organic medium [93]. Since then, a wide range of RAFT agents became commercially available that can be used in aqueous solution [94, 102, 103]. The living character of the RAFT process can be exploited to realize block structures by first synthesizing a PMAA block which can serve as a macro-RAFT agent to initiate the subsequent polymerization of the second block (*e.g.* PEGMA).

Although offering the advantage of precisely tailoring the molecular structure, RAFT synthesis is still inferior to FRC on industrial scale due to cost reasons. However, there have been some patents filed currently with the intention to make use of gradient and block-PCEs as SPs in high performance concretes with significantly reduced mixing time [104].

1.6. Characterization of Average Parameters

1.6.1. PCE Composition

Various studies indicate that the microstructure of the combs is a key parameter to understand the performance of PCEs as dispersing agent. Indeed, several researchers have aimed to correlate the microstructure of PCEs and their effect on cement hydration and rheology [28, 105]. However, these studies often refer to average molecular parameters and neglect the impact of dispersity. While very useful, such results should always be considered to represent average effects of a distribution. To provide reliable predictions, it is inevitable to go beyond the determination of average properties of PCEs and consider their structural heterogeneity on the molecular level.

As pointed out in the previous sections, the molecular composition of PCEs is highly complex. In a first approximation, averaged information can be useful

to get an idea about the molecular parameters. With the charge density driving the adsorption process, it is of special interest. It can be determined by acid-base titration [106, 107] or polyelectrolyte titration using a cationic polyelectrolyte such as poly(diallyl dimethyl ammonium) chloride (PDADMAC) [108].

The charge density is correlated with the ratio between carboxylic acid groups and side chain bearing units (C/E) along the PCE backbone. The simplest way to calculate C/E is from the conversion of the polymerization reaction. Alternatively, $^1\text{H-NMR}$ can be used to access C/E [6]. In addition to $^1\text{H-NMR}$ measurements, complementary $^{13}\text{C-NMR}$ offer a unique tool to investigate the microstructure of PCEs. Carboxylate groups and esterified units appear at different shifts in the ^{13}C spectrum and can be used to study the repartition of monomers along the backbone [55, 109–111]. In general, NMR characterization works reliably for many acrylic and methacrylic based PCEs, however certain PCEs do not feature suitable proton or carbon signals allowing to access the composition and/or repartition.

Another spectroscopy method applied to gather information about the composition of a PCE is infrared (IR) spectroscopy. Here, carboxylic acid, carboxylate as well as ether bonds can be detected. The relative intensity of the signals allows to draw conclusions regarding the copolymer composition [112–114].

Besides the direct determination of the molecular parameters, also the ability of a PCE to bind calcium can be of interest to foresee its affinity for the cement surface. The amount of calcium chelated by a PCE can be determined by depletion of calcium ions from solution using calcium selective electrodes. This parameter usually increases with increasing C/E, but also depends significantly on the type of charges [76].

1.6.2. Conformation in Solution

In polymer analytics, the most important parameters that characterize the solution conformation are the hydrodynamic radius (R_{H}) and the radius of gyration (R_{G}). Both radii can be obtained from scattering experiments. The ratio $R_{\text{G}}/R_{\text{H}}$, also often referred to as “shape factor” or “asymmetry factor” gives valuable information about the conformation of the polymer in solution [115]. Typical values for $R_{\text{G}}/R_{\text{H}}$ are listed in Table 1.1. For PCEs, $R_{\text{G}}/R_{\text{H}}$ was reported to be < 0.77 [36]. The value is surprisingly low and indicates a very compact structure that might be due to the

highly branched architecture of the molecules. To this end, it should be mentioned that, the study [36] that reports R_G/R_H for PCEs added Ca^{2+} salts to the PCE solution which can induce inter- and intramolecular crosslinking.

Table 1.1. Dimensionless shape factor for various geometries and molecular architectures as reported by Burchard *et al.* [115]. Θ -solvent refers to the condition when the polymer molecule behaves like an ideal chain that can be described by random walk coil dimensions.

Architecture	Solvent	R_G/R_H
Homogeneous hard sphere		0.778
Gaussian "soft" sphere <i>e.g.</i> dendrimers > 10 generations		0.977
Linear random coil (low dispersity)	Θ Good	1.504 1.78
Linear random coil (high dispersity)	Θ Good	1.73 1.205

Dynamic scattering is a common tool to access the hydrodynamic size of a specimen. In contrast, static scattering techniques are the method of choice to access the radius of gyration. A typical size range for R_H of a PCE is approximately between 5 and 20 nm. Although being at the lower end of resolution, dynamic light scattering (DLS) can be applied to target R_H . The radius of gyration (typically < 5 nm) is too small to be sufficiently resolved in a scattering experiment using a visible light laser. Here, small angle neutron scattering (SANS) must be applied. Gelardi *et al.* [36] carried out SANS experiments using homogeneously grafted PCEs whereas Emaldi *et al.* [38] applied SLS (close to resolution limit). Their results confirm that Equation 1.2 provides a suitable scaling relation to calculate R_G for copolymers with flexible backbone worm geometry.

1.6.3. Molar Mass Averages

As indicated in *Section 1.1.3*, PCEs are multicomponent materials. All their molecular parameters, in particular the backbone length and the C/E are distributed. Therefore, the molar mass of PCEs is not given by a single value, but rather by a distribution. The shape and width of the molar mass distribution (MMD) can be described referring to statistical averages of the distribution. Most frequently used are the number-average molar mass (M_n) and the weight-average molar mass (M_w). The width of the distribution can be indicated by the dispersity index \mathfrak{D} . Hereby, \mathfrak{D} is given by the

ratio of M_w to M_n (Equation 1.7). The apparent MMD of PCEs is usually obtained from size exclusion chromatography (SEC) in aqueous media [36, 39, 41, 116].

$$\mathcal{D} = \frac{M_w}{M_n} \quad (1.7)$$

1.7. Characterization of Parameter Distributions

1.7.1. The Importance of Liquid Chromatography

In many research papers, the heterogeneity of PCEs is solely characterized as ratio between M_w and M_n . While this is very useful to get a first impression of the dispersity in molar mass, it is not accounting sufficiently for the variations in the chemical composition. Indeed, the total heterogeneity of a PCE has to be described by superimposing all aspects of dispersity [41].

To access molar mass distribution (MMD) and chemical composition distribution (CCD) various analytical techniques are needed. Each technique should be selective and target one specific aspect of heterogeneity. Combining multiple selective analysis methods gives access to a multi-dimensional map of molecular heterogeneity in a polymer sample [41].

As described in *Section 1.6*, spectroscopy and scattering experiments are widely used for the analysis of PCEs. When carried out in batch mode, these techniques lack information about distributions and only give an average value over the whole sample (bulk characteristics). Distribution analysis can only be performed after separation of the inhomogeneous polymer mixture into its components. To this end, liquid chromatography (LC) techniques are a widely used tool [117]. Besides, also field flow fractionation [118, 119] and electrophoretic techniques [120, 121] can be considered to fraction a disperse sample. In the following sections, the importance of LC-based techniques for polymer characterization is highlighted.

For comprehensive analysis, LC can be used as a first step to fraction polymer samples. Subsequently, the different fractions can be subjected to spectroscopic characterization. Best results are achieved by using a combination of selective detection methods (*e.g.* spectroscopic, scattering, viscometry) [116, 117, 122, 123].

Whereas size exclusion chromatography (SEC) can be used to separate polymers by hydrodynamic size, interaction chromatography (IC), like gradient polymer elution chromatography (GPEC) or LC at critical conditions (LCCC) are suitable to separate polymers by chemical composition or functionality [117, 123].

For complex copolymers that feature dispersity in two dimensions (*e.g.* molar mass and chemical composition), a combination of separation methods is needed to fully map molecular heterogeneity. In the past two decades, numerous methods of online coupling of two LC techniques (LCxLC) have been published. Besides LCxLC, there is the possibility to combine LC techniques with mass spectrometry (LCxLC-MS) [116, 117, 122, 123].

1.7.2. Basics about Liquid Chromatography Modes

A standard LC setup is composed of a solvent reservoir containing the mobile phase, a solvent pump, a sample injector, and a chromatographic column filled with packing material (stationary phase). At the end of the column, a detector continuously records a chromatogram and signals the elution of compounds from the column [107]. Figure 1.13 shows a schematic LC setup.

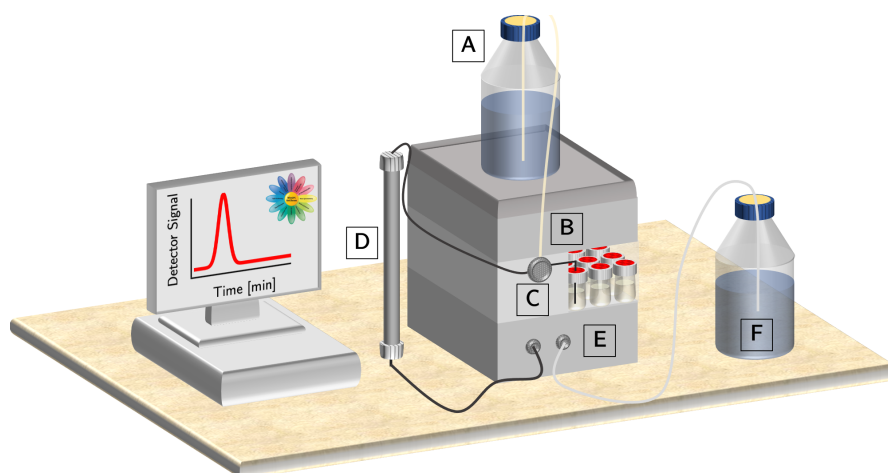


Figure 1.13. Schematic of a liquid chromatography setup: (A) Solvent reservoir, (B) Pump, (C) Injector, (D) Column, (E) Detector, (F) Waste.

For an isocratic LC experiment, the solute (*i.e.* polymer sample) is dissolved and injected into the chromatography column while the mobile phase is continuously being pumped. The different solute components migrate through the column at

different velocities. Generally speaking, the chromatographic separation mechanism depends on the partition of solute components between stationary phase and mobile phase. This partition can be described with the distribution coefficient K_D , which is given by the ratio of solute concentration in the stationary phase (c_s) and the corresponding concentration in the mobile phase (c_m) (Equation 1.8).

$$K_D = \frac{c_s}{c_m} \quad (1.8)$$

Moreover, the equilibrium of components between both phases can be described thermodynamically, referring to the *Gibbs' Energy* (ΔG) [41]:

$$\Delta G = \Delta H - T\Delta S = -RT \cdot \ln K_D \quad (1.9)$$

where ΔH is the enthalpic term and $T\Delta S$ the entropic term. Depending on the ratio between both terms, three different modes of chromatography are distinguished, namely size exclusion chromatography (SEC), liquid chromatography at critical conditions (LCCC) and liquid adsorption chromatography (LAC). In SEC, molecules are separated by entropic exclusion ($\Delta H = 0$), while LAC separates molecules due to enthalpic interactions between polymer and stationary phase ($T\Delta S = 0$). For the special case of LCCC, entropic and enthalpic contributions compensate each other ($\Delta G = 0$) [41].

Evidently, the time span for which a solute molecule is retained depends on its hydrodynamic size and its interactions with the stationary phase. Hence, the retention volume, V_R , can be expressed with Equation 1.10 [41, 117]:

$$V_R = V_i + K_{SEC} \cdot V_p + K_{LAC} \cdot V_s \quad (1.10)$$

where V_i is the interstitial volume, V_p the pore volume and V_s is the stationary phase volume. K_{SEC} and K_{LAC} represent the chromatographic distribution coefficients for steric exclusion and for adsorption, respectively.

For all LC modes, the dependence of the retention volume (often also referred to as elution volume) on the molar mass is depicted in Figure 1.14. Throughout this thesis, the terms "retention volume" and "elution volume" are used as synonyms. In SEC experiments, retention is decreased with increasing molar mass, while the opposite

trend is found for LAC. In a typical LCCC experiment, elution is independent of the molar mass. The different chromatography modes are described in more detail in the following sections: SEC (*Section 1.8*), LCCC (*Section 1.9*), LAC (*Section 1.10*).

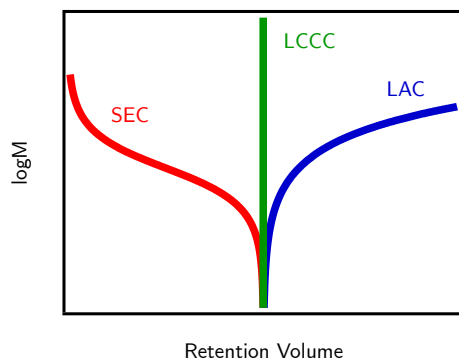


Figure 1.14. Dependence of the molar mass (M) on the retention volume for different LC modes. In SEC, molecules of low M are retained longer, while the opposite trend is found for LAC. In LCCC elution occurs independent of M .

1.8. Size Exclusion Chromatography

1.8.1. Basics about SEC

Under ideal SEC conditions, there are no enthalpic interactions between the stationary phase and the solute and the separation mechanism is purely entropic ($\Delta S \leq 0$). Consequently, for $dH = 0$, the steric distribution coefficient can be calculated after rearranging Equation 1.9 as follows [41]:

$$K_D = K_{SEC} = \exp\left(\frac{\Delta S}{R}\right) \quad (1.11)$$

For SEC, a thermodynamically good solvent for the solute must be chosen as mobile phase to avoid enthalpic interactions between solute and column material. For ionic polymers, the addition of salt to the mobile phase is recommended to shield interactions. The stationary phase is given by porous column packing materials. Depending on their size, solute molecules can penetrate the pores. Subsequently, the path they travel through the column is increased and molecules are retained based on their hydrodynamic dimensions. For ideal SEC, the separation process is purely

based on entropic exclusion ($K_{LAC} = 0$). K_{SEC} varies between 0 for large molecules that cannot enter the pores and 1 for small molecules that are able to access all pore sizes ("total permeation"). Thus, retention decreases with increasing molecule size [41, 117, 124].

At the end of the column, several detectors can be connected to record the eluting fractions. The most common detectors are concentration detectors (*e.g.* refractive index or diode arrays) but also molar mass sensitive detectors (*e.g.* multi angle laser light scattering or viscosity) [41, 117, 124].

In common SEC setups, concentration sensitive detectors signalize the concentration of an eluting fraction. Prior to the analysis of a sample with unknown molar mass, the SEC setup must be calibrated. For this purpose, a series of polymer standards (of known molar mass and narrow dispersity) is run through the SEC device. Subsequently, a calibration curve can be calculated connecting each slice of the chromatogram with the molar mass of the standard. The obtained calibration curve can be used to determine the relative molar mass of a sample with unknown characteristics. Notably, this method only gives reliable results when the standards and the samples feature the same chemistry. PEG/PEO, PAA and PMAA are standard polymers for the characterization of hydrophilic polymers in aqueous SEC [41, 117, 124].

However, PCEs are comb copolymers and none of the linear standards mentioned above allows to access their exact MMD. Nevertheless, SEC with PEG/PEO standards is a widespread method to estimate the MMD of a PCE. For this purpose, polar column materials in combination with water as mobile phase have proven to be appropriate. It is essential to add salt to the mobile phase (*e.g.* Na_2HPO_4 , NaNO_3 , NaCl) to eliminate interactions between the PCE and the column material [125].

Gelardi *et al.* [36, 39] opted for a better use of SEC in PCE analysis and encouraged to prefer SEC with multi angle laser light scattering (MALLS) over conventional standard calibration. Indeed, MALLS provides the absolute molar mass and potentially also the radius of gyration of an eluting sample. A MALLS detector measures the scattering intensity of an eluting species at various angles. The excess intensity $R(\Theta)$ of scattered light at an angle Θ is related to the weight average molar mass M_w according to Equation 1.12 [119, 124]:

$$\frac{K_{opt} \cdot c}{R(\Theta)} = \left[\frac{1}{M_w} \cdot P(\Theta) \right] + 2A_2c \quad (1.12)$$

$$\text{with } K = \frac{4\pi^2 n_0^2 \left(\frac{dn}{dc}\right)^2}{\lambda_0^4 \cdot N_A}$$

where K_{opt} is the optical constant, $P(\Theta)$ the form factor, A_2 the second virial coefficient and c the sample concentration. Moreover, λ_0 is the wavelength of the laser, N_A the Avogadro constant, n_0 the refractive index of the mobile phase and dn/dc the refractive index increment of the sample.

Subsequently, a *Zimm plot* can be used to determine R_G and M_w (Figure 1.15). To this end, $(K_{opt} \cdot c)/R(\Theta)$ is plotted against $\sin^2(\Theta/2)$. M_w is then obtained from the intercept, whereas R_G can be calculated from the slope. Notably, samples with a radius of gyration smaller than 10 nm scatter light isotropically (*Rayleigh scattering*). This hinders accessing the radius of gyration, however, M_w can still be obtained by extrapolation ($c \rightarrow 0$) [119].

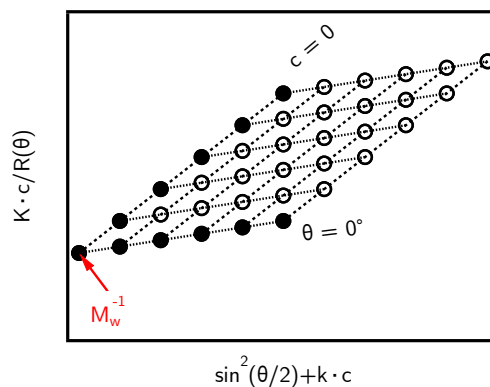


Figure 1.15. Schematic representation of a Zimm Plot. Linear regression of the data points allows to elucidate information on M_w and R_G of a dissolved molecule or particle.

To obtain reliable results, the dn/dc of a sample is required. It can be determined with the help of the concentration signal, or offline in batch mode. An imprecise dn/dc decreases the accuracy of the molar mass determination significantly. For homopolymers, dn/dc values for many polymer-solvent combinations are tabulated in literature [126]. With PCEs being copolymers, it is more difficult to accurately account for the dn/dc . In many studies, the dn/dc is taken as the dn/dc of PEG

(0.135 mL/g in aqueous solution) assuming that the refractive index increment of the PCE is equal to the value of its side chains [127]. As shown by Emaldi [38] and Gelardi [39], this is an insufficient approximation. However, also the online determination method of the dn/dc can be problematic for chemically heterogeneous samples. In this case, the dn/dc is not given by one exact value for all fractions [128], but might be different for each eluting copolymer fraction. More precisely, variations in the dn/dc cause problems when it comes to the determination of MMDs due to imprecise calculations of eluting polymer concentrations [128]. However, SEC with MALLS/RI detection was proven to give a good estimate of the MMD for PCEs [36, 38].

When approaching the MMD from SEC chromatograms, it is assumed that the hydrodynamic size of a polymer coil is mainly determined by its chain length (*i.e.* degree of polymerization). However, the molecular architecture (*i.e.* branching) and up to a certain extent also the chemical composition of a polymer chain have an impact on hydrodynamic dimensions [115]. In this context, the comb-shaped architecture of PCEs must be considered. It is feasible that two PCE molecules of different backbone length and different grafting ratio happen to feature the same R_H . As SEC strictly separates by hydrodynamic size, both molecules elute simultaneously. This phenomenon is often referred to as coelution [129]. Notably, the problem of coelution cannot be solved by refining the detection mechanism. Hence, SEC experiments only allow to approach the MMD and do not give exact values.

1.8.2. Dual Concentration Detection

SEC is commonly applied to gather information on the MMD, however, the combined use of multiple concentration sensitive detectors gives access to elucidate quantitative information on the composition of chemically heterogeneous samples such as copolymers [130–133] and polymer blends [130, 131].

For this purpose, the same number of concentration detectors as number of (co)monomers found in the sample must be applied. For instance, for a copolymer comprised by two comonomers, two concentration detection methods are needed. Regarding copolymers containing a chromophore, simultaneous RI and UV detection is the method of choice [117]. The use of two concentration detectors for investigating the chemical composition of copolymers in dependence on their size is often referred to as SEC with dual concentration detection.

To understand dual concentration detection, Equation 1.13-1.14 are essential. The intensity of the RI and UV signal (S^{RI} and S^{UV}) are proportional to the polymer concentration c_P , where the proportionality constant is given by a polymer-specific response factor k . Hence, the signal from the i^{th} slice of the chromatogram can be calculated as follows:

$$S_i^{RI} = k^{RI} \cdot c_{i,P} \quad (1.13)$$

$$S_i^{UV} = k^{UV} \cdot c_{i,P} \quad (1.14)$$

It should be mentioned that k^{RI} is equal to the dn/dc of a polymer when the detector constant of the RI detector is known, however, this requires precise calibration of the instrument prior to dual detection analysis.

The response factor of a copolymer is related with its chemical composition and may be expressed as a function of the corresponding values of the homopolymers. For instance, the RI response factor of a copolymer “AB” can be calculated from the response factors of homopolymer A and B (k_A^{RI} and k_B^{RI}) as follows [126, 130]:

$$k^{RI} = k_A^{RI} \cdot \omega_A + k_B^{RI} \cdot \omega_B \quad (1.15)$$

with $\omega_A = 1 - \omega_B$

where ω_A and ω_B are given by the weight fraction of comonomer A and B contained in the copolymer. The response factor k^{UV} of copolymer AB can be calculated analogously when k_A^{UV} and k_B^{UV} are known. Notably, Equation 1.15 is only valid, when neighboring group effects which might impact the response factor can be excluded.

Looking at the SEC chromatogram of a copolymer, the response factors can only be described by one distinct value, when all eluting fractions have the same composition (*i.e.* ω_A and ω_B are constant over the whole peak). Variations in the molecular composition cause changes of the response factors along the elution axis. While this is problematic for MMD determination (see *Section 1.8*), dual concentration

detection capitalizes on this phenomenon. Considering that the response factors of copolymers depend on the chemical nature of the eluting fraction, Equation 1.13 and Equation 1.14 can be rewritten as follows:

$$S_i^{RI} = c_{i,P} \cdot [\omega_{i,A} \cdot k_A^{RI} + \omega_{i,B} \cdot k_B^{RI}] \quad (1.16)$$

$$S_i^{UV} = c_{i,P} \cdot [\omega_{i,A} \cdot k_A^{UV} + \omega_{i,B} \cdot k_B^{UV}] \quad (1.17)$$

$$\text{with } \omega_{i,A} = 1 - \omega_{i,B}$$

where $\omega_{i,A}$ and $\omega_{i,B}$ refer to the weight fraction of comonomer A and B in the i^{th} slice of the chromatogram. Knowing the response factors of the homopolymers, a set of equations with three unknowns (*i.e.* $c_{i,P}$, $\omega_{i,A}$ and $\omega_{i,B}$) can be solved as described in literature [117, 128, 130, 133] to yield information on the concentration and composition of the eluting fractions. Hence, the sample composition along the elution axis can be monitored. Notably, SEC with dual concentration detection shows a valuable tool to gather information on the chemical composition of copolymers in dependence on their molecular size. However, the dual concentration method does not allow to reveal the CCD [117].

1.9. Liquid Chromatography at Critical Conditions

1.9.1. Basics about LCCC

The term critical referring to polymer solubility has to be put in context with the *Flory-Huggins Theory*, where the critical point describes the limited solubility of polymers in solution [53]. Below the critical point, polymer-solvent interactions are favorable, and the polymer stays in solution. Exceeding the critical point induces phase separation, as polymer-polymer interactions are favored.

In the 1970s, Russian scientists [134, 135] elaborated a concept to transfer the phase separation behavior of polymers in solution to chromatographic conditions. Here, “critical” does not refer to the miscibility behavior between polymer-solvent

and polymer-polymer, but it describes the interactions between polymer-solvent (better polymer-eluent) and polymer-stationary phase.

If polymer and stationary phase do not interact with each other, molecules are strictly separated by entropic exclusion (SEC mode). However, when enthalpic interactions between polymer segments and column material are favored, the polymer molecules start adsorbing to the stationary phase (LAC mode) [123, 136].

LCCC refers to chromatographic conditions when entropic and enthalpic contributions are balanced ($\Delta G = 0$, $K_D = 1$). Under critical conditions all molecules with the same monomeric composition are chromatographically “invisible” meaning that they are not separated and elute simultaneously. This can be seen from Figure 1.14 (green vertical line) where polymer molecules elute independent of their molar mass. Therefore, the retention behavior solely depends on chemical differences. LCCC is widely applied to separate telechelic polymers according to their end groups [137] or block copolymers according to block length [132].

In praxis, the critical chromatography conditions of a polymer depend on a series of factors such as mobile phase, column properties, temperature, or pressure. A change of one of these parameters can dramatically impact the retention of the polymer. Thus, critical conditions found in literature can only serve as a guideline and exact conditions have to be precisely established prior to each experiment by adjusting the above-mentioned parameters [138].

1.9.2. LCCC of PCEs

Regarding PCE synthesis, LCCC can be useful to characterize the purity of the applied educts, *i.e.* PEGMA macromonomer or MPEG [137]. LCCC experiments of PEG derivatives are commonly carried out on hydrophobic columns using solvent combinations of methanol/water [116, 137], acetonitrile/water [39, 137] or acetone/water [137] as mobile phase.

For instance, LCCC experiments of MPEG allow the identification of residues of $\alpha - \omega$ -dihydroxy-PEG. This bifunctional PEG can cause undesired crosslinking of PCEs during a grafting reaction. Moreover, PEGMA macromonomers often contain residual MPEG, which cannot be incorporated into the PCE during a copolymerization and will remain as an impurity. Upon application in cement, ungrafted MPEG side chains can cause excess air entrainment [88].

Besides analyzing educts, LCCC experiments can also be directly applied to PCEs. For instance, Adler *et al.* successfully used semi-preparative LCCC in combination with IR-detection [112, 116] and MALDI-ToF [116] as well as online 2D-chromatography (*i.e.* LCCC×SEC) [116] to investigate PCEs prepared by free radical copolymerization. In the first dimension, they established critical conditions of PEG/PEO using a mixture of water and methanol. In this way, PCE molecules were separated from byproducts of the synthesis. However, these conditions did not allow to detect heterogeneity in grafting.

1.10. Liquid Adsorption Chromatography

1.10.1. Basics about LAC

Liquid adsorption chromatography (LAC) is also often referred to as interaction chromatography (IC). LAC and IC are commonly used as “umbrella terms” covering a large variety of chromatographic methods based on enthalpically-driven separation processes [129]. In a typical LAC experiment, we find $K_{LAC} \gg 1$. This occurs when the eluent strength of the mobile phase is decreased. Consequently, solute molecules start interacting with the stationary phase and can adsorb to it ($\Delta H < 0$). Typical interactions are dispersion forces, but also hydrogen bonding or Coulomb interactions. Moreover, adsorptive interactions contribute to the total retention time [117].

In an ideal LAC experiment, the separation mechanism is purely enthalpic. For $T\Delta S = 0$, the enthalpic distribution coefficient, K_{LAC} can be calculated using Equation 1.9.

$$K_D = K_{LAC} = \exp\left(\frac{-\Delta H}{RT}\right) \quad (1.18)$$

However, in practice, this condition is often not fulfilled, meaning that besides enthalpic interactions, also size exclusion effects have to be considered [41].

In LAC, a rapid increase in retention can be observed with increasing molar mass of a polymer (Figure 1.14, blue curve). This phenomenon is described by *Martin’s Rule* (Equation 1.19), an empirical equation that correlates the retention factor k_{LAC} with the degree of polymerization DP_n [136, 139].

$$\log(k_{LAC}) \propto DP_n \quad (1.19)$$

where $k_{LAC} = \frac{t_{solute} - t_0}{t_0}$

where t_{solute} is the retention time of the solute and t_0 is the elution time of the injection solvent [129]. The retention factor k_{LAC} and distribution coefficient K_{LAC} are related as described in Equation 1.20 [129]:

$$k_{LAC} = \frac{K_{LAC} \cdot V_s}{V_0} \quad (1.20)$$

where V_s refers to the volume of the stationary phase and V_0 gives the volume of the mobile phase.

High molar mass polymers strongly interact with the column material as their high degree of polymerization favors the formation of multiple bonds with the stationary phase. For high molar mass polymers, irreversible adsorption is often observed. As a consequence of such strong enthalpic interactions, LAC experiments require the use of gradients. This contrasts with SEC and LCCC experiments, which are isocratic techniques. In the following section, gradient polymer elution chromatography (GPEC) is described more detailed. More precisely, solvent gradient interaction chromatography (SGIC) and temperature gradient interaction chromatography are highlighted (TGIC).

1.11. Gradient Polymer Elution Chromatography

1.11.1. Solvent Gradient Interaction Chromatography

In a typical SGIC experiment, a polymer is injected into a column while using a weak eluent as a mobile phase. Depending on the solvent quality of the eluent, and the stationary phase, the polymer molecules either precipitate or adsorb to the stationary phase. Subsequently, the eluent strength is gradually increased by adding a strong solvent. The volume fraction of strong solvent is given by ϕ . Upon increasing ϕ , the polymer desorbs, dissolves, and starts eluting. Here, separation occurs according to the affinity of the polymer molecules for adsorption to the stationary phase.

Notably, the affinity for adsorption depends on chemical composition and molar mass [117, 129].

For a certain eluent composition, critical conditions are reached. Generally, two cases must be distinguished. In the first scenario, the polymer is completely dissolved, when critical conditions are reached. This means that $\phi_{crit} > \phi_{sol}$. Here ϕ_{crit} refers to the volume fraction of strong solvent at critical conditions and ϕ_{sol} is the volume fraction of strong solvent that is needed to dissolve the polymer completely [117].

In a typical experiment, low molar mass fractions of the sample desorb/dissolve first and elute. Subsequently, ϕ_{sol} is reached and all polymer fractions desorb and dissolve. Upon reaching ϕ_{crit} , the remaining high molar mass fractions of the sample elute in LCCC mode, independent of their molar mass, only dependent on chemical composition and functionality of the polymer fractions [117].

The second scenario is given for $\phi_{crit} < \phi_{sol}$. In this case, critical conditions are reached before all polymer fractions desorb and dissolve. Thus, elution of the fractions depends on molar mass and chemical composition [117].

Because of the changing eluent composition, there is a limited number of detection methods available for GPEC. Most often UV detectors or evaporative light scattering detectors (ELSD) are applied [117, 129].

GPEC allows to analyze the CCD of copolymers [129, 140]. Moreover, copolymers can be separated by architecture as demonstrated by Glöckner *et al.* [141] who applied GPEC to differentiate copolymers of styrene and t-butyl methacrylate according to their statistical and block constitution.

Silica is a widely used stationary phase in LAC/IC applications. However, for hydrophilic polymers the use of bare silica columns is problematic as the molecules tend to irreversibly adsorb to the column material [142]. Here, columns packed with C18-functionalized silica are commonly used in combination with mixtures of water and organic solvents as mobile phase. This type of chromatography using hydrophobic columns and polar eluents is often referred to as reversed-phase high performance liquid chromatography (RP-HPLC) [41].

In 2018, Perrier *et al.* [142] suggested a gradient RP-HPLC method to analyze hydrophilic copolymers (containing ionic groups) according to their composition. They showed that GPEC using water/acetonitrile and water/methanol gradients can

separate various water-soluble copolymers by composition but also by architecture (*i.e.* statistical and multiblock).

1.11.2. Temperature Gradient Interaction Chromatography

Besides changing the eluent quality, the retention behavior of polymers can be triggered by changing the temperature. This type of chromatography experiments is referred to as temperature gradient interaction chromatography (TGIC). In praxis, TGIC can be applied for molar mass separation with high resolution [143]. Moreover, copolymers and blends can be investigated regarding chemical composition distribution [144, 145].

In contrast to SGIC, TGIC experiments are commonly carried out isocratically at a fixed eluent composition [117]. However, eluent and temperature gradients can be combined to separate copolymers or blends with high efficiency [146].

The useful range of temperatures is bracketed by the physical properties of the mobile phase (*i.e.* freezing and boiling point) [129]. Compared to eluent gradients, where the quality of the mobile phase can be adjusted within a wide range, changing the temperature only allows moderate variations of the solvent quality. This complicates the method development and analysis of broadly disperse or multicomponent samples. Consequently, the mobile phase has to be chosen carefully in TGIC experiments [129].

For the analysis of a polymer with an upper critical solution temperature (UCST), the sample is injected into the column at a temperature below critical condition ($T < T_{LCCC}$). Consequently, the molecules adsorb to the column material. An increase in temperature improves the solubility of the UCST polymer in the mobile phase, and desorption and the onset of elution is induced. On the contrary, LCST polymers (*Chapter 1.1.5*) may require reversed temperature gradients as solubility increases upon cooling [129].

1.12. 2D-Chromatography

Complex polymers are disperse in more than one dimension, meaning that besides a distribution of molar mass (MMD) also a distribution of the chemical composition

(CCD) and possibly also in architecture and end groups has to be considered. Indeed, the total heterogeneity of a complex polymer has to be described by superimposing all aspects of dispersity [41]. To this end, the combined use of multiple LC techniques is essential [147, 148].

The combination of two chromatographic techniques to characterize polymer samples is referred to as two-dimensional (2D)-chromatography. Theoretically, all kinds of separation methods can be coupled with each other. To map molecular heterogeneity as precise as possible, it is recommended to choose two orthogonal techniques. Orthogonality refers to the independence of both dimensions. If both separation dimensions work completely independent, each dimension discloses one specific molecular characteristic [149]. In practice, many conceivable combinations of LC techniques potentially suffer from incompatibility issues. For instance, the mobile phase of the first dimension might impact the separation in the second dimension [150].

A widely applied procedure is the combination of LCCC in the first dimension and SEC in the second dimension. Alternatively, SGIC can be coupled with SEC. In this way, information on CCD and MMD of the sample can be revealed. Notably, up to a certain degree, all mentioned techniques, LCCC, SGIC and SEC depend on the molar mass indicating that they are not perfectly orthogonal. The coupling of these methods can be carried out offline or online [149–151].

In a typical offline experiment, multiple fractions eluting from the first dimension are collected (by hand or with the help of a fraction collector) and then manually transferred and injected into the second dimension. Offline experiments are work intense and in many cases only few fractions from the first dimension are selected and injected into the second dimension. This selective approach is often referred to as "heart cutting" technique and is denoted as LC-LC [149].

The fractionation and transfer process can be automatized using a multiport valve system. In a comprehensive online experiment, all fractions from the first dimension are continuously transferred to the second dimension [41] which is often referred to as LCxLC. Online coupling provides a maximum insight into heterogeneity within a sample as no fraction is discarded [149].

When the LC methods of each dimension are operated individually, each LC separation gives a chromatogram. In contrast, the result of an online 2D-analysis can be visualized using a contour plot. The x and y-axis give the elution volumes of

the first and second dimension, while the intensity of the (second) detector is coded using a color scale.

For the purpose of illustration, the analysis of PEGMA using LCCC (at critical conditions of MPEG) and SEC is presented in Figure 1.16, where Figure 1.16a and Figure 1.16b show the chromatograms obtained when both dimensions are applied individually. Additionally, Figure 1.16c shows a contour plot obtained *via* online LCCC \times SEC. Notably, the presented data was calculated for illustration purpose and not experimentally measured.

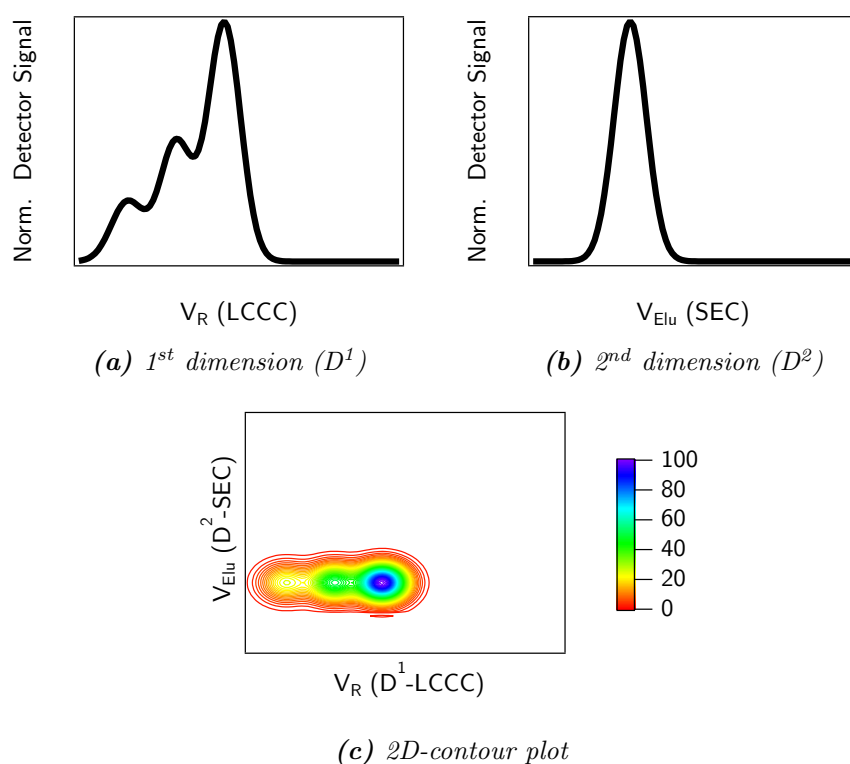


Figure 1.16. Hypothetical 2D-analysis of PEGMA. The data presented in this Figure was not measured but calculated assuming Gaussian distributions in both dimensions. (a)-(b) Chromatograms obtained from independent LCCC and SEC analysis of PEGMA. (c) Contour plot obtained via LCCC \times SEC of PEGMA.

In the hypothetical LCCC data of PEGMA, three different peaks can be identified (Figure 1.16a). The SEC analysis of the same sample shows only one well-defined peak (Figure 1.16b). Consequently, the sample contains three species which are chemically different, but which adopt a similar hydrodynamic size (similar molar mass).

PEGMA is a macromonomer that is often applied in PCE synthesis and which is obtained *via* esterification of methacrylic acid (MAA) with poly(ethylene glycol) (PEG). Normally, Methoxy poly(ethylene glycol) (MPEG) is applied for the esterification, however, MPEG (mono-functional) potentially contains traces of $\alpha - \omega$ -dihydroxy-PEG (bi-functional).

LCCC reveals three species, consequently, it can be assumed that the macromonomer contains impurities of both PEG derivatives due to an incomplete esterification process. The order of elution of the different species is directly related with the polarity of their end groups. $\alpha - \omega$ -dihydroxy-PEG is very polar due to two hydroxy moieties, while PEGMA is rather hydrophobic due to the double bond attached to its end. On a typical reverse phase column (*e.g.* C18 column), the retention time increases with decreasing polarity of the solute.

All in all, this example emphasizes that the combined use of two LC techniques (LCxLC) is a powerful tool enabling to access information on dispersity in chemical functionality and molar mass within a polymer sample.

Regarding PCEs, the work of Adler *et al.* [116] is prime example for 2D-chromatography. Similar to the hypothetical example shown in the previous section, they combined LCCC under critical conditions of MPEG with SEC measurements. This allowed them to separate and identify PCEs from impurities (*e.g.* residual macromonomer and MPEG) and byproducts (*e.g.* homopolymerized macromonomer) of the PCE synthesis.

1.13. Implications of the State of the Art

This state-of-the-art chapter has emphasized that PCEs are interesting research subjects from two perspectives. First of all, their comb copolymer architecture and polyelectrolyte characteristics make them highly relevant for polymer science and analytics. Secondly, their ability to plasticize cement pastes makes them an indispensable part of modern concrete technology with large scale applications.

In common admixture research, several PCEs are compared in regard to their plasticizing abilities. As pointed out in the previous sections, PCE synthesis can produce countless structures with different chemistry and composition. Consequently, it becomes increasingly difficult to select and compare PCEs on a meaningful basis.

Moreover and most generally, the macroscopic performance of PCEs is the sum of processes on the (sub)molecular level. Hence, a better understanding of the molecular level is essential to comprehend and predict the performance of PCEs as superplasticizers.

As previously described, the dispersing mechanism of PCEs heavily relies on their adsorption onto the cement surface. Here, literature falls short of studies that characterize the adsorption behavior of PCEs considering their molecular parameters and their molecular heterogeneity. There are several reasons for this research gap. For instance, common characterization methods to study adsorption, such as total organic carbon measurements, do not directly reveal molecular level effects. Moreover, correlations between molecular architecture and adsorption can only be drawn, when the exact molecular composition of the PCE is known. Therefore, it is important to characterize PCEs beyond average characteristics. However, accessing the dispersity within PCEs calls for more elaborated analytical methods than normally used.

As pointed out in the second part of the state-of-the-art, there have been several studies on PCE characterization by spectroscopy and chromatography. However, these were solely focused on the PCE characterization itself and this is where the main problem of PCE research lies. In many cases, researchers are either focused on admixture research and neglect the polymer analytics or *vice versa*.

A main objective of this thesis is to contribute to overcoming this division. Thereby, its approach relies both on deriving meaningful models that relate the PCE molecular structure with their macroscopic performance, as well as developing advanced characterization of methods to provide more substantial information on PCE dispersity.

Synthesis of Poly(carboxylate ethers)

Parts of the present chapter were published in the Results and Appendices of the research articles listed below. All elements that were taken from these publications were entirely written by S. A. Weckwerth and revised by Prof. Flatt.

Weckwerth *et al.*, *Cement and Concrete Research*, **2022**, Volume 151, 106523,
[doi:10.1016/j.cemconres.2021.106523](https://doi.org/10.1016/j.cemconres.2021.106523)

Weckwerth *et al.*, *Polymers*, **2021**, 13(12):1921,
[doi:10.3390/polym13121921](https://doi.org/10.3390/polym13121921)

2.1. Context

The synthesis of poly(carboxylate ethers) (PCEs) with systematic variations in molecular structure is essential for admixture research. In this regard, it is important to underline that publications on the subject have moved towards providing full molecular structures, something which was not initially the case. In this sense, the work by the group of Prof. Johann Plank has clearly contributed to a “more open book” position in the field.

Concerning working mechanisms, on the one hand, PCEs with distinct molecular properties are needed to study their adsorption behavior at the cement surface and to investigate structure-performance relations of superplasticizers. But importantly, PCEs with well-defined characteristics are also needed for the development of characterization methods to study the dispersity within PCEs.

The present chapter provides comprehensive information on synthesis and characterization of PCEs that were used throughout this thesis. PCEs with systematic variations in molecular structure (*i.e.* grafting ratio, backbone length and side chain length) were synthesized pursuing different synthesis pathways. Synthesis and characterization protocols are described at length. Notably, this chapter is not purely descriptive, as the outcome of various synthesis and characterization experiments is discussed.

All in all, the present chapter provides the means to synthesize a library of PCEs with systemic variations of their molecular characteristics. Hence, it lies the groundwork for the development of liquid chromatography based analysis of molecular dispersity (*Chapter 3* and *Chapter 4*) and the studies on PCE adsorption at the cement surface (*Chapter 5* and *Chapter 6*).

2.2. Nomenclature of PCEs

Throughout this work, MPEG-type PCEs (see *Chapter 1.4*) with a poly(methacrylic acid) (PMAA) backbone were used. These PCEs were produced pursuing different strategies. The synthesis method is indicated by a *prefix*. PCEs from RAFT polymerization are termed R-PCE. PCEs obtained *via* free radical copolymerization are termed FRC-PCE and such from polymer-analogous esterification (= grafting of a precursor PMAA) are labelled G-PCE.

C/E and side chain length P are indicated as *suffix*. Here, C/E refers to the numeric ratio between carboxylate groups (C) and side chain bearing ester groups (E) along the PCE backbone. P gives the number of ethylene oxide (EO) repeating units of the side chain. A representative molecular structure of a PCE is shown in Figure 1.1.

Example: G-PCE-4.0-22 refers to a PCE synthesized by grafting of a precursor backbone with MPEG side chains consisting of 22 units ($M_w \approx 1000$ g/mol). The C/E of this PCE is 4.0 as determined from $^1\text{H-NMR}$ of the purified polymer.

2.3. RAFT Polymerization

2.3.1. Chemicals

The following chemicals were purchased from Sigma Aldrich (now Merck) and were used as received: 2-Methacrylic acid (MAA, 99 % with 250 ppm MEHQ as inhibitor), poly(ethylene glycol) methyl ether methacrylate (Table 2.1), 4-(((2-Carboxyethyl)thio) carbonothioyl) thio)-4-cyanopentanoic acid (CTA, RAFT agent), 4,4-Azobis (4-cyanopentanoic acid) (ACPA, radical initiator) and 1,3,5-Trioxane (≥ 99 %, internal reference for $^1\text{H-NMR}$ analyses). Furthermore, D_2O (99.9 atom % D) was used as solvent for $^1\text{H-NMR}$ spectroscopy). All organic solvents were of analytical grade. Water was purified by a Millipore Milli-Q filtration system from Merck ($\text{TOC} \leq 2$, $\rho = 18.2 \text{ M}\Omega \cdot \text{cm}$).

Table 2.1. Applied PEGMA Monomers. All chemicals were purchased from Sigma Aldrich (now Merck) and used without further purification. M_n is given in g/mol. P refers to the number of EO repeating units in the PEGMA macromonomer.

	M_n	P	Inhibitor (ppm)
PEGMA-4	300	4	BHT (300)+MEHQ (100)
PEGMA-9	500	9	BHT (200)+MEHQ (100)
PEGMA-19	950	19	BHT (300)+MEHQ (100)
PEGMA-43	2000	43	-

2.3.2. Synthesis Protocol

PCEs of different C/E and different side chain lengths P were synthesized by RAFT copolymerization of MAA and the macromonomers shown in Table 2.1. The aimed backbone length of all PCEs can be adjusted by the ratio between monomer and RAFT agent. It was approximately 60:1 in all polymerizations. The ratio between RAFT agent and initiator was kept as low as possible (10:1) to guarantee initiation of the polymerization but avoid uncontrolled propagation.

Table 2.2 gives information about the educts involved in further synthesis. Water was preferably chosen as solvent for the polymerization. Notably, organic solvents were added for the synthesis of PCEs with high C/E or shorter side chains to guarantee solubility of the PCE and to adjust the reaction rate of MAA and PEGMA macromonomer.

2. Synthesis of Poly(carboxylate ethers)

MAA and PEGMA were dissolved in the chosen solvent (ultrapure water or mixture with dioxane). The solution was filled into a round bottom flask that was sealed with a septum. Subsequently, CTA and 1,3,5-trioxane (0.1 mol/L) were added. The CTA can optionally be dissolved in 1-2 mL of dioxane prior to addition to improve its solubility in the reaction mixture. Subsequently, the solution was degassed by bubbling with nitrogen. After 60 minutes, the nitrogen stream was turned off and the radical initiator was added. The polymerization was initiated by increasing the temperature to 80 °C using an oil bath. During the polymerization, the temperature was kept constant at 80 °C and the reaction mixture was continuously stirred with a magnetic stirring bar. Small samples were withdrawn to monitor conversion over time. For this, the aliquot was injected into cooled D₂O to stop the polymerization. The monomer conversion was calculated from 1H-NMR spectroscopy by relative integration of the protons of trioxane and the vinylic monomers, as described in Section 2.6.3.

Table 2.2. Experimental conditions and conversions of several RAFT copolymerizations. The molar ratio [Monomer]:[CTA] was kept at 60:1 and [CTA]:[ACPA] was 10:1. Water was used as solvent. For PCEs with higher charge and/or lower side chains lengths, dioxane was added to improve the solubility and adjust reaction rates. The volumetric ratio between water and dioxane was 1:1. The monomer conversion was calculated from 1H-NMR. The nomenclature of all PCEs follows the following pattern: R-PCE-C/E-P.

R-PCE	$\frac{[\text{MAA}]}{[\text{PEGMA}]}$	[Monomer] (mol/L)	Solvent	Time (min)	Conv. (%)	
					x _{MAA}	x _{PEGMA}
R-PCE-0.7-19	0.5	0.21	water	240	100	100
R-PCE-1.2-19	1.1	0.20	water	270	97	95
R-PCE-2.0-19	2.0	0.20	water	455	95	95
R-PCE-2.8-19	3.0	0.20	water	480	93	90
R-PCE-4.0-19	4.0	0.20	water/diox	600	90	89
R-PCE-9.0-19	8.0	0.49	water/diox	630	95	90
R-PCE-1.7-4	2.1	0.19	water	600	87	81
R-PCE-1.7-9	2.0	0.20	water	480	100	91
R-PCE-1.7-9	2.0	0.20	water/diox	540	89	84
R-PCE-2.0-43	2.0	0.50	water	1710	92	91

Upon stagnation of the conversion, the reaction was stopped by cooling with an ice bath. The product was purified by dialysis and dried *via* lyophilization when needed. Lyophilization is essential when the R-PCEs are stored for longer times to prevent end group hydrolysis. However, it has to be noted that lyophilization might cause partial decarboxylation of the carboxylic acid group in the backbone (see Chapter 3.7). The C/E ratio of the dried product was calculated from 1H-NMR

(Section 2.6.3) and the molar mass distribution was obtained from aqueous SEC (Section 2.6.2).

2.3.3. Calculation of Molecular Parameters

The controlled nature of the RAFT process allows to calculate the theoretical molar mass M_{theo} and the ratio $(C/E)_{theo}$ of the product according to Equation 2.1 and 2.2, where M_{MAA} is the molar mass of the methacrylic acid monomer and M_{PEGMA} the molar mass of the macromonomer. M_{CTA} is the molar mass of the RAFT agent. $[MAA]_0$ and $[PEGMA]_0$ are the initial monomer concentrations of the comonomers prior to initiation of the reaction and $[CTA]_0$ is the corresponding concentration of the RAFT agent. x_{MAA} and x_{PEGMA} are the conversions of the monomers calculated from 1H-NMR relative to the trioxane peak (Table 2.2).

$$M_{n,theo} = M_{CTA} + \frac{(M_{MAA} \cdot [MAA]_0) \cdot x_{MAA}}{[CTA]_0} + \frac{(M_{PEGMA} \cdot [PEGMA]_0) \cdot x_{PEGMA}}{[CTA]_0} \quad (2.1)$$

$$(C/E)_{theo} = \frac{[MAA]_0 \cdot x_{MAA}}{[PEGMA]_0 \cdot x_{PEGMA}} \quad (2.2)$$

$M_{n,theo}$ can be regarded as a number-averaged molar mass. When comparing the calculated value to the measured value from SEC, a good agreement can be found for all samples (Table 2.3). Analog to the molar mass, also the C/E ratio of the PCE can be calculated ($(C/E)_{theo}$). $(C/E)_{theo}$ values are in good agreement with the $(C/E)_{NMR}$ for the purified PCE (Section 2.6.3). C/E can be varied by changing the molar ratio between MAA and PEGMA. Assuming both monomers show similar reactivity rates, a homogeneously grafted PCE of narrow dispersity is obtained.

This emphasizes the advantage of a living polymerization technique such as RAFT over conventional free radical copolymerization. The molecular parameters of the PCE (*i.e.* C/E and backbone length) can be predicted and adjusted from the stoichiometry of the reactants. For instance, the degree of polymerization can be tailored by changing the ratio between monomers and CTA. This allows to adjust the backbone length. As can be seen in Table 2.3, most reactions showed a total

2. Synthesis of Poly(carboxylate ethers)

monomer conversion of 90 % or higher. As an alternative to changing $\frac{[Monomer]_0}{[CTA]_0}$, the reaction can be stopped as soon as the desired conversion is reached.

Table 2.3. Information on number-average molar mass and C/E ratio of several R-PCEs. The individual monomer conversion was used to calculate the theoretical molar mass $M_{n,theo}$ according to Equation 2.1 and $(C/E)_{theo}$ according to Equation 2.2. The theoretical values are compared with M_n obtained from SEC and the grafting density obtained from 1H -NMR. Molar masses are given in kg/mol.

R-PCE	$M_{n,theo}$	$M_{n,SEC}$	\mathfrak{D}	$(C/E)_{theo}$	$(C/E)_{NMR}$
R-PCE-0.7-19	38.0	47.5	1.05	0.5	0.7
R-PCE-1.2-19	29.2	31.5	1.01	1.1	1.2
R-PCE-2.0-19	21.5	23.3	1.04	2.0	2.0
R-PCE-2.8-19	17.1	18.6	1.05	3.0	2.8
R-PCE-4.0-19	14.2	15.2	1.01	3.9	4.0
R-PCE-9.0-19	10.5	11.5	1.01	7.6	9.0
R-PCE-1.7-4	8.2	11.0	1.03	1.9	1.7
R-PCE-1.7-9	13.3	14.7	1.01	1.9	1.7
R-PCE-1.7-9	12.0	9.0	1.01	1.9	1.7
R-PCE-2.0-43	35.8	44.0	2.12	2.3	2.0

2.3.4. Molar Mass Distribution

For polymerizations where the chain growth is well controlled by the RAFT agent and where side reactions such as termination or homopolymerization do not occur, Equation 2.1 gives a good estimate for the M_n of the PCE. Living polymerization techniques usually allow the synthesis of macromolecules of low dispersity ($\mathfrak{D} < 1.05$). The dispersity in molar mass of a PCE cannot be estimated from calculations. This calls for SEC measurements.

The dispersity index of all R-PCEs-C/E-19 ($P=19$) is below 1.1 indicating a low heterogeneity of the polymers regarding molar mass (*i.e.* hydrodynamic size). The corresponding chromatograms of the samples are shown in Figure 2.1a. All PCEs elute in well-defined, narrow peaks. Although showing significantly different grafting densities, all R-PCE-C/E-19 have similar elution volumes (24-28 mL) and the elution peaks are overlapping significantly. This is due to similar hydrodynamic sizes of the comb shaped polymers. With increasing grafting density, the elution peak is shifted slightly to lower volumes.

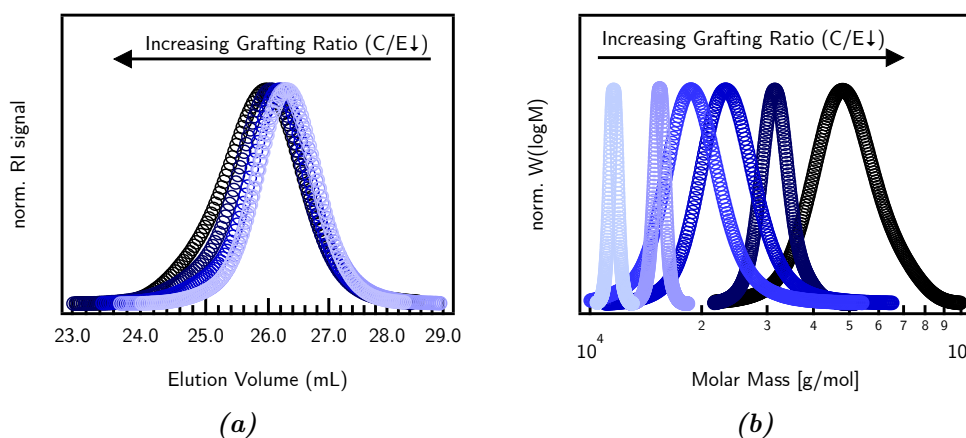


Figure 2.1. a) Chromatograms of R-PCEs-C/E-19 synthesized by RAFT copolymerization of PEGMA-19 and MAA. Information on the synthesis and molar mass of the PCEs can be found in Table 2.2 and Table 2.3. All samples elute at similar elution volumes in well-defined elution peaks, indicating a low dispersity. As all R-PCEs feature a similar backbone length, the minimal variations in the peak maximum are caused by the grafting ratio. With decreasing C/E, the peak is slightly shifted to lower volumes. (b) Molar mass distribution of the chromatograms shown in (a). With increasing grafting ratio, the molar mass increases due to a higher number of side chains in the PCE comb.

Notably, a PCE of high grafting density (low C/E) and short backbone can adapt the same hydrodynamic volume as a PCE with low grafting density (high C/E) and long backbone. This leads to coelution of PCEs with different molecular composition. For homogeneously grafted PCEs obtained from controlled synthesis, coelution phenomena are less relevant. However, PCEs synthesized by free radical techniques are composed by a variety of molecules with different C/E and backbone length. Therefore, coelution has to be considered to impact the molar mass distribution (MMD).

The MMDs shown in Figure 2.1b are absolute molar masses obtained from SEC with MALLS/RI detection. With increasing grafting density, the MMD is shifted to higher masses due to the presence of more side chains in the polymer comb.

2.3.5. Monitoring the Reaction Progress

To verify if both comonomers are consumed at similar rates, the conversion of MAA and PEGMA was monitored. Figure 2.2 shows the conversion of the comonomers in dependence on the reaction time for several R-PCEs with a constant side chain length of $P=19$. The C/E ratio varies between 0.7 and 9.0. For $1.2 \leq C/E \leq 4.0$,

2. Synthesis of Poly(carboxylate ethers)

both monomers are consumed at similar rates indicating a statistic distribution of MAA and ester groups along the formed PCE backbone (Figure 2.2b-2.2e)

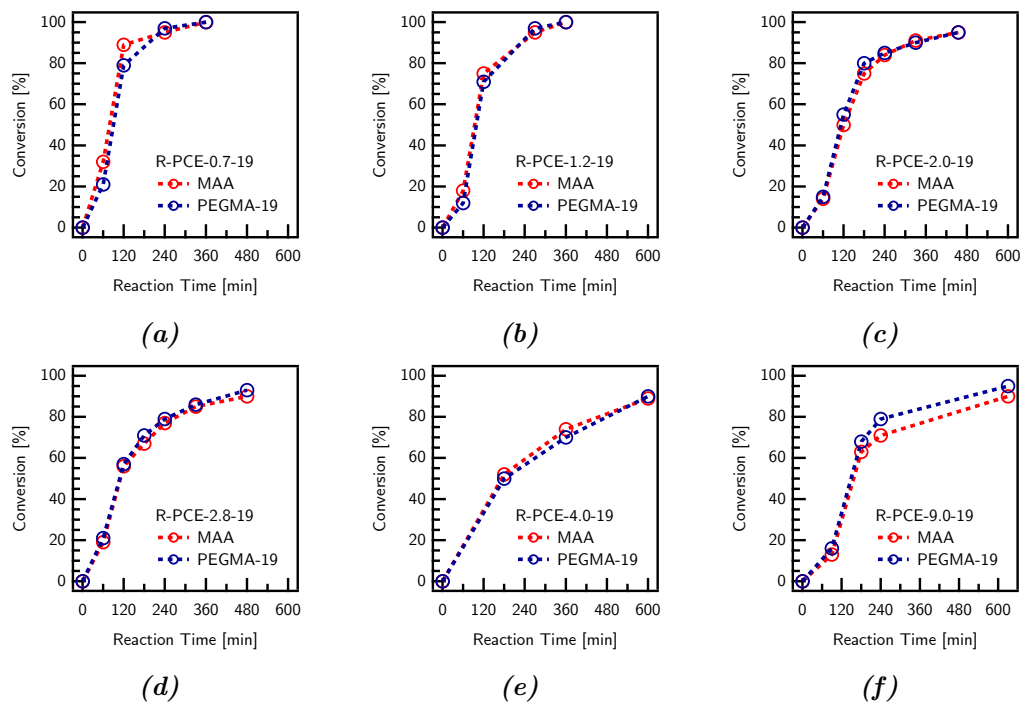


Figure 2.2. a) Conversion of comonomers (PEGMA-19 and MAA) in dependence of time. a) PCE with a high grafting density. MAA is faster consumed within the first 120 minutes of polymerization, leading to a gradient distribution of charges and side chains along the backbone b-e) Both monomers are consumed at similar rates. The resulting R-PCE is homogeneously grafted. f) PCE with a low grafting density (high charge density). The macromonomer is preferentially incorporated in the beginning, leading to a gradient structure.

For the lowest C/E (R-PCE-0.7-19; Figure 2.2a), methacrylic acid is consumed slightly faster within the first 120 minutes of polymerization, leading to a PCE with increased charged density in the beginning of the backbone. In contrast, the PCE with the lowest grafting ratio (R-PCE-10.0-19; Figure 2.2f) reveals an increased incorporation of the macromonomer during the beginning of the polymerization.

2.3.6. Different Side Chain Lengths

Different reactivity of MAA *vs.* PEGMA is of particular importance when synthesizing PCEs with different side chain lengths. As can be seen from Figure 2.3a-2.3b, PEGMA-4 and PEGMA-9 are preferentially incorporated into the PCE when polymerized in aqueous solution. The reactivity rates depend on multiple factors

such as stability of the formed radical, pH or used solvent. By adding dioxane (polar, aprotic solvent) to the reaction mixture, the reactivity of PEGMA-9 and MAA was adjusted to yield a homogeneous comb structure (Figure 2.3c).

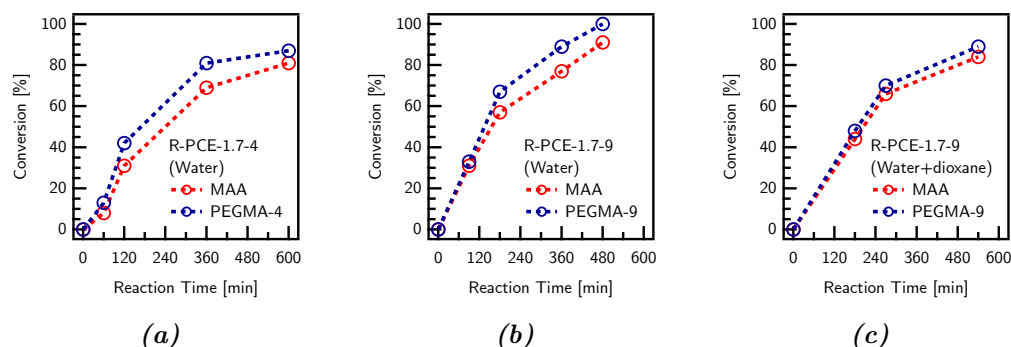


Figure 2.3. Synthesis of R-PCEs with short side chains. The conversion of the comonomers is plotted against time. For the synthesis of R-PCE-1.7-4 (a) and R-PCE-1.7-9 (b), the macromonomer is preferentially incorporated into the PCE, causing a gradient structure. (c) The addition of a polar aprotic solvent allowed to adjust the reactivity rates of PEGMA-9 and MAA to yield a homogenous grafted comb.

Regarding the synthesis of R-PCEs with increased side chain length, steric hindrance has a major impact on the chain growth. According to Figure 2.4a, the synthesis progresses significantly slower compared to the previously discussed polymerizations involving shorter side chains. After 10 hours of polymerization, less than 40 % of the monomers have been converted. The monomers seem to be consumed at similar rates, however, the corresponding molar mass distribution (Figure 2.4b) is very broad ($\bar{M}_w/\bar{M}_n=2.12$, Table 2.3) and reveals a shoulder at high molar masses. The increased dispersity hints at a lack of control during the reaction and termination by recombination. Moreover, it is feasible that the comonomers homopolymerized leading to PMAA (low molar mass fraction) and PPEGMA (high molar mass fraction).

The polymerization procedure for R-PCEs with long side chains was not improved further. Nonetheless, an increase of the monomer concentration might help to optimize the reaction rates. Moreover, a change of solvent, pH and/or CTA might be necessary to yield homogeneously grafted R-PCEs. The synthesis of R-PCE-2.0-43 emphasizes the importance of characterizing R-PCEs with size exclusion chromatography. Indeed, M_n can be estimated using Equation 2.1. Nonetheless, this calculation is only valid when the RAFT synthesis is well controlled by the CTA. The dispersity in molar mass is only revealed by chromatography.

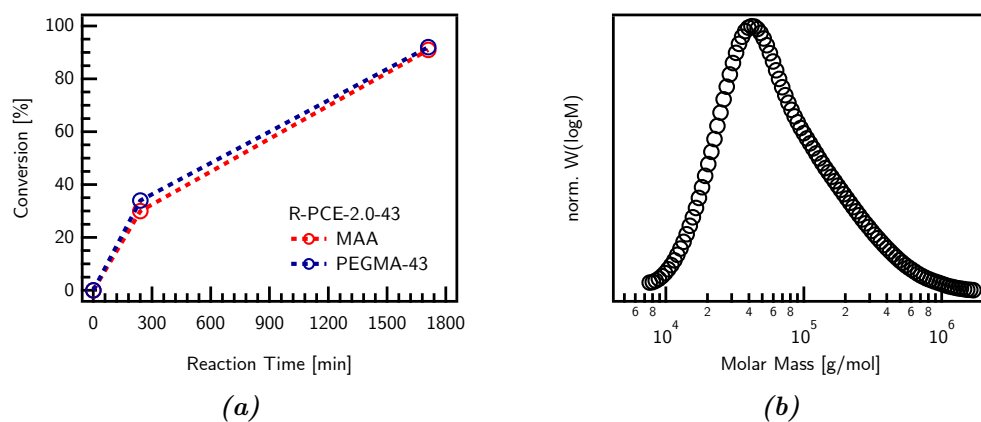


Figure 2.4. Synthesis of R-PCES with long side chains. Information on monomer conversion (a) and molar mass distribution (b) of R-PCE-2.0-43. The MMD is very broad ($\mathcal{D} > 2$) and shows a shoulder at high molar masses.

2.3.7. Living Character of RAFT

The CTA added to the RAFT synthesis controls the growing chain end. Termination and chain transfer processes are suppressed. Thus, the RAFT process can be considered a “living polymerization technique”. For this type of polymerization, a particular dependence of monomer concentration $[M]$ and reaction time t can be found:

$$\frac{-d[M]}{[M]} = \text{const} \cdot dt \quad (2.3)$$

The proportionality constant of this expression depends on multiple factors (*i.e.* the propagation rate and the CTA concentration). Integration of Equation 2.3 from 0 to t and inserting the monomer conversion x results in the following expression (Equation 2.4):

$$-\ln(1-x) = \text{const} \cdot t \quad (2.4)$$

with $x = 1 - \frac{M(t)}{M_0}$

A linear increase of $-\ln(1-x)$ with reaction time was found for all copolymerization of MAA with PEGMA described in Table 2.2. Exemplarily, the data for

three R-PCEs was replotted according to Equation 2.4 (Figure 2.5). The slope of the lines gives information about the reaction velocity. As a general trend it was found that the reaction progresses faster when a lower C/E (higher grafting density) is targeted underlining the high reactivity of the macromonomer. However, a detailed quantification and comparison of the slopes is not meaningful as the polymerizations were carried out in different solvents.

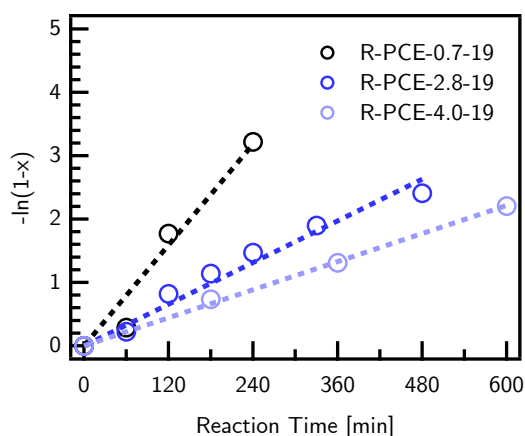


Figure 2.5. Living Character of the RAFT synthesis. The characterization follows the kinetics of a living polymerization according to Equation 2.4

This chapter is focused on the synthesis of statistical copolymers of MAA and PEGMA. However, the living character of the RAFT process allows the synthesis of block copolymers in two steps. Theoretically, one block could be synthesized first (*e.g.* homopolymerization of MAA). The resulting PMAA chains carry a RAFT group at each chain end. Thus, the first block can be considered as a RAFT-macroinitiator. Further addition of PEGMA (and initiator) will result in the polymerization of a second block onto the first one.

2.3.8. Concentration Detection via UV-Vis Spectroscopy

Many chain transfer agents applied for RAFT polymerization are thiocarbonyl based. In this study, CTAs with trithiocarbonate chemistry were applied. The RAFT polymerization mechanism leads to an $\alpha - \omega$ chain end modification of the synthesized polymer. The so-called Z-group at the backbone end (thiocarbonyl moiety) features genuine absorption bands in the UV and visible range. Thus, RAFT synthesized polymers are commonly colored in shades of yellow, orange or red due to a weak absorption of the thiocarbonyl group in the visible range ($n - \pi^*$ transition).

2. Synthesis of Poly(carboxylate ethers)

Figure 2.6 shows an absorption spectrum of R-PCE-1.9-19 recorded in the wavelength range between 260 and 600 nm. For wavelengths longer than 400 nm the absorption values were multiplied with factor 100 for magnification. The weak $n - \pi^*$ transition is found for $\lambda = 440$ nm (blue spectrum).

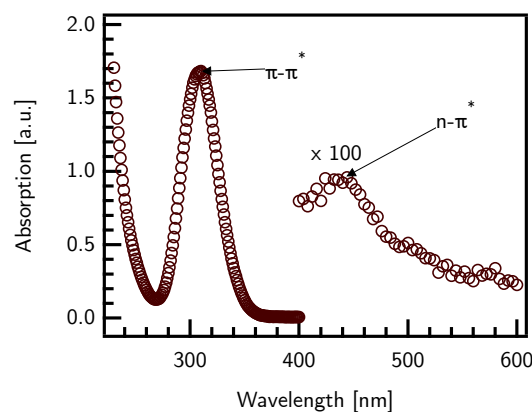


Figure 2.6. UV-Vis absorption spectra of R-PCE-1.9-19 recorded between 260 and 800 nm. For longer wavelengths, the absorption values were multiplied with factor 100 for magnification. At 440 nm a weak absorption peak is visible. Moreover, a strong absorption is found near the UV range (309 nm).^a

Consequently, the R-PCE solution appears to be yellow to the human eye. Additionally, thiocarbonyl groups feature a very strong absorption band ($\pi - \pi^*$ transition) near the UV range (typically around 305-315 nm). Due to its strong absorptivity, this band can be used for end-group analysis using UV-Vis absorption spectroscopy.

Assuming that each chain end is modified with a Z-group, the strong absorption of R-PCEs was used to calculate their concentration in solution according to *Lambert-Beer's Law*. For R-PCE-1.9-19, the maximum of absorption was found at 309 nm. The absorption value at this wavelength ($Abs@309$) was determined for a series of polymer solutions of known concentration (Figure 2.7a). Figure 2.7b shows that $Abs@309$ and concentration are direct proportional (*Lambert-Beer's Law*). The specific absorptivity coefficient of the R-PCE (α_{309}) was determined from a linear regression of a line passing through the origin, as shown in Figure 2.7b. It has to

^aThe absorption spectrum shown in Figure 2.6 exemplifies the absorption behavior of the R-PCEs synthesized and applied in this thesis. Notably, for different PCEs from different batches and synthesis, the absorption peaks and maxima can be slightly shifted even when the same RAFT-agent was applied.

be emphasized that for each R-PCE a new calibration has to be measured. Even if two R-PCEs carry the same functional group, the slope of the calibration line can be significantly different. With the attached chromophore being sensitive to hydrolysis, the calibration of a R-PCE has to be renewed frequently.

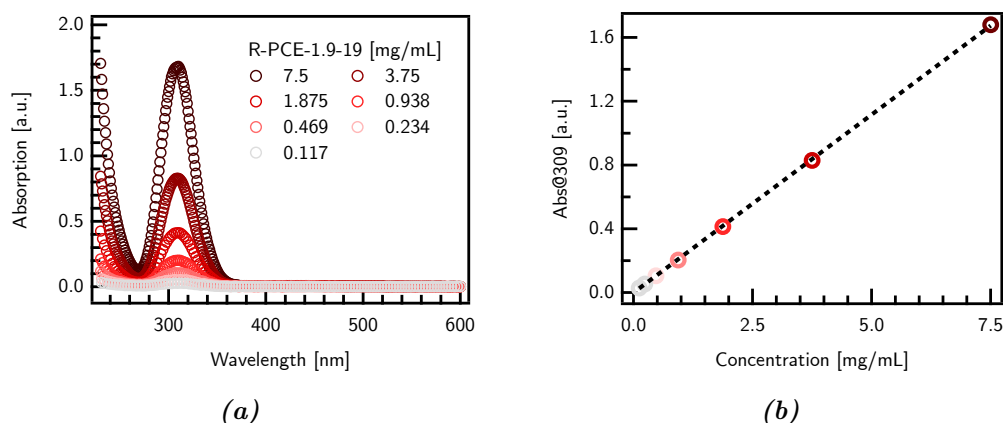


Figure 2.7. (a): UV-Vis absorption spectra of R-PCE-1.9-19 solutions with concentrations between 0.78 and 25 mg/mL; (b) Abs@309 vs. concentration. The absorption value increases linearly with the concentration of the polymer in solution. The slope of the regression line was found to be $0.1036 \frac{\text{a.u.}\cdot\text{mL}}{\text{mg}}$.

Subsequently, the amount of R-PCE in a solution of unknown concentration c_{PCE} can be calculated according to Equation 2.5. This procedure was followed to determine the concentration of R-PCE in pore solution (see *Chapter 5* and *Chapter 6*).

$$Abs@309 = \alpha_{309} \cdot c_{PCE} \quad (2.5)$$

2.3.9. Hydrolytic Stability of the RAFT group

Directly after the RAFT synthesis, each PCE backbone carries a Z-group. However, these moieties are connected *via* a labile thiocarbonylthio bonds that can be cleaved by hydrolysis, UV radiation or oxidation. When the thiocarbonylthio moiety is cleaved and in turn a thiol is formed, the strong UV activity is lost. For R-PCEs, high pH values are of concern due to the alkalinity of the pore solution. To verify the stability at different pH values, two solutions of R-PCE-1.9-19 (5 mg/mL; pH 4.7 and pH 13) were prepared. Figure 2.8a shows the evolution of the absorption value at 309 nm over the course of two weeks. The absorption on day 0 was set to 100 %, the remaining absorption was taken relative to this value.

2. Synthesis of Poly(carboxylate ethers)

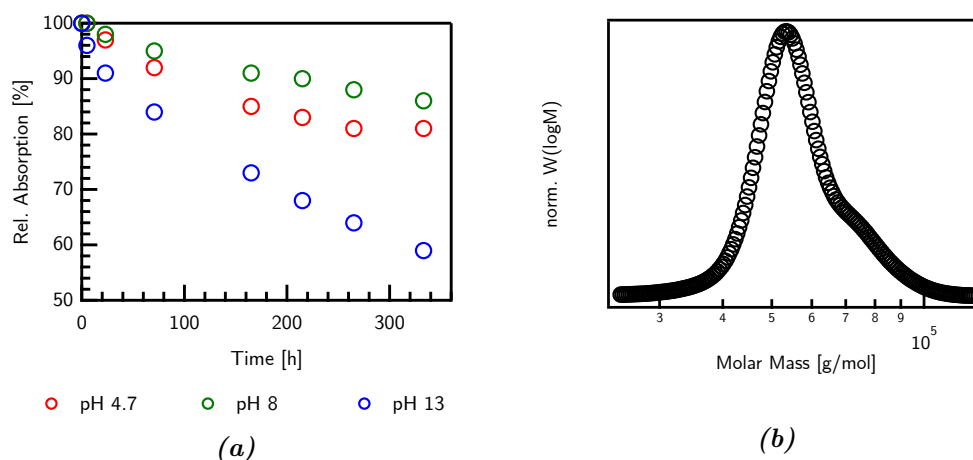


Figure 2.8. (a) Hydrolytic stability of R-PCE-1.9-19 at different pH value of the polymer solution. (b) Molar mass distribution of a R-PCE stored in alkaline solution prior to SEC analysis. A bimodal distribution was found due to the formation of disulfide bonds.

Within the first 5 hours, the solution of pH 4.7 and pH 8 remains at 100 % absorption. For the highly alkaline solution (pH 13), the relative absorption drops slightly to 96 % indicating that a high pH accelerates the hydrolysis of the RAFT end group. The two solutions of lower pH remain above 90 % relative absorption up to 72 hours after preparation, whereas the alkaline solution decreases to 84 %. As a general trend, it can be observed that the R-PCE undergoes the fastest hydrolysis at pH 13. Interestingly, the acidic solution hydrolysis faster than the solution of pH 8. The change in the absorption behavior upon hydrolysis must be considered when the end group is used for calculations of the concentration. Solutions should always be prepared freshly to achieve the highest accuracy.

Upon the hydrolysis, the R-PCE thiocarbonylthio moiety is cleaved and each backbone is terminated by a thiol group which does not feature UV absorption. However, thiol groups are well known to form disulfide bonds. This means that two PCE backbones can connect with each other *via* disulfide coupling. This phenomenon can be verified in the molar mass distribution. Besides the usual peak of the R-PCE, a second peak arises at roughly the double molar mass (Figure 2.8b).

Generally, trithiocarbonates were found to be more stable against hydrolysis than dithioester-based CTAs. For short term storage, R-PCE solutions were kept in the fridge and protected from light. If a R-PCE was stored for longer periods, it is recommended to lyophilize or freeze the PCE to prevent the loss of Z-groups by hydrolysis.

2.4. Free Radical Copolymerization

2.4.1. Chemicals and Synthesis Protocol

FRC-PCEs with different grafting densities were obtained from free radical copolymerization of methacrylic acid (MAA; contains 250 ppm 4-Methoxyphenol (MEHQ) as inhibitor; 99 %) and poly(ethylene glycol) methyl ether methacrylate (PEGMA-19, M_n 950 g/mol, Table 2.1) in aqueous media. As a chain regulator sodium 3-mercaptopropionic acid (MPA; for synthesis; Sigma Aldrich) was used and potassium persulfate ($K_2S_2O_8$; ACS reagent grade 99.0 %, Sigma Aldrich) was applied as a radical initiator. Water was purified by a Millipore Milli-Q filtration system from Merck ($TOC \leq 2$ ppb, $\rho = 18.2 M\Omega \cdot cm$). The exact amounts of educts are listed in Table 2.4.

Table 2.4. Applied Chemicals for free radical copolymerization of PCEs with different grafting degree. The nomenclature of the FRC PCEs follows the following pattern: FRC-PCE-C/E-P. Solution A and B were pumped at constant feed rates of 0.225 mL/min (A) and 0.141 mL/min (B). The time until complete addition of each solution is noted.

(a) Solution A

FRC-PCE	$\frac{[MAA]}{[PEGMA]}$	MAA [mmol]	PEGMA [mmol]	water [mL]	MPA [mmol]	time [min]
FRC-PCE-1.7-19	1.5	23.3	15.5	4.4	1.3	93
FRC-PCE-2.8-19	3.0	29.1	9.7	3.0	1.3	65
FRC-PCE-5.0-19	5.0	58.1	11.6	4.0	2.3	89

(b) Solution B

FRC-PCE	K_2SO_4 [mmol]	water [mL]	time [min]
FRC-PCE-1.7-19	0.4	18.0	119
FRC-PCE-2.8-19	0.4	12.2	87
FRC-PCE-5.0-19	0.8	16.1	114

(c) Reactor

FRC-PCE	water [mL]
FRC-PCE-1.7-19	11.2
FRC-PCE-2.8-19	8.3
FRC-PCE-5.0-19	10.8

Prior to synthesis, two solutions are prepared. Solution A contains the comonomers (MAA and PEGMA-19), ultrapure water, and mercaptopropionic acid. Solution B contains potassium persulfate dissolved in ultrapure water. A five neck round bottom flask (total volume 100 mL) was filled with water and was subsequently heated to 80 °C while being flushed with nitrogen to remove oxygen from solution.

2. Synthesis of Poly(carboxylate ethers)

The solution was stirred with an overhead stirrer (IKA[®] Eurostar power control visc). The nitrogen bubbling was continued during the whole synthesis process. After 20 minutes of heating and degassing, solution A and B were added to the reactor. For this purpose, a peristaltic pump (Ismatec ISM831C) was used to maintain a constant flow rate. Solution A was pumped with a rate of 0.225 mL/min (\approx 13.5 mL/h) and B was added at 0.141 mL/min (\approx 8.5 mL/h). After the addition of both solutions was finalized, the polymer solution was stirred for one more hour at 80 °C. During the reaction, the viscosity of the solution increased significantly. After cooling to room temperature, a viscous polymer solution was obtained, which was purified by dialysis. Subsequently, the C/E ratio of the PCEs was determined from ¹H-NMR measurements.

2.4.2. Molar Mass and Grafting Density

After purification, the grafting ratio of the PCEs was determined from ¹H-NMR measurements (Table 2.6). The obtained average C/E is close to the ratio of the comonomers in the educt solution. According to literature, the copolymerization parameters for MAA and PEGMA-19 in acidic aqueous media are similar. However, without further characterization it cannot be stated if the obtained FRC-PCEs are statistical copolymers or if they there are gradients regarding the repartition of charges and side chain along the backbone.

Table 2.6. Information on SEC and ¹H-NMR characterization of the FRC-PCEs. The molar mass is given in kg/mol.

FRC-PCE	M _w (GPC)	Đ	C/E _{NMR}
FRC-PCE-1.7-19	67.1	1.7	1.7
FRC-PCE-2.8-19	51.6	1.9	2.8
FRC-PCE-5.0-19	23.4	1.7	5.0

Figure 2.9a shows the chromatograms of the FRC-PCEs. All PCEs elute in well-defined peak between 21.0 and 29.0 mL. The normalized RI peaks are entirely overlapping. Corresponding molar mass distributions were obtained using online MALLS and RI detection (Figure 2.9b). As a general trend, the average molar mass increases with increasing grafting ratio. Nonetheless, it is not possible to draw further conclusions regarding the molecular parameters. In contrast to R-PCEs where a homogeneous grafting density and similar sized backbones are obtained, FRC-PCEs

do not feature distinct parameters for C/E and backbone length, but parameter distributions that demand further analysis.

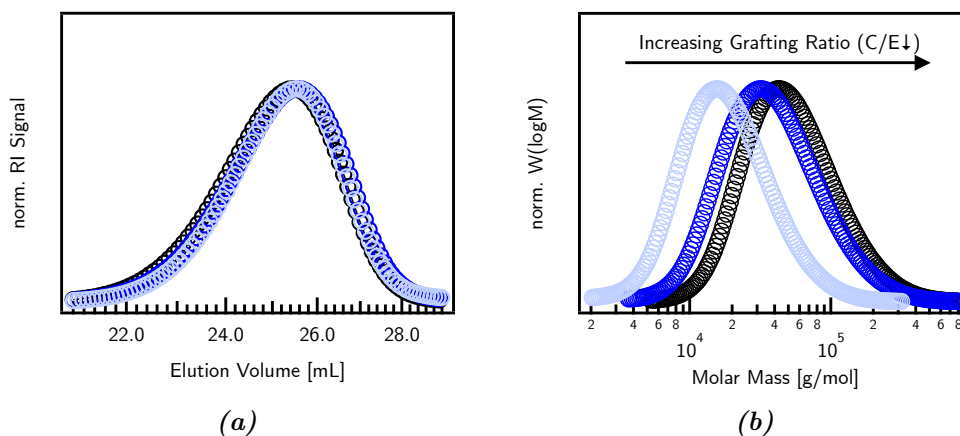


Figure 2.9. (a) Chromatograms of FRC-PCEs synthesized by free radical copolymerization of PEGMA-19 and MAA. Information on the synthesis and molar mass of the PCEs can be found in Table 2.4 and 2.6. (b) Molar mass distribution of the chromatograms shown in (a) With increasing grafting ratio, the molar mass increases. It is not possible to draw conclusions regarding backbone length.

The dispersity index \mathbb{D} of all FRC-PCEs is bigger than 1.7 indicating a higher dispersity regarding molar mass compared to R-PCEs (Table 2.6). Due to side reactions and termination by recombination or disproportion, a value of \mathbb{D} close to 2 or even higher is typical for polymers synthesized by free radical techniques. The results of NMR and SEC analysis of all FRC-PCEs are summarized in Table 2.6.

2.5. Grafting via Polymer-analogous Esterification

Grafted PCEs (G-PCEs) were obtained *via* grafting of a precursor backbone with MPEG in a polymer-analogous esterification process. The process can be regarded as an acid-catalyzed *Fischer-Esterification*. The reaction was carried out in melt to yield high conversions. Hence, high temperature and low vacuum are needed. In *Section 2.5.1*, a standard protocol for grafting poly(carboxylic acid) backbones is presented. The process is explained for the esterification of a poly(acrylic acid) (PAA) backbone with MPEG. The procedure can also be applied for grafting of PMAA precursors. However, all methacrylic G-PCEs that were applied throughout this thesis were prepared and supplied by Sika AG, Switzerland.

2.5.1. Standard Grafting Protocol

Precursor backbone (PAA, M_w 5760 g/mol, \bar{D} =1.98, DP_n =40, 9.4 g, 0.003 mol) and side chains (MPEG-22, M_w 1000 g/mol, \bar{D} = 1.0, 32.6 g, 0.033 mol) were filled into a round bottom flask and dissolved in ultrapure water (10 mL). In case of 100 % conversion, a PCE with $C/E = 3.0$ will be obtained. $(C/E)_{100\%}$ can be estimated using Equation 2.6, where $[PAA]$ and $[MPEG]$ are the molar concentrations of precursor and side chains in the starting solution and DP_n is the number-averaged degree of polymerization of the PAA precursor.

$$(C/E)_{100\%} = \frac{[PAA] \cdot DP_n}{[MPEG]} - 1 \quad (2.6)$$

The pH of the solution was adjusted to 2.2 using sulfuric acid. At this pH, more than 95 % of the carboxylic groups of the precursor are protonated. To obtain a homogeneous solution, the mixture was heated to 90 °C using an oil bath while being constantly stirred by an overhead stirrer (IKA[®] Eurostar power control visc). Subsequently, light vacuum was applied to remove water from the reaction mixture. During this step, the temperature was kept at 90 °C. Upon removal of the solvent, the consistency of the mixture became wax-like. In the next step, the temperature was increased to 180 °C and the vacuum was decreased to 0.1 mbar.

The onset of the esterification process could be observed by the formation of gas bubbles (water vapor). Temperature and vacuum were kept constant until gas formation ended. The reaction product (PCE melt) was cooled down to 90 °C while maintaining the vacuum. Subsequently, ambient pressure was restored, and ultrapure water (75 mL) was added while stirring constantly. The product was stirred until a homogeneous solution was obtained. Finally, the PCE solution (solid content approximately 20-25 wt%) was allowed to cool to room temperature. The product was characterized with SEC to verify if the esterification was successful and to determine the amount of residual (ungrafted) MPEG. For this purpose, the product was not purified prior to characterization.

2.5.2. Size Exclusion Chromatography

Figure 2.10 shows several chromatograms of MPEG, PAA precursor and the G-PCE. Due to its small hydrodynamic size, MPEG elutes as last component at 30.0 mL, right before the system peak. The ungrafted backbone elutes between 24.0 and 30.0 mL in a well-defined peak. The RI trace of the G-PCE reveals two peaks. The main peak between 21.0 and 29.0 mL signalizes the elution of PCE molecules. Compared to PAA, the PCE elutes earlier, indicating an increase in the hydrodynamic size due to successful grafting of side chains onto the backbone. The second peak shows a maximum at 30.0 mL indicating that some educts of the grafting reaction are left.

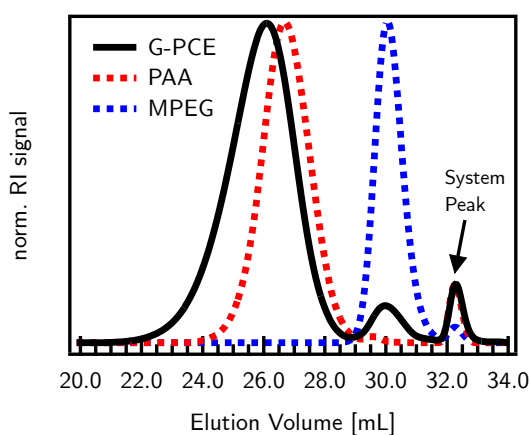


Figure 2.10. Chromatogram of an unpurified G-PCE with PAA backbone and MPEG-22 side chains. The traces of the synthesis educts, MPEG and PAA are also shown. All peaks were normalized to the peak maxima.

2.5.3. Methacrylic G-PCEs

Various MPEG-type PCEs with PMAA backbone were provided by Sika AG, Switzerland. The polymers were prepared by grafting MPEG of different molar mass (Table 2.7a) onto preformed PMAA (Table 2.7b) *via* an esterification process. The applied synthesis protocol is similar to the process described for grafting of PAA in the previous section, however, details are not disclosed. Grafted PCEs will be referred to as G-PCEs. All G-PCEs were purified by dialysis and freeze-dried when needed. Molar mass distributions were obtained from SEC, and $^1\text{H-NMR}$ was used to determine the grafting density. More than 15 G-PCEs with different charge density and side chain length were applied. Detailed information on these PCEs can be

2. Synthesis of Poly(carboxylate ethers)

found in the materials and methods sections of *Chapter 3*, *Chapter 5*, *Chapter 4* and *Chapter 6*.

Table 2.7. Information on MPEG side chains (a) and PMAA precursor backbones (b) used in polymer-analogous esterification synthesis of PCEs. Molar masses are given in g/mol

(a) MPEG			(b) PMAA precursor			
	M_n	P		M_w	\bar{D}	DP_n
MPEG-10	500	10		5200	1.4	44
MPEG-22	1000	22	PMAA-5k	5300	1.4	45
MPEG-67	3000	67		5400	1.4	45
MPEG-113	3000	113	PMAA-8k	8100	1.5	64

2.6. Materials and Characterization Protocols

2.6.1. Purification and Storage

When needed, PCEs were purified by dialysis against ultrapure water to remove impurities such as residual educts or organic solvents. For PCEs with high charge density, the pH of the dialysis bath was increased using NaOH to avoid precipitation of the PCE in the dialysis bag. In order to reduce the content of free side chains (MPEG or PEGMA), the cutoff of the dialysis membrane was chosen accordingly. Dialysis membranes of type SpectraPor™ 6, MWCO 1 kDa, 2 kDa 3.5 kDa and 8 kDa were used for this purpose. Subsequently, the PCEs were stored as aqueous solution, frozen or freeze-dried.

2.6.2. Size Exclusion Chromatography

Standard SEC Protocol

SEC analysis was performed on an Agilent 1260 Infinity system (Agilent Technologies, Santa Clara, CA, USA) equipped with a RI detector (Agilent Technologies, G1362A) and a MALLS detector (SLD7100, PSS Polymer Standards Service, Mainz, Germany). A series of three PSS Suprema columns (individual dimensions 0.8 cm x 30 cm, particle size 10 μm) of different pore sizes (30 \AA , 1000 \AA , 1000 \AA) was used. The combination

of MALLS and online RI was used for measuring molar mass distributions. The mobile phase (0.1 M Na₂HPO₄ in ultrapure water) was pumped with a flow rate of 1 L/min. The sample concentrations ranged between 1.5–3.0 mg/mL. For this, an adequate amount of polymer was dissolved in the eluent. For each analysis a volume between 50 and 100 µL of polymer solution was injected. Data analysis was carried out using PSS WinGPC Software (Polymer Standards Service, Mainz, Germany).

MALLS with online RI detection allows to determine absolute MMDs of polymers. In case of chemically disperse samples such as PCE copolymers, the refractive index increment might be different for each eluting copolymer fraction. These variations might cause problems when it comes to determination of MMDs due to imprecise determination of eluting polymer concentrations. However, MALLS/RI was proven to give a good estimate of the MMD for PCEs.

The SEC chromatogram can also be applied to determine the fraction of free side chains or macromonomer that were not consumed during the PCE synthesis. When PCE and MPEG (or PEGMA) are baseline separated, both peaks of the RI signal can be integrated. A good example for well separated PCE and MPEG peaks is given in Figure 2.10. Assuming that the refractive index increment of PCE and MPEG (*i.e.* PEGMA) is identical, the fraction of free (=ungrafted) side chains can be approximated from the peak integrals according to Equation 2.7.

$$f_{SC} = \frac{A_{SC}}{A_{SC} + A_{PCE}} \quad (2.7)$$

where A_{SC} is the area below the RI signal of MPEG or PEGMA and A_{PCE} the corresponding integral below the PCE main peak.

SEC with Dual Concentration Detection

For SEC with dual concentration detection, the same column setup as described in the previous section was used. A second concentration detector, more specifically, a diode array detector (Agilent Technologies, G1315D, operated at $\lambda=220$ nm) was connected to allow dual concentration detection. Moreover, the mobile phase was changed to 0.1M NaCl (pH adjusted to 10 using 5M NaOH). The change of the salt in the mobile phase is essential to shift the UV cutoff to lower wavelengths. More

detail on the chromatographic setup used for dual detection experiments is described in Chapter 3.3.2.

2.6.3. ¹H-NMR

Determination of C/E

All ¹H-NMR measurements were carried out on a Bruker 300 MHz spectrometer using D₂O as a solvent. Figure 2.11 shows a typical spectrum of a PCE with PMAA backbone and MPEG side chains, including peak assignments.

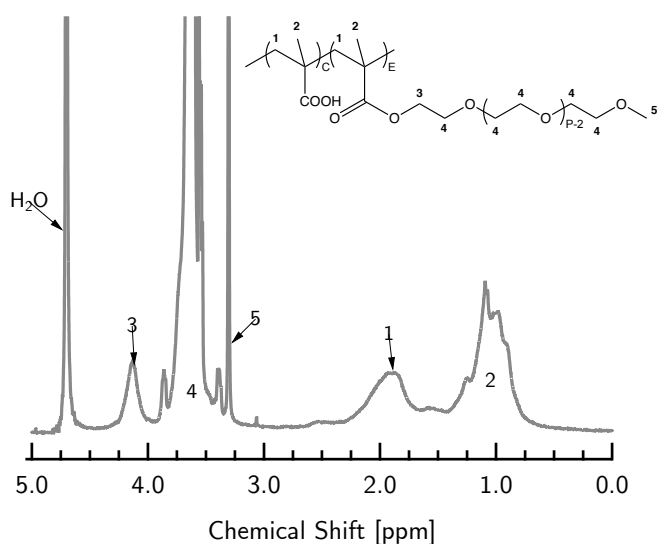


Figure 2.11. ¹H-NMR spectrum of a PCE with PMAA backbone and MPEG side chains including peak assignments.

The C/E (= $N-1$) can be calculated using the protons of the backbone (5 protons in peak 1 and 2) and those of the terminal methyl-group of the side chain (3 protons in peak 5). To this end, peak 1, 2 and 5 were integrated and normalized by the corresponding number of protons. Subsequently, the C/E can be calculated as follows:

$$C/E = \frac{(I_1 + I_2 - I_5)}{I_5} \quad (2.8)$$

where I_1 , I_2 and I_5 represent the normalized integrals of peak 1, 2 and 5 as shown and assigned in Figure 2.11.

Monitoring the Reaction Progress

$^1\text{H-NMR}$ measurement were also applied to monitor the progress of the RAFT polymerization. For different times of the reaction, aliquots were extracted and diluted with D_2O . The monomer conversion was calculated by relative integration of the protons of 1,3,5-trioxane (peak 1) and the vinylic protons of MAA (peak 2) and PEGMA macromonomer (peak 3). All relevant peaks are shown in Figure 2.12. The ratio for $t=0$ min refers to 0 % conversion

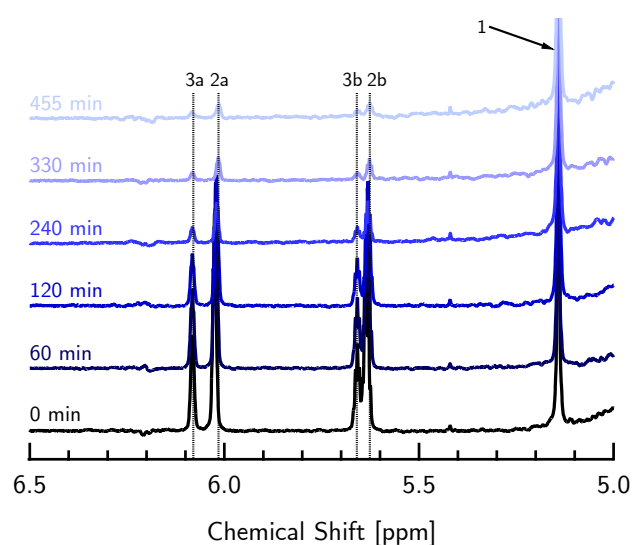


Figure 2.12. $^1\text{H-NMR}$ spectrum of aliquots extracted during the RAFT synthesis. The relative integral ratio between the trioxane peak (1) and the vinylic protons of the monomers MAA (2) and PEGMA (3) can be used to calculate the conversion of each monomer. With increasing reaction time, the area below the vinylic peaks decreases as monomers are consumed and incorporated into the R-PCE.

2.6.4. Titration

Throughout this manuscript, all reported C/E ratios were determined from $^1\text{H-NMR}$ of purified PCEs as described in the previous section. Alternatively, the C/E can be estimated from acid-base titration. For titration, an automatic titration system (EasyPro[™] titrator, Mettler Toledo, Switzerland) equipped with a pH electrode and temperature sensor was used.

In a typical titration experiment, the polymer was dissolved in ultrapure water. A suitable sample concentration is 10-50 mg/mL. Subsequently, the solution was

2. Synthesis of Poly(carboxylate ethers)

acidified using HCl to decrease the pH until $\text{pH} < 1.8$. At this pH, all carboxylate groups of the PCE are protonated. Subsequently, the solution was titrated using potassium hydroxide solution (KOH). The exact concentration of the titrant was determined prior to titration. A suitable concentration range is 0.05-0.5 M. The titrant is added to the polymer solution while recording the pH. Titration is finished as soon as the second equivalence point (EP_2) is reached. A typical titration curve is shown in Figure 2.13a.

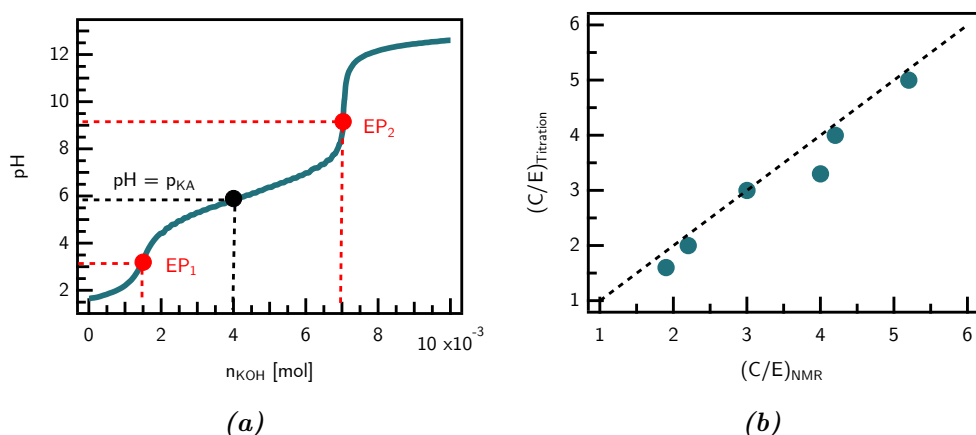


Figure 2.13. Titration of PCEs. (a) Titration curve of an acidified PCE solution with KOH. Two equivalence points can be identified. Moreover, the pK_A of the carboxylate groups in the backbone can be estimated from the half-equivalence point. (b) Comparison of C/E values determined from $^1\text{H-NMR}$ and titration. Both values are in good agreement and follow the trend of a bisecting line.

Up to the first equivalence point (EP_1), excess HCl in solution is consumed (Equation 2.9). The addition of further KOH causes deprotonation of carboxylate groups (C). Hence, the EP_2 corresponds to the titration of all carboxylate groups present in the PCE (Equation 2.10).

$$n_{\text{KOH},1} \stackrel{EP_1}{=} n_{\text{HCl}} \quad (2.9)$$

$$n_{\text{KOH},2} \stackrel{EP_2}{=} n_{\text{KOH},1} + n_C \quad (2.10)$$

where $n_{\text{KOH},1}$ and $n_{\text{KOH},2}$ are the molar amounts of titrant added to the sample solution at the equivalence points. n_C is the number of carboxylate moieties in the PCE sample to be titrated and n_E the respective number of side chain bearing ester units.

Consequently, $(C/E)_{Titration}$ can be calculated using Equation 2.11-2.12.

$$(C/E)_{Titration} = n_C/n_E \quad (2.11)$$

$$\text{where } n_E = \frac{m_{PCE} - n_C \cdot M_C}{M_E} \quad (2.12)$$

$$\text{and } m_{PCE} = m_{Polymer} \cdot (1 - f_{sc}) \quad (2.13)$$

where M_C is the molar mass of MAA and M_E is given by the molar mass of the macromonomer. m_{PCE} is the amount of PCE to be titrated. When free (=ungrafted) side chains or residual macromonomer are present in the sample, m_{PCE} can be calculated using Equation 2.13. In this case, the fraction of side chains (f_{sc}) has to be determined beforehand. Here, $m_{Polymer}$ refers to the total amount of polymer (PCE and ungrafted side chains) that were dissolved in the titration sample.

Titration only allows to estimate the C/E ratio. Equation 2.9-2.10 assumes that all carboxylate groups of the PCE will eventually be titrated by one equivalent of KOH. However, the type and radius of the counter ion (here K^+) can significantly impact the titration result [152]. For G-PCEs with a C/E ratio ranging between 1 and 6 titration and NMR are in good agreement (Figure 2.13b).

Moreover, titration gives information on the pKA value of PCEs. For all titrated MPEG-type PCEs with PMAA backbone, the pKA ranges between 5.9 and 6.1. This value is of particular importance for understanding the degree of dissociation, α , of carboxylate groups in the PCE backbone. A factor that significantly impacts its solubility. The degree of dissociation can be estimated with Equation 2.14 according to the *Henderson Hasselbalch* equation for weak acids of low molecular weight. Notably, α can only be approximated with this equation as the *polyelectrolyte effect* is not considered.

$$\alpha = \frac{10^{-pK_A}}{10^{-pH} + 10^{-pK_A}} \quad (2.14)$$

2.6.5. UV-Vis-Spectroscopy

All absorption spectra presented in this thesis were measured with a Lambda 650 UV-Vis spectrophotometer from Perkin Elmer. The spectra were recorded between 190 and 600 nm with wavelength steps of 1 nm. The solutions were filled into a quartz cuvette (Hellma[®], QS Quartz Glass High performance, path length 10 mm). A baseline was measured using ultrapure water as reference.

Chapter

3

Liquid Chromatography - Part I SEC with Dual Concentration Detection

The content of *Chapter 3* was published in the following research article:

*"A METHOD FOR CHARACTERIZING THE CHEMICAL HETEROGENEITY
OF COMB-COPOLYMERS AND ITS DEPENDENCE
ON SYNTHESIS ROUTES"*

Polymers, **2021**, 13(12):1921, [doi:10.3390/polym13121921](https://doi.org/10.3390/polym13121921)

Stefanie Anne Weckwerth is the first author of this publication. She carried out all experiments, evaluated and visualized data as well as wrote the first draft of the paper. The experimental strategy and concept was elaborated in collaboration with *Dr. Radke*, who consulted the work with his profound expertise in polymer science and chromatography. The final manuscript was written by *Ms. Weckwerth*, guided by *Dr. Radke* and *Prof. Flatt*.

3.1. Context

The heterogeneity in chemical structure of polymers is difficult to characterize and consequently remains an often-overlooked factor in mechanistic studies of functional polymers, such as poly(carboxylate ethers) (PCEs). In the field of PCE research, the role of molecular parameter averages has been much studied [28, 68, 77, 109, 153–156], but their variations have received little attention [157]. However, information

about the dispersity in molar mass and chemical composition is essential to predict, understand and tailor the performance of dispersants.

Liquid chromatography is a powerful tool to study dispersity in polymers. Common size exclusion chromatography (SEC) gives access to the molar mass distribution, but does not provide information on chemical composition. In the present chapter, an analytical method is established that provides a deep insight into the molecular heterogeneity of PCEs. More precisely, a protocol for SEC with dual concentration detection in aqueous media is developed that allows to monitor the grafting ratio of PCEs in dependence on their molecular size. By applying this analytical tool to various PCE samples (*i.e.* G-PCEs and FRC-PCEs), this chapter reveals that the synthesis pathways can lead to a clearly different chemical heterogeneity within a PCE.

The results of our dual concentration detection SEC experiments not only exemplify the development of methods to characterize chemical dispersity, but also establish its relevance to better understand how various synthetic routes may affect polymer performance at equivalent average composition.

3.2. Strategy

In a typical experiment, we use a multi angle laser light scattering (MALLS) setup with online refractive index (RI) detection to target the MMD. Along with this, simultaneous UV detection enables us to quantify the copolymer composition, *i.e.* the comonomer content of the PCEs along the elution axis. More information on the theory of copolymer analysis using SEC with dual concentration detection is given in *Chapter 1.8.2*.

The study is divided in two parts. First, homopolymer mixtures of PMAA (precursor backbone) and PPEGMA (100 % grafted backbone, poly(poly(ethylene glycol methacrylate))) of known composition are measured. These mixtures were used to evaluate the accuracy of the dual detection approach and allowed to exclude the influence of neighboring group effects that might compromise the reliability of the dual detection results for PCE copolymers. Subsequently, in the second part of the chapter, various PCE samples obtained by different synthesis pathways (*i.e.* free radical copolymerization and grafting) are subjected to dual concentration detection SEC experiments.

3.3. Materials and Methods

3.3.1. Applied Polymers for Dual Detection

For this study, various PMAA and PPEGMA homopolymers as well as PCE copolymers were applied. The homopolymers were obtained by free radical homopolymerization (FRP) in aqueous media. These homopolymers serve as test materials for our dual detection study (see *Section 3.4.2*). The PMAA homopolymer refers to the reference case of an ungrafted backbone ($C/E = \infty$) and PPEGMA corresponds to the case of a 100 % grafted backbone ($C/E = 0$). Here, C/E refers to the numeric ratio of methacrylic acid groups to ester groups in the PCE sample.

Moreover, six methacrylic PCEs with a C/E between 1.60 and 5.0 were prepared for the second stage of this study (see *Section 3.5.2*). These PCEs were obtained by grafting of a precursor backbone (PMAA; $M_w = 5300$ g/mol; $D = 1.4$) with methoxy poly(ethylene glycol) (MPEG, $M_w = 1000$ g/mol) side chains. The samples were provided by Sika AG, Switzerland. The C/E of the PCEs was determined from $^1\text{H-NMR}$ spectroscopy.

To investigate the influence of the synthetic approach, three additional methacrylic PCEs were synthesized via free radical copolymerization (FRC) in aqueous media. Again, C/E was calculated from $^1\text{H-NMR}$ spectroscopy. More details about synthesis and NMR evaluation can be found in *Chapter 2.6.3*. Information on the molecular characteristics of all polymers is summarized in Table 3.1.

Figure 3.1 shows the representative molecular structure of a PCE composed by MAA (C) and PEGMA (E) repeating units. The side chain length of the macromonomer is given by P repeating units of ethylene oxide.

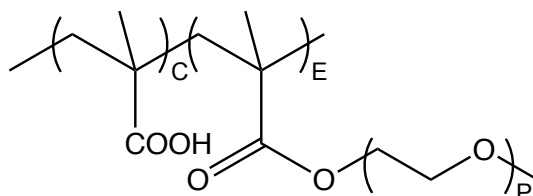


Figure 3.1. Molecular structure of a comb shaped PCE featuring a PMAA backbone and PEG side chains with P repeating units. C notes the number of MAA units in the backbone and E refers to the number of side chain bearing backbone units. Details about molecular parameters of all applied PCEs are listed in Table 3.1.

Table 3.1. Average Molecular characteristics of applied PCEs. The numeric ratio between the comonomers (C/E) was obtained from 1H -NMR spectroscopy. The corresponding weight fractions of component C and E were calculated according to Equation 3.1. P gives the number of repeating units in the PEG side chain. M_w and the dispersity index, \mathcal{D} , were measured via SEC using online RI and MALLS detection.

Name	Synthesis	C/E (NMR)	ω_C	ω_E	P	M_w	\mathcal{D}
PPEGMA	FRP	0.00	0.00	1.00	22	339.6	3.2
PMAA	FRP	∞	1.00	0.00	-	5.3	1.4
G-PCE-1.6		1.6	0.112	0.888	22	25.4	1.6
G-PCE-2.0		2.0	0.135	0.865	22	22.5	1.5
G-PCE-2.5	Grafting of	2.5	0.164	0.836	22	18.0	1.5
G-PCE-3.0	Precursor	3.0	0.190	0.810	22	17.7	1.5
G-PCE-3.3	Backbone	3.3	0.203	0.797	22	15.1	1.5
G-PCE-4.0		4.0	0.239	0.761	22	13.2	1.6
G-PCE-5.0		5.0	0.281	0.719	22	16.6	1.8
FRC-PCE-1.7	FRC	1.7	0.132	0.868	19	67.1	1.7
FRC-PCE-2.8	FRC	2.8	0.200	0.800	19	51.6	1.9
FRC-PCE-5.0	FRC	5.0	0.309	0.691	19	23.4	1.7

The numeric ratio between the comonomers C and E (see Figure 3.1) can be used to calculate the weight fraction of each component (ω_C and ω_E) according to Equation 3.1, where M_C is the molar mass of MAA and M_E the number-average molar mass of the macromonomer (PEGMA).

$$\omega_C = \frac{C \cdot M_C}{C \cdot M_C + E \cdot M_E} \quad (3.1)$$

where $\omega_E = 1 - \omega_C$

3.3.2. Size Exclusion Chromatography

SEC analysis was performed on an Agilent 1260 Infinity system (Agilent Technologies, Santa Clara, CA, USA) equipped with a RI detector (Agilent Technologies, G1362A) a diode array detector (Agilent Technologies, G1315D, operated at $\lambda = 220$ nm) and a MALLS detector (SLD7100, PSS Polymer Standards Service, Mainz, Germany). A series of three PSS Suprema columns (individual dimensions 0.8 cm x 30 cm, particle size 10 μm) of different pore sizes (30 \AA , 1000 \AA , 1000 \AA) was used. The combination of MALLS and online RI was used for measuring molar mass distributions. The

corresponding weight-average molar mass, M_w , and dispersity index, \mathcal{D} , are presented in Table 3.1.

The mobile phase (0.1M NaCl aqueous solution, pH 10 adjusted by addition of 10M NaOH) was pumped with a flow rate of 1 mL/min. An alkaline pH of the mobile phase is required to achieve complete deprotonation of the carboxylate groups. Moreover, the addition of salt is essential to shield interactions between the solute and the stationary phase.

The sample concentrations ranged between 1.5–3.0 mg/mL. For this, an adequate amount of polymer was dissolved in the eluent. For each analysis a volume between 50 and 100 μL of polymer solution was injected. Data analysis was carried out using PSS WinGPC Software (Polymer Standards Service, Mainz, Germany).

The calibration of the MALLS detector was done using a monodisperse Pullulan sample (M_w 110 000 g/mol, \mathcal{D} = 1.12) that does not show angular dependence in scattering. The same sample was used to determine the detector constant of the RI detector, as well as inter-detector delays.

3.3.3. Mobile Phase and Detection Wavelength

Figure 3.2a shows the UV-Vis spectra of several aqueous buffer solutions (*i.e.* Na_2HPO_4 , and $\text{CH}_3\text{COONH}_4$) that are frequently used as mobile phases for SEC analysis of PCEs [39]. These buffers feature a UV cutoff ≥ 220 nm (Figure 3.2b), hence the absorption of carbonyl groups, which feature their absorption maximum approximately at this wavelength, cannot be detected. In contrast, the addition of NaCl (and NaOH) results in a UV cutoff at 210 nm allowing to detect the carboxylate and ester peak.

3.3.4. Response Factor Determination

As already mentioned above, conventional SEC data processing using a single concentration detector does not give access to the comonomer composition of a copolymer. In order to quantify the amount of comonomers, the same number of independent concentration detector signals as number of comonomers contained in the sample is needed [6,37]. With the type of PCEs considered in this study

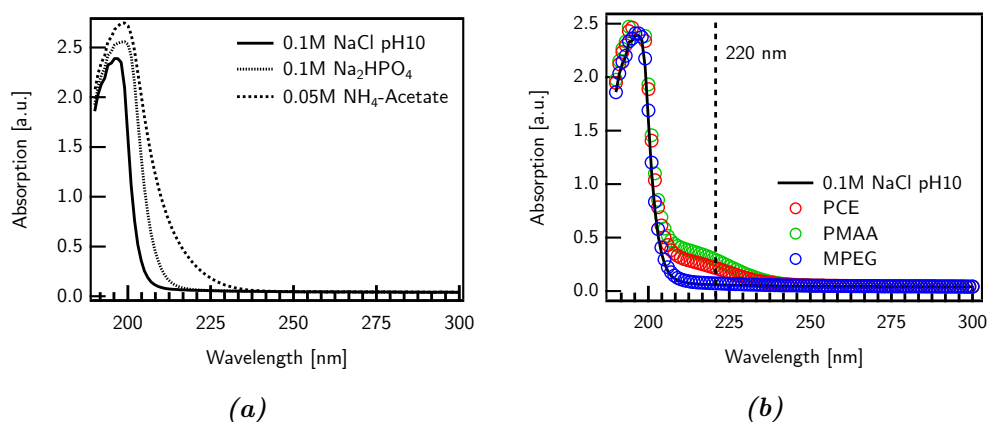


Figure 3.2. UV-Vis absorption spectra recorded between 190 and 300 nm: (a) Different aqueous salt/buffer solutions that are frequently used in SEC analysis of PCEs. The addition of salt/buffer affects the cutoff wavelength. All absorption spectra were measured in the wavelength range between 190 nm and 300 nm using air as reference. (b) Various polymers dissolved in 0.1M NaCl at pH 10. The UV cutoff of this solvent is located at approximately 210 nm. For PCE and PMAA solution, an absorption peak was found at 220 nm. MPEG does not show an absorption peak in the recorded range.

being binary copolymers, two signals (e.g. RI and UV) are needed to calculate the composition distribution and the overall bulk composition.

The DAD detector was operated at $\lambda = 220$ nm, where both the carboxylic acid groups and the ester groups show an absorption. Thus, both concentration detectors are able to detect both comonomers of the PCE. Notably, UV absorption is only due to the carbonyl groups in the backbone since the PEG side chains do not absorb at 220 nm (Figure 3.2b). The chromatograms (RI and UV signal) for PMAA and PPEGMA (corresponding to $C/E = \infty$ and $C/E = 0$, respectively) are plotted in Figure 3.3a-b.

A series of PMAA and PPEGMA samples with exact concentrations were injected into the chromatography setup. RI and UV signals were integrated over the eluting peaks and the peak areas were plotted against the injected mass. The integrals of both signals turn out to be proportional to the injected mass of homopolymer as shown in Figure 3.3c-d.

The slopes of peak area versus injected mass provide the response factor for each homopolymer-detector combination. The response factor of PMAA in RI detection will be referred to as k_C^{RI} and in UV detection k_C^{UV} . The response factors of PPEGMA are termed analogously k_E^{RI} and k_E^{UV} .

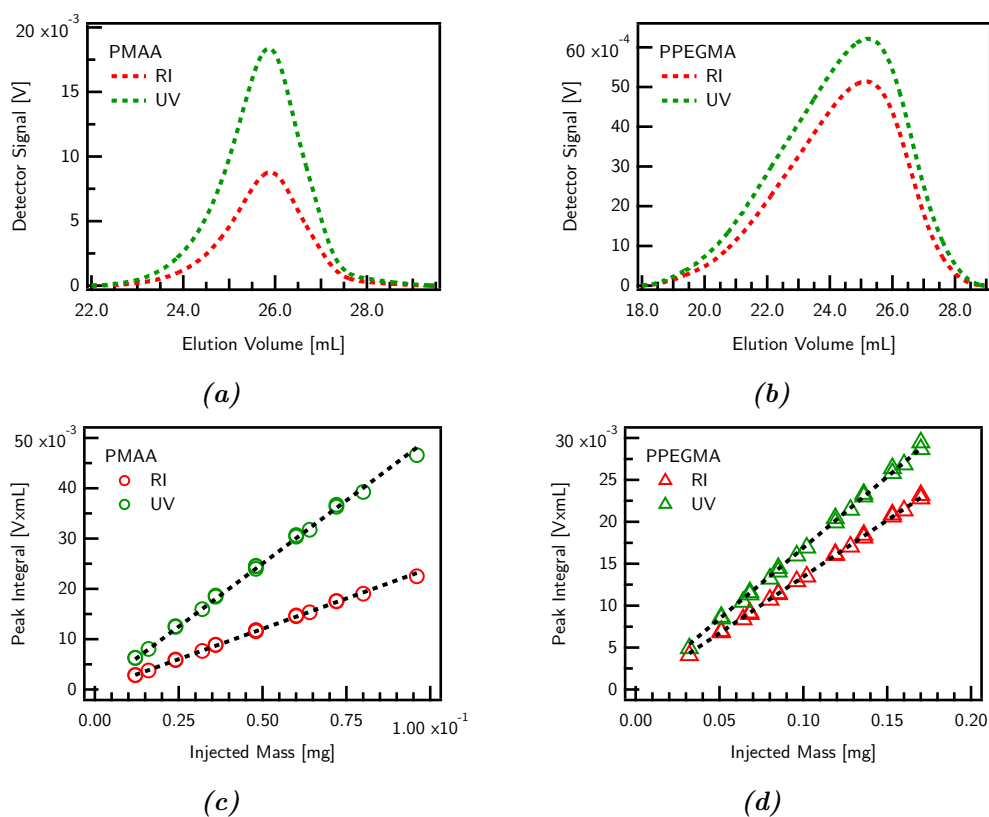


Figure 3.3. Above: Chromatogram of PMAA (a) and PPEGMA (b) homopolymers. These correspond respectively to C/E values of ∞ and 0. The signals from RI and UV detector are plotted against the elution volume. Below: Determination of response factors in RI and UV detection of PMAA (c) and PPEGMA (d) by linear regression. The results of the linear regressions are shown in Table 3.2.

Notably, the determination of response factors for polyelectrolytes is delicate. The method described above is suggested in literature [126, 158] to ensure an equilibrium distribution of counter ions in the vicinity of the polymer and the bulk solution.

3.4. Results and Discussion

3.4.1. Evaluation of Dual Concentration Results

The signals of both detectors, S^{RI} and S^{UV} are concentration sensitive and depend on the chemical nature of the sample. Hence, for copolymers, the signal from the i^{th}

Table 3.2. Response factors for PMAA and PPEGMA. The UV response factors were determined for a detection wavelength of 220 nm. The response factors are given in [(V x L)/g].

Sample	k^{RI}	k^{UV}
PMAA	0.241	0.501
PPEGMA	0.135	0.169

slice of the chromatogram is given by the signal contribution of each component [124, 130, 133].

$$S_i^{RI} = c_{i,P} \cdot [\omega_{i,C} \cdot k_C^{RI} + \omega_{i,E} \cdot k_E^{RI}] \quad (3.2)$$

$$S_i^{UV} = c_{i,P} \cdot [\omega_{i,C} \cdot k_C^{UV} + \omega_{i,E} \cdot k_E^{UV}] \quad (3.3)$$

$$\text{with } \omega_E = 1 - \omega_C \quad (3.4)$$

where $c_{i,P}$ refers. to the concentration of the polymer in the i^{th} fraction of the chromatogram, while $\omega_{i,C}$ and $\omega_{i,E}$ are the weight fractions of comonomers in that i^{th} slice. Here, the indices C and E refer to MAA and PEGMA as comonomers. k^{RI} and k^{UV} are the response factors of the homopolymers (Table 3.2).

From the above, for each slice, we have a system of three equations for the three unknowns ($c_{i,P}$, $\omega_{i,C}$ and $\omega_{i,E}$) that can be solved to yield information on the concentration and composition of the eluting fraction as described in literature [128, 130]. Equation 3.2-3.4 can be used to follow the sample composition along the elution axis by considering the signal ratio at time i . Moreover, the overall composition of a sample can be calculated by considering the integral over the complete RI and UV peak.

3.4.2. Mixtures of PMAA and PPEGMA Homopolymers

In contrast to most applications of SEC with dual concentration detection, both comonomers of our PCEs give rise to a response in both detectors, thereby challenging analysis. In order to find out if the method is capable of correctly quantifying relative amounts of C and E, we decided to analyzing homopolymer mixtures before changing to PCEs. For this purpose, a series of 20 homopolymer (PMAA and PPEGMA)

mixtures of known compositions were prepared and analyzed. The composition of the mixtures is given according to their weight fraction of PMAA. For instance, $\omega_C^{weight} = 0.05$ corresponds to a mixture with 5 wt% of PMAA and 95 wt% of PPEGMA.

An example of a chromatogram obtained for such mixtures is shown in Figure 3.4a for the mixture with $\omega_C^{weight} = 0.7$. The sample elutes between 18 and 28 mL, which agrees with the elution volume of the homopolymers (Figure 3.3a-b).

The composition of the eluting species was calculated across the peak using RI and UV-detection. Upon the onset of elution (18-22 mL), both concentration signals are weak. Hence, the calculated composition, $\omega_{i,C}^{Dual}$ cannot be considered precise. For volumes higher than 22 mL, $\omega_{i,C}^{Dual}$ is lower than 0.5 indicating that mainly PPEGMA is eluting from the column. With increasing elution volume $\omega_{i,C}^{Dual}$ increases until a value of 0.63. The increase in $\omega_{i,C}^{Dual}$ with elution volume agrees with the elution profile of the homopolymers. Due to its larger hydrodynamic volume, PPEGMA starts eluting earlier than PMAA (see Figure 3.3a-b).

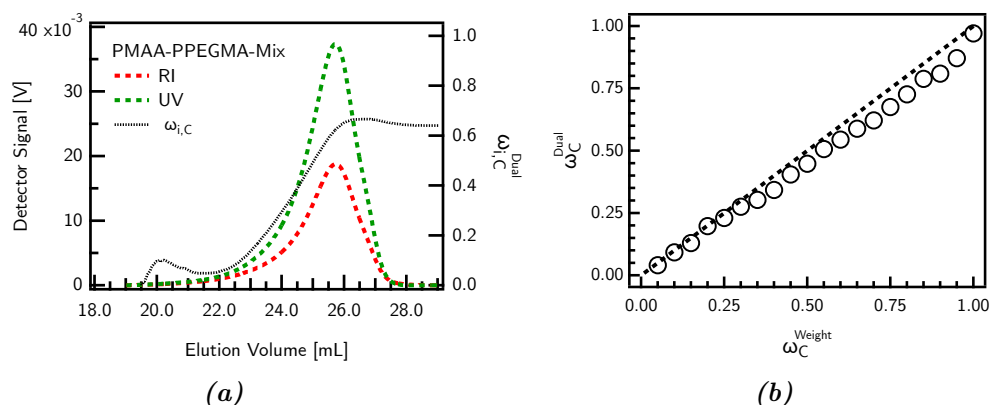


Figure 3.4. Analysis of homopolymer mixtures using dual detection. (a) Chromatogram of a sample with $\omega_C^{Weight} = 0.7$. The composition of the eluting fractions was monitored. (b) Comparison of $\omega_C^{Weight} = 0.7$ with $\omega_C^{Dual} = 0.7$ for 20 homopolymer mixtures of different PMAA and PPEGMA content.

To obtain information on the overall composition of the sample, the RI and UV signals shown in Figure 3.4a were integrated and ω_C^{Dual} of the complete mixture was calculated as described in Section 3.4.1. The calculated value of $\omega_C^{Dual} = 0.62$ is lower than the expected fraction of 0.70 for the specific sample shown in Figure 3.4a.

For a more detailed analysis of the deviation, the integration was carried out for all homopolymer mixtures. The determined weight fractions of PMAA were plotted against the weighted amounts. Figure 3.4b shows that all data points follow the trend of a bisecting line, indicating that ω_C^{Weight} and ω_C^{Dual} are in good agreement. For samples with low PMAA content (high PPEGMA), the data points show an almost perfect match. However, for samples with high PMAA content (low PPEGMA), ω_C^{Dual} is systematically smaller than ω_C^{Weight} . This deviation may be due to the lower UV response factor of PPEGMA compared to PMAA (Table 3.2). For low concentrations of PPEGMA, it only has a small contribution to the overall UV signal. If the signal contribution is below the detection limit, the composition of the mixture will not be captured correctly. Notably, this deviation is not expected to impact PCE characterization of the samples in the present investigation, as all relevant PCEs have a PMAA content lower than 0.35 (Table 3.1).

3.5. Dual Detection SEC of PCEs

3.5.1. Comparison with 1H-NMR

The above results show that dual detection can quantify amounts of monomers C and E in mixtures of pure reference compounds (homopolymers). To verify if this also applies to quantification of comonomers in PCEs, the method was compared to 1H-NMR data. For this, all PCEs shown in Table 3.1 were investigated by dual detection SEC. The overall weight fraction of comonomer C (ω_C^{Dual}) in each sample was calculated according to Equation 3.2-3.4 after integration over the whole RI and UV signal. The obtained weight fractions were compared to the average composition calculated from 1H-NMR spectra (ω_C^{NMR}) (Figure 3.5).

Figure 3.5 shows a plot of ω_C^{Dual} vs. ω_C^{NMR} for G-PCEs and FRC-PCEs and a bisecting line (dashed line). In case of perfect agreement between both analytical techniques, the data points are expected to fall on this line. Indeed, for PCEs with a high grafting ratio (low weight fraction of ω_C), the analysis by NMR and dual detection are in good agreement. For $\omega_C^{NMR} > 0.2$, the weight fractions determined from dual detection are slightly higher than the corresponding NMR values but still a clear trend can be observed. Only for G-PCE-5.0 ($\omega_C^{NMR} = 0.281$), NMR and dual detection analysis deviate significantly. Possible reasons for the deviation are briefly addressed in *Section 3.7*. However, G-PCE-5.0 was excluded from further

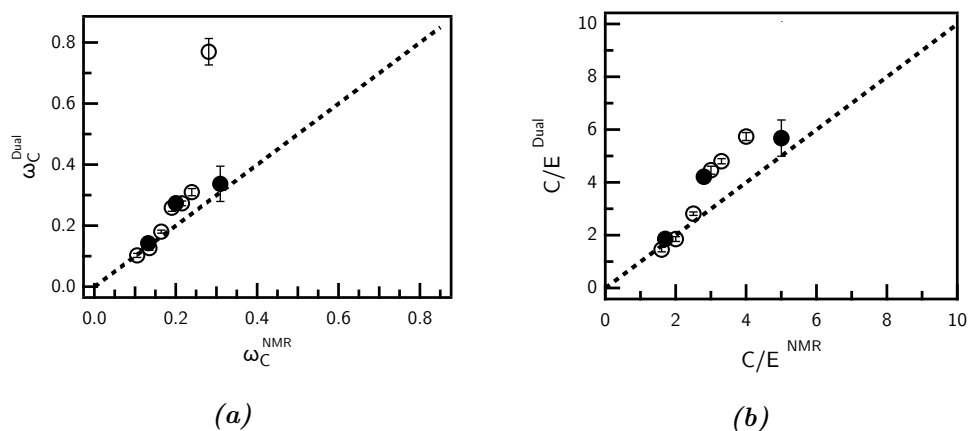


Figure 3.5. Comparison of copolymer composition in G-PCEs (\circ) and FRC-PCEs (\bullet) calculated from $^1\text{H-NMR}$ data and dual concentration detection SEC expressed as weight fraction of comonomer C (ω_C) (a) and C/E ratio (b). The results for sample G-PCE-5.0 are excluded from graph (b).

dual detection analysis in the second part of this chapter. Notably, FRC-PCE-5.0 ($\omega_C^{NMR} = 0.281$), that has a very similar molar composition to G-PCE-5.0 follows the trend of the bisecting line.

The agreement between ω_C^{Dual} and ω_C^{NMR} proves that the comonomer content in PCEs can precisely be quantified using dual detection SEC without being compromised by neighboring group effects. This result brings us to the next part of this chapter, where we will focus on tracing the PCE composition along the elution axis of the chromatogram.

3.5.2. Homogeneity of PCEs produced by Esterification

Grafting of precursor backbones is a widely used technique for the preparation of PCE model structures for research purpose. It is often claimed that grafting leads to a homogeneous distribution of side chains along the backbone. Moreover, independence of grafting ratio on backbone length is commonly assumed. However, lately some doubts have been raised about whether the dispersity of the backbone length in the precursor P(M)AA might impact the grafting ratio [39].

Dual detection SEC offers the opportunity to monitor the composition of the grafting ratio along the elution peak in a chromatogram. Figure 3.6 shows the

chromatogram (RI and UV signal) and the content of C ($\omega_{i,C}^{Dual}$) within six different G-PCE samples.

For all PCEs, $\omega_{i,C}^{Dual}$ seems to be rather constant, with only a slight decrease in $\omega_{i,C}^{Dual}$ with increasing elution volume. Thus, early eluting fractions (larger hydrodynamic volume) contain a slightly higher weight fraction of C than late eluting fractions. This behavior is more pronounced for PCEs with low C/E ratio (high grafting degree). For instance, G-PCE-1.6, $\omega_{i,C}^{Dual}$ decreases by 6.6 wt% between 24 and 28 mL. This corresponds to a change in C/E from 2.7 to 1.5, which is substantial in regard to PCE performance as superplasticizers. In contrast, $\omega_{i,C}^{Dual}$ of G-PCE-4.0 is almost constant at 30.3 wt% throughout the chromatogram. It has to be mentioned that the calculated values of $\omega_{i,C}^{Dual}$ are fluctuating at peak start and end. These uncertainties are due to low concentrations and corresponding weak detector signals of the eluting species in this area.

According to Figure 3.6, it appears that PCEs with smaller hydrodynamic size (early elution) feature a slightly higher content of C than bigger molecules. It is conceivable that such differences in the grafting ratio are related to the backbone length of the precursor. Indeed, the backbone of the G-PCEs features a M_w of 5300 g/mol, with dispersity index $\mathbb{D}=1.4$ meaning that the molar mass ranges approximately between 100 and 20 000 g/mol. The impact of backbone length on grafting ratio is further discussed in the next section.

3.5.3. Impact of Backbone Length

In order to verify if the backbone length impacts the C/E ratio of the PCE, a G-PCE was produced by grafting a mixture of two backbones with different molar masses. This mixture included the previously used PMAA-5k backbone and a larger one: PMAA-8k (M_w 8100; $\mathbb{D}= 1.5$) in proportions of 1:1 by weight. The mix is referred to as PMAA-6k, whereby its average molar mass is M_w 6400 g/mol with $\mathbb{D}= 1.4$. With this mix, the molar mass range of the grafted PCE was extended to higher molar masses (up to 40 000 g/mol). The molar mass distributions of all PMAAs are shown in Figure 3.7a.

The results in Figure 3.6 show that the heterogeneity of the C/E ratio is more pronounced for G-PCEs with C/E ratio below approx. 2.5. Therefore, a C/E of

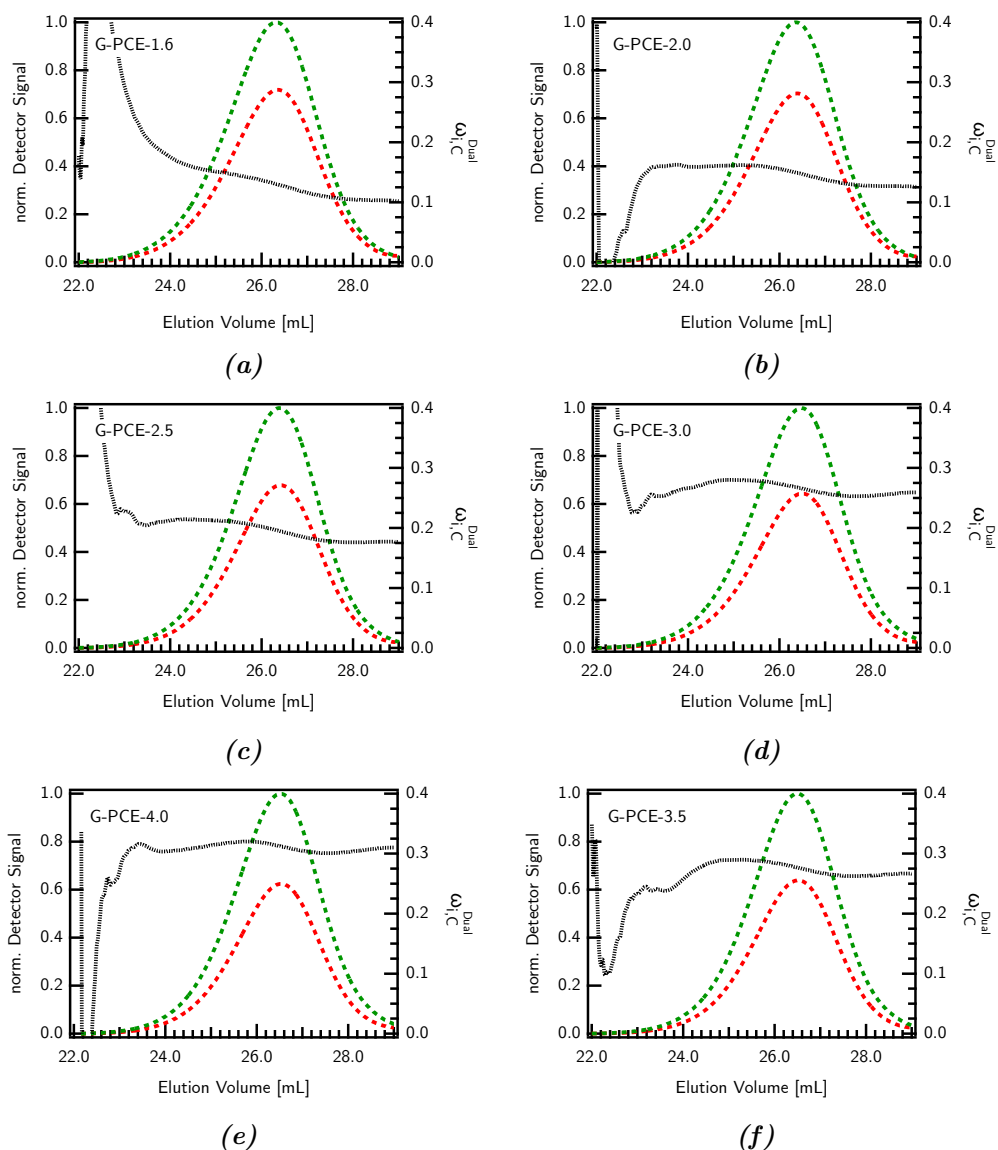


Figure 3.6. (a)-(f) Chromatograms of various G-PCE samples with different C/E ratio. The green curve is the UV-signal, and the red curve corresponds to the RI signal. The signals were normalized with regard to the maximum of the UV-peak. The dashed black line indicates the composition of the eluting species monitored by dual detection.

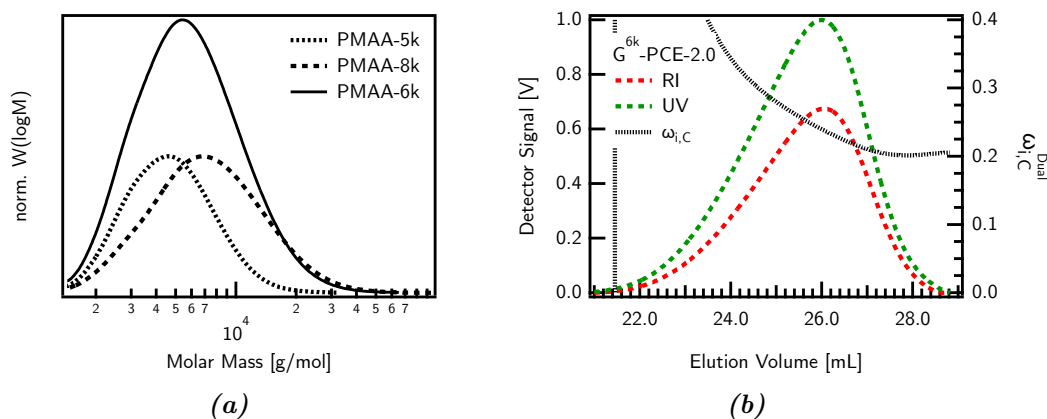


Figure 3.7. (a) Molar mass distributions of PMAA. PMAA-5k was used for the G-PCEs shown in Table 3.1. The molar mass range of this PCE was increased by adding PMAA-8k. The resulting backbone mix contains PMAA molecules with molar masses between approximately 100 and 40 000 g/mol. (b) Dual detection SEC analysis of G^{6k} -PCE-2.0.

2 was targeted when grafting side chains onto PMAA-6k. The resulting G-PCE is termed G^{6k} -PCE-2.0.

As can be seen in Figure 3.7b, the dual detection analysis of G^{6k} -PCE-2.0 shows that $\omega_{i,C}^{Dual}$ decreases along the elution axis. Early eluting PCE fractions feature a higher methacrylic acid content compared to later eluting species. Between onset and end of the elution peak, the weight fraction of C decreases by more than 13 wt%. This corresponds to a change in C/E from 3.9 to 1.7. This decrease is significantly stronger than for G-PCE-2.0, where the weight fraction of C is reduced by roughly 3.1 wt% meaning that the C/E varies between 2.4 and 1.9. Comparing G-PCE-2.0 and G^{6k} -PCE-2.0 confirms that the length of the precursor backbone impacts the grafting density of the PCE. It appears that small backbones tend to feature a higher grafting degree than longer backbones.

3.5.4. PCEs from Free Radical Copolymerization

On industrial scales, PCEs are most often obtained by free radical copolymerization. To reflect this mode of production, three different FRC-PCEs were characterized with dual detection SEC in order to investigate the methacrylic acid content across the elution peak (Figure 2.9a). As can be seen from Figure 2.9a, the $\omega_{i,C}^{Dual}$ increases with increasing elution volume, indicating that larger molecules (early elution) are more extensively grafted than smaller molecules (late elution). Thus, the trend is

reversed compared to G-PCEs. Notably, the differences in $\omega_{i,C}^{Dual}$ between onset and end of the elution peak are more pronounced for PCEs with high C/E ratio. For FRC-PCE-1.7, the $\omega_{i,C}^{Dual}$ is increased by approximately 6.0 wt%. Consequently, its C/E ranges between 0.9 and 1.9. For FRC-PCE-2.8 and FRC-PCE-5.0, $\omega_{i,C}^{Dual}$ is increased by more than 17 wt%. Hence, the C/E increases by more than 4.0 units between beginning and end of the elution peak.

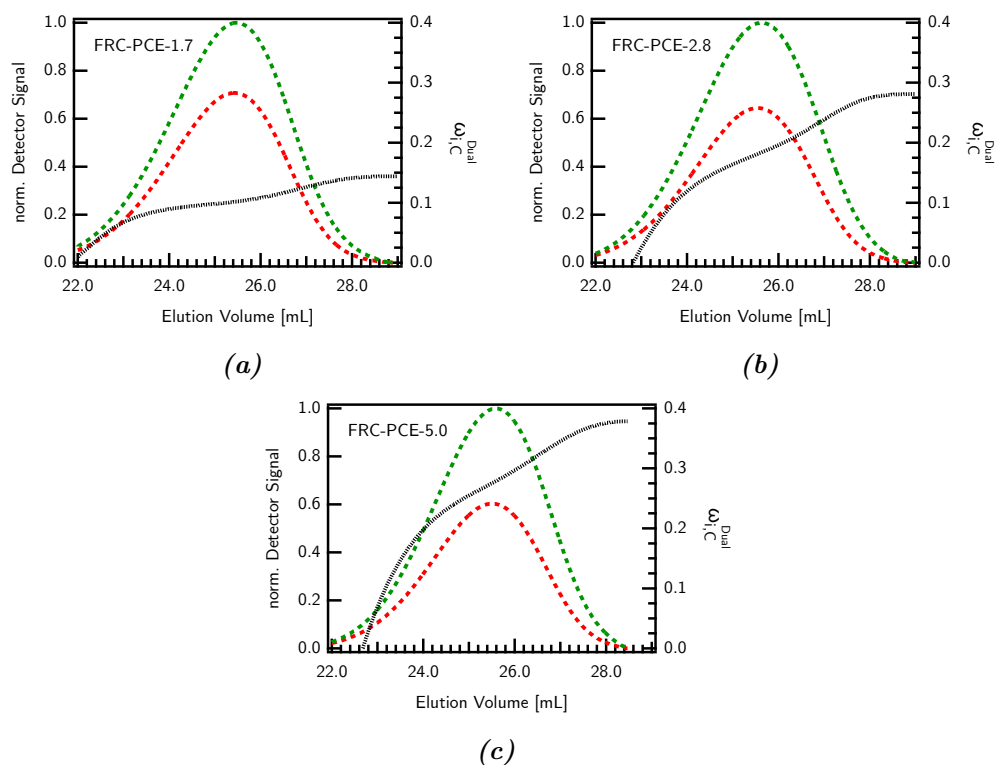


Figure 3.8. (a)-(c) Chromatogram of various FRC-PCE samples with different C/E ratio. The green curve is the UV-signal, and the red curve corresponds to the RI signal. The signals were normalized with regard to the maximum of the UV-peak. The dashed black line indicates the composition of the eluting species monitored by dual detection.

Generally speaking, it is difficult to ascribe the dispersity of the grafting density to one particular impact factor during FRC synthesis. The molecular architecture of FRC-PCEs depends on many factors among them the reactivity ratio [43, 47] of the comonomers, the monomer feed during synthesis, but also the choice of chain transfer agent or possible side reactions such as radical transfer and termination have to be considered. While the topic deserves further investigation, these results underpin the existence of this inhomogeneity, representing an additional factor that should be considered when studying the working mechanisms of such compounds or seeking to improve their performance.

3.6. Conclusion

It has been shown that aqueous size exclusion chromatography with dual concentration detection is a suitable tool to characterize the comonomer composition of PCEs. It was revealed that the synthesis pathway has a significant impact on the variation of grafting density with molar mass.

Polymer-analogous esterification revealed a weak correlation between backbone length and grafting ratio. It appeared that smaller backbones carry more side chains than larger ones. Variations in the grafting ratio are more expressed when a high grafting density is targeted during synthesis. This result is of particular interest for admixture research, where G-PCEs are often used as model structures. It is often assumed that within a G-PCE sample all backbones feature the same grafting ratio and are only dispersed with regard to the backbone length. However, this study proves that PCEs from esterification are dispersed in a second dimension, *i.e.* comonomer content. For the synthesis of optimal model structures where the chemical heterogeneity can be neglected, the use of narrowly distributed precursor backbones is recommended.

Having said this, PCE from free radical copolymerization show much stronger variation of grafting ratio with molar mass. While larger molecules are highly grafted, smaller molecules have a higher methacrylic acid content. Consequently, the correlation between molar mass and grafting ratio is reversed for FRC-PCEs compared to G-PCEs. For FRC-PCEs, dual concentration detection SEC can be considered a useful tool to get a deeper insight into the polymerization process. Therefore, we suggest to withdraw aliquots during the synthesis and investigate the comonomer composition of the samples. Additional ^{13}C NMR measurements could contribute to a better understanding of comonomer reactivity.

In literature, it has been shown, that the charge density significantly impacts the affinity of PCE molecules for adsorption on the cement surface [16,19,46]. And also in this work, (*Chapter 5*), we will show that PCE molecules with high C/E ratio preferentially adsorb over molecules with shorter backbones and high grafting degree. PCEs with decreased efficiency demand higher dosages to achieve the same workability of the concrete. Hence, the suggested dual detection method offers a tool to identify fractions within a PCE sample that are potentially less effective regarding their plasticizing ability. This suggests that new strategies to adapt

the synthesis conditions may enable the production of more efficient PCEs with tailormade molecular structure.

Liquid chromatography is a well-established tool to characterize polymers. With regard to PCE analysis, the simple addition of a second concentration detector to a standard SEC setup can provide new insight into the chemical dispersity of PCEs. Revealing their chemical heterogeneity gives access to a better understanding of their molecular heterogeneity.

In this study, different G-PCEs and FRC-PCEs were investigated. In contrast, R-PCEs are not suitable for dual concentration detection due to their strongly absorbing RAFT end group. When end group and repeating unit show an overlap in their absorption spectra, dual concentration detection might not allow to correctly quantify the copolymer composition, when the detection wavelength is located within the overlap region.

Generally speaking, the detection wavelength has to be selected appropriately that the end group contribution compared to absorption of the repeating units is negligible. In particular for high molar mass polymers, this requirement is often fulfilled as the number of repeating units is much higher than the number of end groups. However, the strongly absorbing thiocarbonylthio-moieties in R-PCEs do not allow to detect the carbonyl repeating units.

While this chapter has been focused on PCEs, it is suggested that the dual detection method in aqueous media can also be applied to other types of water-soluble copolymers with different components and architectures. For this purpose, only suitable detector response factors for the comonomers have to be established.

The most important characteristic that conditions the suitability of dual concentration detection is a sufficiently different response of the comonomers in at least one detector. When neighboring group effects can be excluded, the method is equally suitable for random copolymers, gradient and (multi)block structures. Besides PCEs, further copolymers containing (meth)acrylic acid or maleic acid as comonomer can be characterized by dual concentration detection. Moreover, acrylamide, N-isopropyl acrylamide vinyl acetate or lactic acid containing copolymers can potentially be subjected to this method, too.

All in all, dual detection SEC in aqueous media is a versatile and promising tool to understand molecular heterogeneity in water-soluble copolymers. The collected

information is of particular interest to comprehend structure-performance relations of functional polymers, as exemplified here in the case of superplasticizers extensively used in cementitious materials.

3.7. Appendix Chapter 3

Dual concentration detection SEC was validated as a suitable method to investigate the comonomer composition of PCEs. For the majority of PCE samples subjected to this method, the results were in agreement with $^1\text{H-NMR}$ data. However, in case of G-PCE-5.0 one outlier was observed (see *Section 3.5.1*). For this sample, the composition determined from both methods deviates significantly.

In order to exclude that impurities in the sample affect the measurement of G-PCE-5.0, the synthesis of this PCE was repeated, the corresponding polymer has a C/E ratio of 5.0 and is termed G-PCE²-5.0. The result of the dual detection analysis for this sample is included in Figure 3.9 (red circle). Similar to G-PCE-5.0, also G-PCE²-5.0 lies above the bisection, indicating that ω_{PMAA}^{Dual} is not in agreement with the $^1\text{H-NMR}$ analysis. Notably, FRC-PCE-5.0 that has a very similar molar composition to G-PCE-5.0 and G-PCE²-5.0 follows the trend of the bisecting line.

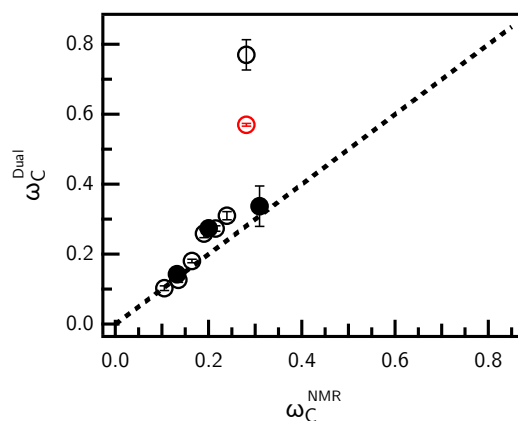


Figure 3.9. Comparison of copolymer composition in G-PCEs (\circ) and FRC-PCEs (\bullet) calculated from $^1\text{H-NMR}$ data and dual concentration detection SEC expressed as weight fraction of comonomer C (ω_C). The black data points were reprinted from Figure 3.5. The result for G-PCE²-5.0 was added (\circ , red). Similar to G-PCE-5.0, the data point is located above the bisecting line.

The main difference between the polymers is the synthesis route. While the FRC-PCE was obtained by aqueous copolymerization, the G-PCEs were synthesized *via* esterification of MPEG with a PMAA precursor backbone. For the grafting process elevated temperature ($> 160\text{ }^{\circ}\text{C}$) and strong vacuum are needed to yield high conversions.

It is known that high temperatures can cause degradation of P(M)AA *via* two possible pathways, namely condensation of adjacent carboxylic groups and/or decarboxylation of acid groups (Figure 3.10). These degradation reactions were also observed for G-PCEs synthesized *via* esterification in melt [77].

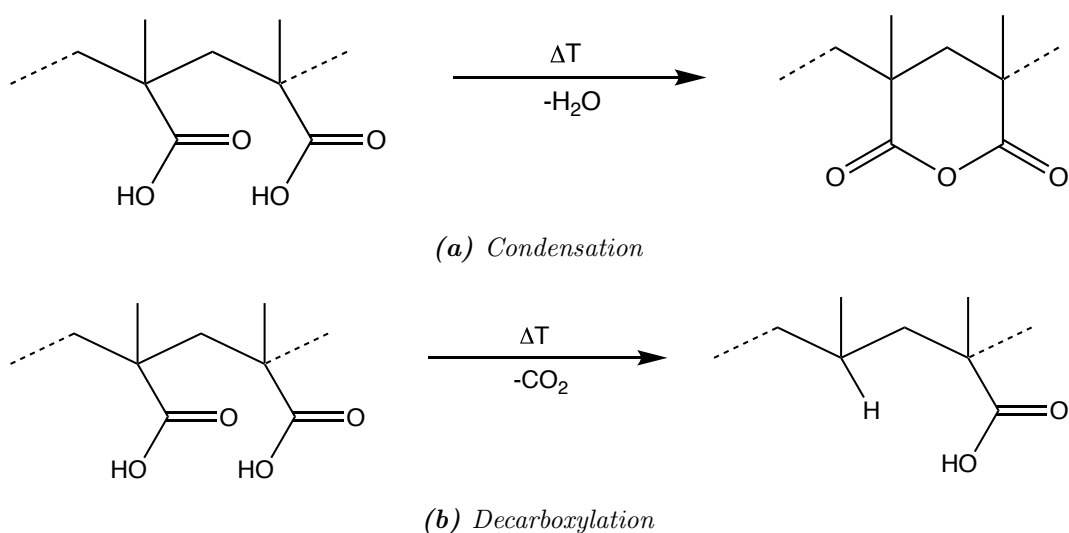


Figure 3.10. Possible degradation mechanisms of carboxylic acid groups within the PCE backbone. Excessive heat can cause condensation of adjacent groups (a) or decarboxylation of individual units (b). More information on this subject can be found in literature [77]

The anhydride formation can be reversed by dissolution of the PCE in aqueous media. On the contrary, the loss of CO_2 is permanent and has to be regarded as a major modification of the chemical structure. Indeed, a PCE that has undergone partial decarboxylation has to be treated as a terpolymer from a chemical point of view. The refractive index increment and in particular the ability to absorb UV light are modified upon decarboxylation. Consequently, k^{UV} and k^{RI} that are essential for dual detection analysis are not accurate anymore. Thermal degradation of PCEs gives a plausible explanation for the outlier shown in Figure 3.9. However, the effect of elevated temperatures (and vacuum) on highly charged PCEs ($C/E > 5.0$) was not further investigated.

Besides thermally induced processes, also vacuum might cause polymer degradation. In several examples, we observed changes of the RI/UV signal upon freeze-drying. In Figure 3.11, the chromatogram of G-PCE-3.0 is shown before and after lyophilization. While the shape and position of the elution peak was barely changed, the ratio of the concentration detector signals was modified (Table 3.3).

Table 3.3. Ratio RI/UV signal of G-PCE-3.0 before and after freeze-drying the sample. The signal ratio was obtained from the ratio of the peak integrals.

Sample	RI/UV before	RI/UV after
G-PCE-3.0	0.62	0.42

This indicates that the size of the PCE remained constant, while the response factors have undergone a change. It can be assumed that backbone length and side chains mainly determine the size of the polymer coil. Upon condensation and decarboxylation, small moieties are cleaved off. It is feasible that this does not significantly impact the hydrodynamic dimensions, while it causes a change in the response factors.

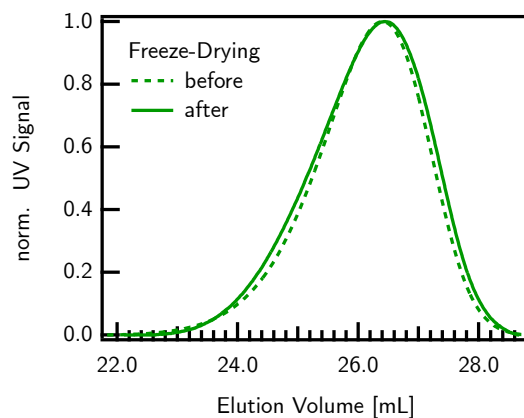


Figure 3.11. Chromatogram of G-PCE-3.0 before and after freeze-drying. The signals were normalized to the maximum of the UV-peak.

Table 3.3 shows that RI/UV decreases upon lyophilization indicating an increased absorption of UV relative to the RI response. Notably, the assumption that the UV activity of PCEs is mainly connected with the number of carboxylate groups in the backbone contradicts a loss of carboxylate groups by decarboxylation. However, the exact impact of decarboxylation on the response factors remains unknown.

Obviously, the issue of thermally or vacuum induced degradation of PCEs is delicate and deserves further investigation. In order to find out if and how the molecular structure of PCEs is affected by exposure to high temperatures and vacuum, additional $^1\text{H-NMR}$, $^{13}\text{C-NMR}$ and IR measurements as well as potentiometric titration and a thermogravimetric study could contribute to a better understanding of possible degradation processes and their reversibility. Moreover, the refractive index increment and specific absorption coefficient for several PCEs should be determined before and after exposure to damaging conditions. In addition to degradation of the backbone, also the decay or cleaving of MPEG side chains should be considered [39]. Notably, this topic was not further investigated in this thesis. However, the concerns raised in this section show the importance of sample history and sample preparation for proper method development.

Liquid Chromatography - Part II

RP-HPLC with Solvent Gradients

The content of *Chapter 4* was not (yet) submitted to a scientific journal. However, the results are potentially considered for publication at a later point in time. The experimental strategy was elaborated by *Stefanie Anne Weckwerth*, who carried out all experiments and entirely wrote this chapter. *Dr. Radke* was consulted for data evaluation. The present chapter, in particular the section addressing implications for admixture research, was revised by *Prof. Flatt*.

4.1. Context

In the previous chapter (*Chapter 3*), it is shown how the addition of a second concentration detector (*i.e.* UV detector) to a traditional size exclusion chromatography (SEC) setup with refractive index (RI) detection allows to quantify the comonomer content of poly(carboxylate ethers) (PCEs) along the elution axis. In other words, this method allows to reveal information on the chemical composition in dependence on the hydrodynamic size of the molecules. While this information is extremely valuable for a better understanding of the molecular heterogeneity within PCEs, it does not give access to the precise chemical composition distribution (CCD) of PCEs.

Indeed, the characterization of the CCD in copolymers is not trivial. In particular for water-soluble copolymers, there is a lack of available methods for characterizing chemical heterogeneity. In the past, interaction-based chromatography (IC) has been proven a suitable tool to reveal information on the chemical dispersity of copolymers. Herein, molecules are separated based on enthalpic interactions with the stationary phase. While IC for polymers is commonly carried out on C18 columns using organic solvents, it is also possible to use solvent mixtures with water. Thus,

reverse-phase high performance liquid chromatography (RP-HPLC) is also suitable for the characterization of more hydrophilic copolymers, such as PCEs. In the present chapter, the potential of RP-HPLC with solvent gradients for characterization of PCEs is investigated.

4.2. Strategy

RP-HPLC experiments are carried out on a C18 column using solvent gradients of acetonitrile and water as mobile phase. A series of PCEs with well-defined composition that were obtained from RAFT (short for reversible addition-fragmentation chain transfer) copolymerization are used to demonstrate the impact of the grafting ratio (*i.e.* C/E ratio) on retention. Subsequently, further PCE samples with systemic variations in their molecular parameters are subjected to RP-HPLC to validate the method.

Finally, PCEs with higher dispersity are studied. The obtained fractions from the RP-HPLC experiments are investigated by complementary SEC measurements in the second dimension. Thus, we aim to thoroughly investigate PCEs using a combination of LC techniques. The findings will be compared to the results obtained from SEC with dual concentration detection presented in *Chapter 3*.

4.3. Applied Polymers

In this study, various PMAA and PPEGMA homopolymers as well as PCE copolymers with different C/E ratio ranging between 0.7 and 9.0 were applied. Here, C/E refers to the numeric ratio of methacrylic acid groups (C) to ester groups (E) in the PCE sample. The poly(methacrylic acid) (PMAA) homopolymer refers to the reference case of an ungrafted backbone (C/E = ∞) and PPEGMA (poly(poly(ethylene glycol methacrylate))) shows the case of a 100% grafted backbone (C/E = 0). The homopolymers were essential for developing appropriate solvent gradients. The weight averaged molar mass (M_w) and dispersity index (\mathbb{D}) of all polymers was obtained using SEC with MALLS and online RI detection. The C/E ratio was calculated from ¹H-NMR as described in *Chapter 2.6.3*. Information on all PCEs is summarized in Table 4.1.

Table 4.1. Molecular characteristics of applied PCEs obtained from various synthesis routes. C/E was obtained from 1H -NMR spectroscopy, M_w [kg/mol] and \bar{D} were measured via SEC.

(a) **R-Polymers** obtained from RAFT (co)polymerization. While there are differences of the C/E , all PCEs (except R-PCE-1.7-9) feature the same side chain length ($P=19$). R-PMAA refers to the case of an ungrafted backbone, and R-PPEGMA gives the case for a 100% grafted backbone.

R-Polymer	C/E	M_w	\bar{D}	P
R-PPEGMA	0	77.4	1.28	19
R-PCE-0.7-19	0.7	49.9	1.05	19
R-PCE-2.2-19	2.2	24.4	1.01	19
R-PCE-4.5-19	4.5	23.0	1.01	19
R-PCE-9.0-19	9.0	11.5	1.01	19
R-PCE-1.7-9	1.7	12.1	1.01	9
R-PMAA	∞	5.5	1.11	-

(b) **G-PCEs** obtained via grafting of MPEG onto precursor backbones with different molar mass.

G-PCE	C/E	M_w	\bar{D}	P	Backbone
G-PCE-1.5-22	1.5	21.9	1.59	22	PMAA-5k
G-PCE-3.5-22	3.5	17.2	1.50	22	PMAA-5k
G-PCE-5.0-22	5.0	14.4	1.44	22	PMAA-5k
G-PCE-2.0-11	2.0	26.1	2.3	11	PMAA-5k
G-PCE-2.0-22	2.0	15.1	1.8	22	PMAA-5k
G-PCE-1.5-22	1.5	46.3	2.00	22	PMAA-8k
G-PCE-3.5-22	3.5	37.0	1.89	22	PMAA-8k
G-PCE-5.0-22	5.0	34.5	2.02	22	PMAA-8k

(c) **FRC-PCEs** obtained via free radical (co)polymerization of MAA and PEGMA-19.

FRC-PCE	C/E	M_w	\bar{D}	P
FRC-PCE-1.7-19	1.7	67.1	1.7	19
FRC-PCE-2.8-19	2.8	51.6	1.9	19
FRC-PCE-5.0-19	5.0	23.4	1.7	19

4.3.1. Nomenclature

The nomenclature of PCEs follows a similar pattern as in the previous chapters: Homopolymers and PCEs were obtained *via* various synthesis strategies, which are indicated by a prefix. R-Polymer refers to polymers obtained *via* RAFT (co)polymerization, FRC is the prefix for free radical copolymerization and G- refers to the grafting method. For PCEs, their C/E ratio is indicated as a suffix. Moreover, the number of ethylene oxide (EO) repeating units in the side chains (P) is added as a second suffix when needed. For instance, R-PCE-2.0-19 describes a PCE with a C/E ratio of 2 synthesized by RAFT. The side chain length of this R-PCE is 19 EO units.

4.3.2. RAFT-Polymers

Firstly, we tested if RP-HPLC with gradient elution can be applied to separate PCEs with different chemical composition (*i.e.* C/E ratio). Therefore, a solvent gradient is developed while using polymer samples of low dispersity. These polymers were synthesized by RAFT polymerization as described in *Chapter 2.3*. The backbone length of the polymers was controlled by adjusting the molar ratio between monomer and RAFT agent and controlling the conversion. This ratio was kept at 60/1 for all samples. All R-PCEs feature a similar backbone length. Information on R-PCEs is given in Table 4.2a.

4.3.3. Grafting of Precursor Backbones

A second set of PCEs was obtained by grafting of PMAA precursor backbones with different molar mass (PMAA-5k, $M_w \approx 5$ kDa; PMAA-8k, $M_w \approx 8$ kDa, Table 2.8b) with MPEG of different length (MPEG-11 and MPEG-22, Table 2.8a) *via* polymer-analogous esterification. Here, different grafting ratios between 2 and 5 were aimed for. PCEs obtained *via* grafting are termed G-PCEs. All G-PCEs and the precursor backbones were supplied by Sika AG, Switzerland. More information about the grafting process and all applied educts can be found in *Chapter 2.5*. Information on all applied G-PCEs is summarized in Table 4.2b.

4.3.4. Free Radical Copolymerization

For comparison of the synthesis techniques, three additional PCEs were synthesized *via* free radical copolymerization of MAA and PEGMA in aqueous media. Information on FRC-PCEs is shown in Table 4.2c. The applied synthesis protocol can be found in *Chapter 2.4*. The same PCEs are subjected to SEC with dual concentration detection in *Chapter 3*.

4.4. Instrumentation

4.4.1. Size Exclusion Chromatography

All PCEs applied in this chapter were characterized using size exclusion chromatography. More precisely, a combination of multi angle laser light scattering (MALLS) and online RI detection was used for approaching absolute molar mass distributions (MMDs). More information about the instrumental setup and the characterization protocol can be found in *Chapter 2.6.2*.

4.4.2. RP-HPLC

RP-HPLC chromatograms of the (co)polymers were recorded on an Agilent 1260 Infinity HPLC instrument using evaporative light scattering detection (SOFTA Model 1400 ELSD) The temperature of the spray chamber was set to 30 °C and the one of the drift tube is 60 °C.

The HPLC system was equipped with a Waters XTERRA MSC18 column (150 mm \times 4.6 mm, 5 μ m diameter particle size, 8 nm pore size). The column was kept in a column oven (TCC6000, Polymer Standard Service, Mainz, Germany) and the temperature was set to 35 °C. Acetonitrile (ACN, HPLC gradient grade, \geq 99.9 %) was used as solvent A and water was used as solvent B. The water was purified using a Millipore filtration system. Moreover, 0.1 vol% of TFA was added to the aqueous solvent. All (co)polymers were dissolved in ultrapure water. For gradient experiments, the concentrations ranged between 5-10 mg/mL and the applied injection volumes were between 50-100 μ L. During isocratic experiments, sample concentrations were 1.0 mg/mL and 1-5 μ L were injected. In all experiments,

the flow rate was kept constant at 1.00 mL/min. The column temperature was kept at 35 °C during all RP-HPLC experiments. For solvent compositions with a volume fraction of more than 47 vol% ACN ($\phi_A > 47$ vol%), MPEG elutes in SEC mode. For $\phi_A < 47$ vol%, MPEG elutes in liquid adsorption chromatography (LAC) mode, meaning that big molecules are retained longer than small ones due to increased interactions between solute and stationary phase.

4.4.3. Development of the Solvent Gradient

The solubility of PCEs is strongly influenced by the chemistry of their side chains. For the determination of critical conditions of MPEG, RP-HPLC experiments were carried out under isocratic conditions using different combinations of solvent A and B. MPEG with different molar masses (350, 500, 1000, 3000, 5000 and 7500 g/mol provided by Sika AG, Switzerland) were injected. For a solvent composition of 47 vol% of A and 53 vol% of B critical conditions were found meaning that MPEG elutes independent of its molar mass ($V_{LCCC} = 1.25$ mL, Figure 4.1a).

In Figure 4.1b, three R-PCEs with variations in their C/E ratio were subjected to isocratic RP-HPLC experiments using critical conditions of MPEG. All samples have their elution maximum at approximately 1.25 mL meaning that the R-PCEs elute at the same retention volume as MPEG. At 1.1 mL the peaks feature a shoulder indicating the elution of a second species. It is conceivable that the R-PCE samples contain residual macromonomer, PEGMA. However, as a consequence of the rather unpolar double bond attached to each macromonomer, PEGMA is expected to elute slightly after the PCE. Alternatively, the shoulder is possibly due to the elution of $\alpha - \omega$ - dihydroxy-PEG, an impurity contained in the macromonomer. While, isocratic RP-HPLC only allows to separate remaining macromonomer or impurities from the PCEs it does not provide the means to distinguish molecules by C/E ratio. Therefore, a solvent gradient was developed (Figure 4.1c).

All gradient experiments started with an eluent composition of 5 vol% A (ACN) and 95 vol% B (water). Upon injection, the volume fraction of A was linearly increased from 5 to 30 vol% within 20 minutes. Subsequently, the volume fraction of A was further increased linearly up to 50 vol% within another 30 minutes. In the final stage A was increased linearly up to 80 vol% within additional 25 minutes (Figure 4.1c). Hence, the polarity of the mobile phase was gradually decreased.

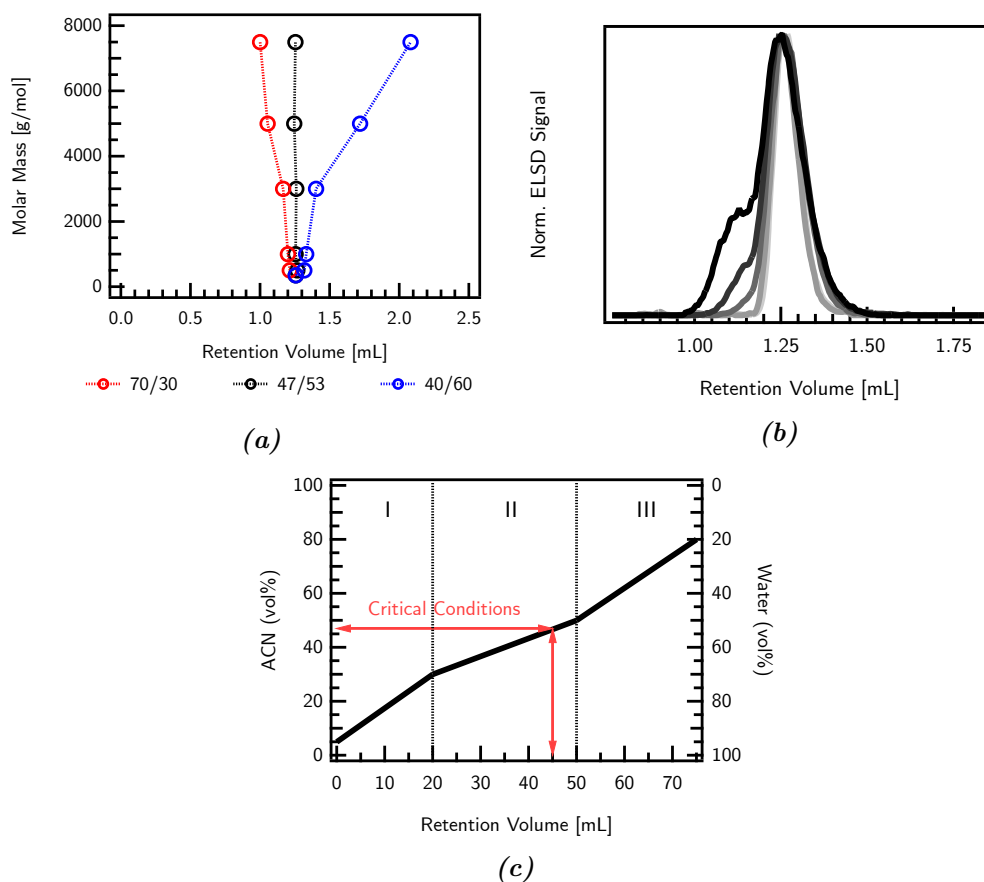


Figure 4.1. (a) Establishing critical conditions for MPEG on a C18 column. For 47 vol% ACN and 53 vol% water ($A/B=47/53$) MPEG elutes independent of its molar mass. A higher volume fraction of ACN results in steric exclusion, while a decrease in ACN allows interaction between the solute and the stationary phase). (b) Chromatogram of various R-PCEs at critical conditions of MPEG as found in (a). The elution peaks of all samples are overlapping. (c) Gradient for RP-HPLC measurements of PCEs. The composition of the mobile phase was gradually changed from 5/95 to 80/20.

Referring to MPEG, the solvent composition changes from LAC conditions to SEC conditions (see *Chapter 1.7.2*).

4.5. Results and Discussion

4.5.1. Gradient RP-HPLC of Polymers with Low Dispersity

The polarity and solubility of PCEs is significantly impacted by their grafting ratio. Thus, also enthalpic interactions between PCE molecules and the C18 column are expected to be influenced by the comonomer composition of PCEs. Generally speaking, more hydrophobic PCE molecules (low C/E) are expected to interact stronger with the stationary phase (= longer retention) than more hydrophilic ones (high C/E). To validate this assumption, a small library of R-Polymers (Table 4.2a) was investigated.

In a first step, R-PMAA (ungrafted backbone) was subjected to the previously described gradient. In the chromatogram one elution peak is found at 16 mL (Figure 4.2, top). For solvent compositions with a high volume fraction of water, R-PMAA was found to adsorb to the column material. Due to the high polarity of carboxylic acid groups, R-PMAA mainly interacts with the C18 column *via* the methyl groups of the backbone. Interactions occur for very polar solvent compositions. With increasing volume fraction of ACN (decreasing polarity of the mobile phase), hydrophobic interactions are decreased and R-PMAA is flushed out from the column. More specifically, R-PMAA elutes during stage I of the applied solvent gradient.

C18 stationary phases are commonly produced by modifying the surface of silica particles with octyldecyl silane. As a result of incomplete surface modification, several silanol groups remain on the silica surface. These silanol groups could strongly interact with the carboxylic acid units of R-PMAA *via* formation of hydrogen bonds [159], possibly causing irreversible adsorption of the solute molecules to the column packing material. However, as R-PMAA elutes upon increasing the ACN content, it can be expected that the retention of R-PMAA is dominated by hydrophobic interactions between the methyl groups of the R-PMAA backbone and the C18 chains.

In a second step, R-PPEGMA (100% grafted backbone) was investigated. In the corresponding chromatogram, three elution peaks can be identified. The first two peaks show a modulation (Figure 4.2) indicating the elution of polymer molecules with slightly different degree of polymerization. The first peak is caused by PEG molecules, which are impurities contained in the PEGMA macromonomer. The second peak is caused by residues of PEGMA itself. PEG elutes before PEGMA due

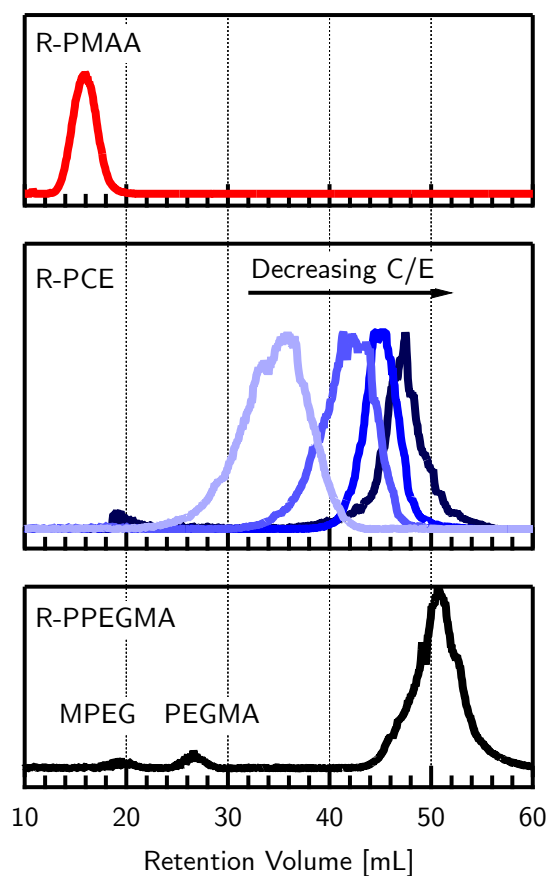


Figure 4.2. RP-HPLC experiments using solvent gradients of water and ACN for several R-Polymers. All polymers were obtained from RAFT (co)polymerization with MAA and/or PEGMA-19. The elution peak of PMAA is located at 15.8 mL. The R-PCEs have C/E ratios between 9.0 and 0.7 and elute at the following retention volumes: 35.5 mL (R-PCE-9.0-19), 42.5 mL (R-PCE-4.5-19), 45.3 mL (R-PCE-2.2-19) and 47.2 mL (R-PCE-0.7-19). R-PPEGMA elutes at 50.8 mL. More information on the molecular characteristics of all applied R-Polymers is shown in Table 4.2a.

to its higher polarity. The hydroxy end groups of the PEG are more polar than the methacrylate moiety of PEGMA.

The main peak indicates the elution of R-PPEGMA between 44.0 and 60.0 mL. Thus, R-PPEGMA elutes significantly later than R-PMAA revealing a stronger interaction with the column material. Hence, the presence of side chains increases the retention time. Notably, for approximately 45 mL, the solvent composition of the mobile phase is equal to critical conditions of MPEG. Consequently, R-PPEGMA starts desorbing from the column shortly before the critical point is reached.

The elution peak of R-PMAA and R-PPEGMA are clearly separated from each other. PCEs are expected to elute in between both peaks. In order to find out if a separation according to the C/E ratio is possible, a series of R-PCEs with C/E ranging between 0.7 and 9.0 is investigated. As can be seen from Figure 4.2 (middle), the PCEs elute between 26.0 and 56.0 mL. With decreasing C/E ratio, the elution maxima are shifted to higher retention volumes, meaning that highly charged PCEs elute closer to R-PMAA while highly grafted PCEs elute closer to R-PPEGMA.

However, it is only possible to distinguish PCEs with significant differences in C/E ratio from each other. The peaks of R-PCE-9.0-19 and R-PCE-2.2-19 are baseline separated. On the contrary, the peaks of R-PCE-4.5-19, R-PCE-2.2-19 and R-PCE-0.7-19 are overlapping. While the elution maxima are shifted to higher volumes with decreasing C/E, the peaks are not baseline separated.

The results presented in Figure 4.2 confirm that RP-HPLC with solvent gradients of ACN/Water allows to separate PCEs by grafting ratio as a consequence of enthalpic interactions between PCE and stationary phase. Two types of interactions were identified to contribute to the total retention: The methyl groups of the backbone and the side chains can interact with the C18 column material. This means that a change in backbone length, but also a change in side chain length, potentially contributes to the total retention time of a PCE. Importantly, all R-Polymers have a similar backbone length and identical side chain length. Hence, the retention was only impacted by changes in C/E (*i.e.* grafting degree). In order to reveal how a change in the length of backbone or side chain is reflected in the chromatogram, a series of PCEs with systemic variations in these parameters was investigated. Understanding the impact of these variations is essential to properly interpret the chromatograms of PCEs with higher dispersity.

4.5.2. Variations of Side Chain Length

R-PCE-2.2-19 and R-PCE-1.7-9 have a similar backbone length and C/E ratio, but differ in side chain length. Figure 4.3a shows the chromatogram of the corresponding RP-HPLC experiments. According to Figure 4.3a, no particular effect of *P* on retention is observed. Both R-PCEs elute between 35.0 and 55.0 mL. The elution maximum of R-PCE-1.7-9 is very slightly shifted to higher volumes, however, this could be due to the small difference in the grafting degree (C/E 1.7 *vs.* 2.2). To

confirm these conclusions, an additional investigation of the effect of P was carried out, as described below.

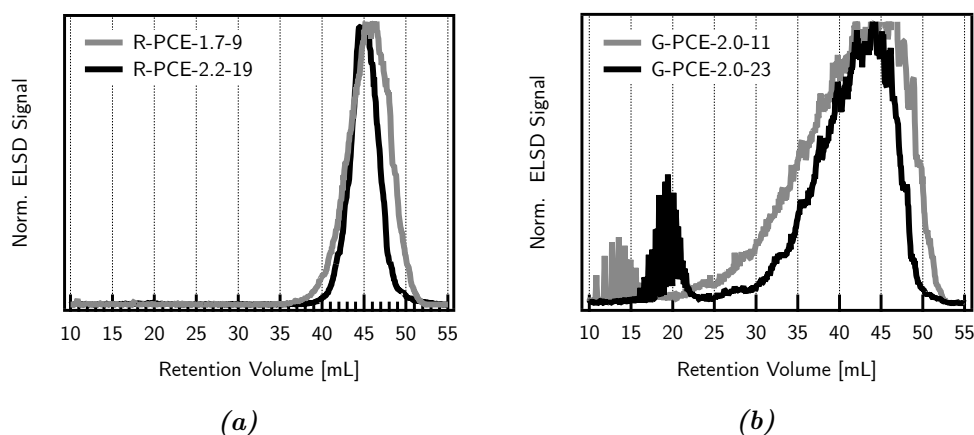


Figure 4.3. Impact of side chain length on retention of PCEs in a RP-HPLC experiment with solvent gradients. (a) R-PCEs: Both R-PCEs have a very similar backbone length (degree of polymerization) and also their C/E ratio is comparable. (b) G-PCEs: Both G-PCEs were grafted onto the same PMAA-5k precursor. Moreover, the C/E ratio of both G-PCEs was found identical from $^1\text{H-NMR}$ measurements. For both types of PCE the side chain length does not significantly impact the retention.

This time, two G-PCEs with identical backbone (PMAA-5k) and identical C/E ratio were used. Figure 4.3b shows the chromatograms of the RP-HPLC experiments. For both G-PCEs, two elution peaks can be distinguished. The first peaks (at lower retention volume) are modulated, as previously found for R-PPEGMA (see Section 4.5.1). These peaks indicate the elution of residual MPEG that was not grafted onto the backbone. Notably, MPEG-11 elutes earlier than MPEG-22 revealing that the interaction between MPEG and stationary phase depends on the length of the side chains. Thus, the EO units of MPEG interact with the column material. Besides EO, also the hydroxy and methoxy end groups of each chain can interact with the stationary phase.

The main peak of the chromatogram (between 25.0 to 55.0 mL) signalizes the elution the G-PCEs. Similar to the two R-PCEs, both G-PCEs, elute simultaneously. However, their elution peaks are significantly broader than for the R-PCEs. This can be explained by their higher dispersity, in particular the dispersity regarding backbone length is likely to cause peak broadening.

It appears that the side chain length does not notably influence the retention behavior. It might have an effect when PCEs with big differences in P are compared.

However, most common PCEs used in concrete technology are composed by one type of side chain. Hence, the effect of P on retention is not of particular importance for the RP-HPLC analysis of PCEs. In contrast, variations in the backbone length have to be considered when dealing with disperse PCEs.

4.5.3. Variations of Backbone Length

The impact of backbone length on the retention behavior is investigated in Figure 4.4. Here, two series of PCEs are compared with each other. The first series of PCEs was obtained by grafting MPEG-22 onto PMAA-5k (Figure 4.4, bottom). The precursor used for the second series of G-PCEs was PMAA-8k (Figure 4.4, below).

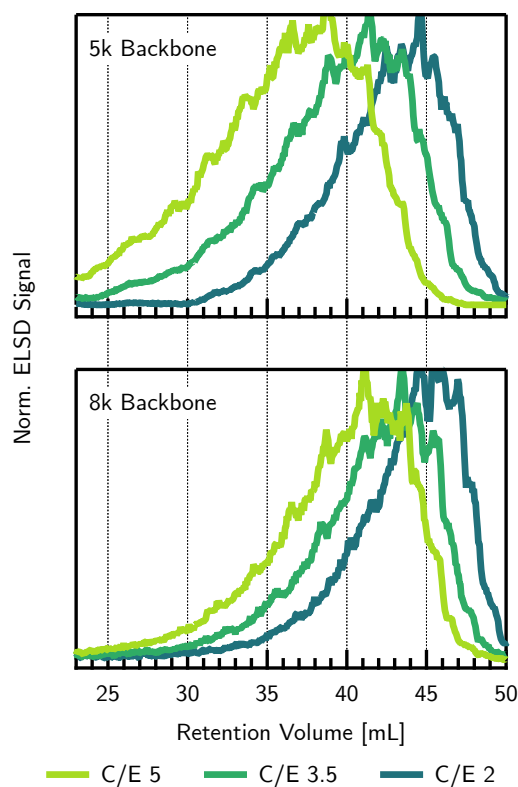


Figure 4.4. Impact of backbone length on retention of G-PCEs in a RP-HPLC experiment with solvent gradients of ACN/Water. The side chain length of all PCEs shown here is $P=22$. An increase in backbone length causes a slight shift of the elution peak to higher volumes.

It appears that for a given C/E ratio and fixed P , PCEs are retained longer, when the backbone length is increased. This is plausible, as an increase in backbone

length coincides with a higher number of groups that can potentially interact with the stationary phase. Besides, interactions between the backbone itself and the column material, an increase of the degree of polymerization also results in more contacts between side chains and column material. Hence, compared to SEC, where bigger molecules elute earlier, the order of elution is reversed.

Evidently, the retention of PCEs during the gradient experiment depends on multiple factors, most importantly grafting degree, but also backbone length. Changes in both parameters impact the elution. Hence, an important factor that always has to be considered when characterizing polymers by 1D-chromatography (LAC and SEC) are coelution phenomena. Regarding the gradients, this means that PCEs with a long backbone and high C/E (low grafting), might coelute with shorter and higher grafted molecules.

4.5.4. Gradient Experiments of PCEs from Free Radical Copolymerization

In the previous sections, the impact of molecular parameters on the retention behavior was investigated by using PCEs with distinct molecular properties. However, most commercially relevant PCEs are obtained from free radical copolymerization which means that they are likely to contain a variety of molecules with different backbone length, C/E ratio and possibly even different architectures (*i.e.* gradients, blocks *etc.*)

In order to determine whether RP-HPLC can be used to get an insight into the molecular heterogeneity of more broadly dispersed PCEs, we subject FRC-PCEs to the gradient method. In contrast to R-PCEs and G-PCEs, where the length of the backbone is known, we only hold information about the average C/E ratio of the FRC-PCEs. The chromatograms, of three FRC-PCEs are shown in Figure 4.5a. With decreasing C/E ratio, the elution peak is shifted to higher volumes. This is in agreement with the retention behavior found for G-PCEs and R-PCEs in the previous sections. All FRC-PCEs elute approximately between 30 and 55 mL. Thus, the overall width of the elution peaks is comparable to the one of G-PCEs.

The width of the elution peak is determined by the overall dispersity of the samples regarding degree of polymerization and chemical composition. In Figure 4.5b the elution behavior of PCEs with similar C/E and P , but different dispersity is compared. While R-PCE-2.2 elutes in a well-defined peak, the two G-PCEs and

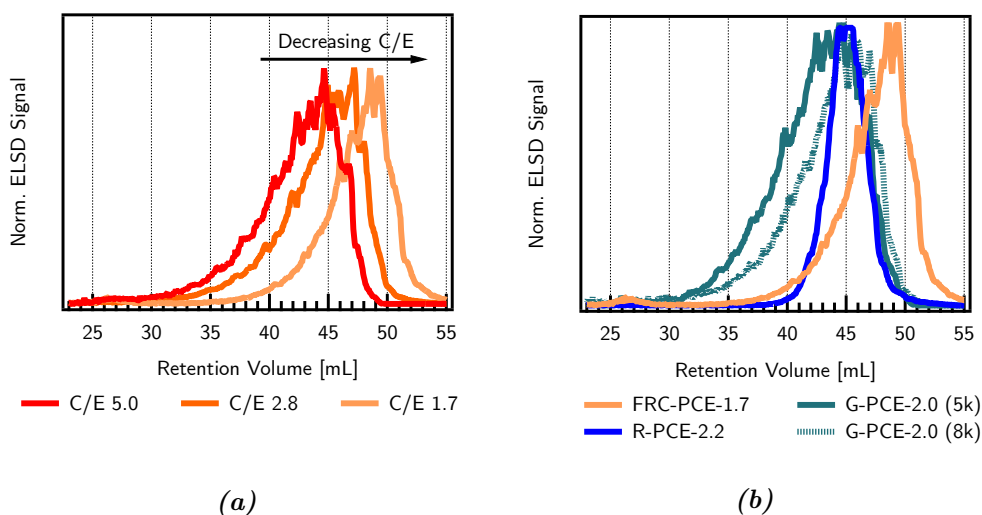


Figure 4.5. (a) RP-HPLC experiments using solvent gradients of water and ACN for several FRC-PCEs. All polymers were obtained from free radical copolymerization of MAA and PEGMA-19.

FRC-PCE have a significantly broader elution peak. Notably, the peak of FRC-PCE-1.7 elutes later than the other samples (Figure 4.5b, orange). This might due to the slightly lower C/E ratio. Alternatively, this can be caused by the presence of FRC-PCEs with very high degree of polymerization (long backbone). It is noteworthy, that the applied gradient method is capable of separating the peak maximum of these FRC-PCEs. In SEC experiments (*Chapter 2*, Figure 2.9), the elution peaks of these polymers completely overlapped.

In *Chapter 3*, dual concentration SEC experiments revealed a correlation between molecular size and C/E ratio for G-PCEs and FRC-PCEs. While this correlation is moderate for G-PCEs, FRC-PCEs show more significant changes in C/E ratio with molecular size. It appeared that small molecules tend to have a higher C/E ratio than larger ones. Theoretically, the gradient method is capable of separating small and highly charged PCEs (early elution) from big and highly grafted PCEs (longer retention). However, coelution phenomena always have to be considered in 1D-chromatography of polymers. Specifically, as previously mentioned PCE molecules with high charge density (low grafting density) and long backbone potentially elute simultaneously with molecules that are higher grafted (low charge density) but short.

Despite the different separation mechanism in SEC, which is driven by entropy, similar parameter contributions of C/E and backbone length (*i.e.* degree of polymerization, DP_n) can cause coelution. Also in SEC, a long and highly charged

PCE might elute simultaneously with such molecules that are short but highly grafted. Hence, it becomes evident that the information obtained from SEC and RP-HPLC always has to be evaluated carefully while considering coelution phenomena. Moreover, as the retention in both techniques is impacted by C/E and DP_n , SEC and RP-HPLC cannot be considered orthogonal. Consequently, RP-HPLC does not provide the exact CCD and SEC does not give the exact MMD. Both analytical methods only allow to approach CCD and MMD.

4.5.5. Fractionation and 2D-Chromatography

In order to get a more comprehensive picture of the molecular heterogeneity within FRC-PCEs, the gradient method was complemented by additional SEC measurements using the so called "heart-cutting" technique (see *Chapter 1.12*). To this end, the chromatograms shown in Figure 4.5a were divided into multiple fractions ("heart cuts"), which were manually collected using a fraction collector. More precisely, between 27 and 55 mL, 28 fractions were collected (each with a volume of 1 mL). Subsequently, each fraction was investigated by SEC in the second dimension. The results of this offline 2D-approach (*i.e.* RP-HPLC–LC) are presented in Figure 4.7 as contour plots. The RI signal in the second dimension was coded using a color scale and, for illustration purpose, the data between the points was interpolated. The interpretation of these 2D-plots is complex, as the combined effects of C/E and backbone length have to be considered in each dimension.

Before analyzing the contour plots of the PCEs, it is helpful to have a look at Figure 4.6. This figure shows a schematic 2D-analysis of a homopolymer (*e.g.* PEG) with high molar mass. The hypothetical PEG is subjected to the same gradient as the PCEs in this chapter. It is assumed that all PEG molecules are monofunctional (MPEG). This means that they carry the exactly same end groups and are only disperse with regard to their chain length P (*i.e.* degree of polymerization, DP_n).

For early HPLC fractions, a dependence of the HPLC retention volume (V_R), on the elution volume of the SEC experiment (V_{Elu}), can be observed. With increasing V_R , V_{Elu} decreases slightly, indicating a molar mass dependence of the HPLC separation. Molecules that elute early from the second dimension have a big hydrodynamic volume. Consequently, with increasing V_R , the molar mass of PEG increases. For late HPLC fractions, the elution in the first dimension is independent of V_{Elu} .

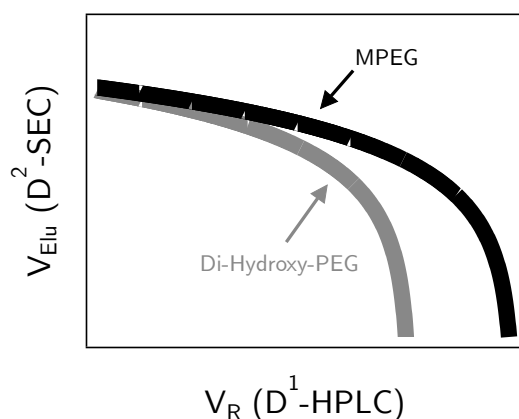


Figure 4.6. Schematic 2D-analysis (RP-HPLC \times SEC) of a linear, monofunctional MPEG homopolymer (black curve) and a bifunctional PEG (grey curve). For early HPLC fractions, a dependence of V_R on V_{Elu} can be observed. At high HPLC retention volumes, the separation in the first dimension occurs independent of V_{Elu} (= independent of molar mass). Hence, the corresponding 2D-plot has a curved shape that was referred to as "bananagram" by Schoenmakers et al. [147]

The 2D-plot (schematic illustration Figure 4.6) displays a curved "banana shape". This particular shape indicates that the separation in the first dimension occurred on the adsorption side of the critical point. Notably, this particular plot can be obtained for homopolymers, which contain only one type of monomer and is solely the consequence of dispersity in the degree of polymerization [147, 148]. If the PEG sample contains a second species (*i.e.* $\alpha - \omega$ -dihydroxy-PEG), interactions between these groups and the stationary phase impact the retention in the first dimension rather than the size in the second dimension. Hence, for this species, another "bananagram" (grey curve) is found. If the gradient is not suitable to separate both species by their functionality, both "bananagrams" will smear out and give one broad contour plot.

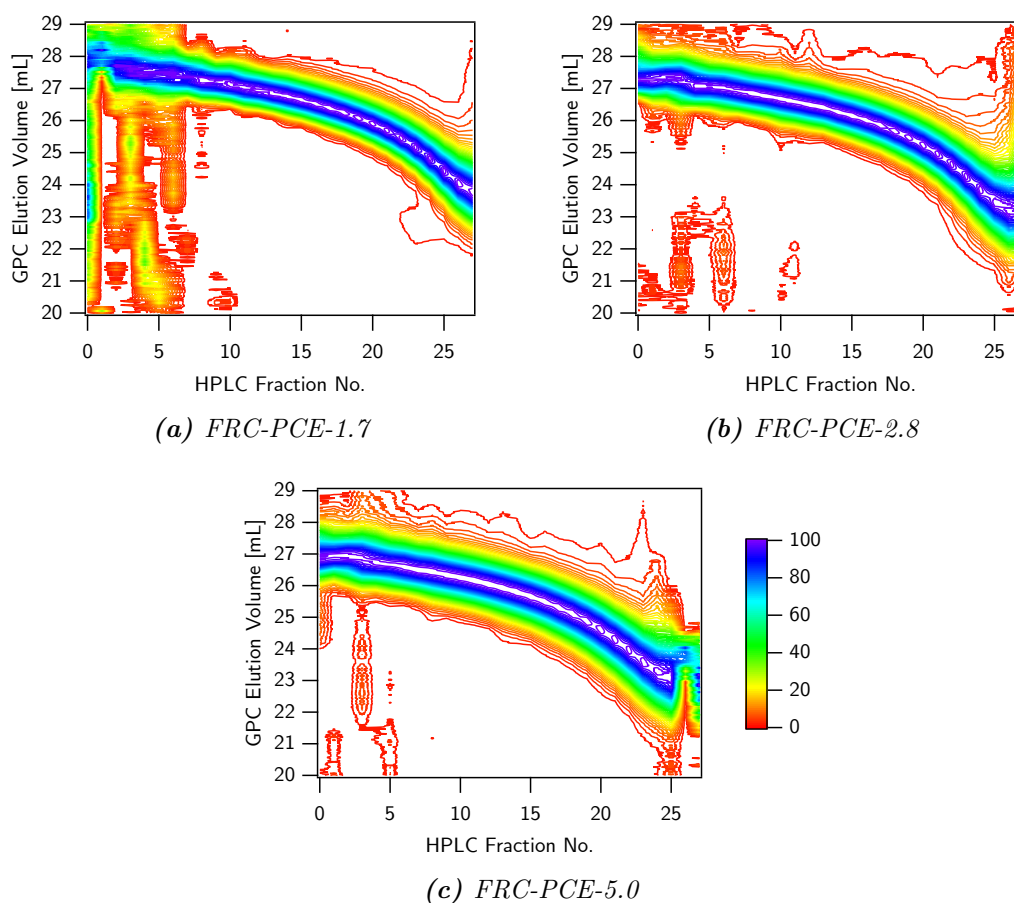


Figure 4.7. (a)-(c) 2D-Chromatography of FRC-PCEs using RP-HPLC in the first dimension and SEC in the second dimension (RP-HPLC-SEC). The results are presented as contour plots. In the first dimension (x -axis) the samples were subjected to gradient RP-HPLC. 28 Fractions were collected and injected into a SEC setup with RI detector in the second dimension. The SEC data is shown along the y -axis. The intensity of the RI detector in the second dimension is coded using the color scale shown below. For illustration purpose, the data between the points was interpolated.

Let's turn our attention to the contour plots of the FRC-PCEs. According to Figure 4.7a, early fractions (Fraction 0-9) from the first dimension of FRC-PCE-1.7 elute between 20 and 29 mL in the second dimension. Thus, these fractions contain molecules with significant differences in hydrodynamic size. For later fractions (Fraction 10-28), the elution peak is visibly less broad. For instance, fraction 10, elutes approximately between 26.0 and 28.5 mL. This indicates that these fractions contain PCE molecules with a well-defined hydrodynamic size. With increasing HPLC fraction number, the SEC peak moves towards smaller elution volumes, indicating the elution of PCE molecules with a higher hydrodynamic volume. Interestingly, the

GPC elution volume decreases moderately (from 29 to 25 mL) for the fractions 1-20, while a more pronounced decrease can be observed for fractions 20-28 (from 25 to 22 mL). This trend causes a particular "banana shape" that was introduced in the previous section. For FRC-PCE-2.8 (Figure 4.7b) and FRC-PCE-5.0 (Figure 4.7c), similar shaped contour plots were found. The "bananagrams" indicate that the separation mechanism in the first dimension occurred on the adsorption side of the critical point [147] confirming that the chosen RP-HPLC gradient separates PCEs according to interactions between solute and stationary phase. Hence, the performed experiments belong to the category of solvent gradient interaction chromatography (SGIC). Notably, for all HPLC fractions, separation depends on hydrodynamic size. Thus, the critical point where elution is independent of molar mass was not reached.

For linear homopolymers, the "bananagram" is the result of dispersity in backbone length. Regarding PCEs, this issue is more complex. Theoretically, the retention in the first dimension can be caused by variations in C/E and/or in the backbone length of the PCE. Looking at the individual HPLC fractions, the majority of these fractions elute in a narrow and well-defined peak in the second dimension, proving that within each fraction, polymer molecules with rather consistent chemical composition and similar backbone length can be found. Only early eluting HPLC fractions reveal a broader dispersity in hydrodynamic volume. With increasing V_R , the SEC peaks are shifted towards smaller V_{Elu} . Overall, the PCE molecules elute between roughly 29 and 20 mL in the second dimension. Thus, the global elution peak in the second dimension is rather broad. A broad elution in SEC is directly related with the presence of molecules with big differences regarding their hydrodynamic size. This indicates that the retention in the first dimension is more likely caused by a disperse backbone than by broad dispersity in C/E. This can be understood by looking at Equation 4.1:

$$R_H \propto \left(\left(\frac{a_N}{a_P} \right)^2 \frac{(1 - 2\chi)}{2} \right)^{0.2} a_P \cdot P^{0.4} (C/E + 1)^{0.2} \cdot n^{0.6} \quad (4.1)$$

where R_H is the hydrodynamic radius of a PCE, a_N represents the backbone monomer size (0.25 nm for methacrylates), and a_P the side chain monomer size (0.36 nm for ethylene oxide, EO). χ is the *Flory-Huggins* parameter accounting for the solubility of the PCE (0.37 for PEO at 25 °C) [10]. n and P are structural parameters of the PCE as described in *Chapter 1.1*.

Equation 4.1[36] shows that the hydrodynamic radius of a (flexible backbone worm) PCE is proportional to the product of $(C/E + 1)^{1/5}$ and $n^{3/5}$. Here n refers to the number of structural units defined by Gay and Raphaël [37] and can be taken as a measure for the DP_n . Consequently, changes in the backbone length cause a more pronounced change in R_H than changes in C/E . Regarding SEC, this means that variations in the backbone length will have a significant impact on the elution volume, while variations in C/E will be less pronounced. This minimal impact of C/E on the elution volume can be understood when looking at Figure 2.1b (see *Chapter 2*), where the SEC chromatograms of various R-PCEs are shown.

Coming back to the contour plot of the FRC-PCEs, the curvature of the "bananagrams" (Fractions 20-28) is probably due to changes in the degree of polymerization at rather constant C/E . However, a certain dispersity in C/E is feasible. The fact that early fractions from the first dimension appear to elute late in the 2nd dimension, also allows the conclusion that the contained PCE molecules are possibly more charged but adopt a smaller hydrodynamic volume than such fractions, which are retained longer in RP-HPLC. This conclusion cannot be drawn solely based on the shape of the "bananagram", but has to be combined with the findings from the SEC experiments with dual concentration detection (*Chapter 3*). Dual detection experiments revealed that FRC-PCE molecules with smaller hydrodynamic size have a higher C/E ratio. Notably, gradient RP-HPLC does not allow to precisely quantify the comonomer composition. The order of elution can only serve as an indicator for the grafting ratio. Indeed, it is difficult to interpret 2D-plots of PCEs that are potentially disperse in multiple parameters. Most information on a sample can be revealed when comparing between the contour plots of various samples of different dispersity.

4.6. Comprehensive LC Analysis of PCEs

Finally, all applied LC techniques applied throughout this thesis are compared and their relevance for PCE characterization is discussed. To this end, all LC experiments which were carried out with FRC-PCEs are summarized and interpreted. Standard SEC experiments (MALLS/RI) revealed broad elution peaks, indicating that the FRC-PCEs contain molecules with significant variations in hydrodynamic size. The steric exclusion mechanism in the SEC was not capable to separate the peaks, which all eluted simultaneously (Figure 2.9a). However, SEC with MALLS and online RI

detection is very useful to approach the MMD (Figure 2.9b). The dispersity index, \mathfrak{D} , gives a first idea of the dispersity in molar mass, or more accurately in hydrodynamic size. For FRC-PCEs \mathfrak{D} was found to be close to 2 (Table 4.1). This value is typical for polymers obtained from free radical polymerization techniques.

By adding a second concentration detector to the SEC device, the comonomer content in PCEs can be monitored along the elution axis. This provided a first insight into the chemical heterogeneity of FRC-PCEs, however, it does not provide the means to reveal details about the CCD. For FRC-PCEs, a dependence of the C/E ratio on the hydrodynamic size was revealed (Figure 3.8, *Chapter 3.5.4*). More precisely, for our FRC-PCEs, late eluting molecules (small hydrodynamic size) have a higher C/E ratio than early eluting molecules (big hydrodynamic size). For instance, for FRC-PCE-5.0, the C/E changed by more than 4.0 units between beginning and end of the SEC elution peak.

In order to get a deeper insight into the CCD, RP-HPLC experiments involving solvent gradients of water and ACN were applied. For FRC-PCEs this method allowed to partially separate the FRC-PCEs by their C/E. This can be seen from the peak shift in Figure 4.5a. For PCEs with low dispersity in backbone length, RP-HPLC separates PCEs exclusively according to their grafting ratio. Thus, this technique offers the means to access the CCD. However, most PCEs are disperse regarding their backbone length. In this case, the retention in RP-HPLC depends on C/E, as well as degree of polymerization.

The separation mechanism of both techniques, SEC and RP-HPLC (*i.e.* SGIC), is fundamentally different. While SEC separates by size, SGIC depends on enthalpic interactions between solute and column material. However, both techniques do not allow an orthogonal separation of PCEs because C/E and DP_n impact the retention in both dimensions. This complicates the interpretation of the 2D-results, but, while this situation is not optimal for 2D-analysis, the contour plot of a PCE is very useful to access and describe its dispersity.

Consequently, RP-HPLC and SEC experiments were combined, and an offline 2D-analysis (RP-HPLC-SEC) was performed. The corresponding contour plots have a curved shape ("bananagram"), which was connected with significant variations in the backbone length. The shape of the contour plot is in agreement with the results from the dual experiments. Small molecules are likely to be higher charged than big molecules. Finally, it can be concluded that all individual LC experiments work like

a puzzle that finally reveal and confirm a complex heterogeneity regarding C/E and backbone length in FRC-PCEs.

4.7. Conclusion

As a preamble to this conclusion section, it is worth noting that all applied PCEs were considered to be statistical copolymers. This assumption is legitimate based on similar copolymerization parameters of the MAA and PEGMA-19 (see *Chapter 1.5.2*). However, possible variations in the molecular architecture (*i.e.* statistical, gradient, block) might also affect PCE retention and cause coelution.

A main outcome of this chapter is to show that RP-HPLC is suitable to separate PCEs according to their grafting ratio. However, the C/E is not the only factor influencing the retention behavior. While the contribution of side chain length on retention appears negligible, variations in the backbone length do impact the separation process. Consequently, besides the chemical composition, also the degree of polymerization impacts the retention volume. Hence, coelution phenomena have to be considered. In particular, highly charged PCEs with a long backbone and such molecules that are highly grafted but shorter in backbone length are expected to elute simultaneously.

Similar coelution phenomena also occur in SEC experiments. While SEC separates by steric exclusion, the separation in the gradient experiments is based on enthalpic interactions. Consequently, similar fractions which are found to coelute in gradient experiments, potentially also show a similar retention behavior under SEC conditions. Moreover, the retention mechanism in both techniques is impacted by C/E and DP_n meaning that RP-HPLC and SEC are not orthogonal when applied to PCEs.

While RP-HPLC–SEC does not allow to completely disclose MMD and CCD, combining both techniques is still useful to get a more comprehensive idea of the heterogeneity within disperse PCEs. To this end, fractions obtained from RP-HPLC can be subjected to SEC in the second dimension. The here presented offline approach provides a first insight into the molecular dispersity of PCEs. However, fully-automated online coupling of both LC techniques (*i.e.* RP-HPLCxSEC) is ultimately aimed for, which can continuously transfer fractions from the first dimension to the second one. As pointed out before, due to coelution, and the fact that RP-HPLC and SEC are not orthogonal, also the 2D-analysis does not give definite answers

regarding MMD and CCD. To this end further analytical methods, possibly dual detection in the second dimension, might be beneficial. In this case, the C/E ratio in each 2D-fraction can be quantified.

In this thesis, the analysis of PCEs was focused on MPEG-type PCEs with PMAA backbone. Gradients of ACN and water have been proven to be applicable to a wide range of hydrophilic copolymers [142]. Thus, we suggest RP-HPLC for PCEs with different chemistry and comonomers as shown in Figure 1.7.

An important lesson learned in this chapter is that neither MMD nor CCD of PCEs can be accessed easily. Both analytical methods can only be used to approach the distributions. Moreover, it was found that 1D-experiments are not sufficient to get a profound insight into the molecular heterogeneity. To this end, it is essential to apply multi-detection methods or carry out complementing LC experiments in a second dimension. Notably, despite the above-mentioned limitations, 2D-separation of PCEs combining RP-HPLC (*i.e.* SGIC) with SEC is a promising tool to reveal heterogeneity within PCEs. Refining gradients and additional detection methods in SEC will allow to disclose more features about MMD and CCD. While it is difficult to interpret a single contour plot of a PCE, comparing between the 2D-analysis of different samples will allow to reveal and understand differences in their molecular heterogeneity.

4.8. Implications for Admixture Research

4.8.1. Mapping Dispersity

In this context, we suggest, that the overall molecular heterogeneity of PCEs including aspects of MMD and CCD should not be characterized solely by 1D-chromatograms and dispersity indices, but rather by a contour plot. The pattern and shapes of this "chromatography map" accurately combine information on composition and hydrodynamic size and allow to draw conclusions regarding molecular heterogeneity. Those maps are best used when comparing between different samples.

4.8.2. Identification of PCE Species

Currently, many researchers aim to correlate molecular characteristics with PCE performance. In *Chapter 5*, we contribute to this research field by showing that highly charged PCE molecules and molecules with a longer backbone show a high affinity for adsorption at the cement interface. Such results indirectly advocate for the need for better characterizing polymer dispersity.

In this sense, a contour plot is helpful to identify fractions within PCEs that are potentially less competitive regarding the adsorption on cement than other molecules. After identifying these fractions, synthesis conditions may be adapted for the production of highly efficient superplasticizers with tailor-made molecular structures.

This scenario is best explained by looking at Figure 4.8, which shows a hypothetical contour plot of a PCE. The plot does not give measurement data, but was calculated assuming *Gaussian* distributions in both LC dimensions. The "2D-map" is divided into four sectors and Table 4.3 explains the characteristics that can be assigned to PCE fractions located in each sector.

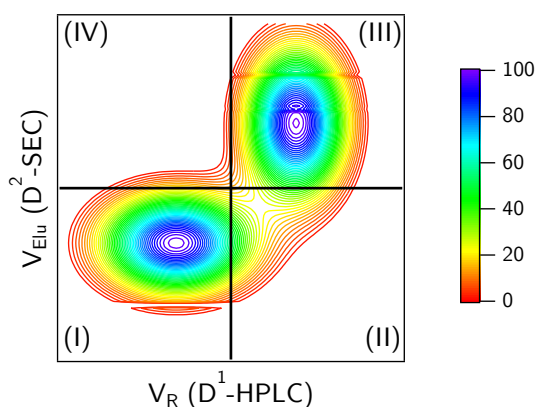


Figure 4.8. Calculated contour plot of a PCE containing two species which differ in their molecular characteristics. The chromatogram area was divided into four sectors.

The pattern of the modelled contour plot reveals that the PCE contains two different species. The fraction in sector I is potentially high in charge and large regarding its hydrodynamic size, which correlates with a long backbone. In contrast, PCEs of sector III tend to be lower in charge and small.

Table 4.3. Characteristics of PCEs located in different sectors of a contour plot obtained by RP-HPLCxSEC as shown in Figure 4.8.

Sector	Characteristics
(I)	high charge, large size
(II)	low charge, large size
(III)	low charge, small size
(IV)	high charge, small size

Based on structure-performance relations, the competitiveness of this PCE for adsorption or also its potential to cause retardation of the cement hydration behavior *etc.* can be predicted. To this end, it is not relevant if the structure-performance relations are based on empirical values or on scientific models, as long as reliable correlations between molecular parameter and performance are drawn. The example presented in Figure 4.8 reveals that chromatography data can be interpreted in a meaningful way when referring to validated structure-performance relations.

4.8.3. Structure-Performance-Relations: An Example

So far, we have stressed multiple times that molecular heterogeneity should be taken into account when aiming to understand the performance of a PCE. While one might argue that considering average parameters is often sufficient, we want to give an example that underlines the relevance of dispersity.

A widely known effect of using PCEs in cement is the fact that they delay hydration. Marchon *et al.* [28, 44, 45] derived an empirical equation that correlates the delay time (Δt) with the number of introduced carboxylate groups. Thus, Δt was successfully correlated with the PCE dosage and the C/E according to Equation 4.2:

$$\Delta t \propto n_{RU}^{tot} \cdot \left(\frac{C/E}{C/E + 1} \right)^{1.5} \quad (4.2)$$

$$\text{where } n_{RU}^{tot} = \frac{d_{PCE}}{M_{RU}}$$

here n_{RU} is the total number of structural repeating units (as defined by Gay, Raphaël [37] and Flatt [10]) that are introduced into the system. M_{RU} is the molar mass of this structural repeating unit and d_{PCE} is the applied PCE dosage.

In her study, Marchon [45] used PCEs of rather low dispersity in C/E, and it can be considered that each PCE contains only one species. For a mixture of PCEs with different molecular characteristics, we suggest calculating the overall delay in hydration (Δt) as the sum of delay times caused by the different species (Δt_i) contained in the sample. Hence, Equation 4.2 can be modified as follows:

$$\Delta t = \sum_{i=1}^S \Delta t_i \propto \sum_{i=1}^S n_{RU,i}^{tot} \cdot \left(\frac{(C/E)_i}{(C/E)_i + 1} \right)^{1.5} \quad (4.3)$$

where S is the total number of different PCE species contained in the sample. For $S=1$, Equation 4.3 is equal to Equation 4.2. $(C/E)_i$ is the C/E ratio of species i and $n_{RU,i}$ the number of repeating of this species added with the dosage.

It should be noted that the hypothesis that the total retardation is the sum of the retardation from the different components should be proven experimentally. However, since the work by Marchon *et al.* [28, 45], shows a linear increase of retardation with dosage of each of the superplasticizers they tested, this assumption should be reasonable.

In the following, we use Equation 4.3 to calculate the delay in hydration for three different PCEs. The characteristics of these PCEs are summarized in Table 4.4. PCE-A contains only molecules with C/E= 3. PCE-B and PCE-C are disperse regarding C/E and can be considered as binary mixtures of molecules, with C/E= 2 and 4 for PCE-B and C/E= 1 and 5 for PCE-C. Notably, the (number) average C/E of all samples is 3.0. In all three scenarios, the same dosage of PCE is applied.

The delay in hydration for PCE-A is used as reference value and is equal to 1.0. For PCE-B, the calculated Δt is only slightly smaller (0.97), showing that the dispersity in C/E is not expected to impact the hydration in this sample. However, for PCE-C, the Δt decreases to 0.86. This means that the calculated delay time is reduced by 14 %. This remains small, but is not insignificant.

Importantly, and as alluded to previously, Equation 4.3 has not been verified with experimental data yet. We have used it to illustrate how to infer possible

Table 4.4. Molecular parameters of the PCE species for the calculation of the delay in hydration Δt according to Equation 4.3. Here, Δt_i is the delay caused by species i . M_{RU} is given in g/mol and was calculated assuming a PMAA backbone ($M_{MAA} = 85\text{g/mol}$) and MPEG side chains with a molar mass of 1000 g/mol. n_{RU} is given in mmol and the total dosage is equal to 1 (g). The corresponding delay times were calculated as multiples of the delay obtained for sample A. Thus, the delay for PCE-A is equal to 1.0.

	PCE-A		PCE-B		PCE-C	
	A	B1	B2	C1	C2	
C/E	3.0	2.0	4.0	1.0	5.0	
M_{RU}	1340	1255	1425	1170	1510	
dosage	1	0.48	0.52	0.44	0.56	
n_{RU}^{tot}	0.75	38	0.36	0.38	0.37	
Δt_i	1.0	0.43	0.54	0.27	0.58	
Δt	1.0	0.97		0.86		

macroscopic effects using mechanistic relations as well as dispersity characterization. Our choice was guided by the arguable additivity of retardation contributions. For other properties, the behavior may be highly non-linear with dosage and even more complex for mixes. However, provided these effects can be described analytically, it becomes possible to better assess the role that dispersity may play in the overall performance of PCEs.

As a final remark, it is important to underline that PCE performance involves a combination of aspects, including dispersion and retardation. These issues have been handled analytically in the work by Marchon [12] and may provide a good basis for further studies considering dispersity. However, in cases when the combination of effects is more delicate to argue for, a more involved analysis would be needed.

At this point, the first part of this thesis which was focused on PCE synthesis and analytics is concluded. The second part is dedicated to competitive adsorption phenomena between PCE molecules with different molecular characteristics, aiming to derive scientifically-based models which enable to predict PCE competitiveness.

Competitive Adsorption - Part I

Impact of Charge Density and Backbone Length

The content of *Chapter 5* was published in the following research article:

"EXPERIMENTAL METHOD AND THERMODYNAMIC MODEL FOR COMPETITIVE ADSORPTION BETWEEN POLYCARBOXYLATE COMB COPOLYMERS"

Cement and Concrete Research, **2022**, Volume 151, 106523,
[doi:10.1016/j.cemconres.2021.106523](https://doi.org/10.1016/j.cemconres.2021.106523)

Stefanie Anne Weckwerth is the first author of this publication. She developed the concept for this work, designed and carried out experiments, evaluated and visualized the data as well as wrote the first draft of the article. The experimental work was supported by *Robert L. Temme*. The thermodynamic model and final paper manuscript are the result of intense discussions and collaboration between *S. A. Weckwerth* and *Prof. Flatt*.

5.1. Context

PCEs are interesting research subjects from two point of views. First of all, their comb copolymer architecture and polyelectrolyte characteristics make them interesting for polymer science. Indeed, their solution conformation and solubility behavior has been intensely studied in the past and well described by convenient scaling laws derived from polymer physics [10, 54]. Moreover, their ability to plasticize cement

pastes makes them an indispensable part of modern concrete technology. In this context, countless efforts have been done to study the performance of various PCEs in correlation with average molecular characteristics. However, there is a severe lack of studies that focus on the behavior of PCEs at the cement surface. Until today, many publications describe the adsorption equilibrium using the *Langmuir* Adsorption Isotherm. However, this model was derived for low molar mass species and is in principle inadequate to describe the adsorption of polymers, even if such adsorption tend to be “well-enough” fitted by the *Langmuir* equation. More importantly, there is a lack of models accurately correlating the PCE structure with their affinity and competitiveness during adsorption.

In the present chapter, we want to close this gap by proposing a thermodynamic model describing the competitive behavior of between PCE molecules at the cement surface, while accurately considering their molecular parameters and their nature as polymers. Therefore, the adsorption and exchange behavior between PCE molecules at the solid-liquid interface in cement paste is investigated. To achieve this, a methodology was developed making it possible to distinguish the adsorption of two similar PCEs. Hence, the existence of competitive adsorption between PCE molecules with different molecular architecture could be established. More precisely, the charge density $N (= C/E+1)$ has been identified as a driving force impacting the competition and quantified accordingly.

The starting point of the study was recognizing that in the past UV-Vis absorption measurements were successfully applied to detect the concentration of UV absorbing SPs like naphthalene sulfonates or poly(styrene sulfonates) [160]. While this is not possible for most commercial PCEs synthesized by grafting or radical copolymerization, PCEs prepared by RAFT polymerization do absorb sufficiently in the UV to be quantified in solution by UV-Vis spectroscopy (*Chapter 2.3.8*).

By combining well-established total organic carbon measurements with UV-Vis spectroscopy, competitive adsorption between PCEs of different structures could not only be revealed but also quantified. Results are interpreted by deriving a fundamental thermodynamic model describing the PCE competition as a dynamic equilibrium between adsorbed and dissolved PCE molecules with different architectures. The model rationalizes the effect of dispersity in charge and backbone length on the adsorption behavior of PCEs and contributes to a fundamental understanding of the PCE working mechanism on the molecular level.

5.2. Strategy

5.2.1. Basic Concept and Methodology

Throughout this chapter, homogeneously grafted PCEs are used. More precisely, the applied PCEs are flexible backbone worms as described in *Chapter 1.1.2*. The molecular parameters N (charge density), and $N \times n$ (backbone length) will play a central role to understand the impact of dispersity onto competition between PCEs.

In order to imitate the heterogeneity of N in a PCE having a distribution of the molecular structure parameter, binary mixtures of well-defined PCEs were used. One component was chosen to be UV-active (R-PCE) and the second one not (G-PCE).

The concept is summarized in Figure 5.1. First, a cement paste is prepared with relatively high water to cement ratio to facilitate subsequent extraction. The superplasticizer is added 15 minutes after the first contact between cement powder and water. Allowing the system to reach the induction period before adding PCE, prevents the PCE molecules from modifying the nucleation of ettringite and thereby modifying the specific surface area of cement [28, 30, 161–163]. As this factor has a major impact on the amount of PCE that can be adsorbed, it appeared the most reasonable choice for this study. Clearly however, the questions of how and to what extent PCEs impact ettringite nucleation is of high practical importance, but nevertheless out of the scope of this work [164–170].

As schematically represented in Figure 5.1, the aqueous phase was separated 15 minutes after having added the PCE. This was done using pressure filtration. The combined adsorption of both components was monitored by TOC measurements of extracted pore solutions. This was complemented by UV-Vis absorption measurements to determine the R-PCE adsorption. Thus, the combination of both techniques gives access to the exact weight fractions of adsorbed PCE species.

5.2.2. Assessing Molecular Level Effects

The above-presented strategy allows to verify competitive adsorption between PCE molecules of different charge density in cement. It makes it possible to go beyond only measuring effects of average properties of PCEs [28, 68, 77, 153–156]. However, it also called for well-planned experiments to be able to draw conclusive observations on

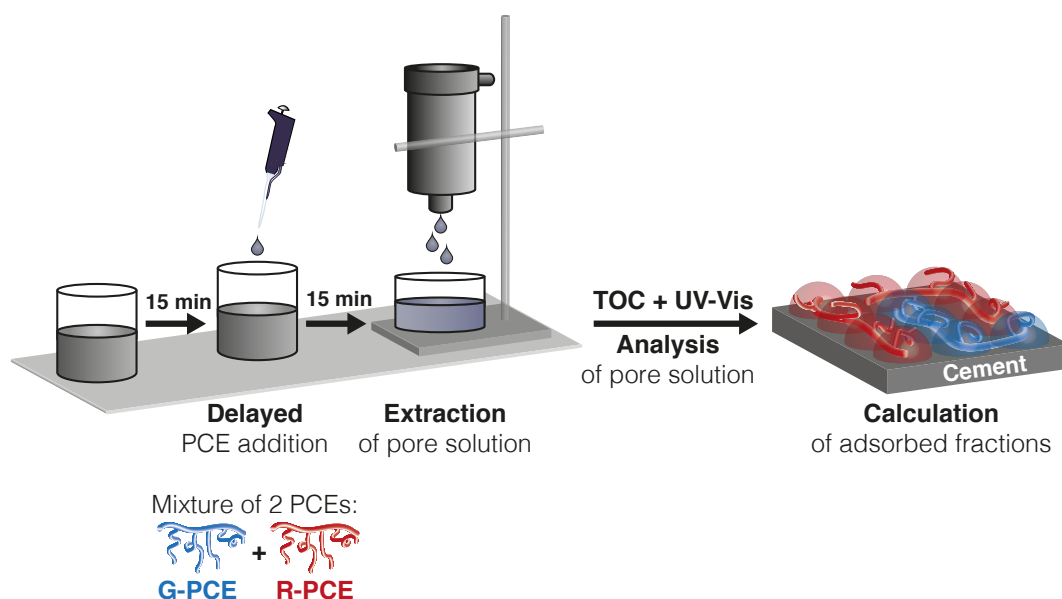


Figure 5.1. Schematic describing the concept of this study. A combination of TOC and UV-Vis absorption measurements gives access to the adsorbed fractions of PCEs with different charge density.

how molecular structure variations affect competitive adsorption within a dispersed polymer. For this study, we focused on the charge density N for a couple of reasons.

First, the dispersity of length in side chains (P), while not inexistent is rather limited and does not appear as a primary factor of concern. Second, as far as adsorption goes, the backbone length ($N \times n$) should not play a major role either on the adsorbed mass per unit area, or on the adsorbed layer thickness. However, the side chain spacing, related to the ionic density of the backbone, is expected to play a major role in the affinity of a PCE for cement surfaces. Thus, this factor is considered to play a major role in competitive adsorption. Moreover, it is often advocated that the widely used route of copolymerization may lead to PCEs with inhomogeneous side chain distributions.

All in all, it appears that the most pressing factor to examine competitive adsorption among PCEs is indeed the charge density N . Consequently, G-PCEs of different charge density ($N = 3.0, 4.3, 6.7$) were chosen to compete against a R-PCE ($N = 2.9$) obtained *via* RAFT-synthesis. A binary mix of one G-PCE and the R-PCE was added either simultaneously or sequentially after each other to a cement paste. Subsequently, the adsorbed fractions of each PCE were identified by combined TOC

and UV-Vis measurements, as suggested above. Considering these fractions, the competitive adsorption behavior is aimed to be correlated with the charge density N .

5.3. Materials

5.3.1. Cement

For this study, ordinary Portland type CEM I 52.5 R (Holcim Normo 5R, Siggenthal) was used. Its chemical composition was obtained from XRD– analysis. (Table 5.1). BET measurements were applied to determine the specific surface area (SSA_{BET}) as described in [171]. SSA_{BET} of the anhydrous cement powder was found to be $0.9742 \pm 0.0086 \text{ m}^2/\text{g}$. The surface of the cement paste ($W/C = 1.1$) after 15 minutes of hydration was $1.7715 \pm 0.0122 \text{ m}^2/\text{g}$. For this, hydration was stopped using isopropanol.

Table 5.1. XRD analysis of the applied cement powder (%).

C_3S	C_2S	C_3A	C_4AF	Gypsum	Anhydrite	Calcite
64.5	8.4	6.2	10.8	7.5	1.1	1.4

5.3.2. PCEs

All PCEs for this study feature a methacrylic backbone and the side chains are given by methoxy poly(ethylene glycol) (MPEG). Whereas side chain length and backbone length are similar among all PCEs, the grafting ratio (*i.e.* charge density) of the comb copolymers varies. Throughout this chapter, the charge density will be expressed as N , referring to the number of repeating units in one structural unit N . N varied between 3.0 and 6.7. All macromolecules can be considered to be homogeneously grafted flexible backbone worms as defined in literature [10]. More information about the model by Gay, Raphaël and Flatt can be found in *Chapter 1.1.2*. An example of the molecular structure is shown in Figure 5.2. In contrast, to the previous chapters, where the PCE nomenclature included the C/E ratio, we use the charge density N ($N = C/E + 1$). The nomenclature in the present chapter follows the pattern: *R-PCE-N* and *G-PCE-N*.

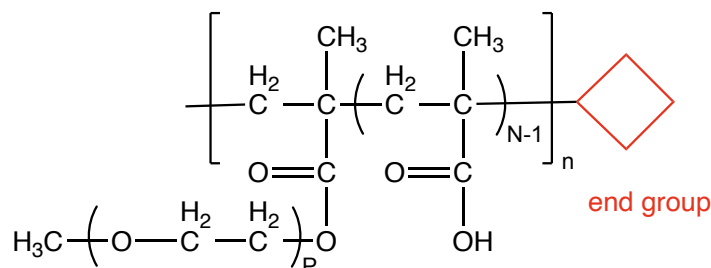


Figure 5.2. Molecular structure of a PCE with a poly(methacrylic acid) backbone and poly(ethylene glycol) side chains using the notation according to Gay, Raphaël and Flatt[10]. In case of R-PCEs, a UV-absorbing end group is attached to the backbone end. Details about molecular parameters of all applied PCEs are listed in Table 5.2.

In this study, two different types of PCEs are distinguished. Although backbone and side chains feature the same chemical components, different synthesis strategies were pursued. The first kind of PCE was obtained by grafting of MPEG (M_n 1000 g/mol) onto preformed poly methacrylic acid (PMAA, M_w 5400 g/mol, \mathcal{D} = 1.6) via an esterification process. This type of PCEs will be referred to as G-PCEs. All G-PCEs were supplied by Sika AG, Switzerland. More information on the grafting process is given in *Chapter 2.5*.

A second type of PCEs was obtained by RAFT- copolymerization of methacrylic acid (MAA) and the macromonomer poly(ethylene glycol) methyl ether methacrylate (PEGMA, M_n = 950 g/mol). This PCEs will be referred to as R-PCE. Due to the RAFT-process, an additional functional group is attached to the backbone of the R-PCEs. This group features absorption bands in the UV spectrum (*Chapter 2.3.8*).

Details on the synthesis of the PCEs are pointed out in *Chapter 2*. Prior to use, all PCEs were purified by dialysis to reduce the content of free side chains. Subsequently, the PCEs were freeze-dried. This allows to dose the PCE as precise as possible by weight. Information on structural parameters of all PCEs is summarized in Table 5.2. M_w refers to the weight-averaged molar mass and \mathcal{D} is the dispersity index of the molar mass distribution.

Table 5.2. Molecular characteristics of applied PCEs. N was obtained from $1H$ -NMR spectroscopy, M_w [kg/mol], \mathcal{D} and free side chains (wt%) were measured via size exclusion chromatography using online refractive index and multi angle light scattering detection. All PCEs are homogeneously grafted comb copolymers with flexible backbone worm characteristics as suggested in literature [10]. While there are differences of the charge density, all PCEs have a similar side chain length. The nomenclature of the PCEs follows the pattern: R-PCE- N and G-PCE- N .

	N	n	$N \times n$	P	M_w	\mathcal{D}	free side chains
R-PCE-2.9	2.9	15.2	44	19	20.9	1.1	2.0
G-PCE-3.0	3.0	13.2	40	22	20.6	2.0	6.0
G-PCE-4.3	4.3	9.2	40	22	18.8	1.9	4.3
G-PCE-6.7	6.7	5.9	40	22	14.9	1.8	2.9
G-Backbone	-	-	40	-	5.2	1.6	-

5.4. Experimental Methods

5.4.1. Standard Mixing Protocol

All cement pastes were prepared at room temperature with a W/C ratio of 1.1 by weight. This rather high W/C was chosen to optimize the extraction of non-adsorbed PCE in pore solution. Further information on issues regarding PCE extraction is described in *Section 5.8.2*. All cement pastes were prepared using ultrapure water from a Millipore Milli-Q system from Merck (TOC < 2 ppb, $\rho = 18.2 M\Omega \cdot cm$). Whereas W/C was kept constant, PCEs of different dosages and different N were used. The mixing protocol can be divided into different steps: preparation of cement paste, addition of PCEs and extraction of pore solution. The sequence of steps was precisely timed with the experimental time starting upon first contact between water and cement powder.

The first step was equal for all experiments. 10.00 g of cement powder was added to 11.00 mL of ultrapure water and mixed for 90 s at 1000 rpm using an overhead stirrer (IKA[®] Eurostar power control visc). The paste was left sitting until 15 minutes. In a second step, 1.00 mL of PCE solution was added, and the paste was mixed again for 90 s at 1000 rpm. The PCE dosage ranged between 0.1 g/g_{cem} to 10.0 mg/g_{cem}. The addition of the PCE solution leads to an increase in the W/C to 1.2. It has been shown in literature that the dilution of cement pastes during their induction period does not impact their hydration behavior up to the hydration

peak [171, 172]. Moreover, BET measurements confirmed that the available surface is not significantly impacted by the addition of PCE and additional water.^a

At 15 minutes, the cement paste was shortly vortexed and poured into a pressure filtration vessel. Compressed air was applied to filter the pore solution through a filter membrane (Polyamide, 0.45 μm , Sartorius Stedim Biotech). The obtained pore solution was acidified by adding 100 μL HCl (Sigma Aldrich, 37%, ACS reagent) and subsequently characterized by total organic carbon and UV-Vis absorption measurements.

5.4.2. Competitive Adsorption Protocol

It was aimed to investigate the adsorption behavior of R-PCE-2.9 in presence of a second PCE (G-PCE, see Table 5.2). The addition of the two SPs was carried out either simultaneously or sequentially. The total dosage of added PCEs is 4 $\text{mg}/\text{g}_{\text{cem}}$ in all competition experiments. In case of simultaneous addition, the procedure is equal to the standard mixing protocol. During the second step, 1.00 mL of PCE solution was added, here the solution contained equal amounts (by weight) of G-PCE and R-PCE-2.9. Consequently, the dosage of each competitor is 2 $\text{mg}/\text{g}_{\text{cem}}$, summing up to a total dosage of 4 $\text{mg}/\text{g}_{\text{cem}}$. This is the required dosage to achieve surface saturation (*Section 5.4.3*).

For sequential addition, the standard mixing protocol was modified as follows. The addition of the first PCE (2 $\text{mg}/\text{g}_{\text{cem}}$) was carried out as usual. After the first component was given 15 minutes to adsorb onto cement, the pore solution was not extracted directly, but a second PCE (2 $\text{mg}/\text{g}_{\text{cem}}$ in 1 mL ultrapure water) was added. The paste was mixed for 90 seconds at 1000 rpm. Subsequently, the paste was left for another 13.5 minutes rest, before the pore solution was extracted as described above. All *sequential* experiments were carried out both by adding R-PCE-2.9 first,

^aTo verify if additional water and PCE influence the SSA of cement, additional BET measurements were carried out. In these experiments, a different batch of CEMI 52.5R was used than in the experiments of the chapter. It was found that the SSA is not significantly influenced by the delayed addition of PCE solution. All SSA values are given in m^2/g . The time when the hydration was stopped is indicated as suffix.

- SSA_{15min} (no PCE): 2.15
- SSA_{30min} (no PCE): 2.11
- SSA_{30min} (4 $\text{mg}/\text{g}_{\text{cem}}$ added simultaneously): 2.29
- SSA_{45min} (4 $\text{mg}/\text{g}_{\text{cem}}$ added sequentially (2+2)): 2.09

and the G-PCE component as a second and *vice versa*. Corresponding experiments are denoted *R-First* and *G-First*.

5.4.3. Adsorption Isotherms

The amount of adsorbed PCE was calculated using the so-called depletion method. For this purpose, the amount of PCE in the pore solution was determined by analytical techniques, namely total organic carbon (TOC) or UV-Vis spectroscopy. In all calculations, the amount of free (= non-grafted) side chains was considered. For this correction, the assumption that free side chains do not adsorb onto the cement surface but stay in the pore solution was made. All adsorption isotherms presented in this paper are plotted as the amount of adsorbed PCE *versus* total dosage of PCE. Both values are normalized by the mass of the cement sample.

Total Organic Carbon

The total organic carbon content of extracted pore solutions was measured by a Shimadzu TOC-V CSH. The pore solutions were diluted with 0.05M HCl to meet the calibration range of the TOC analyzer. The pH of all diluted samples was acidic (pH 2) to guarantee removal of inorganic carbon. Subsequently, TOC was measured as the total carbon (TC) of the acidified pore solution. The TOC of a reference material (cement paste without PCE) was measured to consider organic carbon of the cement itself due to grinding aids *etc.* All measurements were corrected with this reference.

Figure 5.3 shows TOC adsorption isotherms of all applied PCEs. The adsorbed amount of PCE increases sharply at low dosages and finally reaches a plateau. The plateau value is equal to surface saturation. Hence, all adsorption sites are occupied, and the surface is fully covered by a PCE monolayer.

All adsorption isotherms feature a rather rounded curve. For the G-PCE samples this could be due to their dispersity (\bar{D} = 1.8-2.0; Table 5.2). With R-PCE-2.9 being substantially monodisperse (\bar{D} = 1.1; Table 5.2), the rounded trend indicates a rather moderate affinity for the cement surface.

For all applied PCEs, surface saturation was found between 1.5-2.0 mg/g_{cem}. A minimum dosage of about 2-3 mg/g_{cem} is needed to achieve surface saturation

(Figure 5.3). This value was crucial for the dosages chosen in competitive adsorption experiments. Here a total dosage of 4 mg/g_{cem} was applied to ensure that all kinetic adsorption and desorption processes occur within the plateau region.

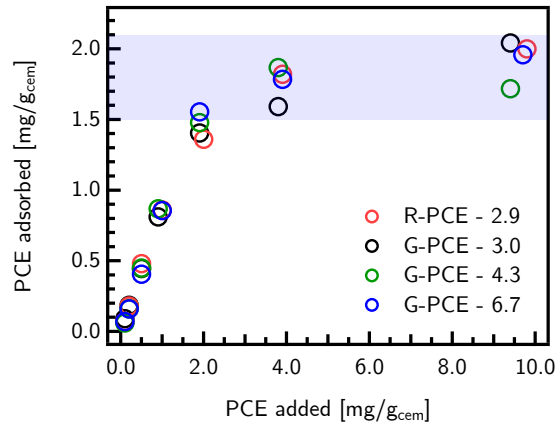


Figure 5.3. Adsorption isotherms of all applied PCEs determined by TOC and depletion calculation. The plateau value for all pastes ranges between 1.5-2.0 mg/g_{cem} (blue zone). A minimum dosage of 2-3 mg/g_{cem} is needed to achieve surface saturation.

UV-Vis-Absorption

TOC only gives access to the total amount of PCE left in the pore solution. It is not possible to distinguish between different types of PCEs. Due to the functional group attached to the backbone, R-PCEs can be detected with UV-Vis spectroscopy. For R-PCE-2.9, a linear calibration was established as described in *Chapter 2.3.8*. This allows to determine the concentration of R-PCE in (pore) solution.

Figure 5.4 shows the absorption spectra of various pore solutions extracted from pastes without added admixture (= reference) and from two plasticized pastes using 5 mg/g_{cem} G-PCE-3.0 and R-PCE-2.9. At 308 nm, an absorption peak can be observed for R-PCE-2.9, whereas G-PCE-3.0 and the reference spectra do not reveal a significant absorption at this wavelength. The concentration of R-PCE-2.9 contained in a pore solution can be calculated using the above-mentioned calibration curve after subtraction of a reference value. As a reference, Abs@308 of a pore solution without admixture was chosen.

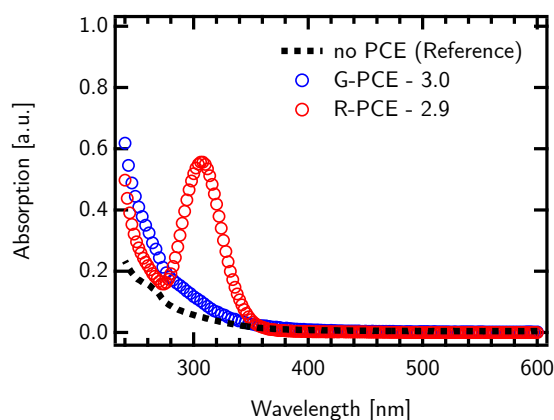


Figure 5.4. UV-Vis absorption spectra of different pore solutions. The pore solution containing R-PCE-2.9 shows an absorption peak at 308 nm, whereas G-PCE-3.0 and the reference pore solution do not feature specific absorption at this wavelength.

TOC versus UV-Vis

In case of R-PCE-2.9 both methods, TOC and UV-Vis, can be used to measure the concentration in solution. For various pore solutions, the content of R-PCE-2.9 was determined *via* both techniques, respective values were plotted against each other (Figure 5.5a). The data obtained from both methods are fully consistent. Corresponding adsorption isotherms for both techniques are in very good agreement (Figure 5.5b).

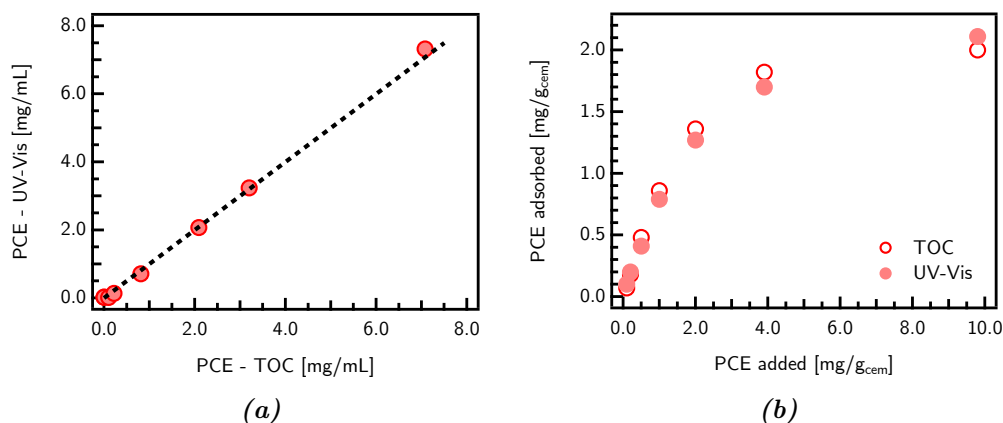


Figure 5.5. (a) Concentrations of R-PCE-2.9 detected by TOC and UV-Vis plotted against each other. The points follow the trend of a bisecting line (dashed); (b) Adsorption isotherm for R-PCE-2.9 measured with TOC and UV-Vis.

The resolution limit (*i.e.* the limit of quantitation) of the UV-Vis method is around 0.1-0.2 mg/mL. Polymer concentrations lower than this value are affected by baseline noise. For concentrations higher than 0.2 mg/mL, UV-Vis and TOC can be applied equally to detect the concentration of R-PCE-2.9. Referring to adsorption isotherms, a dosage of 1 mg/g_{cem} resulted in approximately 0.2 mg/mL of R-PCE-2.9 left in pore solution. It has to be noted that this value highly depends on the W/C ratio. Moreover, it is only valid for this specific R-PCE-2.9. Different chromophores/RAFT-agents might be useful to enhance resolution.

5.5. Results

5.5.1. Calculations and Data Treatment

The objective is to gain a deeper insight into the adsorption process and the adsorption behavior of R-PCE-2.9 in the presence of different G-PCEs. To this end, two parameters are of special interest, *i.e.* the total amount of adsorbed species, $m_{total,ads}$, and the corresponding weight fraction of each compound, $\omega_{G,ad}$ and $\omega_{R,ad}$.

For this, we note that the total organic carbon in the solutions, $c_{TOC,ppm}$, comes both from polymer G, $c_{TOC,ppm}(G)$, and from polymer R, $c_{TOC,ppm}(R)$:

$$c_{TOC,ppm} = c_{TOC,ppm}(G) + c_{TOC,ppm}(R) \quad (5.1)$$

The concentration of organic carbon in solution can be used to calculate the mass of dissolved R polymer, $m_{R,sol}$, and G polymer, $m_{G,sol}$. For this, the conversion factor f_{TOC} of each component has to be determined beforehand. The total mass of PCE dissolved in pore solution is given by the sum of $m_{G,sol}$ and $m_{R,sol}$ (Equation 5.2-5.4):

$$m_{R,sol} = c_{TOC,ppm}(R) \cdot f_{TOC}(R) \quad (5.2)$$

$$m_{G,sol} = c_{TOC,ppm}(G) \cdot f_{TOC}(G) \quad (5.3)$$

$$m_{TOC,sol} = m_{G,sol} + m_{R,sol} \quad (5.4)$$

The TOC method does not allow to distinguish between the two components. But complementary UV-Vis absorption measurements of the pore solution ($m_{UV,sol}$) give selective access to the amount of dissolved R polymer, $m_{R,sol}$ Equation 5.5.

$$m_{R,sol} = m_{UV,sol} \quad (5.5)$$

After combining Equation 5.5 and Equation 5.2, the amount of G polymer in solution can be calculated as follows:

$$m_{G,sol} = \left(c_{TOC,ppm} - \frac{m_{UV,sol}}{f_{TOC}(R)} \right) \cdot f_{TOC}(G) \quad (5.6)$$

Subsequently, the amount of adsorbed R polymer, $m_{R,ad}$, and G polymer, $m_{G,ad}$, can be obtained by the solution depletion method (Equation 5.7)-5.9). While we do not introduce this explicitly in the following equations, we recall that in all competitive adsorption experiments the dosage of each component ($m_{i,dosage}$) was equal to 2 mg/g_{cem}.

$$m_{R,ad} = m_{R,dosage} - m_{R,sol} \quad (5.7)$$

And similarly, using Equation 5.6, we get:

$$m_{G,ad} = m_{G,dosage} - m_{G,sol} \quad (5.8)$$

The total amount of adsorbed polymer, $m_{total,ad}$, is the sum for the mass of adsorbed polymer G, $m_{G,ad}$, and of polymer R, $m_{R,ad}$.

$$m_{total,ad} = m_{G,ad} + m_{R,ad} \quad (5.9)$$

Finally, the weight fraction of each adsorbed compound, $\omega_{G,ad}$ and $\omega_{R,ad}$, can be calculated as follows:

$$\omega_{G,ad} = \frac{m_{G,ad}}{m_{total,ad}} \quad (5.10)$$

$$\omega_{R,ad} = \frac{m_{R,ad}}{m_{total,ad}} \quad (5.11)$$

$$\text{where } \omega_{G,ad} + \omega_{R,ad} = 1 \quad (5.12)$$

5.5.2. Experimental Outcome

Competitive Adsorption Phenomena

Figure 5.6 (top) summarizes the results of all competitive experiments in several bar plots. The height of the bars shows the total amount (in mg/g_{ce}) of adsorbed PCE in each type of experiment. Each bar is composed of two stacked components, indicating the amount of adsorbed G-PCE and the corresponding amount of R-PCE-2.9. At first sight, it is obvious that the total amount of adsorbed PCE (total height of the bars) is relatively constant, although the proportions of the two PCEs change. More specifically, the total adsorption ranges between 1.6-2.0 mg/g_{cem}, which is consistent with the plateau values for the polymers taken individually. (Figure 5.3, blue zone).

Figure 5.6 (bottom) displays the adsorbed weight fraction of the different species (in wt%). In all experiments, the weight fraction of adsorbed G-PCE is higher than the one of R-PCE-2.9. Globally, this indicates that the G-PCEs feature a higher affinity for the cement surface. In all experimental series (*simultaneous* and *sequential*), the weight fraction of adsorbed G-PCE increases with increasing N while the fraction of R-PCE-2.9 is reduced. This trend hints at a competitive adsorption phenomenon between PCE polymers of different N for adsorption sites on the cement surface.

Dynamic Adsorption

However, a closer look at the results reveals that the mode of PCE addition also has an influence on the adsorbed weight fractions of both polymers. The results of the *simultaneous* series and *G-First* are in good agreement, and the corresponding amounts of adsorbed species only differ slightly. In the *R-First* series, the adsorbed

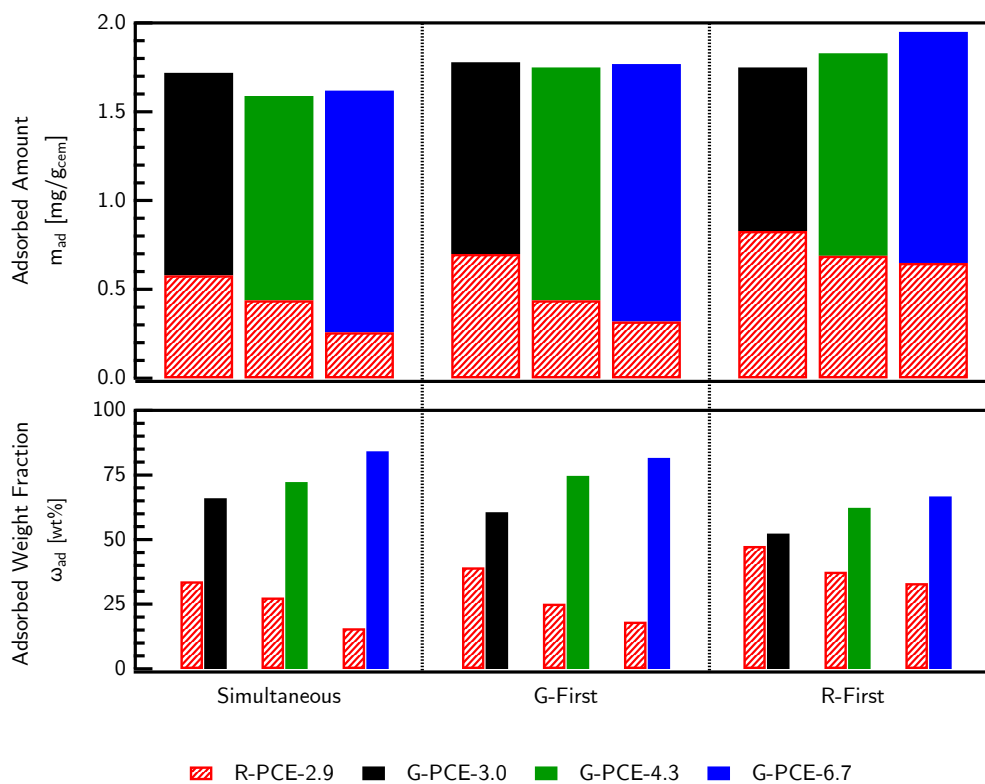


Figure 5.6. Top: Total amount of adsorbed PCEs during competitive adsorption experiments. Bottom: weight fraction of adsorbed species for experiments shown below.

weight fraction of R-PCE is increased compared to the *simultaneous* experiments, hinting at a lower extent of exchange of R-PCE by its competitor.

5.6. Discussion

In order to discuss the above presented results, a simplified but comprehensive model is presented to rationalize affinity of PCEs and to account for enthalpic and entropic forces driving and counteracting the exchange of polymers on the cement surface.

5.6.1. Rationalizing Affinity and Dispersity

The affinity of a PCE is expected to be influenced by its molecular characteristics, *i.e.* charge density (N) and backbone length ($N \times n$). Hence, the affinity of the

5. Competitive Adsorption Part I

PCE is mainly correlated with the number of possible attractive interactions between carboxylate groups and cement surface. A higher charge (or longer backbone) increases the number of electrostatic bonds between PCE and surface. Nevertheless, very high charge densities are expected to attenuate adsorption due to electrostatic repulsion between adjacent carboxylate groups. However, in this study, in all experimental series, the amount of adsorbed G-PCE increases with increasing N , indicating an enhanced affinity when N increases in the range between 3.0 to 6.7.

In all competitive experiments, the amount of adsorbed G-PCE is higher than the one of R-PCE-2.9. This indicates that the G-PCEs feature a higher affinity for the cement surface (Figure 5.6). This also holds for the G-PCE with a similar charge density as the R-PCE, suggesting that the different affinity between these polymers results from the differences in dispersity. Indeed, whereas R-PCE-2.9 contains well-defined molecules with a molar mass between 15 kDa and 30 kDa. The molar mass distribution (MMD) of the G-PCEs ranges approximately between 1.2 kDa and 150 kDa. (Figure 5.7). Although being disperse with regard to molar mass, the charge density N of the G-PCEs can be considered as rather homogeneous. The origin of the broad MMD lies in the dispersity of the backbone ($\mathcal{D}= 1.6$) of the G-PCEs that was synthesized by free radical homopolymerization of MAA before being esterified with MPEG.

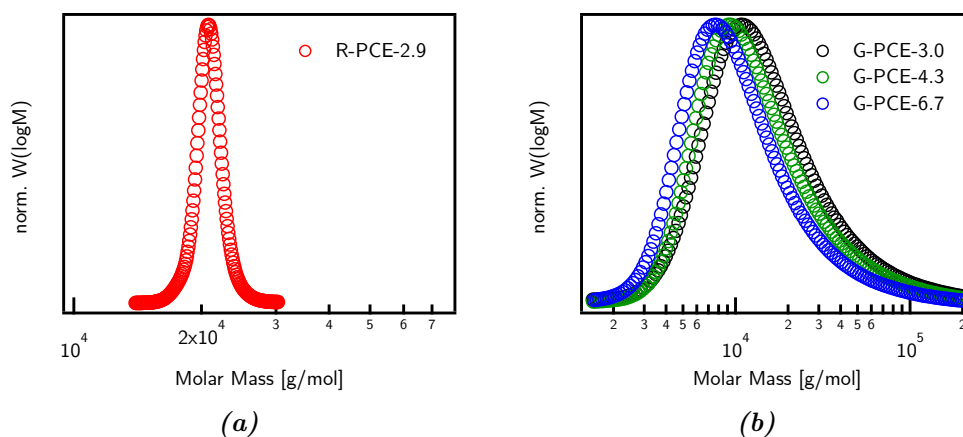


Figure 5.7. Molar mass distribution of all applied PCEs: R-PCE-2.9 (a) and G-PCEs (b). It should be noted that while both graphs use a log-scale, the one on the right shows a range of molecular masses that is about 20 times larger. If the same scale was used on the left than on the right, the R-PCE distribution would appear as a vertical line only. This underlines the difference in breadth of the molecular mass distribution also reflected in Table 5.2.

At constant N , G-PCEs with a longer backbone should show a higher affinity for the cement surface. In a first order, this can be assigned to the increased number of

carboxylate groups that can bond exothermally with the cement surface. In a second order, entropy changes contribute to the affinity, as discussed later in more detail.

The molar mass distribution of the G-PCE backbone can be found in Figure 5.8. The mass range of the PMAA backbone ranges between approximately 750 Da and 30 kDa. This is equal to $N \times n$ values between 10 and 350.

In contrast to G-PCEs, the backbone of R-PCE-2.9 is very uniform. It can be considered as a single fraction (R1) of molecules of low dispersity as evidenced by its chromatogram. However, the exact MMD of the R-PCE is not directly accessible as the backbone was not pre-synthesized but copolymerized along with the inclusion of the side chains. Nevertheless, the RAFT process is known to yield highly uniform polymers. Hence, the dispersity of the R-PCE backbone can be estimated from the MMD of the PCE ($\mathcal{D}= 1.05$).

Globally, the G-PCE backbone can be regarded as a heterogeneous mixture of various PMAA with different M_w . To represent this, the chromatogram of PMAA was divided into five fractions of equal weight noted G1-G5. Each of these can be considered as a monodisperse sub-fraction of the backbone. The characteristics of the sub-fractions are summarized in Table 5.3. Considering a homogeneous grafting of the backbone, the affinity of the sub-fractions should increase from G1 to G5 due to increasing M_w .

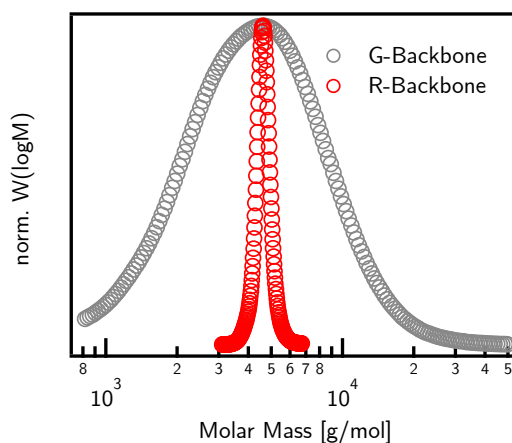


Figure 5.8. Molar mass distribution of the PCE backbones: The G-Backbone distribution was experimentally determined (i.e. PMAA-5k) by SEC. The distribution of the R-backbone was calculated from the data in Figure 5.7.

Figure 5.8 and Table 5.3 emphasize that the competition between R-PCE-2.9 and a G-PCE is better understood as competition between a well-defined R-PCE

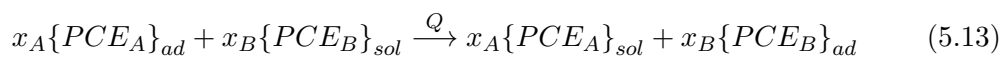
with 5 monodisperse fractions of G-PCE, whereby the backbone of R-PCEs lies in between those of the G-PCEs.

Table 5.3. Sub-fractions of the PCE backbones. The R-PCE backbone is comprised by one narrowly distributed fraction. The disperse G-PCE backbone can be divided into 5 uniform sub-fractions of low dispersity.^b

Fraction	R1	G1	G2	G3	G4	G5
Weight Fraction [wt%]	100	20.5	19.9	20.2	19.5	19.9
M _w [kg/mol]	4.1	1.7	3.0	4.3	6.1	11.1
Đ	1.05	1.09	1.01	1.01	1.01	1.10

5.6.2. Basic Thermodynamics of the Exchange

According to theoretical considerations, an adsorbed PCE (**A**) can be replaced by another PCE (**B**) in order to minimize free energy. The exchange on the cement surface can be rationalized with Equation 5.13. Importantly, in our conditions, the surface is always saturated, and its area is constant. Consequently, we can write this process of polymer exchange similarly to how we would do so for a chemical reaction, where here however the stoichiometric coefficients account for the number of molecules needed to occupy a given surface. Considering that x_A molecules of adsorbed **A** are replaced by x_B molecules of **B** from pore solution, we have:



In order to determine if the replacement takes place, the free energy of exchange, ΔG_{Ex} (“Gibbs free energy”), has to be considered. For $\Delta G_{Ex} < 0$, the process is exergonic and results in energy minimization. ΔG_{Ex} can be calculated as follows:

$$\Delta G_{Ex} = \Delta G_{Ex}^o + RT \cdot \ln(Q) \quad (5.14)$$

^bTo divide the chromatogram into five sub-fractions with equal weight, the integral below the elution peak (RI Signal) was split into 5 equal parts. For each sub-fraction M_w and M_n were calculated to access the corresponding dispersity index.

where ΔG_{Ex}^o is the standard free energy of the exchange process and Q the reaction product given by:

$$Q = \left(\frac{[PCE_A]_{sol}}{[PCE_A]_{ad}} \right)^{x_A} \left(\frac{[PCE_B]_{ad}}{[PCE_B]_{sol}} \right)^{x_B} \quad (5.15)$$

where $[PCE_A]_{sol}$ and $[PCE_B]_{sol}$ refer to the concentration of PCE **A** and **B** in solution and $[PCE_A]_{ad}$ and $[PCE_B]_{ad}$ are approximated by the surface fraction of each adsorbed polymer.

Now, Y_A and Y_B are defined as the partition of dissolved over adsorbed species of **A**, respectively **B**:

$$Y_A = \frac{[PCE_A]_{sol}}{[PCE_A]_{ad}} \quad Y_B = \frac{[PCE_B]_{sol}}{[PCE_B]_{ad}} \quad (5.16)$$

Together with Equation 5.15, this gives:

$$Q = Y_A^{x_A} \cdot Y_B^{-x_B} \quad (5.17)$$

For ideal systems, the value of Q is purely related to mixing entropy. It is an entropic term based on the concentrations in solution and on the surface for each system considered. This mixing term changes to minimize free energy and bring the system to a chemical equilibrium.

At equilibrium conditions, $\Delta G_{Ex} = 0$ and the reaction product Q is equal to the equilibrium constant K . This allows to correlate K with the standard free energy of exchange. Hence, ΔG_{Ex}^o is directly related with the partition of adsorbed and desorbed species at equilibrium conditions:

$$\Delta G_{Ex}^o = -RT \cdot \ln(K) \quad (5.18)$$

Substitution into Equation 5.14 gives:

$$\Delta G_{Ex} = RT \cdot \ln \left(\frac{Q}{K} \right) \quad (5.19)$$

While this general result is well known, the important step here is to consider stoichiometric coefficients relating to a unit surface area. Very importantly, the molecular parameters of the PCEs influence those stoichiometric coefficients, and this is an important part of our discussion of how changes in molecular structure can impact the outcome of competitive adsorption between “relatively similar” polymers.

5.6.3. Exchange on a Unit Surface

As mentioned above, in order to rationalize the exchange of PCEs from a free energy perspective, it is useful to refer to the exchange taking place on a unit area. The standard free energy of an exchange, $\Delta G_{Ex}^{o,Area}$, on a given surface can be calculated as follows:

$$\Delta G_{Ex}^{o,Area} = \Delta G_B^{o,Area} - \Delta G_A^{o,Area} \quad (5.20)$$

where $\Delta G_A^{o,Area}$ and $\Delta G_B^{o,Area}$ are the standard adsorption free energies for **A** and **B** for occupying a reference unit area. The standard free energy of exchange, $\Delta G_{Ex}^{o,Area}$, includes an enthalpic contribution ($\Delta H_{Ex}^{o,Area}$) and an entropic one ($T\Delta S_{Ex}^{o,Area}$):

$$\Delta G_{Ex}^{o,Area} = \Delta H_{Ex}^{o,Area} - T\Delta S_{Ex}^{o,Area} \quad (5.21)$$

$$\text{where } \Delta H_{Ex}^{o,Area} = \Delta H_B^{o,Area} - \Delta H_A^{o,Area} \quad (5.22)$$

$$\text{and } \Delta S_{Ex}^{o,Area} = \Delta S_B^{o,Area} - \Delta S_A^{o,Area} \quad (5.23)$$

The number of molecules of PCE_{*i*} adsorbed on a unit surface (X_i) can be calculated as suggested by Flatt *et al.* [10] using Equation 5.24:

$$X_i = \frac{\sqrt{2}}{(\pi \cdot a_N a_P)} \cdot \left(2\sqrt{2}(1 - 2\chi) \frac{a_N}{a_P} \right)^{-0.4} P_i^{-0.9} \cdot N_i^{-0.3} \cdot n_i^{-1.0} \quad (5.24)$$

Here a_N represents the backbone monomer size (0.25 nm for methacrylates), and a_P the side chain monomer size (0.36 nm for ethylene oxide). χ is the *Flory-Huggins* parameter accounting for the solubility of the PCE (0.37 for PEO at 25 °C). Equation 5.24 can be applied to calculate the stoichiometric coefficients x_A and x_B .

PCE Activities and Lattice Model

For the calculation of Q , polymer activities in solution and on the surface have to be approximated by their concentrations. In our approach, we use a simplified lattice model (similar to the *Flory-Huggins* theory) to estimate PCE concentrations in solution and on the surface.

Briefly speaking, polymer concentrations in solution (Equation 5.25) are given with respect to the number of water molecules in pore solution. Specifically, we define L_{sol} as the total number of lattice sites of the solution and L_{PCE_i-sol} the number of sites occupied by PCE_i:

$$[PCE_i]_{sol} \approx \frac{L_{PCE_i,sol}}{L_{sol}} \quad (5.25)$$

Since the solution is very dilute, L_{sol} can roughly be approximated by the number of water molecules in pore solution ($L_{sol} \approx L_{water}$). With regard to L_{PCE_i-sol} , we consider that each monomeric unit of the PCE backbone occupies one lattice site.

Analogously, the surface fraction of adsorbed PCEs is calculated as ratio between surface sites occupied by the PCE (L_{PCE_i-ad}) and the total number of sites of the surface lattice ($L_{surface}$).

$$[PCE_i]_{ad} \approx \frac{L_{PCE_i-ad}}{L_{surface}} \approx \omega_{ad}(i) \quad (5.26)$$

The total amount of adsorbed polymers is roughly constant in all competitive experiments (Figure 5.6) and similar to the plateau values of the polymers taken individually (Figure 5.3). Hence, the surface fractions can be considered to be equal to the adsorbed mass fractions $\omega_{ads}(G)$ and $\omega_{ads}(R)$ (Equation 5.10), which substantially simplifies the subsequent analysis.

Enthalpy Contribution

The adsorption enthalpy of a PCE_i, $\Delta H_i^{o,Area}$, is assumed to be proportional to the number of electrostatic bonds between carboxylate groups and Ca²⁺ ions on the surface. So, based on Equation 5.22, the exchange enthalpy, $\Delta H_{Ex}^{o,Area}$, should be proportional to the difference between these. Therefore, let us first consider the adsorption of a single type of PCE. The formation of the above-mentioned bonds is exothermic and favors adsorption. The number of formed bonds per unit area can be estimated from the number of charges per unit area, Z_i , which is given by the product between X_i and the number of charges per PCE molecule, *i.e.* $(N_i - 1) \cdot n$. This gives:

$$Z_i = X_i \cdot n_i \cdot (N_i - 1)$$

$$= \frac{\sqrt{2}}{(\pi \cdot a_N a_P)} \cdot \left(2\sqrt{2}(1 - 2\lambda) \frac{a_N}{a_P} \right)^{-0.4} P_i^{-0.9} N_i^{-0.3} (N_i - 1) \quad (5.27)$$

Comparing PCEs with constant side chain length, Z_i increases with increasing N_i . In first approximation, this also indicates an increased number of electrostatic interaction points. Exemplarily, X_i and Z_i for all applied PCEs of this study were calculated for an area of 100 nm² and given in Table 5.4. The stoichiometric coefficients x_i of the polymers are calculated with reference to $X_{R-PCE-2.9}$.

Table 5.4. Number of molecules (X_i) and charges (Z_i) per 100 nm². The values were calculated using Equation 5.24 and 5.27 assuming $a_N = 0.25$ nm, $a_P = 0.36$ and $\chi = 0.37$. The stoichiometric coefficients were calculated using $X_{R-PCE-2.9}$ as a reference.

	X_i [molecules/100 nm ²]	Z_i [COO ⁻ /100 nm ²]	x_i $x_i = X_i/X_{R-PCE-2.9}$
R-PCE-2.9	1.64	47	1.00
G-PCE-3.0	1.65	44	1.01
G-PCE-4.3	2.13	64	1.30
G-PCE-6.7	2.90	98	1.77

Moving on to the thermodynamics of adsorption, we state that the enthalpy change h_i that occurs upon adsorption of PCE_i is proportional to the number of formed electrostatic bonds, Z_i :

$$\begin{aligned}
h_i &= -\alpha_H Z_i \\
&= -\alpha_H \cdot \frac{\sqrt{2}}{\pi \cdot a_N a_P} \cdot \left(2\sqrt{2}(1 - 2\lambda) \frac{a_N}{a_P} \right)^{-0.4} P_i^{-0.9} N_i^{-0.3} (N_i - 1) \quad (5.28) \\
&\text{with } \alpha_H > 0
\end{aligned}$$

where the proportionality constant α_H is taken positive and can be seen as a measure for the exothermic binding strength between Ca^{2+} and carboxylate groups of the PCE. The choice of taking α_H explains the negative sign in the above equation, since the formation of these electrostatic bonds considered is exothermic.

Importantly, it has to be pointed out that according to Equation 5.27, Z_i is independent of n_i meaning that the number of charges present per unit area should not change with molar mass when N_i and P_i are held constant. Hence, for a given charge density and side chain length, also h_i should be roughly independent of the molar mass. This means that the number of formed bonds per unit surface is the same, no matter if few PCEs with long backbones or more PCEs with shorter backbones are occupying a given unit surface.

This becomes important for understanding the impact of backbone dispersity on PCE adsorption. A long backbone can form more bonds with the surface. *A priori*, this could suggest a higher affinity of PCEs with high n_i compared to those with small n_i . However, when looking at a fully covered unit surface, differences in backbone length do not impact adsorption from an enthalpic point of view.

Entropy Contribution Solvent

With regard to entropy changes, we must distinguish polymer and solvent contributions. When considering a single type of polymer, its adsorption implies the desorption of a large number of solvent molecules. This represents a substantial entropy gain that favors polymer adsorption. Typically, this would override losses of configurational entropy undergone by the adsorbing polymer. However, in the case of competitive adsorption between polymers, we need to consider the difference in number of desorbing solvent molecules with respect to the adsorption of each polymer taken individually.

To estimate this difference, we first consider the number of desorbed solvent molecules per unit area for the adsorption of a given polymer, PCE_i. We note this s_i and assume that it is proportional to the backbone length ($N_i \times n_i$) with α_S being the proportionality constant:

$$\begin{aligned}
 s_i &= \alpha_S \cdot X_i \cdot N_i \times n_i \\
 &= \alpha_S \cdot \frac{\sqrt{2}}{\pi a_N a_P} \left(2\sqrt{2} (1 - 2\chi) \frac{a_N}{a_P} \right)^{-0.4} P_i^{-0.9} N_i^{0.7} \quad (5.29) \\
 &\text{with } \alpha_S > 0
 \end{aligned}$$

Equation 5.29 reveals that, similarly to h_i , s_i also does not depend on the number of repeat units, n_i . Hence, for a given value of P_i and N_i , the entropy term linked to solvent desorption is not affected by the molar mass. Coming back to competitive adsorption, this means that the same number of solvent molecules will be released per unit surface no matter if a species with long or short backbones are going to fully occupy that surface.

Entropy Contribution Polymer

Let us also briefly consider the entropy related to the PCEs. We assume that the penalty for conformational changes is roughly similar, so that the main effect would be the translational entropy. This term is linked to the difference in number of adsorbing chains per unit surface area. Equation 5.24 shows that with increasing n_i , less molecules occupy a unit surface. Thus, in case of long backbones, less molecules are immobilized per unit area, which is beneficial from an entropic point of view. This becomes important when rationalizing the effect of backbone dispersity on adsorption affinity. PCEs with longer backbones are expected to adsorb preferentially over shorter ones.

While the above section suggested that solvent exchange effects cancel out, polymer exchange entropy would not. However, it can be expected to remain a second order contributor to $\Delta G_{Ex}^{O,Area}$. It is important to underline that this argument is only about the role of polymer entropy with regard to the standard free energy. The

exchange free energy retains mixing entropy effects, though the polymer structure dependence of stoichiometric coefficients that is accounted for in Equation 5.19.

5.6.4. Rationalizing Free Energy and Partition

So far, we pointed out that ΔG_i^{Area} of an adsorption process of an individual PCE is related with its molecular parameters. Let us now substitute Equation 5.28 into 5.22 and 5.23 to extend this concept to a binary system where PCE_A is previously adsorbed and then displaced by PCE_B. Looking at this for a reference surface area, the enthalpy of this exchange, $\Delta H_{Ex}^{o,Area}$, can be estimated from $h_B - h_A$ and the entropic term, $\Delta S_{Ex}^{o,Area}$, can be related with $s_B - s_A$:

$$\begin{aligned}\Delta H_{Ex}^{o,Area} &= h_B - h_A \\ &= -\alpha_H \cdot \beta_x \cdot [P_B^{-0.9} N_B^{-0.3} (N_B - 1) - P_A^{-0.9} N_A^{-0.3} (N_A - 1)]\end{aligned}\quad (5.30)$$

$$\begin{aligned}\Delta S_{Ex}^{o,Area} &= s_B - s_A \\ &= \alpha_S \cdot \beta_x \cdot [P_B^{-0.9} N_B^{0.7} - P_A^{-0.9} N_A^{0.7}]\end{aligned}\quad (5.31)$$

$$\text{with } \beta_x = \frac{\sqrt{2}}{\pi a_N a_P} \left(2\sqrt{2} (1 - 2\chi) \frac{a_N}{a_P} \right)^{-0.4}$$

Based on the previous sections, we can infer that $\Delta H_{Ex}^{o,Area}$ and $\Delta S_{Ex}^{o,Area}$ (*i.e.* solvent contribution) are independent of the molar mass of a PCE when N_i and P_i are kept constant. Thus, also $\Delta G_{Ex}^{o,Area}$ is not influenced by the molar mass of the adsorbing species. Coming back to competitive adsorption, this means that $\Delta G_{Ex}^{o,Area}$ will remain constant if for one competitor only n_i is changed, but that N_i and P_i are constant. As a consequence, also the value of the equilibrium constant K will be the same (Equation 5.18).

Understanding Partition

At this point, we need to have a closer look at the equilibrium constant, K . Equation 5.19 defines that at equilibrium Q should be equal K . If K changes, owing for example to a change in the structure of the polymers considered, then Q

must change accordingly. This can happen by a concerted change in Y_A and Y_B , the partition of polymers **A** and **B** between the surface and the solution (Equation 5.16 and 5.17). However, and very importantly for this paper, the value of Q can also be changed as a result of the “polymer structure dependent stoichiometric coefficients” x_i (Equation 5.17). Consequently, there may be cases where a change in the polymer structure does not affect K , but does affect Q . In response to this and to maintain chemical equilibrium, the solution and surface concentrations will change (even if K is constant).

This may be counter-intuitive, because most often when handling chemical reactions, one is used to taking the stoichiometric coefficients as a given, and then looking at how systems modify their concentrations as Q to reach K . We are not used to thinking that equilibrium concentrations may change if K is constant. What happens here, is that by changing the structure of PCE **A** or **B** is equivalent to changing the stoichiometry of the reaction. In what follows, various consequences of changes in molecular structure are discussed with the aim of explaining how the distribution of species can be affected by changes in molecular structure. More precisely, we will create three scenarios in order to discuss the impact of n_i and N_i onto partition and equilibrium conditions.

In **scenario 1**, the cement surface is fully covered by PCE **A1** and PCE **B** is dissolved in pore solution to compete for adsorption. The equilibrium of adsorbed and desorbed species can be described with K_1 . In order to reveal how a change in x_A affects the equilibrium situation, we use Equation 5.17. Plotting $Y_A^{x_A}$ against $Y_B^{x_B}$ gives a line with slope K . For instance, the black line in Figure 5.9 describes all possible combinations of $Y_A^{x_A}$ and $Y_B^{x_B}$ that allow a system of PCE **A** and **B** to be in equilibrium K_1 . The specific equilibrium situation (S1) of **scenario 1** is indicated with the black marker in Figure 5.9.

When the stoichiometric parameter x_A is increased, the value of $Y_A^{x_A}$ is decreased. For this, we need to recall that the activities in solution are much lower than those on the surface ($L_{sol} \gg L_{surface}$), so that the partition of a species **A** ($Y_A = \frac{[PCE_A]_{sol}}{[PCE_A]_{ad}}$) is smaller than 1. This also implies that an increase in x_A would decrease the value of Q . In Figure 5.9, this situation is indicated with the grey marker (S*), which is located below the black trendline. In order to come back to equilibrium, Q has to be increased to meet K (Figure 5.9, red and blue arrow). Therefore, the partitions of Y_A and Y_B need to undergo changes. This is directly related with desorption and adsorption of species **A** and **B**. In the following we describe two explicit scenarios,

where a change in backbone length (**scenario 2**) or charge density (**scenario 3**) cause dynamic processes.

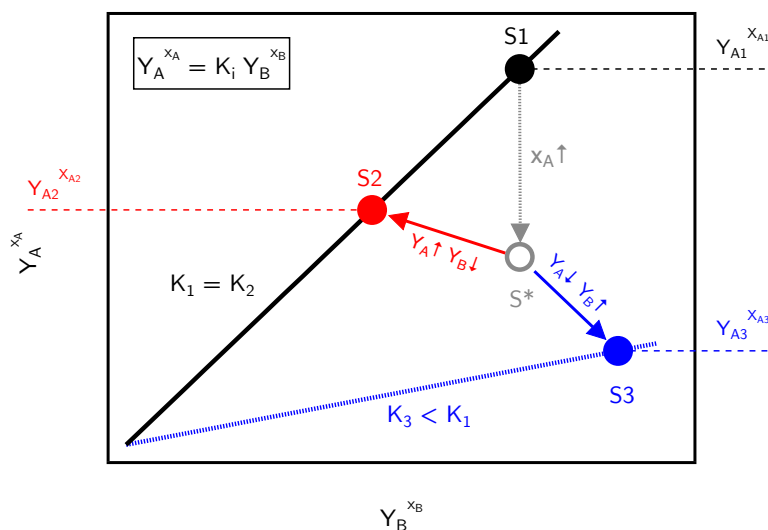


Figure 5.9. Schematic describing how a change in the molecular parameter x_A results in dynamic processes to re-establish equilibrium conditions. $S1$ gives the equilibrium situation of **scenario 1**, where two PCE species **A** and **B** are adsorbed in equilibrium K_1 . An increase in the stoichiometric parameter x_A , leads to a decrease of $Y_A^{x_A}$ (S^*). Consequently, also Q (Equation 5.17) is decreased. Desorption of **A** ($Y_A \uparrow$) and adsorption of **B** ($Y_B \downarrow$) raises the value of Q and brings the system back to an equilibrium situation ($S2$). On the contrary, further adsorption of **A** ($Y_A \downarrow$) and desorption of **B** ($Y_B \uparrow$) brings Q to equilibrium $S3$. Equilibrium situations are described by the black and blue trendline, which give all possible equilibria between PCE **A** and **B** with value K_i . The value of K_i is represented in the slope of the trendline.

Influence of Molar Mass

In **scenario 2**, the equilibrium state of **scenario 1** is perturbed by replacing **A1** by **A2** which has the same values of P and N as **A1** but a shorter backbone ($n_{A2} < n_{A1}$). Moreover, this replacement is done in such a way that **A2** covers the same surface and has the same activity in solution as **A1** at equilibrium. Under these conditions, we change x_A , but keep Y_A , Y_B and x_B constant.

The equilibrium state between **A2** and **B** is described with K_2 . As pointed out in the sections above, $\Delta G_{Ex}^{o,Area}$, is supposed to be independent of n_i . Therefore, in terms of standard free energy, **scenario 2** is equal to **scenario 1**, so that both

equilibrium constants have the same value: ($K_1 = K_2$). Thus, the equilibrium for **scenario 2** is described by the same line as for **scenario 1** in Figure 5.9 (black line).

Now in the case where **A2** has a smaller backbone, more molecules can be adsorbed per unit surface as $x_{A2} > x_{A1}$. As previously explained, this implies that an increase in x_{A2} results in a decrease of $Y_A^{x_A}$ (as Y_A is smaller than 1). In Figure 5.9 this means that the initial equilibrium point S1 is shifted to an out of equilibrium position below it in that same figure (noted S*). To come back to equilibrium, the system must increase Y_A and simultaneously decrease Y_B (with x_A and x_B now being constant). This is shown schematically in Figure 5.9 with the red arrow from S* to S2. An increase in $Y_A^{x_A}$ means that Y_A increases, which implies a desorption of **A2**. Thereby, the new equilibrium point S2 illustrates that **A2** which has a smaller backbone is less competitive with respect to **B** than **A1**.

Understanding the partition of dissolved and adsorbed species in dependence on n_i is crucial to access the role of backbone dispersity on competitive adsorption. From this example, we see that smaller polymers are less competitive in terms of adsorption than larger ones, even if the standard adsorption free energy for the polymer exchange is not or only barely affected by the molar mass of the polymers.

Influence of Charge Density

Let us we now turn our attention to polymers with varying grafting density, but a constant backbone length (constant $N_i \times n_i$). This is essential to comprehend the effect of charge density on competitive adsorption. We aim to explain the influence of N_i on the competition by referring to an exchange **scenario 3**.

Similarly, to **scenario 2**, we start from the equilibrium reached in **scenario 1** and replace **A1** by **A3**. In this case, **A3** and **B** have the same backbone and side chain length, but different charge densities. We consider that **A3** has a higher charge density than **A1**: $N_{A3} > N_{A1}$. At constant backbone length, we find $x_{A3} > x_{A1}$.

As for **scenario 2**, we initially consider a replacement of **A1** in such a way that **A3** occupies the same surface and has the same activity in solution. This ensures that our initial step keeps Y_A , Y_B and x_B constant. As in the previous case, the value of x_A increases, and this results in a decrease of $Y_A^{x_A}$ because Y_A is smaller than one. This moves the system from the equilibrium point S1 to a lower point S* Figure 5.9.

As before, this moves the system out of equilibrium, and we must discuss how equilibrium can be re-established. In contrast to **scenario 2**, the situation considered here modifies the equilibrium constants. Indeed, when looking at Equation 5.30, we see that an increase in the value of N_A , causes the term in the brackets to decrease, so that the enthalpy becomes less negative. For the entropy, Equation 5.31 indicates that if N_A is increased, then the change in entropy decreases, making the process less favorable. Therefore, both entropy and enthalpy changes indicate that increasing the charge density of **A** should reduce the equilibrium constant K (for the displacement of **A** by **B**).

From the above, we have $K_3 < K_1$, so that a new equilibrium for **scenario 3** should be added to Figure 5.9, which is illustrated by the blue line with a slope K_3 smaller than K_1 . With the new equilibrium line being below S^* , our system that we moved from $S1$ to S^* , should move to its new equilibrium by concerted changes of Y_A and Y_B (having to be in opposite direction). We show that by the arrow from S^* to $S3$, which is indicated with a blue marker in Figure 5.9.

Specifically, this return to equilibrium involves a decrease of Y_A and an increase of Y_B . Similarly, $Y_A^{x_A}$ decreases and $Y_B^{x_B}$ increases. In other words, we get further adsorption of **A** and desorption of **B** (with respect to **scenario 1**). This illustrates that an increase in charge density, increases the competitive adsorption ability of a PCE.

Influence of Side Chain Length

So far, the impact of P on the adsorption equilibrium was not considered as in all experiments of this chapter PCEs with constant side chain length were applied. For the sake of completeness, we want to emphasize that changes in P potentially also impact the adsorption equilibrium. More specifically, at constant backbone length and constant charge density N , a reduced side chain length causes the stoichiometric parameter x_A to increase. At the same time, a change in P modifies the equilibrium constant K . In a **scenario 4**, where $P_{A4} < P_B$, a similar situation as illustrated for **scenario 3** will be created ($K_4 < K_1$) (Figure 5.9) that involves desorption of species **B** to give further access to the surface for the PCE with shorter side chains (**A4**). Consequently, PCEs with shorter side chains are potentially more competitive. The role of side chains in competitive adsorption will be addressed in detail in *Chapter 6*.

All in all, the different scenarios emphasize how the change in molecular parameters of one competing species induces exchange of PCE molecules at the cement surface to establish equilibrium conditions, which can be described with the constant K .

5.6.5. Connecting Theory with Results

At this point, we want to connect and verify the derived thermodynamics with our experimental results.

Influence of Charge Density

The effect of charge density on the adsorption behavior of PCEs can be seen in all experiments (*simultaneous* and *sequential*). Overall, it can be stated that a higher N of the G-PCE, coincides with an increased affinity for the surface. This observation is aimed to be connected with the suggested model. Let us turn our attention to the *R-First* series. In all *R-First* experiments, R-PCE-2.9 was added to the cement paste prior to the G-PCE. Hence, we note R-PCE-2.9 as component A, respectively, B refers to the different G-PCEs. For, *G-First* experiments, component **A** (G-PCE) and **B** (R-PCE) have to be treated *vice versa*.

Assuming that $\Delta G_{Ex}^{o,Area}$ is dominated by enthalpic effects and considering entropic contributions to be negligible ($\Delta S_{Ex}^{o,Area} \approx 0$), Equation 5.30 can be rewritten as follows:

$$\begin{aligned}
 \text{For } \Delta G_{Ex}^{o,Area} &\approx \Delta H_{Ex}^{o,Area} = h_B - h_A \\
 \Delta G_{Ex}^{o,Area} &= \alpha_H^* \cdot \Delta [N_i^{-0.3}(N_i - 1)] \\
 \text{where } \Delta [N_i^{-0.3}(N_i - 1)] &= [N_B^{-0.3}(N_B - 1)] - [N_A^{-0.3}(N_A - 1)] \\
 \text{and } \alpha_H^* &= \frac{\alpha_H}{P_A^{0.9}} \cdot \beta_x; \quad \alpha_H > 0; \quad P_A = P_B
 \end{aligned} \tag{5.32}$$

From a theoretical point of view, we therefore expect that $\Delta G_{Ex}^{o,Area}$ should be proportional to $\Delta [N_i^{-0.3}(N_i - 1)]$. From an experimental point of view, we used the measured solution concentration and adsorption values to determine Y_A and

Y_B . With the stoichiometric coefficients listed in Table 5.4, we can calculate K and thereby infer the value of $\Delta G_{Ex}^{o,Area}$ from our experiments. Thus, in order to test our theoretical predictions, we then plot $\Delta G_{Ex}^{o,Area}$ against $|\Delta N_i^{-0.3} (N_i - 1)|$ in Figure 5.10. For means of comparison, we plot absolute values and consider the simultaneous experiment as a benchmark. In this series, the PCEs purely adsorb according to their affinity for the surface, as both competitors are added at the same time to the cement paste.

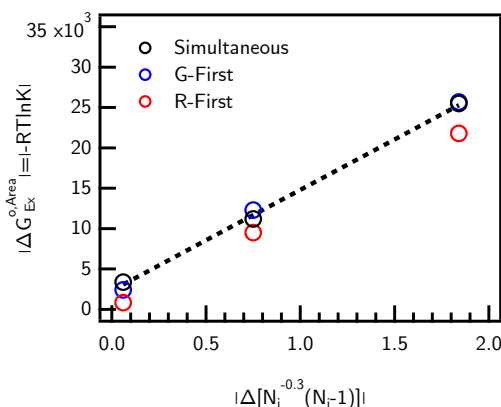


Figure 5.10. Verification of Equation 5.32. The data of the simultaneous experiment was fitted by linear regression. The slope (α_H^*) was found to be 12.5 kJ/mol per unit of $|\Delta [N_i^{-0.3} (N_i - 1)]|$. For an average side chain length with 20 repeating units this is equal to a bonding strength, $\alpha_H \approx 37.9$ kJ per mol of carboxylate. The offset of the regression line is 2.3 kJ/mol.

For all experimental series, a linear relation is found between $\Delta G_{Ex}^{o,Area}$ and $|\Delta [N_i^{-0.3} (N_i - 1)]|$. While this strongly supports our theoretical prediction, it does not fully validate it, because the line does not exactly go through the origin (offset ≈ 2.3 kJ/mol). There are different possible reasons for this offset.

One possibility is that the charge density of the G-PCE is not properly assessed. The average of the G-PCEs was calculated from 1H-NMR, which should be quite accurate. However, it is possible that there are slight inhomogeneities in the grafting ratio between smaller and longer backbones. This might impact the distribution of adsorbed species and the value of K that causes the offset. It is worth mentioning that the regression would pass the origin, if N of the R-PCE was 2.6 instead of 2.9. The rather close values underline that our model appears to be capturing main effects rather well, at least in terms of underlying basic principles.

Another reason for the offset in Figure 5.10 may be that G-PCE has a much larger dispersity than the R-PCE. This is discussed in the next section. Before that, however,

it is worth mentioning that the slope of the linear regression in Figure 5.10 provides the value of α_H^* , which according to its definition can be used to calculate the binding strength α_H (Equation 5.32). Assuming $P_A=P_B= 20$ and taking $\alpha_H^*= 12.5$ kJ/mol, the binding strength between each carboxylate group in the PCE and Ca^{2+} would have to be 37.9 kJ per mol of carboxylate (*i.e.* methacrylate). This is substantially higher than recently reported binding enthalpies for acrylate-based PCEs adsorbed on Calcium-Silicate-Hydrate surfaces. Determined by molecular dynamics, they were found to be in the range between 0 and 20 kJ per mol of acrylate monomer (at room temperature)[173].

However, this discrepancy should not be given too much weight as our model relies on scaling relations for which the numerical constants (proportionality factors) cannot be quantified accurately. On the other hand, the linear relation in Figure 5.10 indicates that our model correctly captures the nature of how changes in molecular structure parameters affect competitive adsorption between PCEs.

The Issue of Backbone Dispersity

In *Section 5.6.4*, we described changes in surface affinity for PCEs of equal charge density, but different backbone lengths. This section builds upon those results to examine whether dispersity and dosage may account for the offset in Figure 5.10. For this, as introduced in *Section 5.6.4*, we consider R-PCE-2.9 as monodisperse and the G-PCEs a dispersed polymer composed of the five monodisperse fractions defined in Table 3.

Under such circumstances, each G-PCE fraction competes with the other G-PCE fractions and with R-PCE. The reaction of each competition can be described by rewriting Equation 5.13 (here: any given G-PCE fraction being component A):

$$\phi_i x_{G,i} \{PCE_G\}_{ad} + \phi_i x_R \{PCE_R\}_{sol} \xrightarrow{Q_i} \phi_i x_{G,i} \{PCE_G\}_{sol} + \phi_i x_R \{PCE_R\}_{ad} \quad (5.33)$$

$$\text{with } \phi_i = \frac{m_{G,i,ad}}{m_{G,ad}} \quad \text{and} \quad \sum_{i=1}^f \phi_i = 1$$

where f is the total number of sub-fractions and ϕ_i is the abundance of sub-fraction i in G-PCE, given as the mass of fraction adsorbed G-PCE. Moreover, $x_{G,i}$ is

the stoichiometric coefficient of the G-PCE sub-fraction i . Consequently, the global reaction Equation 5.13 is equivalent to the following expression:

$$\sum_{i=1}^f \phi_i x_{G,i} \{PCE_G\}_{ad} + x_R \{PCE_R\}_{sol} \xrightarrow{Q_i} \sum_{i=1}^f \phi_i x_{G,i} \{PCE_G\}_{sol} + x_R \{PCE_R\}_{ad} \quad (5.34)$$

Assuming equilibrium conditions, it can be shown that using the same approach as in *Section 5.6.2*, the equilibrium constant K_i for the exchange between any fraction i and R-PCE can be written as:

$$K_i = K^{\phi_i} = Y_{G,i}^{\phi_i x_G} \cdot Y_R^{-\phi_i x_R} \quad (5.35)$$

Rearranging Equation 5.35 leads to:

$$Y_{G,i}^{x_G} = K \cdot Y_R^{x_R} \quad (5.36)$$

with $Y_{G,i} = \left(\frac{[PCE_{G,i}]_{sol}}{[PCE_{G,i}]_{ad}} \right)$

This is an important result, because it means that in a given experiment the term $Y_{G,i}^{x_G}$ has the same value regardless of which G-PCE fraction is considered. It also means that the value of $Y_{G,i}$ can be determined with the measured equilibrium concentrations of R-PCE and the appropriate values of $x_{G,i}$. Knowing $Y_{G,i}$ and K , the adsorbed mass $m_{G,i,ad}$ of each fraction can be calculated.

However, the value of K is not known exactly *a priori*. Indeed, the determination of equilibrium constants in the previous section only represents a first approximation. It has to be considered that those values of K might not be exact, since they were calculated from the experimental results of the *simultaneous* series without proper consideration of the dispersity of the G-PCE.

To verify the suggested dispersity model (Equation 5.34-5.36), we calculated the adsorbed amount of each fraction $m_{G,i,ad}$. In a first step, $[PCE_{G,i}]_{ad}$ was obtained using Equation 5.36. Subsequently, Equation 5.26 allows to access $m_{G,i,ad}$. Then, the total amount of adsorbed G-PCE is given by the sum of the adsorbed fractions:

$$m_{G,ad} = \sum_{i=1}^f m_{G,i,ad} \quad (5.37)$$

5. Competitive Adsorption Part I

Using the previously determined values of K (Equation 5.17, $Q = K$ in equilibrium) for the calculation of $m_{G,ad}$ leads to only minor deviations from the experimentally found values. This is shown in Figure 5.11a, where the first two bars reveal a slight deviation. Here, the first bar gives the amount of adsorbed PCE calculated according to the dispersity model as described in the previous paragraph. As this calculation requires the use of K (Equation 5.17), the corresponding bars are referred to as "Model-K". The second bar gives the adsorbed amount of PCE, which was experimentally determined using simultaneous TOC and UV detection. (Equation 5.7-5.9).

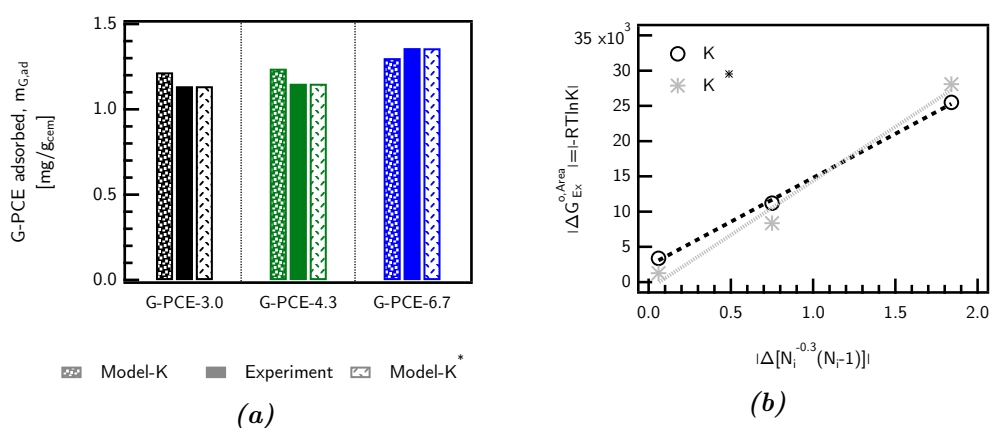


Figure 5.11. (a) Adsorbed amount of G-PCE, $m_{G,ad}$. Comparison between experimental data of the simultaneous series and calculated values according to the dispersity model (Equation 5.34-5.37). Using K results in slight deviations compared to the experimental data. (b) K^* was obtained as the best fit for the calculation of $m_{G,ad}$.

Figure 5.11a also shows a third bar (Model-K*), giving very good agreement with the experiment. These values were calculated using K^* as equilibrium constant. Values of K^* were obtained as the best fit for the calculation of $m_{G,ad}$ according to the dispersity model. All values of K and K^* are provided in Table 5.5. While we cannot say if any of these changes taken individually makes sense, we can examine whether taken together this new set of values does.

Table 5.5. Equilibrium constants: K was determined according to Equation 5.15. K^* shows the best fit of K to calculate $m_{G,ad}$ according to the dispersity model (Equation 5.34 - 5.37).

	G-PCE-3.0	G-PCE-4.3	G-PCE-6.7
K	$2.55 \cdot 10^{-1}$	$1.09 \cdot 10^{-2}$	$3.39 \cdot 10^{-5}$
K^*	$5.96 \cdot 10^{-1}$	$3.42 \cdot 10^{-2}$	$1.17 \cdot 10^{-5}$

In order to verify the accuracy of K^* , we use the values of K^* to determine $\Delta G_{Ex}^{o,Area}$ and examine the relation between $\Delta G_{Ex}^{o,Area}$ and $|\Delta [N_i^{-0.3} (N_i - 1)]|$. As shown in Figure 5.11b (black line), this is once again linear, but this time with an intercept closer to zero (offset = -0.97 kJ/mol instead of 2.3 kJ/mol previously). This supports our argument that the offset in Figure 5.10, also seen from the grey line in Figure 5.11b, is most probably due to the greater dispersity of G-PCE than R-PCE. Our model is thus globally consistent, and we can now take a step further to examine more detailed consequences of dispersity, *i.e.* the partition and distribution of adsorbed species with regard to the backbone length.

Results for the partition of the G-PCE fractions, using K^* values from, Table 5.5 are shown in Figure 5.12a. This shows that fractions with backbone lengths below 30 units barely adsorb, while ones above 40 adsorb almost entirely. Another representation of this is shown in Figure 5.12b, where the partition of each fraction between the surface and the solution is given.

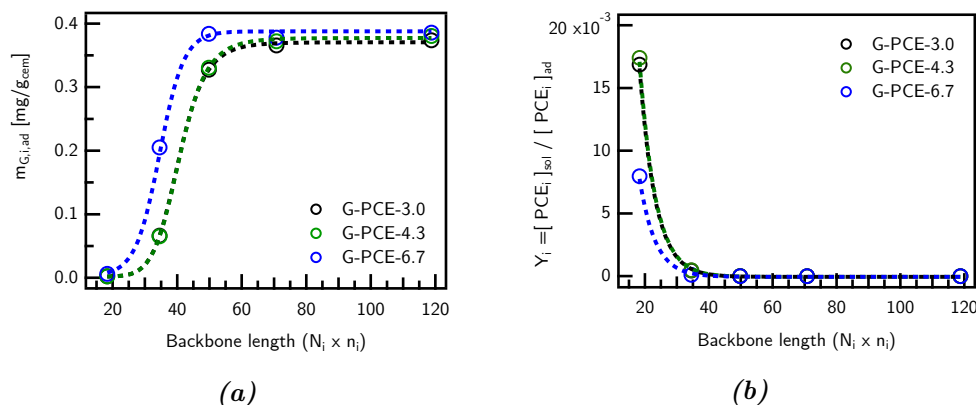


Figure 5.12. Distribution of partition, $Y_{G,i}$ and adsorbed mass, $m_{G,i,ad}$ of the sub-fractions within the G-PCE calculated with K^* . With increasing length of the backbone adsorbed masses increase. This is equal to a decrease in partition for PCEs with long backbones.

As alluded to above, the adsorbed masses shown in Figure 5.12a) reveal that there is a threshold backbone length of approximately 35-40 units for which all applied G-PCEs are majoritarily to be found on the surface rather than in solution. For $N_i x n_i > 40$ the G-PCE, sub-fractions adsorb almost completely, whereas shorter ones barely access the surface. This threshold turns out to be very close to the backbone length of the competing R-PCE, which confirms that the R-PCE loses the direct competition with long G-PCEs and wins against shorter ones. Evidently, the total extent of adsorbed amounts is also affected by the charge of the competitors. But the backbone length has a significant impact on the competitiveness of a PCE.

Dynamic Processes and Excluded Fractions

Figure 5.12 highlights that the greatest difference for the adsorption of the three polymers concerns the fraction of intermediate backbone length which are similar to the backbone of the R-PCE. It underlines that dispersity plays an important role, which is why we include it in our analysis of the outcome of the experiments with different sequencing of the polymer addition (*G-First* and *R-First*).

For this, we replot $\Delta G_{Ex}^{o,Area}$ vs. $|\Delta [N_i^{-0.3} (N_i - 1)]|$ in Figure 5.13. As was also the case in Figure 5.10, results of the *simultaneous* experiment and *G-First* are in very good agreement. This could already be anticipated from Figure 5.6 as both experimental series show similar adsorbed amounts and weight fractions of PCEs. In the *G-First* series, the G-PCE was added to the cement prior to R-PCE. Thus, the G-PCE could freely adsorb on the surface before any competition with R-PCE started. The dosage of G-PCE (2 mg/g_{cem}) was sufficient to cover the complete cement surface. Therefore, when the R-PCE is added, it can only adsorb if some G-PCE molecules desorbs to make space on the surface. Such exchange processes are driven by free energy minimization of $\Delta G_{Ex}^{o,Area}$, as we have tried to describe in our model. Assuming that equilibrium is reached, it should not matter from which side one starts, the final state should be the same. Therefore, the accordance between simultaneous and *G-First* is expected. The slight deviation for *R-First* however requires an explanation.

First, we note that in all *R-First* experiments, increased fractions of R-PCE are found on the surface (Figure 5.6). This indicates that the adsorption of the R-PCE is not fully reversible in the case of *R-First*. A possible reason for this might again lie in the dispersity of the G-PCE backbone. Indeed, the G-PCE fractions with

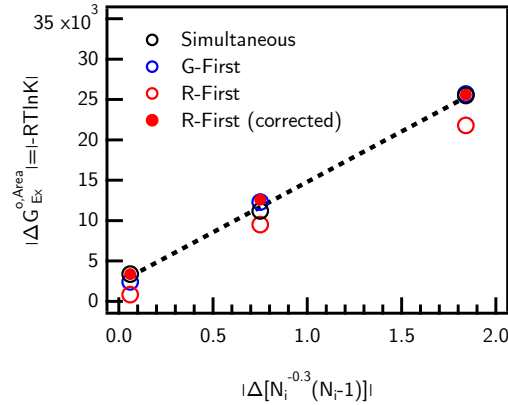


Figure 5.13. Replot of $\Delta G_{Ex}^{o,Area}$ vs. $|\Delta N_i^{-0.3}(N_i - 1)|$. Simultaneous and G-First results are in good agreement, whereas R-First shows a slight deviation with regard to the simultaneous data. We assume that an excess of R-PCE adsorbs as “Excluded G-PCEs” do not replace them sufficiently when being added as a second component. After considering 0.15 mg/g_{cem} of irreversibly adsorbed R-PCE, the corrected R-First values are in good agreement with the simultaneous data.

backbones smaller than 35-40 units may not be able to replace any of the previously adsorbed R-PCE. With regard to the adsorbed masses of these fractions shown in Figure 5.12a, the amount of “Excluded PCE” can be expected to be in the range between 0 and 0.3 mg/g_{cem}.

We recalculated $\Delta G_{Ex}^{o,Area}$ for the *R-First* experiment, assuming that an average of 0.15 mg/g_{cem} R-PCE adsorb irreversibly (do not get replaced by “Excluded” G-PCEs). The recalculated data is in good agreement with the *simultaneous* experiment (Figure 5.13). Thus, the claim that a fraction of R-PCE is not available for exchange by small G-PCEs could be underlined. Nevertheless, it remains an open question if the excess of R-PCE remains adsorbed on hydrating C₃S or if it gets irreversibly linked to aluminate phases (adsorbed on ettringite or possibly intercalated in AFm).

Another factor that could contribute to increased amounts of adsorbed of R-PCE might be attributed to the RAFT end group. However, the influence of this functional group onto adsorption and desorption was not investigated in detail.

Time Effects and Induction Period

The sequence of events in all experiments (paste preparation, PCE addition *etc.*) is precisely timed. Each PCE is given 15 minutes to adsorb to the cement surface and

to displace competing molecules. It is assumed that this period is sufficient to reach an adsorption equilibrium between adsorbed and dissolved species.

All adsorption processes happen during the induction period. During this time, cement hydration is slow, particularly in presence of PCEs. However, anhydrous phase continues to dissolve and hydrates to precipitate. We have selected conditions to have constant specific surfaces to study competitive adsorption without surface area changes, but with a surface chemistry characteristic of cementitious systems.

In real systems, the role of admixtures will be of interest while the surface may be changing, and this should not be forgotten. Very importantly also, any use of PCEs involving their inclusions in the mixing water, should factor in their impact on ettringite nucleation (itself affecting SSA).

Simplifications and Inaccuracies of the Model

An arguable limitation of the model is the nature of the conformation for the adsorbed polymer combs. However, it should be underlined that in first order the main features of this model are that the backbone is adsorbed and not straight, while the coiled side chains extend into solution. These features make sense to what we know about PCEs. In literature, alternative models describing the conformation of adsorbed PCEs can be found. Two alternatives are briefly addressed in *Section 5.8.4*.

The presented adsorption model enables to understand the role of molecular parameters on the competitive adsorption behavior of PCEs. The starting point is fundamental thermodynamics. Subsequently, we include the role of molecular parameters by introducing them *via* the stoichiometry of the exchange reaction.

Equation 5.30 allows to predict the trend of $\Delta G_{Ex}^{o,Area}$ in dependence on molecular and architectural features of the PCE. For constant side chain length, we found a linear relation between $\Delta G_{Ex}^{o,Area}$ and $|\Delta [N_i^{-0.3} (N_i - 1)]|$ (Equation 5.32). This relation was clearly verified with experimental data (Figure 5.10). Importantly, the here presented scaling laws can be transferred to any type of homogeneously grafted PCEs that can be described with flexible backbone worm model of Gay and Raphaël [37], assuming a surface analogue confirmation can be used to describe it when adsorbed [10].

It has to be noted that for the derivation of Equation 5.32, a series of assumptions was made. All simplifications were carefully considered. However, numerical constants such as proportionality factors (*e.g.* binding strength) cannot be quantified accurately. One reason for this is the nature of the scaling laws used to describe the adsorbed conformation. Another reason is the calculation of the concentrations using a lattice model (Equation 5.25-5.26). Moreover, we use a dosage of 2 mg/g_{cem} to guarantee full surface coverage, which includes a slight excess with regard to the surface capacity. This discrepancy, however, should not be given too much weight regarding the importance and general validity of the relation presented above. For completeness of the Discussion, we want to conclude this section by summarizing main assumptions regarding thermodynamics.

Most importantly, our model is based on enthalpic effects driving the adsorption of PCEs onto the cement surface. ($\Delta G_{Ex}^{o,Area} \approx \Delta H_{Ex}^{o,Area}$). Thus, we assume the impact of entropy onto $\Delta G_{Ex}^{o,Area}$ to be negligible (Equation 5.32). While net changes in the entropy possibly plays an important role in adsorption of PCEs onto a plain cement surface, we argue that these contributions ought to cancel out when referring to an exchange of two PCEs, in particular when their structures are not radically different. Nevertheless, the exact role of entropy on PCE exchange and adsorption at high surface coverage remains an open question.

Apart from this, we assume all carboxylic groups along the backbone to equally bind to the cement surface, overlooking neighboring group effects. According to our results, this simplification is legitimate at least for $N= 2.9-6.7$. However, charge densities above this range might be affected by repulsion between adjacent carboxylates.

5.7. Conclusion

We used a dual detection technique to verify competition between PCEs as a result of their molecular architecture, *i.e.* different charge and backbone dispersity. The experiments indicate that PCEs with higher charges preferentially adsorb over lower ones. At first glance, this result seems to be intuitive, however this work is the first one to experimentally prove the occurrence of competitive adsorption between PCEs on the molecular level.

Moreover, we successfully show that adsorption and desorption at the cement surface involves dynamic processes. We underline our experimental outcome by deriving a thermodynamic model that captures all aspects of our experiments. Hence, we are able to describe affinity and competitiveness of PCEs as a consequence of enthalpic and entropic contributions. Drawing on well-established theories of Gay and Raphaël [37] and Flatt *et al.* [10], we relate our model with PCE molecular architecture. In summary, it can be said that the exchange of PCEs on the cement surface is dominated by enthalpic effects. In particular, enthalpy appeared to be well described as linearly scaling with the number of charges per molecule. When it comes to exchange processes between PCEs, the contribution of entropy is of minor importance. Nevertheless, the exact role of entropy on PCE adsorption is still open.

In this context, we want to emphasize that our model captures the thermodynamic effects upon exchange of PCE molecules at the cement surface. In this sense, our equilibrium constants describe the displacement of one PCE by another. We were able to show that competitive adsorption among PCEs at the plateau is dominated by enthalpic effects. In the lower dosage regime, which is of greater practical relevance, PCEs will compete with solvent molecules and other ionic species. While the adsorption enthalpy should remain the same, entropic effects may be quite different. Thus, our results constitute a groundwork to study PCE adsorption at low or intermediate dosage, specifically to determine their partition between solution and surface.

We suggest a way to deal with dispersity in charge and molecular size when dealing with competition between PCEs. The here derived correlations between molecular parameters and competitiveness can be transferred to other comb-shaped polyelectrolytes used for plasticizing cement. Hence, we hope that this model may lay a useful theoretical basis for handling competitive adsorption and PCE adsorption more generally. In the course of this work, we addressed processes occurring at the molecular level. In a continuation of this work, we suggest to include workability tests, *i.e.* spread flow tests and rheology tests in order to verify macroscopic consequences of PCE competition.

All in all, this work makes an important new step towards the mechanistic understanding of structure-property relations of PCEs. Accessing the working mechanism of PCEs on a molecular level is indeed indispensable for molecular design of effective superplasticizers for concrete technology. So far, we validated that our model captures main trends to describe the impact of charge density N onto

competitive adsorption phenomena, in *Chapter 6*, we will prove that also the impact of side chain length P is sufficiently covered by the suggested model.

5.8. Appendix Chapter 5

5.8.1. Influence of W/C

For the study of the adsorption behavior of PCEs onto cement, it is essential to use experimental procedures that allow to extract pore solution and non-adsorbed PCE in a reliable and reproducible way. It was found that the use of low W/C ratios implies some complications for the extraction of dissolved PCEs. In Figure 5.14 the adsorption isotherm of two cement pastes (W/C= 0.45 and W/C= 1.1) is shown. In case of the paste with W/C=0.45, the amount of adsorbed PCE increases linearly with increasing dosage, but no plateau is established. This is not related to incomplete surface coverage, but shows an artifact due to insufficient removal of PCE from the paste.

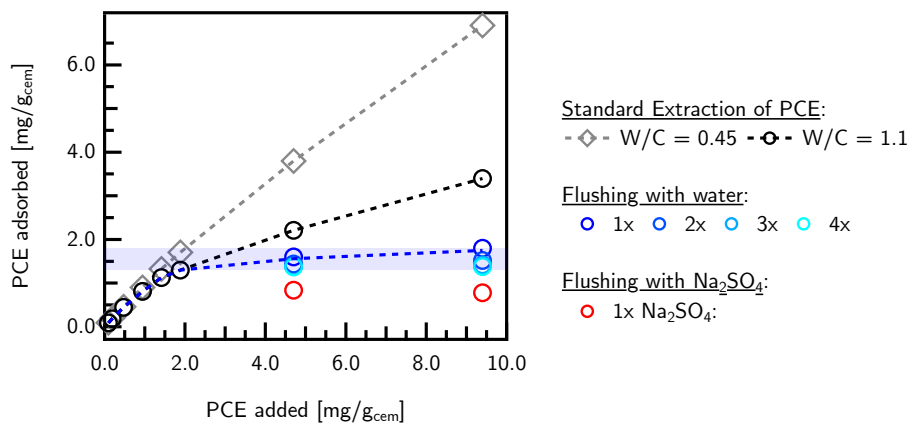


Figure 5.14. Adsorption data illustrating the challenge posed by low W/C pastes and the solution to this issue proposed in the current paper. At W/C 0.45, the adsorption data increases linearly with dosage, while a kink with a continued increase is seen for W/C= 1.1. Flushing the W/C= 1.1 pastes with ultrapure water (1 to 4 times) leads to the common plateau, strongly suggesting that the linear increase without flushing is an artifact that does not represent adsorption. A plateau, of slightly lower magnitude is also obtained with a single flushing with a solution of Na₂SO₄ known to at least partially compete with PCEs. Data shown here refer to G-PCE-3.0. This is done on a paste with W/C 1.1 having already been flushed four times.

In comparison, the trend of the second isotherm ($W/C = 1.1$) follows the same linear increase as described for $W/C = 0.45$ at low dosages. For dosages higher than $2.0 \text{ mg/g}_{\text{cem}}$, the isotherm of $W/C = 1.1$ features a “kink” and a plateau seems to be established. This shows that a higher W/C value is helpful for extraction of non-adsorbed PCE from the paste. Nevertheless, also in case of $W/C = 1.1$, no perfect plateau value is reached. Hence, for high dosages ($> 5 \text{ mg/g}_{\text{cem}}$), a divergence of the isotherm is visible. The use of even higher W/C is not recommended as it results in an increased phase separation of the cement paste that might impair the adsorption of PCE onto the cement surface.

Concerning the origin of the above-mentioned effect, it should not come from an effect of the PCEs on ettringite as we have been using delayed addition. This same addition mode should also limit the role of polymer aggregates [50]. Further investigation of the underlying mechanism is needed, but for the purpose of this paper we may argue that paste with W/C of 1.1 and flushed once provide a reliable representation of PCE adsorption.

5.8.2. Removal of Excess PCE

In order to remove excess PCE from the paste, the cement residue that was obtained after pressure filtration was flushed with ultrapure water. These “flushing steps” were carried out for pastes with PCE dosages $\geq 4.0 \text{ mg/g}_{\text{cem}}$. Below this dosage, they did not show any effect, indicating that pressure filtration was sufficient to remove all excess PCE with the pore solution. During a flushing step, 5 mL of ultrapure water was added to the cement residue after filtration. The paste was quickly redispersed by shaking, and subsequently the water phase was removed again by pressure filtration.

The effect of the flushing procedure is included in Figure 5.14 by the example of a paste with $W/C = 1.1$. As described above, the isotherm does not end in a plateau but diverges (black circles). The adsorbed amount of PCE after various flushing steps is given by the blue circles in Figure 5.14. Already after the first flushing step, excess PCE can be considered as removed. It has to be noted that four (and even more) flushing steps did not lead to a significant desorption of PCE from the surface. By flushing with ultrapure water, the adsorbed amount of PCE does not drop below the plateau region (blue zone, Figure 5.14). The blue dashed line in Figure 5.14 refers to the trend of the adsorption isotherm, including one flushing step. All experiments

presented in this study demanding PCE dosages $\geq 4 \text{ mg/g}_{\text{cem}}$ include one flushing step to guarantee complete PCE removal.

5.8.3. Desorption with Sulfates

As shown in Figure 5.14, flushing with ultrapure water allows to remove excess PCE from the paste, while adsorbed molecules are not affected. However, flushing can also be applied to remove the adsorbed PCEs. For this, a potent competitor has to be added to the flushing solution. For demonstration, the paste of $W/C = 1.1$ was flushed 4 times with ultrapure water (blue circles, Figure 5.14) before one flushing step with Na_2SO_4 , (0.5 mol/L) was carried out. This caused a significant desorption of PCE from the cement surface and the adsorbed amount of PCE drops below the plateau region (red circles, Figure 5.14). This experiment emphasizes the competition between sulfate ions and PCE molecules for the cement surface. All experiments presented in Figure 5.14 summarize that the experimental protocol that is chosen to study adsorption phenomena has to be developed carefully in order to be able to quantify adsorbed species by using depletion calculations.

5.8.4. Alternative Adsorbed Conformation

In literature, multiple approaches to describe the conformation of adsorbed polymer combs in dependence on their molecular parameters can be found. Throughout our study, we focus on the suggested “Hemisphere” model presented by Flatt *et al.* [10]. This model was found most suitable to accurately describe surface coverage and layer thickness of PCEs in dependence on their molecular parameters.

However, we want to refer to two alternative models to capture the number of PCE molecules per unit surface. The simplest attempt to describe the conformation of adsorbed PCEs is assuming that the surface occupancy is proportional to $(N \cdot n)^{-1}$ (Equation 5.38). In this case, the backbone is stretched out on the surface while the uncoiled side chains extend into solution. Hence, the adsorbed area per molecule is not affected by the length of the side chains P .

$$X_i = \alpha_X \cdot N_i^{-1} \cdot n_i^{-1} \quad (5.38)$$

5. Competitive Adsorption Part I

We use Equation 5.38 to recalculate the stoichiometric coefficients of the PCEs applied in this study. Subsequently, we recalculate $\Delta G_{Ex}^{o,Area}$ using the new stoichiometry. As a consequence of Equation 5.38, we find $\Delta G_{Ex}^{o,Area}$ to be proportional to $|\Delta [N_i^{-1} (N_i - 1)]|$ (Equation 5.39).

$$\Delta G_{Ex}^{o,Area} = -\alpha_H^{**} \cdot \Delta [N_i^{-1} \cdot (N_i - 1)] \quad (5.39)$$

The corresponding plot of $\Delta G_{Ex}^{o,Area}$ vs. $|\Delta [N_i^{-1} (N_i - 1)]|$ shows a linear correlation for all experiments. However, the corresponding line is far from passing the origin. Moreover, the determination of K^* leads to a substantially less good agreement with our adsorption results, as can be seen in Figure 5.13. Indirectly, this suggests that assuming a stretched-out backbone and uncoiled side chains is not the right way to represent the adsorbed conformation of PCEs.

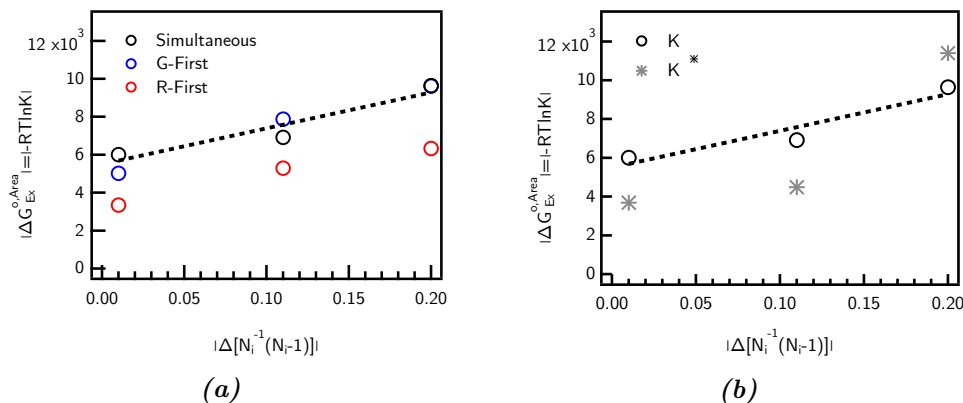


Figure 5.15. (a) Verification of Equation 5.39. The data of the simultaneous experiment was fitted by linear regression. (b) K^* was obtained as the best fit for the calculation of $m_{G,ad}$.

The second alternative model describes the number of molecules per surface, assuming “Mushroom Slices” (Equation 5.40). Details about this model can be found in the appendix of reference [10].

$$X_i = \left(\frac{3}{8}\right)^{0.25} \left(\frac{a_N}{a_P}\right)^{0.25} (1 - 2\lambda)^{-0.25} \left(\frac{1}{a_N a_P}\right) P_i^{-0.75} \cdot N_i^{-9/16} \cdot n^{-1} \quad (5.40)$$

Again, we calculate the new stoichiometric coefficients (Equation 5.40) and recalculate $\Delta G_{Ex}^{o,Area}$ using the new stoichiometry. Hence, we find $\Delta G_{Ex}^{o,Area}$ to be proportional to $\left| \Delta \left[N_i^{-9/16} (N_i - 1) \right] \right|$ (Equation 5.42).

$$\Delta G_{Ex}^{o,Area} = -\alpha_H^{**} \cdot \Delta \left[N_i^{-9/16} \cdot (N_i - 1) \right] \quad (5.41)$$

$$\text{with } \alpha_H^{**} = \left(\frac{3}{8} \right)^{0.25} \left(\frac{a_N}{a_P} \right)^{0.25} (1 - 2\lambda)^{-0.25} \left(\frac{1}{a_N a_P} \right) P_i^{-0.75} \quad (5.42)$$

The corresponding plot of $\Delta G_{Ex}^{o,Area}$ vs. $\left| \Delta \left[N_i^{-9/16} (N_i - 1) \right] \right|$ shows a linear correlation for all experiments (Figure 5.16). Fitting parameters for the *simultaneous* data are 2.8 kJ/mol (offset) and 16.0 kJ/mol per unit of $\left| \Delta \left[N_i^{-0.3} (N_i - 1) \right] \right|$ (slope). For an average side chain length with 20 repeating units, this is equal to a bonding strength of 13.6 kJ/mol per carboxylate. This is closer to the values previously referred to as having been obtained by molecular dynamics. At this stage, it is however, not possible to say if these differences should be considered as an indication that the ‘‘Mushroom Slice’’ model is the better one. In any case, the ‘‘Mushroom Slice’’ model and the ‘‘Hemisphere’’ model yield very similar results. Also, for the ‘‘Mushroom Slices’’, we account for the dispersity and calculate K^* . As can be seen in Figure 5.16, there is an adequate agreement with our adsorption results.

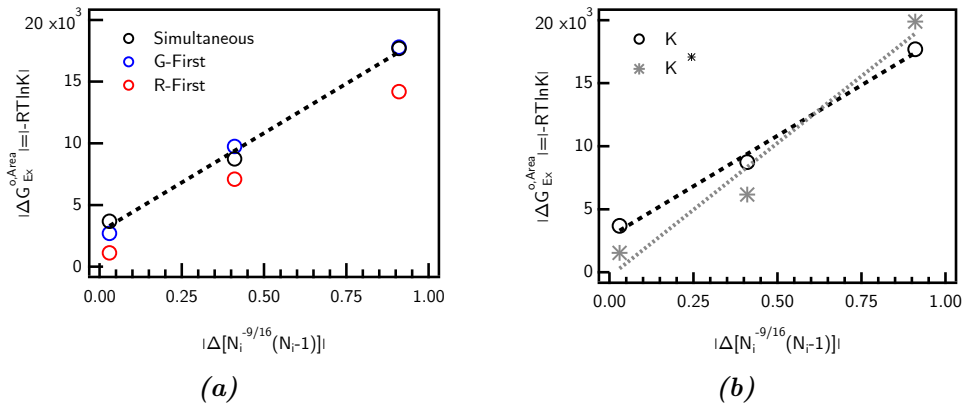


Figure 5.16. (a) Verification of Equation 5.42. The data of the simultaneous experiment was fitted by linear regression. The slope (α_H^{**}) was found to be 16.0 kJ/mol per unit of $\left| \Delta \left[N_i^{-0.3} (N_i - 1) \right] \right|$. For an average side chain length with 20 repeating units, this is equal to a bonding strength, $\alpha_H \approx 13.6$ kJ per mol of carboxylate. The offset of the regression line is 2.8 kJ/mol. (b) K^* was obtained as the best fit for the calculation of $m_{G,ad}$.

5. Competitive Adsorption Part I

At this point, we want to emphasize that for all three suggested models, the derived expression for $\Delta G_{Ex}^{o,Area}$ is independent of n . The close comparison between “Hemisphere” and “Mushroom Slices” model emphasizes the importance of accurately accounting for the stoichiometry of the exchange process when deriving a thermodynamic model describing PCE competition.

Competitive Adsorption - Part II

On the Role of Side Chains

The content of *Chapter 6* was published in the following research article:

*”SIDE CHAINS AND THE COMPETITIVE ADSORPTION BETWEEN
POLY(CARBOXYLATE ETHERS)”*

ACI Conference Paper, Supplementary Volume, Milano, 2022,

13th International Conference on Superplasticizers and Other Chemical Admixtures
in Concrete,
submitted for peer-review

Stefanie Anne Weckwerth is the first author of this publication. She designed and carried out all experiments, evaluated and visualized the data as well as wrote the first draft of the article. The final paper manuscript was elaborated in collaboration with *Prof. Flatt*.

6.1. Context

The molecular structure and dispersity of PCEs have a significant impact on their plasticizing abilities and to date a lot of research empirically describes the impact of average molecular parameters on the performance of PCEs but falls short of predictive models for effects of dispersity. This gap has been filled by the thermodynamic model, which is presented in the previous chapter.

The model in question was shown to properly capture effects of charge density and backbone length on the affinity of PCEs towards the cement surface. In the

present chapter, another significant molecular parameter that affects cement affinity, *i.e.* side chain length, is investigated. For this, the thermodynamic model is extended by focusing on the impact of side chain length onto PCE adsorption and competition. This establishes the means of capturing the effect of all molecular parameters on the thermodynamics of PCE adsorption, representing a fundamental contribution to the understanding of the PCE working mechanism on the molecular level, which is crucial for reliable structure-performance predictions.

All in all, the experiments and results presented in the present chapter complement those of *Chapter 5*. The strategy and concept behind the competitive adsorption experiments is identical as previously described. A cement paste with a W/C of 1.1 was prepared, and a binary mixture of R-PCE and G-PCE was added to a cement paste 15 minutes after the first contact between cement and water. Whereas the R-PCE has a side chain length of 19 EO repeating units, the G-PCEs feature different side chain lengths (*i.e.* variations between P= 11-113).

Competitive adsorption between the PCE species was quantified using combined TOC and UV-Vis measurements of the extracted pore solution. In contrast to *Chapter 5*, where the sequence of PCE addition was varied, all experiments in this chapter were carried out using *simultaneous* addition of the competitors.

This work is being considered for a further journal publication, in which molecular dynamic simulations of PCEs conducted by Dr. Aslam Kunhi Mohammed, a postdoc in the group, would be included. At the moment of completing this manuscript, those simulations seem to indicate a good adequation of adsorption enthalpies per carboxylate group, with respect to those derived from our model in the previous chapter.

6.2. Materials and Methods

6.2.1. Cement

For this study, the same type of cement as in *Chapter 5* (ordinary Portland type CEM I 52.5 R) was applied. However, a different batch was used, leading to small differences in composition and specific surface area. The chemical composition was obtained from XRD analysis (Table 6.1). BET measurements were applied to

determine the specific surface area (SSA_{BET}). SSA_{BET} of the anhydrous cement powder was found to be $0.9024 \pm 0.066 \text{ m}^2/\text{g}$. The surface of the cement paste ($W/C=1.1$) after 15 minutes of hydration was $2.15 \pm 0.16 \text{ m}^2/\text{g}$.

Table 6.1. XRD analysis of the applied cement powder (%).

C_3S	C_2S	C_3A	C_4AF	Gypsum	Calcite
65.6	6.7	3.1	17.6	6.5	0.4

6.2.2. PCEs with different Side Chain Length

Analogue to *Chapter 5*, we used PCEs with methacrylic acid backbone and MPEG side chains. Whereas the backbone length and charge density N are similar among all PCEs ($N \approx 3$), the side chain length of the comb copolymers varies. The molar mass of the side chain lies between 500 and 5000. This is consistent with the structural unit P ranging between 11 and 113. All macromolecules can be considered to be rather homogeneously grafted polymer combs. Due to different side chain lengths, the PCEs can either be described as flexible backbone worms or stretched backbone worms as defined in [10].

Again, various G-PCEs and one R-PCE are chosen as competitors. More information on synthesis is given in *Chapter 2*. G-PCEs were obtained by grafting of MPEG (M_n 500, 1000, 3000 and 5000 g/mol, Table 2.8a) onto preformed poly(methacrylic acid) (PMAA-5k, M_w 5400 g/mol, $D=1.4$, Table 2.8b) *via* an esterification process. All G-PCEs were supplied by Sika AG, Switzerland. Information on the molecular composition of all PCEs is summarized in Table 6.2. The nomenclature of the PCEs follows the pattern *G-PCE-N-P* for the G-PCEs, and *R-PCE-N-P* for the R-PCE competitor.

6.2.3. Adsorption Isothermes from TOC

The total organic carbon content of extracted pore solutions was determined, and adsorption isotherms were calculated using the depletion method. Details about this

^aThe R-PCE used in this chapter is not exactly the same one as the one used in *Chapter 5* as both PCEs were prepared in two different syntheses.

6. Competitive Adsorption Part II

Table 6.2. Molecular characteristics of applied PCEs. N was obtained from $1H$ -NMR spectroscopy, M_w [kg/mol], \mathcal{D} and free side chains (wt%) were measured via size exclusion chromatography using online refractive index and multi angle light scattering detection. All PCEs can be ascribed to the SBW or FBW regime as suggested by Gay, Raphaël and Flatt [10].

	N	n	$N \times n$	P	M_w	\mathcal{D}	free side chains	Regime
R-PCE-2.9-19 ^a	2.9	21.4	57	19	24.7	1.04	0.8	FBW
G-PCE-3.0-11	3.0	15.1	45	11	26.1	2.3	0.2	FBW
G-PCE-3.0-22	3.0	15.1	45	22	26.9	1.8	1.0	FBW
G-PCE-3.2-68	3.2	14.2	45	68	109.4	2.5	13.4	SBW
G-PCE-3.2-113	3.2	14.2	45	113	166.9	2.3	15.2	SBW
G-Backbone	-	-	45	-	5.4	1.4	-	-

method is described in *Chapter 5.4.3*. Figure 6.1 shows TOC adsorption isotherms of all applied PCEs. At low dosages, a sharp increase of the adsorbed amounts can be observed that finally culminates into a plateau. The plateau value indicates surface saturation. Therefore, all adsorption sites are occupied, and the surface is fully covered by a PCE monolayer.

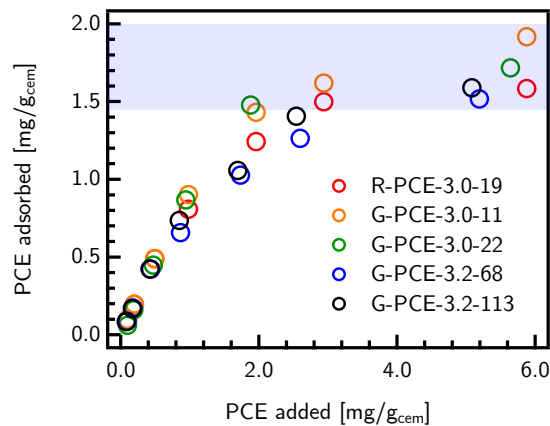


Figure 6.1. Adsorption isotherms of all applied PCEs determined by TOC and depletion calculation. The plateau value for all of the cement pastes ranges between 1.5-2.0 mg/g_{cem} (blue zone). Surface saturation is reached for a minimum dosage of 2-3 mg/g_{cem}.

For all applied PCEs, surface saturation was found between 1.5-2.0 mg/g_{cem}. In order to obtain surface saturation, a minimum dosage of about 2-3 mg/g_{cem} PCE is needed (Figure 6.1). This value was crucial for the dosages chosen in competitive adsorption experiments. Here a total dosage of 6 mg/g_{cem} was applied (3 mg/g_{cem} per competitor) to ensure that all kinetic adsorption and desorption processes occur within the plateau region. The competitors were added *simultaneously* to the cement paste and were given 15 minutes to compete for adsorption on the cement surface

before the pore solution was extracted. A detailed protocol for this type of experiment can be found in *Chapter 5.4.2*.

6.2.4. Mixing Protocol and Data Treatment

The main goal is to gain a deeper insight into the adsorption process and the adsorption behavior of R-PCE-2.9-19 in the presence of different G-PCEs of similar charge density N but different side chain length P . To this end, several parameters are of special interest, *i.e.* the total amount of adsorbed PCE, $m_{total,ads}$, but also the adsorbed amount of each species, $m_{R,ad}$ and $m_{G,ad}$ as well as the corresponding amounts of PCE left in solution termed $m_{R,sol}$ and $m_{G,sol}$. A detailed procedure for the calculation of each parameter is described in *Chapter 5.5.1*. Briefly it can be stated that TOC gives access to the total amount of adsorbed PCE *via* depletion calculation while complementary UV-Vis spectra allow to determine $m_{R,ad}$. Thus, $m_{G,ad}$ is given by the difference $m_{total,ads} - m_{R,ad}$.

6.3. Results and Discussion

6.3.1. Experimental Outcome

The series of bar plots in Figure 6.2a summarizes the outcome of all competitive adsorption experiments. The height of the bars shows the total amount (in mg/g_{cem}) of adsorbed PCE. Each bar is composed of two stacked components indicating the amount of adsorbed G-PCE (with different side chain length P) and the corresponding amount of R-PCE-2.9-19. The total height of the bars is similar in all experiments, indicating that the total amount of adsorbed PCE (total height of the bars) is relatively constant, although the proportions of the two PCEs change. More specifically, the total adsorption ranges between 1.7-2.2 mg/g_{cem}, which is consistent with the plateau values for the polymers taken individually (Figure 6.1, blue zone).

One trend that can be observed is that the mass of adsorbed G-PCE decreases with increasing side chain length. Whereas for $P=11$ and 22 more G-PCE than R-PCE can be found on the surface, the trend is reversed for $P=68$ and 113 . With all G-PCEs featuring the same backbone and a similar grafting density, the differences in

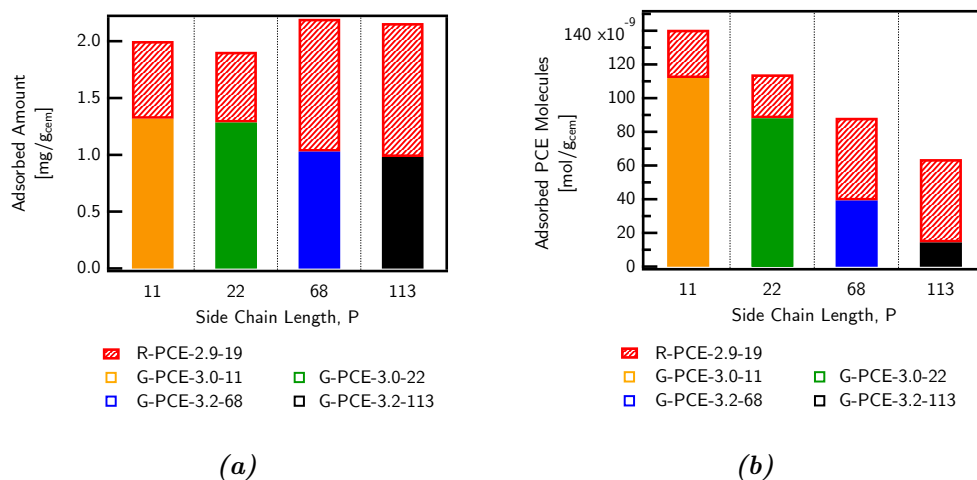


Figure 6.2. (a) Amount of adsorbed PCEs during competitive adsorption experiments. (b) Corresponding number of adsorbed PCE molecules.

affinity for the surface are due to the effect of P on adsorption. The trend that PCEs with shorter side chains adsorb preferentially over PCEs with higher P becomes even clearer when looking at the number of PCE molecules attached to the surface (mol/g_{cem}) (Figure 6.2b).

6.3.2. Thermodynamics of the Adsorption Process

Figure 6.2 clearly shows that P influences the adsorption behavior of a PCE. So far, it can be stated that longer side chains decrease the affinity of PCEs for the surface. We aim to connect this observation with the model presented in *Chapter 5*. To this end, we calculate the equilibrium constant K for all experiments according to Equation 5.17 using the quantified amounts of adsorbed and dissolved species. For this, we take R-PCE-2.9-19 as component A, while B represents the different G-PCEs. For this calculation, the stoichiometric coefficients for each PCE are required. We obtain them with Equation 5.24. The calculated coefficients are tabulated in Table 6.3 and subsequently used to calculate $\Delta G_{Ex}^{o,Area}$ from Equation 5.18.

Enthalpic Contribution

As pointed out before, we consider the adsorption enthalpy to be proportional to the number of charges per area Z_i . To emphasize this correlation, the previously derived equations are reprinted:

$$\begin{aligned}\Delta H_{Ex}^{o,Area} &= h_B - h_A \\ &= -\alpha_H \cdot \beta_x [P_B^{-0.9} N_B^{-0.3} (N_B - 1) - P_A^{-0.9} N_A^{-0.3} (N_A - 1)]\end{aligned}\quad (6.1)$$

$$\begin{aligned}\text{where } h_i &= -\alpha_H Z_i \\ &= -\alpha_H \cdot \frac{\sqrt{2}}{\pi a_N a_P} (2\sqrt{2}(1 - 2\chi) \frac{a_N}{a_P})^{-0.4} P_i^{-0.9} N_i^{-0.3} (N_i - 1)\end{aligned}\quad (6.2)$$

and $\alpha_H > 0$; and $\beta_x = \frac{\sqrt{2}}{\pi a_N a_P} (2\sqrt{2}(1 - 2\chi) \frac{a_N}{a_P})^{-0.4}$

Accordingly, the enthalpic contribution of an adsorbing PCE i solely depends on its charge density N_i and side chain length P_i and is independent of n_i . Notably, all applied PCEs used in this study feature a similar charge. Looking at the values for Z_i , PCEs with shorter side chains feature a higher number of carboxylates per area. This means that for the same value of N , the adsorption of a PCE with shorter chains should be more exothermic than for a competitor with longer side chains. Thus, from a purely enthalpic point of view, PCEs with short side chains are favored to adsorb preferentially over competitors with longer side chains. Indeed, this can be observed in the experimental data (Figure 6.2). G-PCE-3.2-68 and G-PCE-3.2-113 adsorb in significantly smaller amounts than G-PCE-3.0-11 and G-PCE-3.0-22.

Entropic Contribution

We also want to address briefly the role of entropy. Here, polymer and solvent contribution have to be distinguished. The major part of the entropy is considered to be due to the release of solvent molecules from the surface. Upon PCE adsorption, mainly the PCE backbone interacts with the cement surface, causing the release of solvent molecules. Consequently, the entropic contribution per unit surface s_i is proportional to the backbone length of the adsorbing PCE ($N \times n$). Equation 5.29

6. Competitive Adsorption Part II

indicates that s_i is direct proportional to the molecular parameters P and N , where α_S is a proportionality constant. Notably, we investigate the exchange of PCE molecules at full surface coverage. For these conditions, the entropic contribution caused by the solvent is expected to be very similar for any kind of adsorbing PCE species.

Regarding the entropic contribution of the PCE, the number of adsorbed molecules per surface unit X_i have to be considered. With increasing side chain length, less PCEs are required to obtain a full monolayer (Table 6.3). Thus, entropy might favor the adsorption of PCEs with longer side chains as less backbones get immobilized on the surface. In the thermodynamic framework, we consider this contribution to be negligible and relate $\Delta G_{Ex}^{o,Area}$ purely to exothermic bond formation.

Table 6.3. Number of molecules (X_i) and charges (Z_i) per 100 nm². The values were calculated using Equation 5.24 and 5.27 assuming $a_N = 0.25$ nm, $a_P = 0.36$ and $\chi = 0.37$. The stoichiometric coefficients were calculated using $X_{R-PCE-2.9-19}$ as a reference.

	X_i [molecules/100 nm ²]	Z_i [COO ⁻ /100 nm ²]	x_i $x_i = X_i/X_{R-PCE-2.9-19}$
R-PCE-2.9-19	1.17	47	1.00
G-PCE-3.0-11	2.76	84	2.37
G-PCE-3.0-22	1.44	43	1.23
G-PCE-3.2-68	0.55	17	0.47
G-PCE-3.2-113	0.35	11	0.30

In order to verify the thermodynamic model, we modify Equation 6.1 assuming that N_i is constant. Consequently, we find $\Delta G_{Ex}^{o,Area}$ to be proportional to $\Delta[P_i^{-0.9}]$ (Equation 6.3). We then plot $\Delta G_{Ex}^{o,Area}$ against $\Delta[P_i^{-0.9}]$ (Figure 6.3).

$$\Delta G_{Ex}^{o,Area} \approx \Delta H_{Ex}^{o,Area} = h_B - h_A = \alpha_H^* \cdot \Delta[P_i^{-0.9}] \quad (6.3)$$

$$\begin{aligned} \text{with } \Delta[P_i^{-0.9}] &= [P_B^{-0.9} - P_A^{-0.9}] \quad \text{and} \quad N_A = N_B \\ \text{and } \alpha_H^* &= \alpha_H \cdot \beta_x \cdot N_A (N_A - 1) \quad \text{where} \quad \alpha_H > 0 \end{aligned}$$

In Figure 6.3, a linear relation between $\Delta G_{Ex}^{o,Area}$ and $\Delta[P_i^{-0.9}]$ is found. This strongly supports the thermodynamic framework in which we aim to connect the molecular structure with $\Delta G_{Ex}^{o,Area}$. However, our results do not fully validate

the model because the regression line does not exactly pass through the origin (offset ≈ 9.8 kJ/mol). A possible explanation for the offset might be the slight differences of N that are considered to be constant for the sake of this plot. Moreover, the increased dispersity of the G-PCE compared to its rather monodisperse competitor might also result in an offset. Last but not least, also entropic contributions can cause a shift of the trendline.

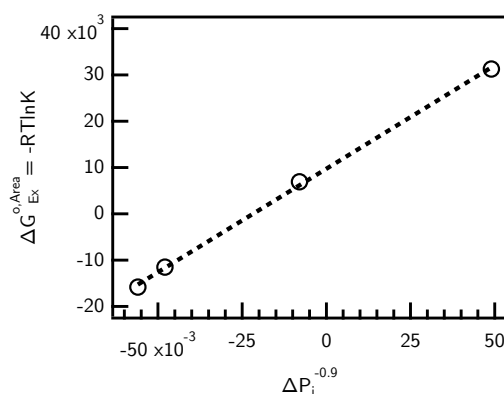


Figure 6.3. Verification of Equation 6.3 The data of the competitive experiments was fitted by linear regression. The slope (α_H^*) was found to be 44.7 kJ/mol per unit of $\Delta P_i^{-0.9}$. The offset of the regression line is 9.8 kJ/mol.

6.3.3. Master Curve

Finally, we aim to combine the effects P and N on the adsorption behavior of PCEs. Our experiments prove that an increasing side chain length decreases the affinity of PCEs for the cement surface. At the same time, our previous work revealed that the affinity increases with increasing N . This means that the affinity of a PCE can be enhanced or reduced by adapting the side chain length and charge density (*i.e.* grafting ratio).

So far, we discussed the adsorption behavior with focus on N and P separately. In the final section of our discussion, we combine our different findings. Consequently, we plot $\Delta G_{Ex}^{o,Area}$ obtained from the data presented in this paper with those reported in *Chapter 5*. To this end, we refer once again to Equation 5.30. However, this time, we plot $\Delta G_{Ex}^{o,Area}$ against $[P_B^{-0.9} N_B^{-0.3} (N_B - 1) - P_A^{-0.9} N_A^{-0.3} (N_A - 1)]$ (Figure 6.4).

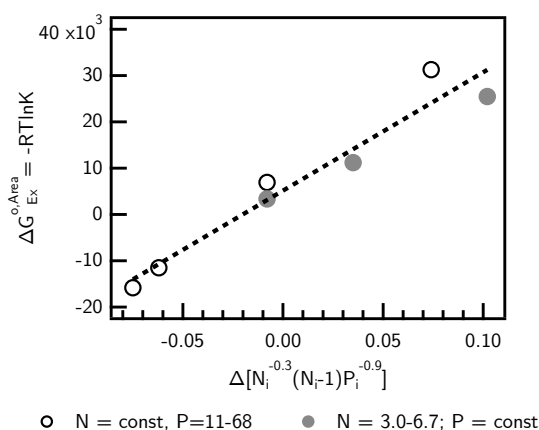


Figure 6.4. Master curve obtained by combining data from competitive adsorption experiments with focus on P and N . Verification of Equation 5.30. The data of the competitive experiments was fitted by linear regression. The slope (α_H^*) was found to be 255.6 kJ/mol per unit of $\Delta[N_i^{-0.3}(N_i - 1) \cdot P_i^{-0.9}]$. This is equal to a bonding strength, $\alpha_H \approx 52.3$ kJ per mol of carboxylate. The offset of the regression line is 5.2 kJ/mol.

Figure 6.4 shows that the results of this study are complementary to the findings in Chapter 5. All data points roughly follow a linear trend. The corresponding regression line is not exactly passing through the origin, but close to it (4.0 kJ/mol). This verifies that Equation 5.32 is an appropriate expression to describe the thermodynamics upon PCE competition in dependence on the molecular parameters.

6.4. Conclusion

Side chains are often only thought of as being the source of steric hindrance, while backbones are considered to dominate the interaction with the cement surface and thereby dominate adsorption. Our study recognizes the key features behind these ideas, but presents a more comprehensive picture of PCE adsorption in regard to their overall molecular structure. In particular, we show that the side chain length affects the thermodynamic equilibrium between adsorbing PCEs of different molecular features. As a general trend, it was revealed that at similar charge density, PCEs with shorter backbones are able to displace combs with longer side chains. This process is mainly driven by enthalpy.

Although side chains do not bind directly to the surface, their coiled conformation demands space and hinders the adsorption of adjacent molecules. In order to cover

a given unit surface, fewer molecules with long side chains are needed, while a higher number of PCEs with short side chains is required. Thus, at same grafting ratio and backbone length, the PCEs with short side chains can form more bonds between carboxylic groups and Ca^{2+} due to a higher charge density per unit area. On the contrary, from an entropic point of view, the adsorption of PCEs with short side chains seems less favorable. This emphasizes the importance of enthalpy and exothermic bond formation during the adsorption process.

The data presented in this study is complementary to the findings in *Chapter 5*. Upon the addition of two PCEs with different molecular parameters, a dynamic equilibrium is established. The adsorbed and desorbed fraction of each PCE can be correlated with its charge, backbone length and side chain length. The calculated equilibrium constant can be regarded as a displacement coefficient that reveals if and to what extent a PCE species preferentially adsorbs over its competitor. Thus, the here presented thermodynamic framework can be considered as a universal tool to predict PCE competition.

Generally speaking, the procedure and model presented can be used as a starting point to investigate competitive adsorption phenomena of PCEs with other chemistries (*i.e.* type of side chains, functional groups) and by adapting the protocol to “direct addition” also the role of PCEs during ettringite nucleation can be investigated with regard to molecular parameter and thermodynamics.

Conclusion and Outlook

7.1. Accomplished Results

7.1.1. PCE Analysis

The presented thesis contributes to the field of poly(carboxylate ether) (PCE) research in the following ways. First of all, it shows that the levels of dispersity within PCEs are complex. Besides the molar mass, also molecular parameters such as backbone length and grafting ratio are distributed. Up to now, this issue has remained an often-overlooked factor in admixture research due to a lack of versatile analytical methods that allow to reveal molecular heterogeneity.

For this purpose, two liquid chromatography (LC) protocols were developed that enable to analyze PCEs regarding dispersity. The first method is given by size exclusion chromatography (SEC) using dual concentration detection. Adding a second concentration detector to a traditional SEC setup allowed to monitor the comonomer composition of PCEs in dependence on their hydrodynamic size. Our results confirm that the synthesis method has a significant impact on the dispersity within PCEs. For PCEs obtained from polymer-analogous esterification, a dependence of the grafting ratio on the molar mass of the precursor was shown. This issue is of particular interest for the synthesis of PCE model structures with distinct molecular properties. Also, for PCEs synthesized by free radical copolymerization (FRC) variations of the comonomer composition with the hydrodynamic volume were revealed. This result is of high practical relevance, as the majority of commercially available PCEs is produced *via* FRC.

Indeed, we do not only exemplify the development of LC methods to characterize chemical dispersity, but reveal that two PCEs with similar average composition can

be composed by a variety of different molecules. This issue is crucial when correlating molecular parameters of PCEs with their performance as superplasticizers and to better understand how various synthetic routes may affect polymer performance at equivalent average composition. All in all, dual concentration SEC offers the means to get a first insight into the heterogeneity of PCEs in hydrodynamic size and chemical composition.

The second LC method developed in this thesis is based on interaction chromatography. More precisely, reverse-phase high performance liquid chromatography (RP-HPLC) in combination with solvent gradients of acetonitrile and water was presented as a powerful tool to separate PCEs by their grafting ratio. Thus, both LC methods target complementary information regarding hydrodynamic size and polarity. When operating SEC and RP-HPLC independently, coelution phenomena have to be taken into account, as branching and molar mass effects cause simultaneous elution of different PCE species in both methods. This makes it increasingly difficult to approach the exact molar mass distribution (MMD) and chemical composition distribution (CCD) of PCEs.

It was shown that 2D-chromatography is capable of solving this issue. Connecting SEC and RP-HPLC (LC×LC) in 2D-experiments was suggested as a powerful tool to identify fractions with different molecular characteristics within PCEs. This type of experiments allowed us to create chromatography maps of PCEs by combining the chromatograms obtained in each dimension. Additionally, we used modelled 2D-data to depict the impact of different levels of dispersity onto the chromatography maps.

However, we highlight that chromatography results of PCEs can only be interpreted in a meaningful way for admixture research when referring to validated structure-performance relations. While the developed chromatography protocols enabled us to identify different species within PCEs, their effect on cement can only be predicted when the impact of molecular parameters on adsorption, hydration and other functions is known. Notably, in this regard, empirical and scientifically-based models are considered equally helpful.

7.1.2. Adsorption Studies and Structure Performance Relations

The affinity of a PCE for the cement surface is an important characteristic that determines their competitiveness for adsorption and ultimately also their performance

as superplasticizer. While it was assumed in the past, that molecular parameters, above all the charge density, impact their tendency to adsorb to the surface, it has not been possible to correlate molecular parameters with affinity.

We developed a dual detection approach combining total organic carbon measurements with UV-Vis spectroscopy to verify competition between PCEs as a result of their molecular composition. Indeed, this work is the first one to experimentally prove the occurrence of competitive adsorption between PCEs on the molecular level and the first work to show that adsorption and desorption at the cement surface involves dynamic processes.

We underlined our experimental outcome by deriving a thermodynamic model that captures all aspects of our experiments. Hence, we were able to describe affinity and competitiveness of PCEs as a consequence of enthalpic and entropic contributions.

All in all, this work makes an important new step towards the mechanistic understanding of structure-property relations of PCEs. Accessing the working mechanism of PCEs on a molecular level is indeed indispensable for molecular design of effective superplasticizers for concrete technology.

We want to encourage systematic research in the field of structure-performance relations, aiming to describe experimental findings with scientifically-based models. While empirical models will always have an important value in admixture research, we are convinced that models combining fundamental knowledge about polymer science and cement chemistry will play a key role in the design of superplasticizers with tailor-made properties. This thesis and the herein presented analytical tools and methods can serve as starting point for further studies aiming to reveal structure-performance relations. At this point, we want to emphasize one more time that performance does not exclusively refer to the impact of PCEs on plasticizing cement, but also on their impact on hydration and setting behavior or ability to modify ettringite nucleation.

7.2. Implications for Admixture Research

Improving the performance of PCEs and choosing the right PCE and the right dosage for different applications are some remaining big challenges in admixture research

and applications. Indeed, we are aware that cement applications will always depend on empirical values and substantially also on trial and error to meet the demands. However, we are convinced that reliable structure-performance relations can make a significant contribution towards the design of superplasticizers with tailor-made characteristics and performance.

We hope that this thesis convinces researchers to rethink the idea of dispersity within PCEs and motivates them to analyze MMD and CCD thoroughly before drawing conclusions regarding efficiency and performance. In particular, when deriving structure-performance relations, molecular heterogeneity within PCEs can be problematic. When the dispersity is not accounted for correctly, misleading conclusions regarding the influence of molecular composition on performance might be drawn. Therefore, we highly encourage a comprehensive analysis of molecular heterogeneity using the LC protocols developed in the course of this thesis.

Indeed, in cement research it has become a standard procedure to analyze cement regarding its composition, available surface and particle distribution. At the same time, the molecular details about the applied admixtures are often neglected. This thesis shows the importance of accurately analyzing PCEs and reporting information about average composition as well as dispersity. In this way, studies conducted by different researchers can be better compared on a meaningful basis, which is essential to validate derived scaling laws.

Moreover, we encourage applying PCEs with well-defined composition when studying structure-performance relations. The RAFT protocol reported in this thesis enables the polymerization of PCEs with narrow distributed composition and well-defined architecture. Thus, the synthesis protocols and LC methods presented in this thesis may contribute to fundamental admixture research aiming to correlate molecular parameters and architecture of PCEs with their effect on affinity, adsorption or hydration in cement.

However, we want to emphasize that dispersity must not be mistaken as a flaw impairing the performance of PCEs as superplasticizers. While a broad distribution of parameters hinders fundamental structure-performance studies, it might be beneficial for the design of robust PCEs covering a wide spectrum of characteristics. With the composition of concrete mixes underlying significant variations regarding the quality of raw materials, the dispersity within PCEs guarantees efficiency for a wide range

of mixes. To this end, the developed LC methods can be applied to understand and tailor the dispersity in CCD and MMD of commercial products.

In conclusion, this thesis emphasizes that knowledge about dispersity combined with validated structure-performance relations provides a deeper insight into of the PCE working mechanism on the molecular level. This knowledge can be used to optimize synthesis methods and PCE structures towards the design of PCEs with tailor-made characteristics. This thesis emphasizes the value of developing analytical protocols for PCE analysis, but also for adsorption studies. In this way, it was proven that combining the disciplines of polymer science and analytics with admixture research and cement chemistry has the potential to guarantee new insights into the working mechanism of PCEs on the molecular level and allows to predict their macroscopic performance.

7.3. Future Opportunities

The research conducted in this thesis used PCEs with MPEG side chains and a PMAA backbone in all experiments. This PCEs can be considered as an "archetype" in admixture research. This was beneficial for this work, as we could pick up scaling relations that were derived for MPEG-type PCEs in the past.

By now, the variety of PCEs with different chemistries has broadened significantly. In many studies, the performance of two PCE species is often compared solely referring to the spread flow at equivalent dosage. We want to encourage researchers to take the analytical methods presented in this thesis and apply them to other types of PCEs. Comparing chromatography results between PCE species with different comonomers might shed light on their different behavior in cement.

All in all, this thesis provides an analytical toolbox that allows to thoroughly characterize PCEs and to reveal processes happening upon adsorption of PCEs at the cement surface on the molecular level. In a continuation of this work, we suggest including further analytical methods such as workability tests, *i.e.*, spread flow tests and rheology tests in order to verify macroscopic consequences of PCE competition as well as calorimetry tests that give information on the hydration behavior.

This thesis shows that competitive adsorption among PCEs at the plateau is dominated by enthalpic effects. For incomplete surface coverage, the adsorption

enthalpy is expected to remain the same. However, the exact role of entropy deserves further attention. To this end, a series of competitive adsorption experiments using low and intermediate dosages of PCEs (and incomplete surface coverage) could contribute to a better understanding of entropic effects. This is of high practical relevance, as in many applications low dosages of PCEs are added.

Of course, the LC protocols also deserve further research. Optimized solvent gradients might allow separating PCEs not only by grafting ratio but could be used to extract information on the architecture (*i.e.* statistical, gradient or block). Besides solvent gradients, we suggest exploiting the lower critical solution temperature (LCST) of PCEs for refining gradient experiments. A first impression on how this issue can be addressed is given in the final section of this thesis (*Appendix A*).

A

Lower Critical Solution Temperature

A.1. Context

Poly(carboxylate ethers) have a complex solubility behavior in aqueous phases that is impacted by multiple factors such as the pH of the solution, but also the molecular parameters of the PCE. Due to the high alkalinity of cement, the solution characteristics of PCEs are often studied with focus on high pH values. Notably, at high pH, most PCE structures are well solubilized. On the contrary, in acidic environment, PCEs exhibit a lower critical solution temperature (LCST) meaning that a reversible phase transition from soluble to insoluble occurs upon heating. Becer *et al.* [54] demonstrated the LCST behavior of PCEs in dependence on C/E and *P*. More information on the LCST is described in *Chapter 1.1.5*.

While the LCST does not impact the performance of PCEs in cement, it could be a very useful feature to investigate PCEs with regard to their molecular characteristics. In this appendix, the solubility behavior, *i.e.* the occurrence of a cloud point (CP) of various PCEs with systematic variations in their molecular composition is demonstrated and potential implications for chromatography are discussed.

A.2. Materials and Methods

A.2.1. Applied PCEs

For this study, a series of G-PCEs obtained from grafting of MPEG-23 (Table 2.8a) onto PMAA-5k (Table 2.8b) was applied. The C/E ratio of these samples ranges

between 1.6 and 5.0. More information on these G-PCEs is given in (*Chapter 3*, Table 3.1). Additionally, three G-PCEs with increased backbone length (precursor PMAA-8k, Table 2.8a) were applied. Information on these samples is given in (*Chapter 4*, Table 4.2b). Moreover, two R-PCE samples were investigated to demonstrate the impact of side chain length ($P=9$ and $P=19$) on the CP. Information on these R-PCEs is presented in *Chapter 4*, Table 4.2a.

A.2.2. Turbidity measurements

The solubility behavior (*i.e.* cloud point, CP) of various PCEs was investigated using turbidimetry. Turbidity measurements were performed in a *Crystal16* device from *Avantum Technologies*. The device allows to monitor the turbidity of 16 samples in dependence on temperature simultaneously. For this purpose, PCE solutions with a concentration of 5 mg/mL were prepared. As solvent, water with 0.1 M NaCl or 0.033 M CaCl₂ was used. The pH of the solutions was precisely adjusted using HCl or NaOH. The ionic strength I of the salt ions in solution is approximately 0.1M and was calculated according to Equation A.1, where c_i is the molar concentration of ion i and z_i is the charge number of that ion. The sum was taken over all salt ions in the solution.

$$I = \frac{1}{2} \sum_{i=1}^n c_i z_i^2 \quad (\text{A.1})$$

In a typical measurement, turbidity was measured by the transmission of red light through the sample vial as a function of the temperature. During the whole experiment, the solutions were stirred with magnetic stirring bars. A temperature ramp between 10 °C and 95 °C was applied. First, the solution was cooled to 10 °C and equilibrated for 15 minutes to guarantee complete PCE dissolution. Subsequently, the solutions were heated until 95 °C at 1 °C/min. Figure A.1 shows a typical plot of transmission *vs.* temperature

At temperatures below CP, the PCE molecules are well dissolved and the solution has 100% transmission. Upon heating, the solubility of the PCE changes. At the CP, the PCE starts forming aggregates and the solution becomes turbid. As a result, the transmission drops to 0. CP was determined as the point of 50% transmission during the first heating ramp. For temperatures beyond the CP, the transmission increases

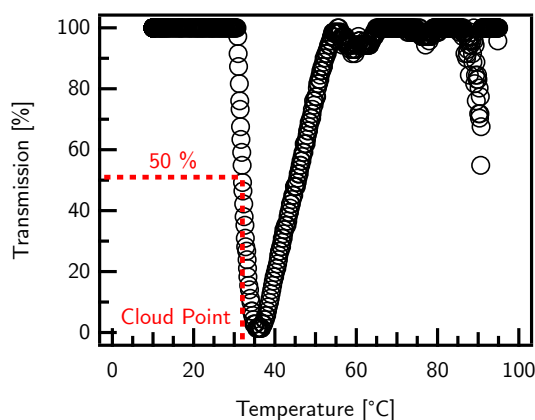


Figure A.1. Plot of transmission vs. temperature as obtained from turbidity measurement of a PCE solution in the temperature range between 10 and 95 °C. The cloud point is determined as the temperature value for 50% transmission during the first heating cycle.

again and fluctuates around 80-100% transmission until the final temperature is reached. This is due to precipitation and sedimentation of the PCE agglomerates at high temperatures.

A.3. Solubility Behavior of PCEs

A.3.1. Impact of C/E and pH

The occurrence of a CP is the consequence of intramolecular interactions (*i.e.* hydrogen bonding) between protonated carboxylate groups and the ethylene oxide (EO) groups in the side chains. Therefore, the CP depends on two main factors, namely the ratio of carboxylic acid groups and side chains (*i.e.* C/E) and degree of dissociation (α). Assuming $pK_A \approx 5.8$, about 99.9 % of the carboxylic acid groups in the PCE backbone are protonated at pH 2 (see *Chapter 2.6.4*; Equation 2.14). For this condition, CP decreases with increasing C/E (Figure A.2a). With increasing C/E, more carboxylic acid groups are incorporated in the PCE backbone, which results in a higher number of intramolecular bonds between carboxylic acid and side chains and induces precipitation. For various PCEs with C/E between 1.6 and 5.0, the CP ranges between approximately 25 °C and 95 °C. Within this range, an almost linear correlation between CP and C/E was found. Notably, at pH 2, CP seems to be independent of backbone length. The CP of G-PCEs with a shorter backbone

(G-PCE-5k) follow the same trend as corresponding G-PCEs with increased backbone length (G-PCE-8k).

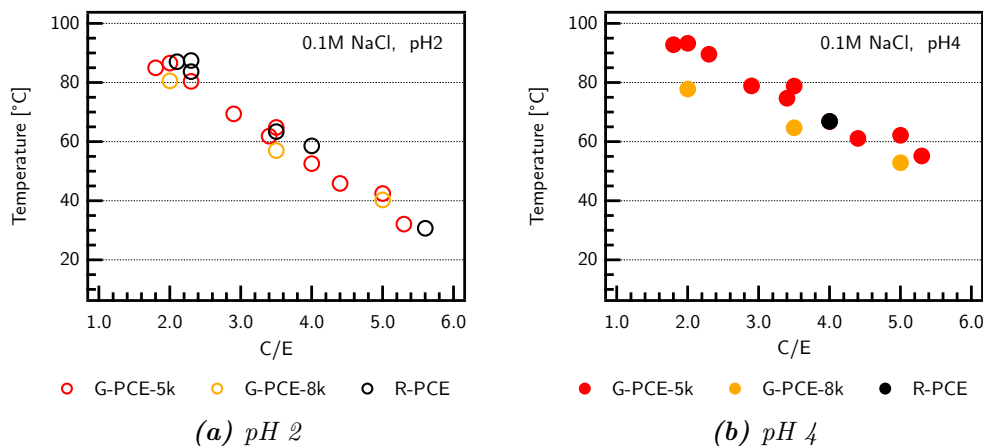


Figure A.2. Cloud points of PCE copolymers as a function of C/E at different pH values estimated by 50% transmittance points of the first heating curves: (a) pH 2, (b) pH 4. For pH higher than pH 6, no CP was observed. All PCE solutions were prepared in 0.1M NaCl ($I=0.1M$), the pH was adjusted using HCl.

Increasing the pH leads to deprotonation of the carboxylic acid groups in the PCE backbone. For pH 4, $\alpha \approx 1.6$ % meaning that approximately 1.6 % of the carboxylic acid groups are deprotonated. Already, this slight decrease in protonation affects the CP. With increasing pH , the CP is shifted to higher temperatures (Figure A.2b). At constant backbone length, there is a linear correlation between CP and C/E . However, it appears that at constant C/E , an increase in backbone length leads to a slight decrease of the CP (Figure A.2b, G-PCE (8k)).

A further increase of the pH results in a shift of the CP to even higher values. Notably, for pH values close to the pK_A and higher, no CP can be observed. Thus, for $pH > 6$, all PCEs shown in Figure A.2 are fully soluble in aqueous solution at all temperatures.

A.3.2. Impact of Side Chain Length

While the backbone length only slightly affects the CP, the side chain length has a significant impact on the solubility behavior of PCEs. In Figure A.3a, the turbidity measurements of two R-PCE solutions (0.1M NaCl pH 2) are shown. Both PCEs have a similar backbone length and C/E but different P . For R-PCE-2.1-19, the CP

is found at 87 °C, while R-PCE-1.9-9 has its CP at 46 °C. Thus, a decrease of the side chain length significantly shifts the CP to lower temperatures.

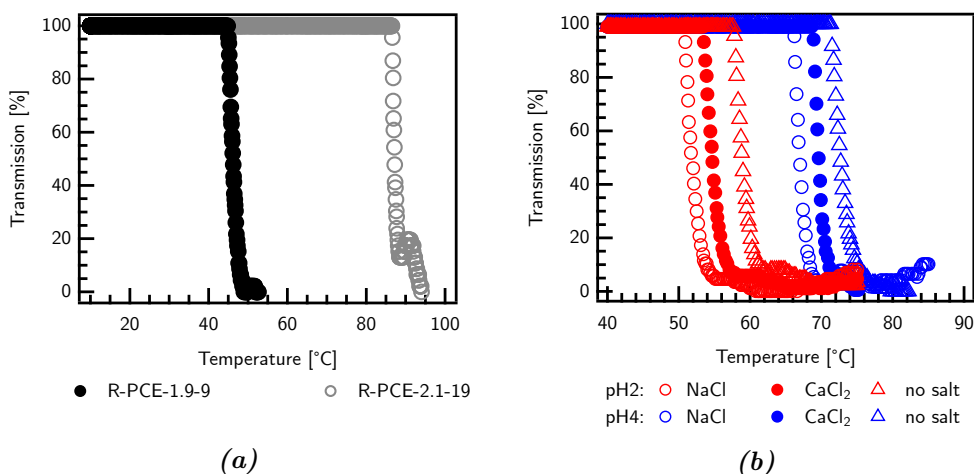


Figure A.3. Plot of transmission vs. temperature as obtained from turbidity measurement of a PCE solution. The impact of different parameters onto the solubility behavior of PCEs was investigated (a) Impact of side chain length (b) Impact of pH and presence of different salts on the solubility of R-PCE-1.9-19. The ionic strength for NaCl and CaCl₂ was adjusted to 0.1M.

A.3.3. Impact of Salt and Ionic Strength

All results shown in Figure A.2 and Figure A.3a used 0.1M NaCl as solvent. Besides pH, also the ionic strength and type of ions in the solvent are expected to have an impact on the CP. In Figure A.3b, the CP of R-PCE-1.9-19 was determined at pH 4 for various solutions. For a solution in ultrapure water (pH 2), CP was found at 59 °C. Addition of salt (*i.e.* NaCl or CaCl₂) causes a shift of the CP to lower temperatures. Here, the salt concentration was chosen in a way that the ionic strength of the solution is comparable. Notably, the addition of Na⁺ causes a bigger shift than Ca²⁺.

A.4. Implications for Chromatography

As can be seen from the previous section, PCEs have a complex solubility behavior. The solubility in aqueous phases correlates with the molecular characteristics and can be adjusted by changing pH, temperature or salt concentration of the solution.

Hence, PCEs are multi-responsive. Indeed, the temperature dependent solubility at acidic pH is of particular interest for developing liquid chromatography-based techniques that allow to separate PCEs by their chemical composition. As shown in Figure A.2a, at pH 2, the LCST is independent of backbone and side chain length and depends solely on the grafting ratio.

In the following, we describe how the LCST behavior of PCEs could possibly be implemented to size exclusion chromatography (SEC) or liquid adsorption chromatography (LAC) of PCEs.

We recall, that the separation mechanism in SEC experiments is based on steric exclusion. In a normal SEC experiment ($T < T_{LCST}$) all PCEs are well-dissolved. Increasing the column temperature will induce changes in the hydrodynamic size of the PCE molecules when T approaches the LCST. As a consequence, PCE fractions with higher charge could potentially be separated from fractions of lower charge.

Indeed, this approach was pursued in some preliminary experiments. For this purpose, two different types of SEC columns (Suprema and Proteema, various pore sizes, Polymer Standard Service, Mainz, Germany) were applied. The mobile phase was 0.1M NaCl (at pH 2 pH 4, adjusted with HCl). However, it was not possible to separate PCEs according to hydrodynamic size. At acidic pH, PCEs interact with the column material at all temperatures. This prevents the separation by steric exclusion.

Nonetheless, interactions between solute and column can be exploited in LAC experiments. For the applied Suprema and Proteema columns, interactions with PCEs occurred independent of their comonomer composition. Besides temperature gradients, also pH gradients (pH 2-pH 7) were preliminary tested to separate PCEs by their C/E. Also here, the molecules revealed a strong tendency to adsorb to the column material. Hence, no selective separation in dependence on the LCST was achieved, neither by steric exclusion nor by enthalpic interactions. However, we encourage to find suitable column materials which are less sensitive to hydrogen bonding to pursue this approach. An ideal column is less prone to interact with PCEs, allows the use of purely aqueous phases, and resists temperature changes in the range between approximately 10 °C and 80 °C.

As soon as a suitable column is found, temperature (or pH) dependent experiments (SEC or LAC based) will allow to separate PCEs according to their grafting ratio. The obtained fractions could be subjected to regular SEC experiments in the second

dimension to create a 2D-contour plot that gives information on the chemical composition in the first dimension and on the molecular size in the second dimension.

Bibliography

- [1] Jiahui Peng, Jindong Qu, Jianxin Zhang, Mingfeng Chen, and Tizhi Wan. Adsorption characteristics of water-reducing agents on gypsum surface and its effect on the rheology of gypsum plaster. *Cement and Concrete Research*, 35(3):527–531, 2005. Type: Journal Article. URL: <https://dx.doi.org/10.1016/j.cemconres.2004.04.016>, doi:10.1016/j.cemconres.2004.04.016.
- [2] Etsuo Sakai, Akira Kawakami, and Masaki Daimon. Dispersion mechanisms of comb-type superplasticizers containing grafted poly(ethylene oxide) chains. *Macromolecular Symposia*, 175(1):367–376, 2001. Type: Journal Article. URL: <https://onlinelibrary.wiley.com/doi/abs/10.1002/1521-3900%28200110%29175%3A1%3C367%3A%3AAID-MASY367%3E3.0.CO%3B2-9>, doi:[https://doi.org/10.1002/1521-3900\(200110\)175:1<367::AID-MASY367>3.0.CO;2-9](https://doi.org/10.1002/1521-3900(200110)175:1<367::AID-MASY367>3.0.CO;2-9).
- [3] Catherine P. Whitby, Peter J. Scales, Franz Grieser, Thomas W. Healy, Glen Kirby, Jennifer A. Lewis, and Charles F. Zukoski. PAA/PEO comb polymer effects on rheological properties and interparticle forces in aqueous silica suspensions. *Journal of Colloid and Interface Science*, 262(1):274–281, 2003. Type: Journal Article. URL: [https://dx.doi.org/10.1016/s0021-9797\(03\)00179-6](https://dx.doi.org/10.1016/s0021-9797(03)00179-6), doi:10.1016/s0021-9797(03)00179-6.
- [4] J. Plank, E. Sakai, C. W. Miao, C. Yu, and J. X. Hong. Chemical admixtures — Chemistry, applications and their impact on concrete microstructure and durability. *Cement and Concrete Research*, 78:81–99, 2015. Type: Journal Article. URL: <https://dx.doi.org/10.1016/j.cemconres.2015.05.016>, doi:10.1016/j.cemconres.2015.05.016.
- [5] John D. Schofield. Extending the boundaries of dispersant technology. *Progress in Organic Coatings*, 45(2-3):249–257, 2002. Type: Journal Article. URL: [https://dx.doi.org/10.1016/s0300-9440\(02\)00041-3](https://dx.doi.org/10.1016/s0300-9440(02)00041-3), doi:10.1016/s0300-9440(02)00041-3.
- [6] G. Gelardi, S. Mantellato, D. Marchon, M. Palacios, A. B. Eberhardt, and R. J. Flatt. Chemistry of chemical admixtures. In *Science and Technology of Concrete Admixtures*, pages 149–218. Elsevier, 2016. Type: Book Section. URL: <https://dx.doi.org/10.1016/B978-0-08-100693-1.00009-6>, doi:10.1016/b978-0-08-100693-1.00009-6.
- [7] Robert J. Flatt, Nicos Martys, and Lennart Bergström. The Rheology of Cementitious Materials. *MRS Bulletin*, 29(5):314–318, 2004. Type: Journal Article. URL: <https://dx.doi.org/10.1557/mrs2004.96>, doi:10.1557/mrs2004.96.
- [8] Johann Plank and Manuel Ilg. The Role of Chemical Admixtures in the Formulation of Modern Advanced Concrete. In William P. Boshoff, Riaan Combrinck, Viktor

- Mechtcherine, and Mateusz Wyrzykowski, editors, *3rd International Conference on the Application of Superabsorbent Polymers (SAP) and Other New Admixtures Towards Smart Concrete*, pages 143–157, Cham, 2020. Springer International Publishing. URL: https://link.springer.com/chapter/10.1007%2F978-3-030-33342-3_16, doi:10.1007/978-3-030-33342-3_16.
- [9] Robert J. Flatt, Nicolas Roussel, and Christopher R. Cheeseman. Concrete: An eco material that needs to be improved. *Journal of the European Ceramic Society*, 32(11):2787–2798, 2012. Type: Journal Article. URL: <https://dx.doi.org/10.1016/j.jeurceramsoc.2011.11.012>, doi:10.1016/j.jeurceramsoc.2011.11.012.
- [10] Robert J. Flatt, Irene Schober, Elie Raphael, Cédric Plassard, and Eric Lesniewska. Conformation of Adsorbed Comb Copolymer Dispersants. *Langmuir*, 25(2):845–855, 2009. Type: Journal Article. URL: <https://dx.doi.org/10.1021/la801410e>, doi:10.1021/la801410e.
- [11] G. Gelardi and R. J. Flatt. 11 - Working mechanisms of water reducers and superplasticizers. In Pierre-Claude Aïtcin and Robert J. Flatt, editors, *Science and Technology of Concrete Admixtures*, pages 257–278. Woodhead Publishing, 2016. Type: Book Section. URL: <http://www.sciencedirect.com/science/article/pii/B9780081006931000114>, doi:10.1016/B978-0-08-100693-1.00011-4.
- [12] D. Marchon, S. Mantellato, A. B. Eberhardt, and R. J. Flatt. Adsorption of chemical admixtures. In *Science and Technology of Concrete Admixtures*, pages 219–256. Elsevier, 2016. Type: Book Section. URL: <https://dx.doi.org/10.1016/B978-0-08-100693-1.00010-2>, doi:10.1016/b978-0-08-100693-1.00010-2.
- [13] P.-C. Aïtcin. Portland cement. In *Science and Technology of Concrete Admixtures*, pages 27–51. Elsevier, 2016. Journal Abbreviation: Science and Technology of Concrete Admixtures. URL: <https://dx.doi.org/10.1016/b978-0-08-100693-1.00003-5>, doi:10.1016/b978-0-08-100693-1.00003-5.
- [14] P. C. Aïtcin. Supplementary cementitious materials and blended cements. In *Science and Technology of Concrete Admixtures*, pages 53–73. Elsevier, 2016. Type: Book Section. URL: <https://dx.doi.org/10.1016/b978-0-08-100693-1.00004-7>, doi:10.1016/b978-0-08-100693-1.00004-7.
- [15] D. Marchon and R. J. Flatt. Impact of chemical admixtures on cement hydration. In *Science and Technology of Concrete Admixtures*, pages 279–304. Elsevier, 2016. Type: Book Section. URL: <https://dx.doi.org/10.1016/b978-0-08-100693-1.00012-6>, doi:10.1016/b978-0-08-100693-1.00012-6.
- [16] Barbara Lothenbach, Karen Scrivener, and R.D. Hooton. Supplementary cementitious materials. *Cement and Concrete Research*, 41(12):1244–1256, 2011. Publisher: Elsevier BV. URL: <https://dx.doi.org/10.1016/j.cemconres.2010.12.001>, doi:10.1016/j.cemconres.2010.12.001.
- [17] Maria C.G. Juenger and Rafat Siddique. Recent advances in understanding the role of supplementary cementitious materials in concrete. *Cement and Concrete Research*, 78:71–80, 2015. Publisher: Elsevier BV. URL: <https://dx.doi.org/10.1016/j.cemconres.2015.03.018>, doi:10.1016/j.cemconres.2015.03.018.

- [18] P.-C. Aïtcin. Accelerators. In *Science and Technology of Concrete Admixtures*, pages 405–413. Elsevier, 2016. Journal Abbreviation: Science and Technology of Concrete Admixtures. URL: <https://dx.doi.org/10.1016/b978-0-08-100693-1.00019-9>, doi:10.1016/b978-0-08-100693-1.00019-9.
- [19] P.-C. Aïtcin. Retarders. In *Science and Technology of Concrete Admixtures*, pages 395–404. Elsevier, 2016. Journal Abbreviation: Science and Technology of Concrete Admixtures. URL: <https://dx.doi.org/10.1016/b978-0-08-100693-1.00018-7>, doi:10.1016/b978-0-08-100693-1.00018-7.
- [20] Claude Bedard and Noel P. Mailvaganam. The Use of Chemical Admixtures in Concrete. Part II: Admixture-Admixture Compatibility and Practical Problems. *Journal of Performance of Constructed Facilities*, 20(1):2–5, February 2006. URL: <http://ascelibrary.org/doi/10.1061/%28ASCE%290887-3828%282006%2920%3A1%282%29>, doi:10.1061/(ASCE)0887-3828(2006)20:1(2).
- [21] S. Mantellato, A. B. Eberhardt, and R. J. Flatt. 15 - Formulation of commercial products. In Pierre-Claude Aïtcin and Robert J Flatt, editors, *Science and Technology of Concrete Admixtures*, pages 343–349. Woodhead Publishing, January 2016. URL: <https://www.sciencedirect.com/science/article/pii/B9780081006931000151>, doi:10.1016/B978-0-08-100693-1.00015-1.
- [22] P. C. Nkinamubanzi, S. Mantellato, and R. J. Flatt. 16 - Superplasticizers in practice. In Pierre-Claude Aïtcin and Robert J. Flatt, editors, *Science and Technology of Concrete Admixtures*, pages 353–377. Woodhead Publishing, 2016. Type: Book Section. URL: <http://www.sciencedirect.com/science/article/pii/B9780081006931000163>, doi:10.1016/B978-0-08-100693-1.00016-3.
- [23] Hela Bessaies-Bey, Robert Baumann, Marc Schmitz, Michael Radler, and Nicolas Roussel. Organic admixtures and cement particles: Competitive adsorption and its macroscopic rheological consequences. *Cement and Concrete Research*, 80:1–9, 2016. Type: Journal Article. URL: <https://dx.doi.org/10.1016/j.cemconres.2015.10.010>, doi:10.1016/j.cemconres.2015.10.010.
- [24] Alexandre Govin, Marie-Claude Bartholin, Wolfram Schmidt, and Philippe Grosseau. Combination of superplasticizers with hydroxypropyl guar, effect on cement-paste properties. *Construction and Building Materials*, 215:595–604, 2019. Publisher: Elsevier BV. URL: <https://dx.doi.org/10.1016/j.conbuildmat.2019.04.137>, doi:10.1016/j.conbuildmat.2019.04.137.
- [25] Rachid Belhadi, Alexandre Govin, and Philippe Grosseau. Influence of polycarboxylate superplasticizer, citric acid and their combination on the hydration and workability of calcium sulfoaluminate cement. *Cement and Concrete Research*, 147:106513, 2021. Publisher: Elsevier BV. URL: <https://dx.doi.org/10.1016/j.cemconres.2021.106513>, doi:10.1016/j.cemconres.2021.106513.
- [26] Johann Plank, Constantin Tiemeyer, Daniel Bülchen, and Nils Recalde Lummer. A Review of Synergistic and Antagonistic Effects Between Oilwell-Cement Additives. *SPE Drilling & Completion*, 28(04):398–404, 2013. Publisher: Society of Petroleum Engineers (SPE). URL: <https://dx.doi.org/10.2118/164103-pa>, doi:10.2118/164103-pa.

- [27] M. Palacios and R.J. Flatt. Working mechanism of viscosity-modifying admixtures. In *Science and Technology of Concrete Admixtures*, pages 415–432. Elsevier, 2016. Journal Abbreviation: Science and Technology of Concrete Admixtures. URL: <https://dx.doi.org/10.1016/b978-0-08-100693-1.00020-5>, doi:10.1016/b978-0-08-100693-1.00020-5.
- [28] Delphine Marchon. *Controlling cement hydration through the molecular structure of comb copolymer superplasticizers*. Thesis, ETH Zürich, 2016. URL: <http://hdl.handle.net/20.500.11850/123827>, doi:10.3929/ethz-a-010798278.
- [29] J. Plank and Ch Winter. Competitive adsorption between superplasticizer and retarder molecules on mineral binder surface. *Cement and Concrete Research*, 38(5):599–605, 2008. Type: Journal Article. URL: <https://dx.doi.org/10.1016/j.cemconres.2007.12.003>, doi:10.1016/j.cemconres.2007.12.003.
- [30] Hela Bessaies Bey, Julie Hot, Robert Baumann, and Nicolas Roussel. Consequences of competitive adsorption between polymers on the rheological behaviour of cement pastes. *Cement and Concrete Composites*, 54:17–20, 2014. Type: Journal Article. URL: <https://dx.doi.org/10.1016/j.cemconcomp.2014.05.002>, doi:10.1016/j.cemconcomp.2014.05.002.
- [31] Hongbo Tan, Xin Li, Jian Huang, Baoguo Ma, Changya Qi, and Lin Chaoliang. Effect of competitive adsorption between polycarboxylate superplasticiser and sodium tripolyphosphate on cement paste fluidity. *Advances in Cement Research*, 27(10):593–600, 2015. Type: Journal Article. URL: <https://dx.doi.org/10.1680/adcr.15.00009>, doi:10.1680/adcr.15.00009.
- [32] Kazuo Yamada, Shoichi Ogawa, and Shunsuke Hanehara. Controlling of the adsorption and dispersing force of polycarboxylate-type superplasticizer by sulfate ion concentration in aqueous phase. *Cement and Concrete Research*, 31(3):375–383, 2001. Type: Journal Article. URL: [https://dx.doi.org/10.1016/S0008-8846\(00\)00503-2](https://dx.doi.org/10.1016/S0008-8846(00)00503-2), doi:10.1016/S0008-8846(00)00503-2.
- [33] Marlene Schmid and Johann Plank. Dispersing performance of different kinds of polycarboxylate (PCE) superplasticizers in cement blended with a calcined clay. *Construction and Building Materials*, 258:119576, 2020. Type: Journal Article. URL: <https://dx.doi.org/10.1016/j.conbuildmat.2020.119576>, doi:10.1016/j.conbuildmat.2020.119576.
- [34] Giorgio Ferrari, Luca Valentini, Vincenzo Russo, Maria C. Dalconi, Marco Favero, and Gilberto Artioli. Improving the performance of PCE superplasticizers in early stiffening Portland cement. *Construction and Building Materials*, 130:83–91, 2017. Publisher: Elsevier BV. URL: <https://dx.doi.org/10.1016/j.conbuildmat.2016.11.015>, doi:10.1016/j.conbuildmat.2016.11.015.
- [35] Jin Young Yoon and Jae Hong Kim. Evaluation on the consumption and performance of polycarboxylates in cement-based materials. *Construction and Building Materials*, 158:423–431, 2018. Publisher: Elsevier BV. URL: <https://dx.doi.org/10.1016/j.conbuildmat.2017.10.004>, doi:10.1016/j.conbuildmat.2017.10.004.

- [36] Giulia Gelardi, Nicolas Sanson, Gergely Nagy, and Robert Flatt. Characterization of Comb-Shaped Copolymers by Multidetector SEC, DLS and SANS. *Polymers*, 9(12):61, 2017. Type: Journal Article. URL: <https://dx.doi.org/10.3390/polym9020061>, doi:10.3390/polym9020061.
- [37] C. Gay and E. Raphaël. Comb-like polymers inside nanoscale pores. *Advances in Colloid and Interface Science*, 94(1-3):229–236, 2001. Type: Journal Article. URL: [https://dx.doi.org/10.1016/S0001-8686\(01\)00062-8](https://dx.doi.org/10.1016/S0001-8686(01)00062-8), doi:10.1016/S0001-8686(01)00062-8.
- [38] Iñaki Emaldi, Amaia Agirre, Agustin Etxeberria, Edurne Erkizia, Jorges Dolado, and Jose R. Leiza. Characterization of Comb Shaped MAA- co -PEGMA Copolymers Synthesized by Free-Radical Polymerization. *Macromolecular Reaction Engineering*, 14(6):2000015, 2020. Type: Journal Article. URL: <https://dx.doi.org/10.1002/mren.202000015>, doi:10.1002/mren.202000015.
- [39] Giulia Gelardi. *Characterization of Comb Copolymer Superplasticizers by a Multi-Technique Approach, 2017*. Thesis, ETH Zürich, Zürich. URL: <http://hdl.handle.net/20.500.11850/208549>, doi:10.3929/ethz-b-000208549.
- [40] Harald Pasch. Hyphenated Techniques in Liquid Chromatography of Polymers. In *New Developments in Polymer Analytics I*, pages 1–66. Springer Berlin Heidelberg, 2000. Type: Book Section. URL: https://dx.doi.org/10.1007/3-540-48764-6_1, doi:10.1007/3-540-48764-6_1.
- [41] Harald Pasch. *Multidimensional HPLC of Polymers*. Springer Laboratory, Manuals in Polymer Science. Springer Berlin Heidelberg, Berlin, Heidelberg, 1st ed. 2013. edition, 2013. Type: Book. doi:10.1007/978-3-642-36080-0.
- [42] Sadao Mori and Howard G. Barth. *Size exclusion chromatography*. Springer, Berlin; London, 2011. Type: Book.
- [43] Iñaki Emaldi, Shaghayegh Hamzehlou, Edurne Erkizia, Jorge Sanchez Dolado, Agustin Etxeberria, and Jose Ramon Leiza. Modelling and control of the microstructure of comb-like poly(MAA-co-PEGMA) water-soluble copolymers. *Polymer Chemistry*, 10(8):1000–1009, 2019. Type: Journal Article. URL: <https://dx.doi.org/10.1039/c8py01599f>, doi:10.1039/c8py01599f.
- [44] Delphine Marchon, Federica Boscaro, and Robert J. Flatt. First steps to the molecular structure optimization of polycarboxylate ether superplasticizers: Mastering fluidity and retardation. *Cement and Concrete Research*, 115:116–123, 2019. Type: Journal Article. URL: <http://www.sciencedirect.com/science/article/pii/S0008884618307907>, doi:<https://doi.org/10.1016/j.cemconres.2018.10.009>.
- [45] Delphine Marchon, Patrick Juilland, Emmanuel Gallucci, Lukas Frunz, and Robert J. Flatt. Molecular and submolecular scale effects of comb-copolymers on tri-calcium silicate reactivity: Toward molecular design. *Journal of the American Ceramic Society*, 100(3):817–841, 2017. Type: Journal Article. URL: <https://dx.doi.org/10.1111/jace.14695>, doi:10.1111/jace.14695.

- [46] Delphine Marchon, Ueli Sulser, Arnd Eberhardt, and Robert J. Flatt. Molecular design of comb-shaped polycarboxylate dispersants for environmentally friendly concrete. *Soft Matter*, 9(45):10719, 2013. Type: Journal Article. URL: <https://dx.doi.org/10.1039/C3SM51030A>, doi:10.1039/c3sm51030a.
- [47] Iñaki Emaldi, Shaghayegh Hamzehlou, Jorge Sanchez-Dolado, and Jose Leiza. Kinetics of the Aqueous-Phase Copolymerization of MAA and PEGMA Macromonomer: Influence of Monomer Concentration and Side Chain Length of PEGMA. *Processes*, 5(4):19, 2017. Type: Journal Article. URL: <https://dx.doi.org/10.3390/pr5020019>, doi:10.3390/pr5020019.
- [48] Tsuyoshi Hirata, Jun Ye, Paulo Branicio, Jianwei Zheng, Alex Lange, Johann Plank, and Michael Sullivan. Adsorbed Conformations of PCE Superplasticizers in Cement Pore Solution Unraveled by Molecular Dynamics Simulations. *Scientific Reports*, 7(1), 2017. Type: Journal Article. URL: <https://dx.doi.org/10.1038/s41598-017-16048-3>, doi:10.1038/s41598-017-16048-3.
- [49] Hans-Jürgen Butt, Kh Graf, and Michael Kappl. *Physics and chemistry of interfaces*. Physics textbook. Wiley-VCH, Weinheim, 2003. Type: Book. URL: <https://onlinelibrary.wiley.com/doi/book/10.1002/3527602313>.
- [50] Francesco Caruso, Sara Mantellato, Marta Palacios, and Robert J. Flatt. ICP-OES method for the characterization of cement pore solutions and their modification by polycarboxylate-based superplasticizers. *Cement and Concrete Research*, 91:52–60, 2017. Type: Journal Article. URL: <https://dx.doi.org/10.1016/j.cemconres.2016.10.007>, doi:10.1016/j.cemconres.2016.10.007.
- [51] Yves F. Houst, Paul Bowen, François Perche, Annika Kauppi, Pascal Borget, Laurent Galmiche, Jean-François Le Meins, Françoise Lafuma, Robert J. Flatt, Irene Schober, Phil F. G. Banfill, David S. Swift, Bernt O. Myrvold, Berit G. Petersen, and Kåre Reknes. Design and function of novel superplasticizers for more durable high performance concrete (superplast project). *Cement and Concrete Research*, 38(10):1197–1209, 2008. Type: Journal Article. URL: <https://dx.doi.org/10.1016/j.cemconres.2008.04.007>, doi:10.1016/j.cemconres.2008.04.007.
- [52] R. Flatt and I. Schober. 7 - Superplasticizers and the rheology of concrete. In Nicolas Roussel, editor, *Understanding the Rheology of Concrete*, pages 144–208. Woodhead Publishing, 2012. Type: Book Section. URL: <http://www.sciencedirect.com/science/article/pii/B9780857090287500078>, doi:10.1533/9780857095282.2.144.
- [53] Michael Rubinstein and Ralph H. Colby. *Polymer physics*. Oxford University Press, Oxford ; New York, 2003. Type: Book.
- [54] C. Remzi Becer, Sabine Hahn, Martin W. M. Fijten, Hanneke M. L. Thijs, Richard Hoogenboom, and Ulrich S. Schubert. Libraries of methacrylic acid and oligo(ethylene glycol) methacrylate copolymers with LCST behavior. *Journal of Polymer Science Part A: Polymer Chemistry*, 46(21):7138–7147, 2008. Type: Journal Article. URL: <https://dx.doi.org/10.1002/pola.23018>, doi:10.1002/pola.23018.

- [55] Pascal Borget, Laurent Galmiche, Jean-Francois Le Meins, and Françoise Lafuma. Microstructural characterisation and behaviour in different salt solutions of sodium polymethacrylate-g-PEO comb copolymers. *Colloids and Surfaces A: Physicochemical and Engineering Aspects*, 260(1-3):173–182, 2005. Type: Journal Article. URL: <https://dx.doi.org/10.1016/j.colsurfa.2005.03.008>, doi:10.1016/j.colsurfa.2005.03.008.
- [56] Li Mei, Rui Xie, Chao Yang, Xiao-Jie Ju, Wei Wang, Ji-Yun Wang, and Liang-Yin Chu. pH-responsive Ca-alginate-based capsule membranes with grafted poly(methacrylic acid) brushes for controllable enzyme reaction. *Chemical Engineering Journal*, 232:573–581, 2013. Type: Journal Article. URL: <https://dx.doi.org/10.1016/j.cej.2013.08.015>, doi:10.1016/j.cej.2013.08.015.
- [57] Matthias Karg, Isabel Pastoriza-Santos, Benito Rodriguez-González, Regine Von Klitzing, Stefan Wellert, and T. Hellweg. Temperature, pH, and Ionic Strength Induced Changes of the Swelling Behavior of PNIPAM-Poly(allylacetic acid) Copolymer Microgels. *Langmuir*, 24(12):6300–6306, 2008. Type: Journal Article. URL: <https://dx.doi.org/10.1021/la702996p>, doi:10.1021/la702996p.
- [58] I. Pochard, P. Couchot, and A. Foissy. Potentiometric and conductometric analysis of the binding of Barium ions with alkali polyacrylate. *Colloid & Polymer Science*, 276(12):1088–1097, 1998. Type: Journal Article. URL: <https://dx.doi.org/10.1007/s003960050350>, doi:10.1007/s003960050350.
- [59] I. Pochard, A. Foissy, and P. Couchot. Conductometric and microcalorimetric analysis of the alkaline-earth/alkali-metal ion exchange onto polyacrylic acid. *Colloid & Polymer Science*, 277(9):818–826, 1999. Type: Journal Article. URL: <https://dx.doi.org/10.1007/s003960050458>, doi:10.1007/s003960050458.
- [60] Cornelia G. Sinn, Rumiana Dimova, and Markus Antonietti. Isothermal Titration Calorimetry of the Polyelectrolyte/Water Interaction and Binding of Ca²⁺: Effects Determining the Quality of Polymeric Scale Inhibitors. *Macromolecules*, 37(9):3444–3450, 2004. Type: Journal Article. URL: <https://dx.doi.org/10.1021/ma030550s>, doi:10.1021/ma030550s.
- [61] J. Lyklema. *Adsorption of Polymers and Polyelectrolytes*. Elsevier, 1995. Type: Book Section. URL: [https://dx.doi.org/10.1016/S1874-5679\(06\)80008-5](https://dx.doi.org/10.1016/S1874-5679(06)80008-5), doi:10.1016/S1874-5679(06)80008-5.
- [62] G. J. Fleer. *Polymers at Interfaces*. Springer Netherlands, 1998. Type: Book.
- [63] P. G. Degennes. CONFORMATIONS OF POLYMERS ATTACHED TO AN INTERFACE. *Macromolecules*, 13(5):1069–1075, 1980. Type: Journal Article. URL: <https://pubs.acs.org/doi/10.1021/ma60077a009>, doi:10.1021/ma60077a009.
- [64] David Platel. *The impact of the polymer architecture on the physico-chemistry properties of cement slurries*. Thesis, Université Pierre et Marie Curie - Paris VI, 2005. URL: <https://pastel.archives-ouvertes.fr/pastel-00001497>.
- [65] Robert Flatt, Yves Houst, Paul Bowen, Heiri Hofmann, J. Widmer, U. Sulser, U. Mäder, and T. Bürge. Interaction of Superplasticizers with Model Powders in

- a Highly Alkaline Medium. In *Proceedings of the 5th Canmet/ACI International Conference on Superplasticizers and Other Chemical Admixtures in Concrete*, 1997. Type: Journal Article. URL: <https://www.concrete.org/publications/internationalconcreteabstractsportal.aspx?m=details&id=6211>, doi: 10.14359/6211.
- [66] J. Zimmermann C. Hampel C. Kurz I. Schober L. Frunz C. Plassard R.J. Flatt and E. Lesniewska. The Role of Adsorption Energy in the Sulfate-Polycarboxylate Competition. *ACI Symposium Publication*, 262, 2009. Type: Journal Article. doi: 10.14359/51663229.
- [67] Sylvie Pourchet, Solenne Liautaud, David Rinaldi, and Isabelle Pochard. Effect of the repartition of the PEG side chains on the adsorption and dispersion behaviors of PCP in presence of sulfate. *Cement and Concrete Research*, 42(2):431–439, 2012. Type: Journal Article. URL: <https://dx.doi.org/10.1016/j.cemconres.2011.11.011>, doi:10.1016/j.cemconres.2011.11.011.
- [68] Song Han and Johann Plank. Mechanistic study on the effect of sulfate ions on polycarboxylate superplasticisers in cement. *Advances in Cement Research*, 25(4):200–207, 2013. Type: Journal Article. URL: <https://dx.doi.org/10.1680/adcr.12.00002>, doi:10.1680/adcr.12.00002.
- [69] J. Zimmermann, C. Hampel, C. Kurz, L. Frunz, and R. Flatt. Effect of Polymer Structure on the Sulfate-Polycarboxylate Competition. In *Ninth ACI International Conference on Superplasticizers and Other Chemical Admixtures*, Seville, 2009.
- [70] Johann Plank, Nils Recalde Lummer, and Fatima Dugonjić-Bilić. Competitive adsorption between an AMPS®-based fluid loss polymer and Welan gum biopolymer in oil well cement. *Journal of Applied Polymer Science*, pages NA–NA, 2010. Type: Journal Article. URL: <https://dx.doi.org/10.1002/app.31865>, doi:10.1002/app.31865.
- [71] Fubing Zou, Hongbo Tan, Yulin Guo, Baoguo Ma, Xingyang He, and Yang Zhou. Effect of sodium gluconate on dispersion of polycarboxylate superplasticizer with different grafting density in side chain. *Journal of Industrial and Engineering Chemistry*, 55:91–100, 2017. Type: Journal Article. URL: <https://dx.doi.org/10.1016/j.jiec.2017.06.032>, doi:10.1016/j.jiec.2017.06.032.
- [72] U. Mäder and I Schober. Performance of blends of polycarboxylate polymers in different cements. In Grieve G and Owens G, editors, *Proceedings 11th International Conference on the Chemistry of Cement (ICCC)*, volume 11, pages 504–513, 2003. Type: Conference Proceedings.
- [73] Hela Bessaies-Bey, Nadia Massoussi, Sudhir Mulik, Robert Baumann, Marc Schmitz, Michael Radler, Giulia Gelardi, Robert J. Flatt, and Nicolas Roussel. Polycarboxylate ester adsorption on cement grains: Influence of polydispersity. *Cement and Concrete Research*, 143:106383, 2021. Type: Journal Article. URL: <https://dx.doi.org/10.1016/j.cemconres.2021.106383>, doi:10.1016/j.cemconres.2021.106383.
- [74] M. A. Cohen Stuart, J. M. H. M. Scheutjens, and G. J. Fleer. Polydispersity effects and the interpretation of polymer adsorption isotherms. *Journal of Polymer Science:*

- Polymer Physics Edition*, 18(3):559–573, 1980. Type: Journal Article. URL: <https://dx.doi.org/10.1002/pol.1980.180180315>, doi:10.1002/pol.1980.180180315.
- [75] E. Pefferkorn, A. Carroy, and R. Varoqui. Dynamic behavior of flexible polymers at a solid/liquid interface. *Journal of Polymer Science: Polymer Physics Edition*, 23(10):1997–2008, 1985. Type: Journal Article. URL: <https://dx.doi.org/10.1002/pol.1985.180231002>, doi:10.1002/pol.1985.180231002.
- [76] J. Stecher and J. Plank. Novel concrete superplasticizers based on phosphate esters. *Cement and Concrete Research*, 119:36–43, 2019. Type: Journal Article. URL: <https://dx.doi.org/10.1016/j.cemconres.2019.01.006>, doi:10.1016/j.cemconres.2019.01.006.
- [77] Raffaella Abile, Alessandro Russo, Claudio Limone, and Fabio Montagnaro. Impact of the charge density on the behaviour of polycarboxylate ethers as cement dispersants. *Construction and Building Materials*, 180:477–490, 2018. Type: Journal Article. URL: <https://dx.doi.org/10.1016/j.conbuildmat.2018.05.276>, doi:10.1016/j.conbuildmat.2018.05.276.
- [78] Ran Li, Lei Lei, Tongbo Sui, and Johann Plank. Effectiveness of PCE superplasticizers in calcined clay blended cements. *Cement and Concrete Research*, 141:106334, 2021. Type: Journal Article. URL: <https://dx.doi.org/10.1016/j.cemconres.2020.106334>, doi:10.1016/j.cemconres.2020.106334.
- [79] L. Lei and J. Plank. A concept for a polycarboxylate superplasticizer possessing enhanced clay tolerance. *Cement and Concrete Research*, 42(10):1299–1306, 2012. Type: Journal Article. URL: <https://dx.doi.org/10.1016/j.cemconres.2012.07.001>, doi:10.1016/j.cemconres.2012.07.001.
- [80] Johann Plank, Christof Schroefl, Mirko Gruber, Matthias Lesti, and Roland Sieber. Effectiveness of Polycarboxylate Superplasticizers in Ultra-High Strength Concrete: The Importance of PCE Compatibility with Silica Fume. *Journal of Advanced Concrete Technology*, 7(1):5–12, 2009. Type: Journal Article. URL: <https://dx.doi.org/10.3151/jact.7.5>, doi:10.3151/jact.7.5.
- [81] Johann Plank and Bernhard Sachsenhauser. Impact of Molecular Structure on Zeta Potential and Adsorbed Conformation of .ALPHA.-Allyl-OMEGA.-Methoxypolyethylene Glycol-Maleic Anhydride Superplasticizers. *Journal of Advanced Concrete Technology*, 4(2):233–239, 2006. Type: Journal Article. URL: <https://dx.doi.org/10.3151/jact.4.233>, doi:10.3151/jact.4.233.
- [82] Lei Lei and Johann Plank. Synthesis and Properties of a Vinyl Ether-Based Polycarboxylate Superplasticizer for Concrete Possessing Clay Tolerance. *Industrial & Engineering Chemistry Research*, 53(3):1048–1055, 2014. Type: Journal Article. URL: <https://dx.doi.org/10.1021/ie4035913>, doi:10.1021/ie4035913.
- [83] My Linh Vo and Johann Plank. Dispersing effectiveness of a phosphated polycarboxylate in α - and β -calcium sulfate hemihydrate systems. *Construction and Building Materials*, 237:117731, 2020. Type: Journal Article. URL: <https://dx.doi.org/10.1016/j.conbuildmat.2019.117731>, doi:10.1016/j.conbuildmat.2019.117731.

- [84] J. Witt and J. Plank. A novel type of PCE possessing silyl functionalities. *American Concrete Institute, ACI Special Publication*, pages 57–70, 2012. Type: Journal Article.
- [85] Wei Fan, François Stoffelbach, Jutta Rieger, Laure Regnaud, Angélique Vichot, Bruno Bresson, and Nicolas Lequeux. A new class of organosilane-modified polycarboxylate superplasticizers with low sulfate sensitivity. *Cement and Concrete Research*, 42(1):166–172, 2012. Type: Journal Article. URL: <https://dx.doi.org/10.1016/j.cemconres.2011.09.006>, doi:10.1016/j.cemconres.2011.09.006.
- [86] Carlos A. Orozco, Byong W. Chun, Guoqing Geng, Abdul H. Emwas, and Paulo J. M. Monteiro. Characterization of the Bonds Developed between Calcium Silicate Hydrate and Polycarboxylate-Based Superplasticizers with Silyl Functionalities. *Langmuir*, 33(14):3404–3412, 2017. Type: Journal Article. URL: <https://dx.doi.org/10.1021/acs.langmuir.6b04368>, doi:10.1021/acs.langmuir.6b04368.
- [87] Johann Plank, Fan Yang, and Oksana Storcheva. Study of the interaction between cement phases and polycarboxylate superplasticizers possessing silyl functionalities. *Journal of Sustainable Cement-Based Materials*, 3(2):77–87, 2014. Type: Journal Article. URL: <https://dx.doi.org/10.1080/21650373.2014.903382>, doi:10.1080/21650373.2014.903382.
- [88] A. Lange and J. Plank. Study on the foaming behaviour of allyl ether-based polycarboxylate superplasticizers. *Cement and Concrete Research*, 42(2):484–489, 2012. Type: Journal Article. URL: <https://dx.doi.org/10.1016/j.cemconres.2011.11.017>, doi:10.1016/j.cemconres.2011.11.017.
- [89] Bethanne L. Smith and John Klier. Determination of monomer reactivity ratios for copolymerizations of methacrylic acid with poly (ethylene glycol) monomethacrylate. *Journal of Applied Polymer Science*, 68(6):1019–1025, 1998. Type: Journal Article. URL: [https://doi.org/10.1002/\(SICI\)1097-4628\(19980509\)68:6<1019::AID-APP15>3.0.CO;2-R](https://doi.org/10.1002/(SICI)1097-4628(19980509)68:6<1019::AID-APP15>3.0.CO;2-R), doi:[https://doi.org/10.1002/\(SICI\)1097-4628\(19980509\)68:6<1019::AID-APP15>3.0.CO;2-R](https://doi.org/10.1002/(SICI)1097-4628(19980509)68:6<1019::AID-APP15>3.0.CO;2-R).
- [90] Sebastian Smolne, Stella Weber, and Michael Buback. Propagation and Termination Kinetics of Poly(Ethylene Glycol) Methyl Ether Methacrylate in Aqueous Solution. *Macromolecular Chemistry and Physics*, 217(21):2391–2401, 2016. Type: Journal Article. URL: <https://dx.doi.org/10.1002/macp.201600302>, doi:10.1002/macp.201600302.
- [91] S. G. Mamedova, N. Sh Rasulov, and Z. M. Rzaev. Alternating copolymerization of maleic anhydride with allyl chloroacetate. *Journal of Polymer Science Part A: Polymer Chemistry*, 25(2):711–717, 1987. Type: Journal Article. URL: <https://dx.doi.org/10.1002/pola.1987.080250222>, doi:10.1002/pola.1987.080250222.
- [92] Bernd Tieke. *Makromolekulare Chemie : eine Einführung*. Wiley-VCH, Weinheim, 2., vollständig überarb. und erweiterte aufl., 2. nachdr. edition, 2009. Type: Book.
- [93] David Rinaldi, Thierry Hamaide, Christian Graillat, Franck D’Agosto, Roger Spitz, Sébastien Georges, Martin Mosquet, and Philippe Maitresse. RAFT copolymerization of methacrylic acid and poly(ethylene glycol) methyl ether methacrylate in the presence of a hydrophobic chain transfer agent in organic solution and in water. *Journal of Polymer*

- Science Part A: Polymer Chemistry*, 47(12):3045–3055, 2009. Type: Journal Article. URL: <https://dx.doi.org/10.1002/pola.23374>, doi:10.1002/pola.23374.
- [94] Metwally Ezzat, Xiaowen Xu, Khadija El Cheikh, Karel Lesage, Richard Hoogenboom, and Geert De Schutter. Structure-property relationships for polycarboxylate ether superplasticizers by means of RAFT polymerization. *Journal of Colloid and Interface Science*, 553:788–797, 2019. Type: Journal Article. URL: <https://dx.doi.org/10.1016/j.jcis.2019.06.088>, doi:10.1016/j.jcis.2019.06.088.
- [95] Tatjana Krivorotova, Aušvydas Vareikis, Daniel Gromadzki, Miloš Netopilík, and Ričardas Makuška. Conventional free-radical and RAFT copolymerization of poly(ethylene oxide) containing macromonomers. *European Polymer Journal*, 46(3):546–556, 2010. Type: Journal Article. URL: <https://dx.doi.org/10.1016/j.eurpolymj.2009.12.001>, doi:10.1016/j.eurpolymj.2009.12.001.
- [96] Graeme Moad, Ezio Rizzardo, and San H. Thang. Living Radical Polymerization by the RAFT Process. *Australian Journal of Chemistry*, 58(6):379, 2005. Type: Journal Article. URL: <https://dx.doi.org/10.1071/ch05072>, doi:10.1071/ch05072.
- [97] Andrew B. Lowe and Charles L. McCormick. RAFT Polymerization in Homogeneous Aqueous Media: Initiation Systems, RAFT Agent Stability, Monomers and Polymer Structures. In *Handbook of RAFT Polymerization*, pages 235–284. John Wiley & Sons, Ltd, September 2008. URL: <https://onlinelibrary.wiley.com/doi/abs/10.1002/9783527622757.ch7>.
- [98] David B. Thomas, Anthony J. Convertine, Roger D. Hester, Andrew B. Lowe, and Charles L. McCormick. Hydrolytic Susceptibility of Dithioester Chain Transfer Agents and Implications in Aqueous RAFT Polymerizations†. *Macromolecules*, 37(5):1735–1741, 2004. Type: Journal Article. URL: <https://dx.doi.org/10.1021/ma035572t>, doi:10.1021/ma035572t.
- [99] Katja Skrabania, Anna Miasnikova, Achille Mayelle Bivigou-Koumba, Daniel Zehm, and André Laschewsky. Examining the UV-vis absorption of RAFT chain transfer agents and their use for polymer analysis. *Polymer Chemistry*, 2(9):2074, 2011. Type: Journal Article. URL: <https://dx.doi.org/10.1039/C1PY00173F>, doi:10.1039/c1py00173f.
- [100] Graeme Moad, Ezio Rizzardo, and San H. Thang. RAFT Polymerization and Some of its Applications. *Chemistry - An Asian Journal*, 8(8):1634–1644, 2013. Type: Journal Article. URL: <https://dx.doi.org/10.1002/asia.201300262>, doi:10.1002/asia.201300262.
- [101] Massimo Benaglia, John Chiefari, Yen K. Chong, Graeme Moad, Ezio Rizzardo, and San H. Thang. Universal (Switchable) RAFT Agents. *Journal of the American Chemical Society*, 131(20):6914–6915, 2009. Type: Journal Article. URL: <https://dx.doi.org/10.1021/ja901955n>, doi:10.1021/ja901955n.
- [102] Isabelle Chaduc, Muriel Lansalot, Franck D’Agosto, and Bernadette Charleux. RAFT Polymerization of Methacrylic Acid in Water. *Macromolecules*, 45(3):1241–1247, 2012. Type: Journal Article. URL: <https://dx.doi.org/10.1021/ma2023815>, doi:10.1021/ma2023815.

- [103] Wenjing Zhang, Franck D'Agosto, Pierre-Yves Dugas, Jutta Rieger, and Bernadette Charleux. RAFT-mediated one-pot aqueous emulsion polymerization of methyl methacrylate in presence of poly(methacrylic acid-co-poly(ethylene oxide) methacrylate) trithiocarbonate macromolecular chain transfer agent. *Polymer*, 54(8):2011–2019, 2013. Type: Journal Article. URL: <https://dx.doi.org/10.1016/j.polymer.2012.12.028>, doi:10.1016/j.polymer.2012.12.028.
- [104] Lukas Frunz, Jürg Weidmann, and Jörg Zimmermann. *Block Copolymer (Patent)*. Sika AG, 2015. URL: <https://patents.google.com/patent/WO2015144886A1/de>.
- [105] Yan-Rong Zhang, Xiang-Ming Kong, Zhen-Bao Lu, Zi-Chen Lu, and Shan-Shan Hou. Effects of the charge characteristics of polycarboxylate superplasticizers on the adsorption and the retardation in cement pastes. *Cement and Concrete Research*, 67:184–196, 2015. Type: Journal Article. URL: <https://dx.doi.org/10.1016/j.cemconres.2014.10.004>, doi:10.1016/j.cemconres.2014.10.004.
- [106] Felix A. Plamper, Harald Becker, Michael Lanzendörfer, Mushtaq Patel, Alexander Wittemann, Matthias Ballauff, and Axel H. E. Müller. Synthesis, Characterization and Behavior in Aqueous Solution of Star-Shaped Poly(acrylic acid). *Macromolecular Chemistry and Physics*, 206(18):1813–1825, 2005. Type: Journal Article. URL: <https://dx.doi.org/10.1002/macp.200500238>, doi:10.1002/macp.200500238.
- [107] Sadao Mori and Howard G. Barth. *Size Exclusion Chromatography*. Springer Berlin Heidelberg, Berlin, Heidelberg, 1999. Type: Book. URL: <https://doi.org/10.1007/978-3-662-03910-6>.
- [108] J. Plank and B. Sachsenhauser. Experimental determination of the effective anionic charge density of polycarboxylate superplasticizers in cement pore solution. *Cement and Concrete Research*, 39(1):1–5, 2009. Type: Journal Article. URL: <https://dx.doi.org/10.1016/j.cemconres.2008.09.001>, doi:10.1016/j.cemconres.2008.09.001.
- [109] Johann Plank, Huiqun Li, Manuel Ilg, Julia Pickelmann, Wolfgang Eisenreich, Yan Yao, and Ziming Wang. A microstructural analysis of isoprenol ether-based polycarboxylates and the impact of structural motifs on the dispersing effectiveness. *Cement and Concrete Research*, 84:20–29, June 2016. URL: <https://www.sciencedirect.com/science/article/pii/S0008884616301594>, doi:10.1016/j.cemconres.2016.02.010.
- [110] Giao Nguyen, Daniel Nicole, Michel Swistek, Marek Matlengiewicz, and Bernard Wiegert. Sequence distribution of the methyl methacrylate-ethyl acrylate copolymer by ^{13}C n.m.r. spectroscopy. *Polymer*, 38(14):3455–3461, 1997. Type: Journal Article. URL: [https://dx.doi.org/10.1016/s0032-3861\(96\)00926-3](https://dx.doi.org/10.1016/s0032-3861(96)00926-3), doi:10.1016/s0032-3861(96)00926-3.
- [111] Yongsin Kim and H. James Harwood. Analysis of sequence distribution in methyl methacrylate–methyl acrylate copolymers by ^{13}C NMR spectroscopy. *Polymer*, 43(11):3229–3237, 2002. Type: Journal Article. URL: [https://dx.doi.org/10.1016/s0032-3861\(02\)00153-2](https://dx.doi.org/10.1016/s0032-3861(02)00153-2), doi:10.1016/s0032-3861(02)00153-2.
- [112] Harald Pasch, Martina Adler, Frank Rittig, and Stefan Becker. New Developments in Multidimensional Chromatography of Complex Polymers. *Macromolecular Rapid*

- Communications*, 26(6):438–444, March 2005. Publisher: John Wiley & Sons, Ltd. doi:10.1002/marc.200400610.
- [113] Gang Chen, Jiaheng Lei, Yong Du, Xiaodi Du, and Xuebing Chen. A polycarboxylate as a superplasticizer for montmorillonite clay in cement: Adsorption and tolerance studies. *Arabian Journal of Chemistry*, 11(6):747–755, 2018. Type: Journal Article. URL: <https://dx.doi.org/10.1016/j.arabjc.2017.12.027>, doi:10.1016/j.arabjc.2017.12.027.
- [114] Liran Zhang, Xia Miao, Xiangming Kong, and Shimin Zhou. Retardation effect of PCE superplasticizers with different architectures and their impacts on early strength of cement mortar. *Cement and Concrete Composites*, 104:103369, 2019. Type: Journal Article. URL: <https://dx.doi.org/10.1016/j.cemconcomp.2019.103369>, doi:10.1016/j.cemconcomp.2019.103369.
- [115] Walther Burchard. Solution Properties of Branched Macromolecules. In *Advances in Polymer Science*, pages 113–194. Springer Berlin Heidelberg, 1999. Type: Book Section. URL: https://dx.doi.org/10.1007/3-540-49780-3_3, doi:10.1007/3-540-49780-3_3.
- [116] Martina Adler, Frank Rittig, Stefan Becker, and Harald Pasch. Multidimensional Chromatographic and Hyphenated Techniques for Hydrophilic Copolymers, 1. *Macromolecular Chemistry and Physics*, 206(22):2269–2277, 2005. eprint: <https://onlinelibrary.wiley.com/doi/pdf/10.1002/macp.200500344>. URL: <https://onlinelibrary.wiley.com/doi/abs/10.1002/macp.200500344>, doi:<https://doi.org/10.1002/macp.200500344>.
- [117] Harry J. A. Philipsen. Determination of chemical composition distributions in synthetic polymers. *Journal of Chromatography A*, 1037(1-2):329–350, 2004. Type: Journal Article. URL: <https://linkinghub.elsevier.com/retrieve/pii/S0021967303023598>, doi:10.1016/j.chroma.2003.12.047.
- [118] Muhammad Imran Malik and Harald Pasch. Field-flow fractionation: New and exciting perspectives in polymer analysis. *Progress in Polymer Science*, 63:42–85, December 2016. URL: <https://www.sciencedirect.com/science/article/pii/S007967001630003X>, doi:10.1016/j.progpolymsci.2016.03.004.
- [119] Stepan Podzimek. *Light scattering, size exclusion chromatography and asymmetric flow field flow fractionation: powerful tools for the characterization of polymers, proteins and nanoparticles*. John Wiley & Sons, 2011. URL: <https://onlinelibrary.wiley.com/doi/book/10.1002/9780470877975>.
- [120] Karl-Heinz Spriestersbach, Frank Rittig, and Harald Pasch. Capillary Electrophoretic Analysis of Synthetic Copolymers with Indirect UV Detection and Contactless Conductivity Detection. *International Journal of Polymer Analysis and Characterization*, 14(3):196–209, March 2009. Publisher: Taylor & Francis eprint: <https://doi.org/10.1080/10236660802673158>. doi:10.1080/10236660802673158.
- [121] D. A. Hoagland, E. Arvanitidou, and C. Welch. Capillary Electrophoresis Measurements of the Free Solution Mobility for Several Model Polyelectrolyte Systems. *Macromolecules*,

- 32(19):6180–6190, September 1999. Publisher: American Chemical Society. doi: 10.1021/ma9903761.
- [122] Daniela Knecht, Frank Rittig, Ronald F. M. Lange, and Harald Pasch. Multidimensional chromatographic techniques for hydrophilic copolymers: II. Analysis of poly(ethylene glycol)-poly(vinyl acetate) graft copolymers. *Journal of Chromatography A*, 1130(1):43–53, October 2006. URL: <https://www.sciencedirect.com/science/article/pii/S0021967306014257>, doi:10.1016/j.chroma.2006.07.050.
- [123] Anja Baumgaertel, Esra Altuntaş, and Ulrich S. Schubert. Recent developments in the detailed characterization of polymers by multidimensional chromatography. *Journal of Chromatography A*, 1240:1–20, 2012. Type: Journal Article. URL: <https://dx.doi.org/10.1016/j.chroma.2012.03.038>, doi:10.1016/j.chroma.2012.03.038.
- [124] Andr M. Striegel, Wallace W. Yau, Joseph J. Kirkland, and Donald D. Bly. *Modern Size-Exclusion Liquid Chromatography*. John Wiley & Sons, Inc., Hoboken, NJ, USA, 2009. Type: Book. URL: <http://doi.wiley.com/10.1002/9780470442876>.
- [125] Anna M. Caltabiano, Joe P. Foley, and André M. Striegel. Aqueous size-exclusion chromatography of polyelectrolytes on reversed-phase and hydrophilic interaction chromatography columns. *Journal of Chromatography A*, 1532:161–174, 2018. Type: Journal Article. URL: <https://dx.doi.org/10.1016/j.chroma.2017.12.007>, doi:10.1016/j.chroma.2017.12.007.
- [126] André M. Striegel. Specific refractive index increment (dn/dc) of polymers at 660 nm and 690 nm. *Chromatographia*, 80(6):989–996, 2017. Type: Journal Article. URL: <https://pubmed.ncbi.nlm.nih.gov/28860670><https://www.ncbi.nlm.nih.gov/pmc/articles/PMC5572220/>, doi:10.1007/s10337-017-3294-2.
- [127] J. Plank, K. Pöllmann, N. Zouaoui, P. R. Andres, and C. Schaefer. Synthesis and performance of methacrylic ester based polycarboxylate superplasticizers possessing hydroxy terminated poly(ethylene glycol) side chains. *Cement and Concrete Research*, 38(10):1210–1216, 2008. Type: Journal Article. URL: <https://dx.doi.org/10.1016/j.cemconres.2008.01.007>, doi:10.1016/j.cemconres.2008.01.007.
- [128] Helmut Schlaad and Peter Kilz. Determination of Molecular Weight Distributions of Diblock Copolymers with Conventional Size Exclusion Chromatography. *Analytical Chemistry*, 75(6):1548–1551, 2003. Type: Journal Article. URL: <https://dx.doi.org/10.1021/ac026002e>, doi:10.1021/ac026002e.
- [129] André M. Striegel. Method development in interaction polymer chromatography. *TrAC Trends in Analytical Chemistry*, 130:115990, 2020. Type: Journal Article. URL: <https://dx.doi.org/10.1016/j.trac.2020.115990>, doi:10.1016/j.trac.2020.115990.
- [130] Ricardo Medrano, M. Teresa R. Laguna, Enrique Saiz, and M. Pilar Tarazona. Analysis of copolymers of styrene and methyl methacrylate using size exclusion chromatography with multiple detection. *Physical Chemistry Chemical Physics*, 5(1):151–157, 2003. Type: Journal Article. URL: <https://dx.doi.org/10.1039/B205461B>, doi:10.1039/b205461b.

- [131] Steven M. Rowland and André M. Striegel. Characterization of Copolymers and Blends by Quintuple-Detector Size-Exclusion Chromatography. *Analytical Chemistry*, 84(11):4812–4820, 2012. Publisher: American Chemical Society (ACS). URL: <https://dx.doi.org/10.1021/ac3003775>, doi:10.1021/ac3003775.
- [132] Wolf Hiller and Mathias Hehn. Investigations of Multiple Detection of Polymers. *Analytical Chemistry*, 86(21):10900–10908, 2014. Type: Journal Article. URL: <https://dx.doi.org/10.1021/ac5031607>, doi:10.1021/ac5031607.
- [133] André M. Striegel and Imad A. Haidar Ahmad. Determining the Chemical-Heterogeneity-Corrected Molar Mass Averages and Distribution of Poly(styrene-co-t-butyl methacrylate) Using SEC/MALS/UV/DRI. *Chromatographia*, 81(5):823–827, 2018. Type: Journal Article. URL: <https://dx.doi.org/10.1007/s10337-018-3512-6>, doi:10.1007/s10337-018-3512-6.
- [134] B. G. Belenky, E. S. Gankina, M. B. Tennikov, and L. Z. Vilenchik. Fundamental aspects of adsorption chromatography of polymers and their experimental verification by thin-layer chromatography. *Journal of Chromatography A*, 147:99–110, 1978. Type: Journal Article. URL: [https://dx.doi.org/10.1016/s0021-9673\(00\)85121-3](https://dx.doi.org/10.1016/s0021-9673(00)85121-3), doi:10.1016/s0021-9673(00)85121-3.
- [135] A. A. Gorbunov and A. M. Skvortsov. The method of “invisibles” in chromatography of polymers and the limits of its applicability. *Polymer Science U.S.S.R.*, 30(4):913–919, 1988. Type: Journal Article. URL: [https://dx.doi.org/10.1016/0032-3950\(88\)90209-2](https://dx.doi.org/10.1016/0032-3950(88)90209-2), doi:10.1016/0032-3950(88)90209-2.
- [136] W. Radke and J. Falkenhagen. Liquid Interaction Chromatography of Polymers. In *Liquid Chromatography*, pages 93–129. Elsevier, 2013. Type: Book Section. URL: <https://dx.doi.org/10.1016/b978-0-12-415806-1.00005-x>, doi:10.1016/b978-0-12-415806-1.00005-x.
- [137] Shazia Abrar and Bernd Trathnigg. Analysis of polyethyleneoxide macromonomers by liquid chromatography along the critical adsorption line. *Analytical and Bioanalytical Chemistry*, 400(8):2577–2586, 2011. Type: Journal Article. URL: <https://dx.doi.org/10.1007/s00216-010-4554-2>, doi:10.1007/s00216-010-4554-2.
- [138] Tibor Macko and David Hunkeler. *Liquid Chromatography under Critical and Limiting Conditions: A Survey of Experimental Systems for Synthetic Polymers*. Springer Berlin Heidelberg, 2003. Type: Book Section. URL: <https://dx.doi.org/10.1007/b11053>, doi:10.1007/b11053.
- [139] A. J. P. Martin. Partition Chromatography. *Annual Review of Biochemistry*, 19(1):517–542, 1950. Type: Journal Article. URL: <https://dx.doi.org/10.1146/annurev.bi.19.070150.002505>, doi:10.1146/annurev.bi.19.070150.002505.
- [140] P. J. C. H. Cools, F. Maesen, B. Klumperman, A. M. Van Herk, and A. L. German. Determination of the chemical composition distribution of copolymers of styrene and butadiene by gradient polymer elution chromatography. *Journal of Chromatography A*, 736(1-2):125–130, 1996. Type: Journal Article. URL: [https://dx.doi.org/10.1016/0021-9673\(95\)01369-5](https://dx.doi.org/10.1016/0021-9673(95)01369-5), doi:10.1016/0021-9673(95)01369-5.

- [141] Gottfried Glöckner and Axel H. E. Müller. Gradient high-performance liquid chromatography of statistical and block copolymers of styrene and t-butyl methacrylate. *Journal of Applied Polymer Science*, 38(9):1761–1774, 1989. Type: Journal Article. URL: <https://dx.doi.org/10.1002/app.1989.070380914>, doi:10.1002/app.1989.070380914.
- [142] Raoul Peltier, Agnieszka Bialek, Agnès Kuroki, Caroline Bray, Liam Martin, and Sébastien Perrier. Reverse-phase high performance liquid chromatography (RP-HPLC) as a powerful tool to characterise complex water-soluble copolymer architectures. *Polymer Chemistry*, 9(46):5511–5520, 2018. Type: Journal Article. URL: <https://dx.doi.org/10.1039/c8py00966j>, doi:10.1039/c8py00966j.
- [143] Taihyun Chang. Polymer characterization by interaction chromatography. *Journal of Polymer Science Part B: Polymer Physics*, 43(13):1591–1607, 2005. Type: Journal Article. URL: <https://dx.doi.org/10.1002/polb.20440>, doi:10.1002/polb.20440.
- [144] Lars-Christian Heinz, Tibor Macko, Harald Pasch, Marc-Stephan Weiser, and Rolf Mülhaupt. High-Temperature Liquid Chromatography at Critical Conditions: Separation of Polystyrene from Blends with Polyethylene and Ethylene-Styrene Block Copolymers. *International Journal of Polymer Analysis and Characterization*, 11(1):47–55, 2006. Type: Journal Article. URL: <https://dx.doi.org/10.1080/10236660500484312>, doi:10.1080/10236660500484312.
- [145] Anthony Ndiripo, Andreas Albrecht, Benjamin Monrabal, Jingbo Wang, and Harald Pasch. Chemical Composition Fractionation of Olefin Plastomers/Elastomers by Solvent and Thermal Gradient Interaction Chromatography. *Macromolecular Rapid Communications*, 39(6):1700703, 2018. Type: Journal Article. URL: <https://dx.doi.org/10.1002/marc.201700703>, doi:10.1002/marc.201700703.
- [146] Anthony Ndiripo and Harald Pasch. Comprehensive Analysis of Oxidized Waxes by Solvent and Thermal Gradient Interaction Chromatography and Two-Dimensional Liquid Chromatography. *Analytical Chemistry*, 90(12):7626–7634, June 2018. Publisher: American Chemical Society. doi:10.1021/acs.analchem.8b01480.
- [147] Xulin Jiang, Aschwin van der Horst, Vincent Lima, and Peter J. Schoenmakers. Comprehensive two-dimensional liquid chromatography for the characterization of functional acrylate polymers. *Journal of Chromatography A*, 1076(1):51–61, May 2005. URL: <https://www.sciencedirect.com/science/article/pii/S0021967305006540>, doi:10.1016/j.chroma.2005.03.135.
- [148] Aschwin van der Horst and Peter J. Schoenmakers. Comprehensive two-dimensional liquid chromatography of polymers. *Journal of Chromatography A*, 1000(1):693–709, June 2003. URL: <https://www.sciencedirect.com/science/article/pii/S0021967303004953>, doi:10.1016/S0021-9673(03)00495-3.
- [149] Jan Blomberg, Peter J. Schoenmakers, Jan Beens, and Robert Tijssen. Comprehensive two-dimensional gas chromatography (GC×GC) and its applicability to the characterization of complex (petrochemical) mixtures. *Journal of High Resolution Chromatography*, 20(10):539–544, 1997. eprint: <https://onlinelibrary.wiley.com/doi/pdf/10.1002/jhrc.1240201005>. URL: <https://onlinelibrary.wiley.com/doi/pdf/10.1002/jhrc.1240201005>.

- //onlinelibrary.wiley.com/doi/abs/10.1002/jhrc.1240201005, doi:10.1002/jhrc.1240201005.
- [150] Gino Groeneveld, Bob W. J. Pirok, and Peter J. Schoenmakers. Perspectives on the future of multi-dimensional platforms. *Faraday Discussions*, 218(0):72–100, 2019. Publisher: Royal Society of Chemistry. URL: <https://pubs.rsc.org/en/content/articlelanding/2019/fd/c8fd00233a>, doi:10.1039/C8FD00233A.
- [151] Maria Shakun. *Neue Charakterisierungsmethoden für Natriumcarboxymethylcellulosen*. Dissertation, Technische Universität, Darmstadt, October 2014. URL: <https://tuprints.ulb.tu-darmstadt.de/4612/>.
- [152] Harry P. Gregor and Michael Frederick. Potentiometric titration of polyacrylic and polymethacrylic acids with alkali metal and quaternary ammonium bases. *Journal of Polymer Science*, 23(103):451–465, 1957. Type: Journal Article. URL: <https://dx.doi.org/10.1002/pol.1957.1202310338>, doi:10.1002/pol.1957.1202310338.
- [153] Frank Winnefeld, Stefan Becker, Joachim Pakusch, and Thomas Götz. Effects of the molecular architecture of comb-shaped superplasticizers on their performance in cementitious systems. *Cement and Concrete Composites*, 29(4):251–262, 2007. Type: Journal Article. URL: <https://dx.doi.org/10.1016/j.cemconcomp.2006.12.006>, doi:10.1016/j.cemconcomp.2006.12.006.
- [154] L. Ferrari, J. Kaufmann, F. Winnefeld, and J. Plank. Multi-method approach to study influence of superplasticizers on cement suspensions. *Cement and Concrete Research*, 41(10):1058–1066, October 2011. URL: <https://www.sciencedirect.com/science/article/pii/S0008884611001840>, doi:10.1016/j.cemconres.2011.06.010.
- [155] Fan-Rong Kong, Li-Sha Pan, Chen-Man Wang, De-La Zhang, and Nai Xu. Effects of polycarboxylate superplasticizers with different molecular structure on the hydration behavior of cement paste. *Construction and Building Materials*, 105:545–553, 2016. Type: Journal Article. URL: <https://dx.doi.org/10.1016/j.conbuildmat.2015.12.178>, doi:10.1016/j.conbuildmat.2015.12.178.
- [156] Florent Dalas, André Nonat, Sylvie Pourchet, Martin Mosquet, David Rinaldi, and Serge Sabio. Tailoring the anionic function and the side chains of comb-like superplasticizers to improve their adsorption. *Cement and Concrete Research*, 67:21–30, 2015. Type: Journal Article. URL: <https://dx.doi.org/10.1016/j.cemconres.2014.07.024>, doi:10.1016/j.cemconres.2014.07.024.
- [157] Hela Bessaies Bey, Nadia Massousi, Robert Baumann, Marc Schmitz, Michael Radler, Robert J. Flatt, and Nicolas Roussel. Polycarboxylate Adsorption on Cement Grains: Influence of Polydispersity. *Cement and Concrete Research*, under revision, 2020. Type: Journal Article.
- [158] Wolfgang Radke. Consequences of on-line dialysis on polyelectrolyte molar masses determined by size-exclusion chromatography with light scattering detection. *Journal of Separation Science*, 39(4):696–702, February 2016. Publisher: John Wiley & Sons, Ltd. doi:10.1002/jssc.201500936.

- [159] Daniela Knecht. *Mehrdimensionale Analytik von hydrophilen synthetischen Copolymeren*. PhD thesis, TU Darmstadt, Darmstadt, 2007. URL: <https://tuprints.ulb.tu-darmstadt.de/epda/000775/>.
- [160] P. J. Andersen, D. M. Roy, J. M. Gaidis, and W.R. Grace & Co. The effects of adsorption of superplasticizers on the surface of cement. *Cement and Concrete Research*, 17(5):805–813, September 1987. URL: <https://www.sciencedirect.com/science/article/pii/S008884687900433>, doi:10.1016/0008-8846(87)90043-3.
- [161] Robert J. Flatt and Yves F. Houst. A simplified view on chemical effects perturbing the action of superplasticizers. *Cement and Concrete Research*, 31(8):1169–1176, 2001. Type: Journal Article. URL: [https://dx.doi.org/10.1016/S0008-8846\(01\)00534-8](https://dx.doi.org/10.1016/S0008-8846(01)00534-8), doi:10.1016/S0008-8846(01)00534-8.
- [162] Johann Plank, Dai Zhimin, Helena Keller, Friedrich V. Hössle, and Wolfgang Seidl. Fundamental mechanisms for polycarboxylate intercalation into C3A hydrate phases and the role of sulfate present in cement. *Cement and Concrete Research*, 40(1):45–57, 2010. Type: Journal Article. URL: <https://dx.doi.org/10.1016/j.cemconres.2009.08.013>, doi:10.1016/j.cemconres.2009.08.013.
- [163] J. J. Thomas, H. M. Jennings, and A. J. Allen. The surface area of cement paste as measured by neutron scattering: evidence for two C-S-H morphologies. *Cement and Concrete Research*, 28(6):897–905, 1998. Type: Journal Article. URL: [https://dx.doi.org/10.1016/S0008-8846\(98\)00049-0](https://dx.doi.org/10.1016/S0008-8846(98)00049-0), doi:10.1016/S0008-8846(98)00049-0.
- [164] Florent Dalas, Sylvie Pourchet, David Rinaldi, André Nonat, Serge Sabio, and Martin Mosquet. Modification of the rate of formation and surface area of ettringite by polycarboxylate ether superplasticizers during early C3A–CaSO₄ hydration. *Cement and Concrete Research*, 69:105–113, March 2015. URL: <https://www.sciencedirect.com/science/article/pii/S000888461400249X>, doi:10.1016/j.cemconres.2014.12.007.
- [165] Chen Shi, Ge Zhang, Tingshu He, and Yimin Li. Effects of superplasticizers on the stability and morphology of ettringite. *Construction and Building Materials*, 112:261–266, June 2016. URL: <https://www.sciencedirect.com/science/article/pii/S0950061816302550>, doi:10.1016/j.conbuildmat.2016.02.198.
- [166] Sylvie Pourchet, Cedric Comparat, André Nonat, and Philippe Maitrasse. Influence of three types of superplasticizers on tricalciumaluminate hydration in presence of gypsum. *ACI Special Publication*, 239, October 2006. URL: <https://www.concrete.org/publications/internationalconcreteabstractsportal.aspx?m=details&id=18377>, doi:10.14359/18377.
- [167] Estelle Poupelloz, Sandrine Gauffinet, and André Nonat. Study of nucleation and growth processes of ettringite in diluted conditions. *Cement and Concrete Research*, 127:105915, 2020. Publisher: Elsevier BV. URL: <https://dx.doi.org/10.1016/j.cemconres.2019.105915>, doi:10.1016/j.cemconres.2019.105915.
- [168] Markus R. Meier and Johann Plank. Crystal growth of [Ca₃Al(OH)₆·12H₂O]₂·(SO₄)₃·2H₂O (ettringite) under microgravity: On the impact of anionicity of polycarboxylate comb polymers. *Journal of Crystal Growth*,

-
- 446:92–102, 2016. Publisher: Elsevier BV. URL: <https://dx.doi.org/10.1016/j.jcrysgro.2016.04.049>, doi:10.1016/j.jcrysgro.2016.04.049.
- [169] Markus R. Meier, Alexander Rinkenburger, and Johann Plank. Impact of different types of polycarboxylate superplasticisers on spontaneous crystallisation of ettringite. *Advances in Cement Research*, 28(5):310–319, 2016. Publisher: Thomas Telford Ltd. URL: <https://dx.doi.org/10.1680/jadcr.15.00114>, doi:10.1680/jadcr.15.00114.
- [170] A.M. Cody, H. Lee, R.D. Cody, and P.G. Spry. The effects of chemical environment on the nucleation, growth, and stability of ettringite $[\text{Ca}_3\text{Al}(\text{OH})_6]_2(\text{SO}_4)_3 \cdot 26\text{H}_2\text{O}$. *Cement and Concrete Research*, 34(5):869–881, 2004. Publisher: Elsevier BV. URL: <https://dx.doi.org/10.1016/j.cemconres.2003.10.023>, doi:10.1016/j.cemconres.2003.10.023.
- [171] Sara Mantellato, Marta Palacios, and Robert J. Flatt. Relating early hydration, specific surface and flow loss of cement pastes. *Materials and Structures*, 52(1), 2019. Type: Journal Article. URL: <https://dx.doi.org/10.1617/s11527-018-1304-y>, doi:10.1617/s11527-018-1304-y.
- [172] Sara Mantellato. *Flow Loss in Superplasticized Cement Pastes*. Doctoral Thesis, ETH Zurich, 2017. Accepted: 2018-05-23T07:17:31Z. URL: <https://www.research-collection.ethz.ch/handle/20.500.11850/265510>, doi:10.3929/ethz-b-000265510.
- [173] Tariq Jamil, Ali Javadi, and Hendrik Heinz. Mechanism of molecular interaction of acrylate-polyethylene glycol acrylate copolymers with calcium silicate hydrate surfaces. *Green Chemistry*, 22(5):1577–1593, 2020. Type: Journal Article. URL: <https://dx.doi.org/10.1039/C9GC03287H>, doi:10.1039/c9gc03287h.

STEFANIE ANNE WECKWERTH

Polymer Chemist

PERSONAL DETAILS



anneckwerth@gmail.com



14th of September, 1991, Germany



www.linkedin.com/in/aweckwerth/

RESEARCH EXPERIENCE

DOCTORATE **PhD Student at Physical Chemistry of Building Materials,**
2016–2021 *ETH ZÜRICH,*
Zürich Contents:

- synthesis and characterization of comb copolymer dispersants
- understanding structure-performance relations of PCEs in cement

SUPERVISOR Prof. Robert J. Flatt

EDUCATION

MASTER **POLYMER SCIENCE (M.SC),**
2014–2016 *Universität Bayreuth,*
Bayreuth Thesis: "Selective Loading of Patchy Micelles with Polymer-Coated Gold Nanoparticles".

BACHELOR **POLYMER AND COLLOIDAL CHEMISTRY (B.SC),**
2011–2014 *Universität Bayreuth,*
Bayreuth Thesis: "Synthesis of Protein Coated Gold Nanoparticles and their Wrinkle-Assisted Linear Assemblies for Application in Anisotropic Optical Materials".

HONORS AND AWARDS

- PROGRAM **Elitenetwork of Bavaria**,
2016–2021 *Study Program "Macromolecular Science"* .
- SCHOLARSHIP **Academic Scholarship "Deutschlandstipendium"**,
2015–2016 *Programme by the German Ministry of Education and Research.*
- AWARD **Award for best Bachelor's Degree**,
2015 *Best Bachelor Student in Polymer and Colloidal Chemistry.*

FURTHER ACTIVITIES

- ETHZ Responsibility for the "Polymer Synthesis and Characterization Laboratory" in the group of Prof. Flatt
2017–2021
- ETHZ Teaching assistant within various lab courses for civil engineers
2017–2020
- REVIEWS Review activity for Cement and Concrete Research, Journal Elsevier
since 2019

PUBLICATIONS (as first author)

- CCR Experimental Method and Thermodynamic Model For Competitive
2021 Adsorption Between Polycarboxylate Comb Copolymers", *Cement and Concrete Research*, 2021, *accepted for publication*
- Polymers "A Method for Characterizing the Chemical Dispersity of Comb Copoly-
2021 mers and its Dependence on Synthesis Routes", *MDPI Polymers*, 2021, doi.org/10.3390/polym13121921
- ACI "Side Chains and the Competitive Adsorption Between Polycarboxylate
2022 Ethers", *ACI Conference Supplementary Volume*, 13th International Conference on Superplasticizers and Other Chemical Admixtures in Concrete, 2022, *submitted*

WORKSHOPS AND CONFERENCES

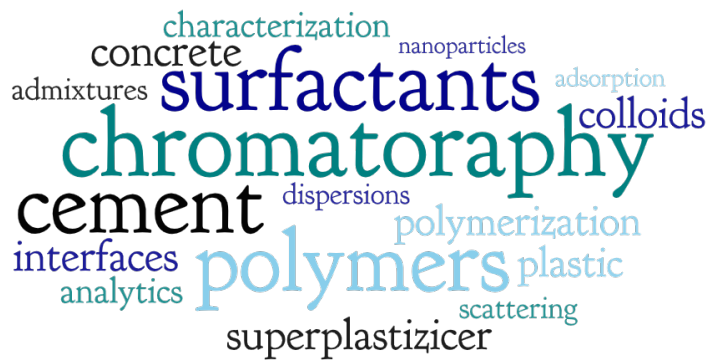
- BASF 136th BASF International Summer Course,
2019 Ludwigshafen, Germany
- BASF BASF Days Construction Chemicals 2019,
2019 Ludwigshafen, Germany

Nanocem Nanocem Knowledge Transfer Workshop,
2019 Madrid, Spain

TUM 2nd and 3rd International Conference on Polycarboxylate Superplasti-
2017&2019 cizers,
TUM München

PSS Practical Workshops focused on Polymer Chromatography,
2016&2020 Polymer Standards Service, Mainz

SKILLS



LANGUAGES



HOBBIES AND INTERESTS



Zürich, July 2021

WECKWERTH S A

